Bulletin
of
The Geological Society of America

VOLUME 67 June 1956 NUMBER 6

CONTENTS

	Pages
Three-dimensional applied potential studies at Austinville, Virginia. By H. V. McMurry and A. D. Hoagland	683–696
Coarse conglomerates of the Middle Ordovician in the southern Appalachian Valley. By John M. Kellberg and Leland F. Grant	697–716
Hemphillian mammalian assemblage from northeastern Oregon. By J. Arnold Shotwell	717–738
Statistical analysis of low-level radioactivity of Pennsylvanian black fissile shale in Illinois. By W. C. Krumbein and H. A. Slack	739–762
Structure and petrology of Enchanted Rock batholith, Llano and Gillespie counties, Texas. By R. M. Hutchinson	763–806
Short Notes	
Unusual patterned ground in Greenland. By A. L. Washburn	807–810
Composition of Westerly granite G-1 and Centerville diabase W-1. By Samuel S. Goldich and Eileen H. Oslund	811–816
Index (January–June)	817–822

Subscription $15.00 per year.

Printing Office: Mt. Royal & Guilford Aves., Baltimore 2, Md.

Communications for publications should be addressed to The Geological Society of America, Dr. H. R. Aldrich, Secretary, 419 West 117 Street, New York, N. Y.

Please give notice of change of address 4 weeks in advance. Claims for nonreceipt of the Bulletin of a given month must be sent to the Secretary of the Society before the end of the second succeeding month.

Entered as second-class matter at the Post Office at Baltimore, Md., under the Act of Congress of July 16, 1894.
Accepted for mailing at special rate of postage provided for in Section 1103 Act of October 3, 1917, authorized on July 8, 1918.

PAPERS IN PRESS FOR FORTHCOMING ISSUES

Classification of Patterned Ground and Review of Suggested Origins. By A. L. Washburn

Chronology of Denudation in Northwest Queensland. By C. R. Twidale

Recent Sediments of Three Wisconsin Lakes. By R. C. Murray

Alteration of Clay Minerals by Weathering in Wisconsin Tills. By J. B. Droste

Geochemistry of Pelitic Rocks. Part III: Major Elements and General Geochemistry. By Denis M. Shaw

Channeled Scabland of Washington: New Data and Interpretations. By J Harlen Bretz, H. T. U. Smith, and George E. Neff

BULLETIN OF THE GEOLOGICAL SOCIETY OF AMERICA
VOL. 67, PP. 683-696 JUNE 1956

THREE-DIMENSIONAL APPLIED POTENTIAL STUDIES AT AUSTINVILLE, VIRGINIA

BY H. V. McMURRY AND A. D. HOAGLAND

ABSTRACT

Applied potential data from diamond-drill holes at Austinville, Virginia, have shown that the host rocks of the ore bodies are of extremely high resistivity and are strongly anisotropic. Triaxial anisotropy is prominent and is thought to be controlled by the mineralization. The delineation of ore bodies by diamond drilling after penetration by a discovery hole has been aided by three-dimensional applied potential surveys. Several field cases are described.

CONTENTS

TEXT

	Page
Abstract	683
Introduction	683
Acknowledgments	683
Analysis of data	687
Appendix	695
References cited	696

Figure	Page
1. Current source in good conductor in Hole 3	684
2. Calculated case: Earth electrically isotropic	685
3. Calculated case: Earth electrically triaxially anisotropic	686
4. Plan of Holes 16 to 21	687
5. Cross section: Current source in high-resistivity zone in Hole 17	687
6. Cross section: Current source in excellent conductor in Hole 17	687
7. Longitudinal section: Current source in high-resistivity zone in Hole 17	688
8. Longitudinal section: Current source in excellent conductor in Hole 17	689
9. Plan of Holes 22 to 38	689
10. Cross section C-C: Current source in ore in Hole 30	690
11. Cross section D-D: Current source in ore in Hole 30	690
12. Cross section A-A: Current source in ore in Hole 30	691
13. Longitudinal section B-B: Current source in ore in Hole 30	692
14. Cross section C-C: Current source in ore in Hole 29	692
15. Cross section D-D: Current source in ore in Hole 29	693
16. Cross section A-A: Current source in ore in Hole 29	694
17. Longitudinal section E-E: Current source in ore in Hole 29	695

INTRODUCTION

The success of the direct-current geophysical method requires an adequate contrast between the resistivities of the host rock and the ore. The primary ore at Austinville, Virginia, is found in pencil-shaped bodies of disseminated sphalerite, pyrite, and galena in dolomite of the Shady formation of Early Cambrian age (Brown, 1935, p. 425; Currier, 1935, p. 74–79).

Sphalerite, the most abundant sulfide, is not a good electrical conductor; however, the associated pyrite and galena are good conductors, and the resistivity of the unmineralized host rock is from 10 to 100 times that of the ore. This contrast in resistivity is well suited to the direct-current applied potential method.

The general procedure followed was to pass current between an electrode embedded in a mineralized body of low resistivity and an electrode so remote that its influence on the current flow in the area under investigation could be neglected. Potentials were measured in volts per ampere between a convenient reference point and closely spaced points in all pertinent drill holes. The data are presented on appropriate vertical sections upon which ore and related mineralized bodies are interpreted.

ACKNOWLEDGMENTS

The writers wish to acknowledge the interest and encouragement of Mr. W. H. Callahan and the late Dr. W. O. Hotchkiss who visualized the

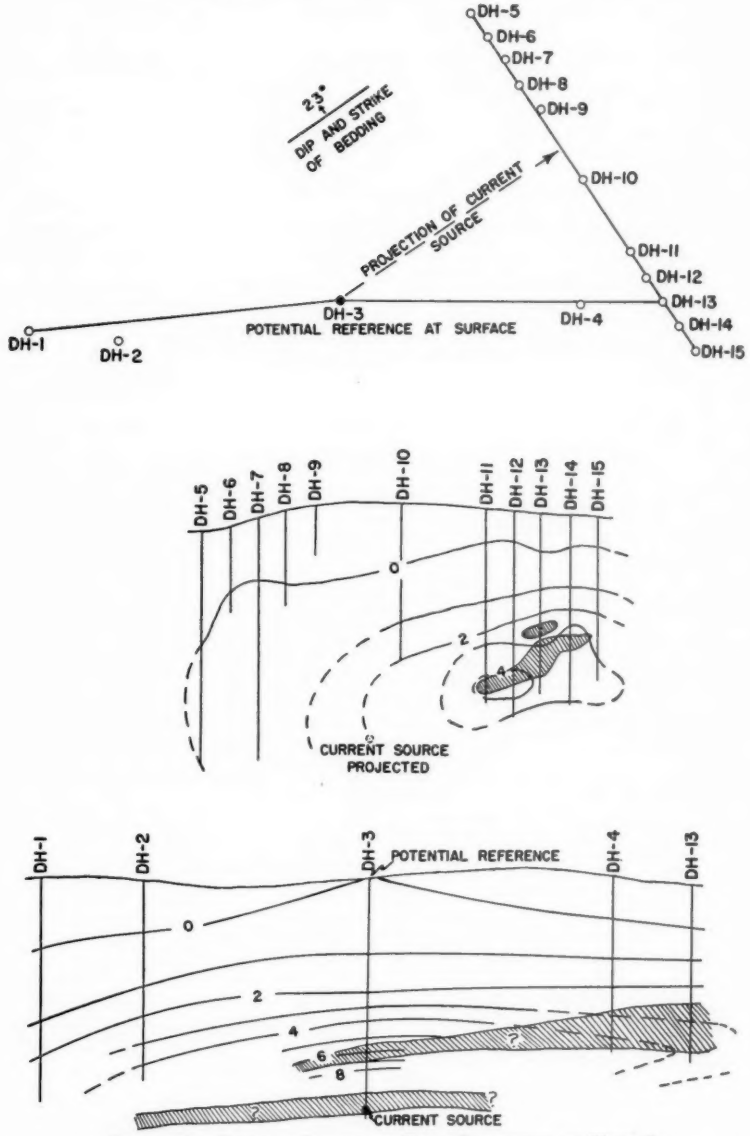

FIGURE 1.—CURRENT SOURCE IN GOOD CONDUCTOR IN HOLE 3

Maximum ellipticity of equipotential contours in plane of holes 1 to 13, lesser ellipticity in the plane of holes 5 to 15 illustrates relationship of ore pencil to low-resistivity zone.

useful application of applied potential studies in drill holes at Austinville. Many helpful suggestions and contributions were made by Messrs. L. B. Slichter, W. H. Brown, R. K. Waring, and D. G. Brubaker. Messrs. J. S. Naratil, R. O. Steel, and E. E. Fulford assisted in the collection of data. Thanks are due Mr. R. M. Knutson for aid in drafting and critical

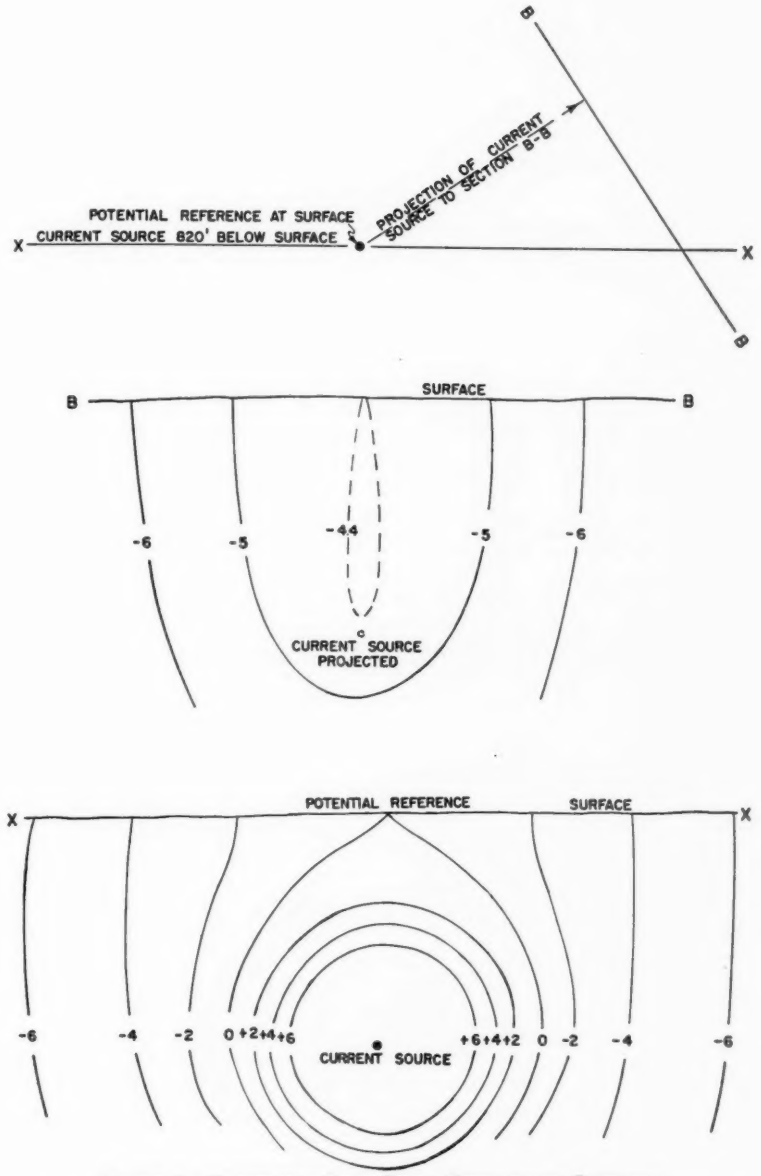

FIGURE 2.—CALCULATED CASE: EARTH ELECTRICALLY ISOTROPIC

Geometry similar to field case shown in Figure 1. Resistivity assumed to be half a million ohm-centimeters.

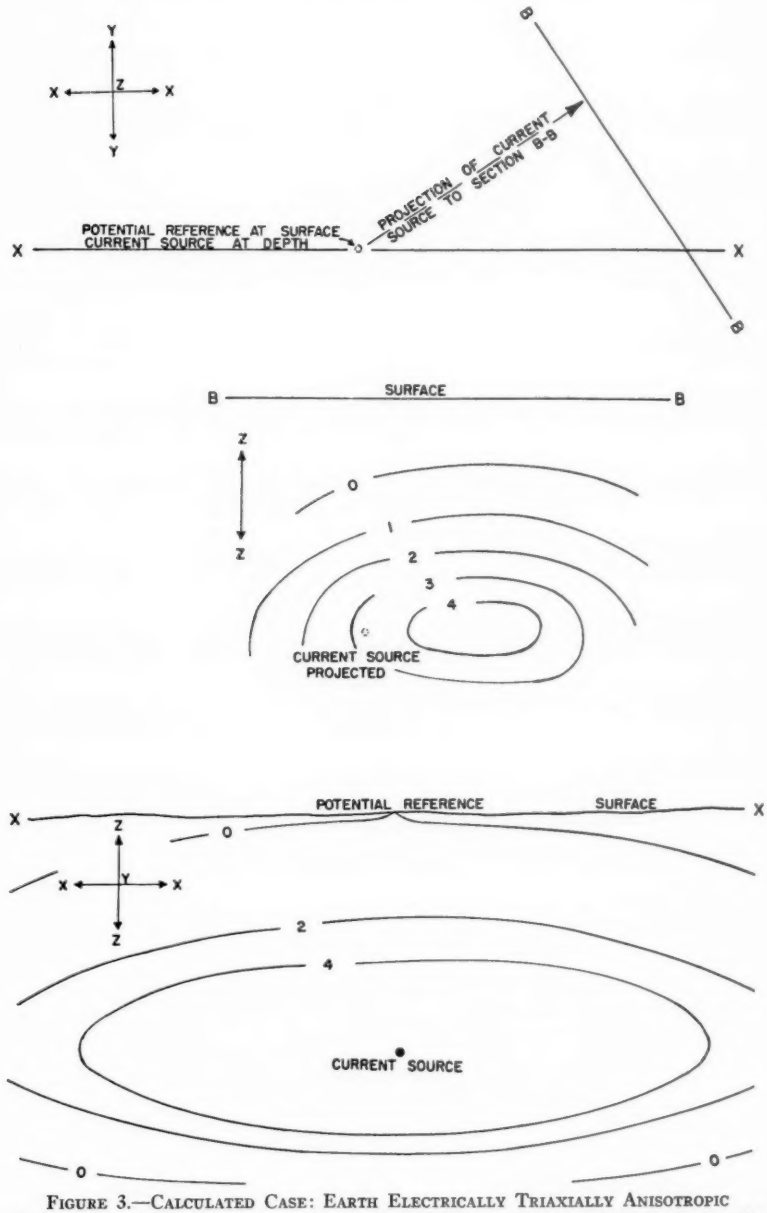

FIGURE 3.—CALCULATED CASE: EARTH ELECTRICALLY TRIAXIALLY ANISOTROPIC

Geometry similar to field case shown in Figure 1. Resistivities are 7 million, 2 million, and half a million ohm-centimeters, respectively, along vertical axes, horizontal axes perpendicular to direction XX, and along axes parallel to XX. Note similarity with field case shown to Figure 1.

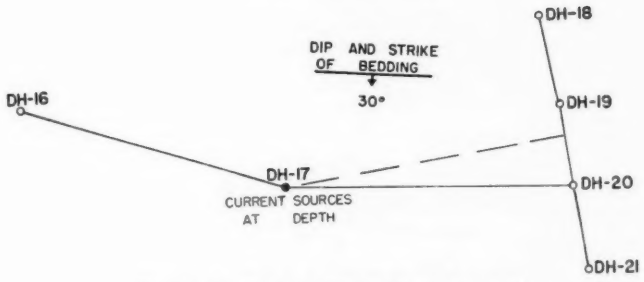

FIGURE 4.—PLAN OF DRILL HOLES 16 TO 21

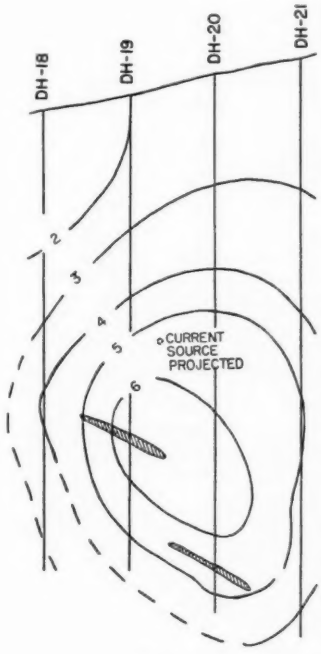

FIG. 5

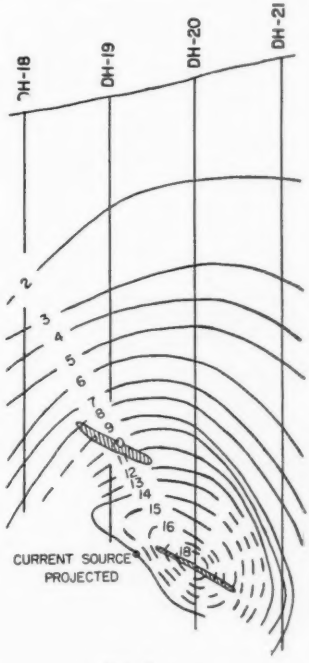

FIG. 6

FIGURE 5.—CROSS SECTION: CURRENT SOURCE IN HIGH-RESISTIVITY ZONE IN HOLE 17
Note low potential on this section indicating at best a weak continuity between conductors on this section and the current source.

FIGURE 6.—CROSS SECTION: CURRENT SOURCE IN EXCELLENT CONDUCTOR IN HOLE 17
High potential area around lower ore zone in hole 20 indicates continuity of this conductor and that in hole 17.

review of the manuscript. The writers wish to thank The New Jersey Zinc Company for permission to publish this paper.

ANALYSIS OF THE DATA

Figure 1 illustrates data from a field case in which current was passed into the lower of two mineralized bodies of low resistivity from an electrode suspended in drill hole 3. As noted, the return electrode was so distant that it had little effect upon the potential distribution in the area to be studied.

The contoured data are shown in the oblique section between holes 5 and 15 and in the

longitudinal section between holes 1 and 13. The axis of elongation of the equipotential contours is in the plane of the bedding in both sections. This is true for each of the cases described.

data of Figure 2. The equipotential surfaces which surround the current source in drill hole 3 are tremendously elongated along the axis joining drill holes 1 and 13 and are flattened along the vertical axis. Of great significance is

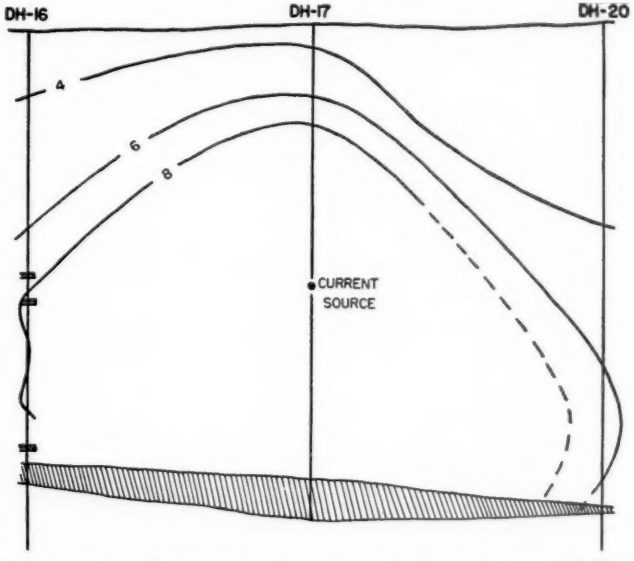

FIGURE 7.—LONGITUDINAL SECTION: CURRENT SOURCE IN HIGH-RESISTIVITY ZONE IN HOLE 17
Minor ellipticity of the equipotential contours in the plane of this section indicates high resistivity between source area and holes 16 and 20.

Figure 2 shows how the two potential distributions would look if the earth were electrically uniform and isotropic. The calculation of Figure 2 was based on a situation in which potentials were referred to a reference station on the surface of the ground directly above the current source and assuming a resistivity for the earth of half a million ohm-centimeters. The geometrical shape of the contours would have been the same regardless of the choice of resistivity, but the magnitudes of the calculated potential gradients are controlled by the resistivity factor. A choice of half a million ohm-centimeters resulted in calculated potential gradients near the current source comparable to those observed in the field. The formula used in making the calculation is a special case of one described in the Appendix.

There is little resemblance between the observed data of Figure 1 and the calculated

the fact that the location of the equipotential maximum in the oblique section is shifted far to the right from its expected position near the projection of the current source upon the section.

The extreme ellipticities of the equipotential surfaces observed here appear to be best explained by a three-dimensional anisotropy in the country rock. The data suggest a situation in which the resistivity along vertical axes is much greater than the resistivity along bedding-plane axes, and further that the resistivity varies with direction in the bedding planes. In the example before us, the resistivity should be a minimum along axes parallel to the longitudinal section containing holes 1, 2, 3, 4, and 13, a maximum along axes normal to the bedding, and should have an intermediate value along bedding-plane axes perpendicular to the directions just described.

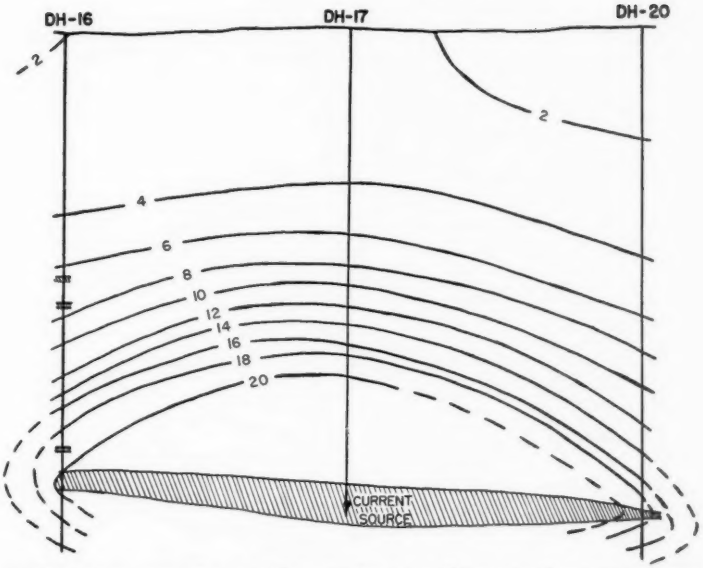

FIGURE 8.—LONGITUDINAL SECTION: CURRENT SOURCE IN EXCELLENT CONDUCTOR IN HOLE 17

Pronounced ellipticity and low-potential gradient indicate electrical continuity between current source and ore zone in holes 16 and 20.

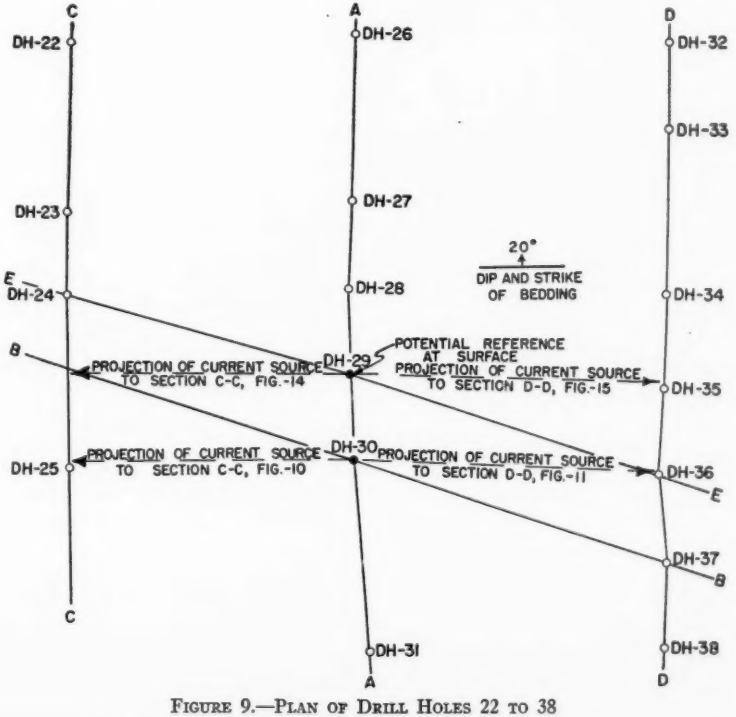

FIGURE 9.—PLAN OF DRILL HOLES 22 TO 38

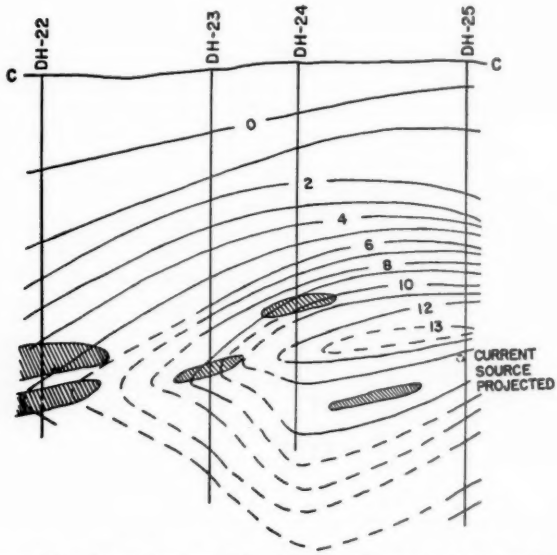

FIGURE 10.—CROSS SECTION C-C: CURRENT SOURCE IN ORE IN HOLE 30

The potential distribution on this section demonstrates that there is no electrical connection between the ore on this section and the ore in which the current source is located in hole 30.

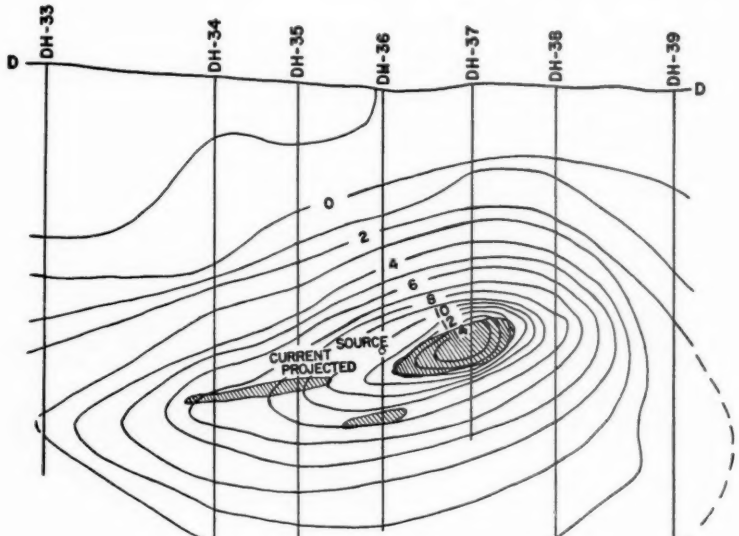

FIGURE 11.—CROSS SECTION D-D: CURRENT SOURCE IN ORE IN HOLE 30

Potential peak in hole 37 indicates electrical continuity between ore in holes 30 and 37.

A large and important conductor has been traced along the axis of minimum bedding-plane resistivity. This conductor penetrates the oblique section in the region of the maximum maximum resistivity along vertical axes of 7 million ohm-centimeters, a minimum resistivity of half a million ohm-centimeters along horizontal axes parallel to section XX, and an

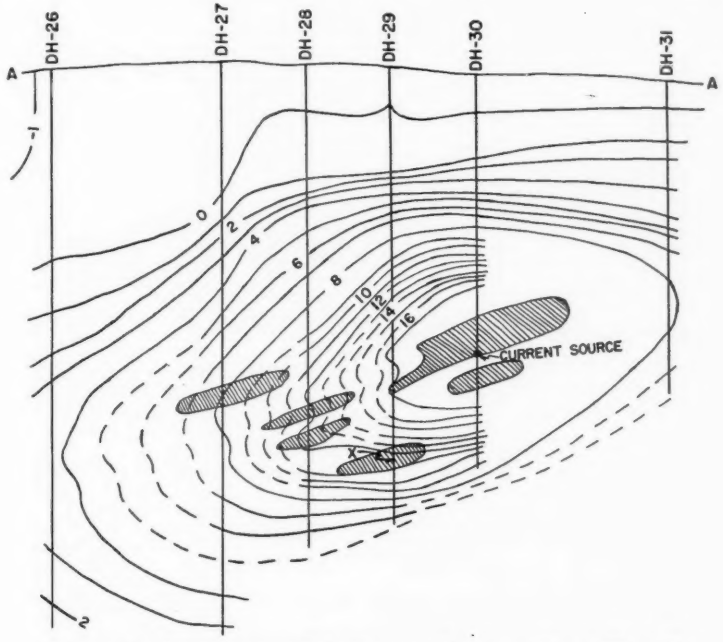

FIGURE 12.—CROSS SECTION A-A: CURRENT SOURCE IN ORE IN HOLE 30

High-potential gradient between hole 29 ore (at X) and current source indicates these two bodies are not electrically connected.

potential. Inspection of these data indicates that drill holes 1 and 2 did not reach the mineralized horizon of drill hole 3. Subsequently holes 1 and 2 were deepened, and both holes found ore at the expected horizon.

It is probable that data from only three drill holes in the area of holes 5 to 10 would have directed attention toward the area containing the mineralized body.

An attempt has been made to fit the field data shown here by calculations based on the assumption of a medium in which the resistivities at all points taken along three perpendicular directions differ. Such a medium is termed triaxially anisotropic. The formula used in these calculations is described in the Appendix.

Figure 3 is a theoretical case illustrating the equipotential surfaces calculated assuming a intermediate resistivity of 2 million ohm centimeters along axes directed at right angles to the above two directions. This combination of resistivities was arrived at after a series of trial calculations. The ratios of the resistivities determine the ellipticities of the equipotential surfaces, and the absolute values of the resistivities fix the magnitudes of the voltages observed.

The calculated data and the field data are in reasonably good agreement, and it is concluded that the resistivities present in the area of this survey are of the same order of magnitude as in the calculated case.

Stratified rock containing interbedded layers of material of relatively good conductivity in many instances possesses biaxial anisotropy whereby the resistivity along axes parallel to

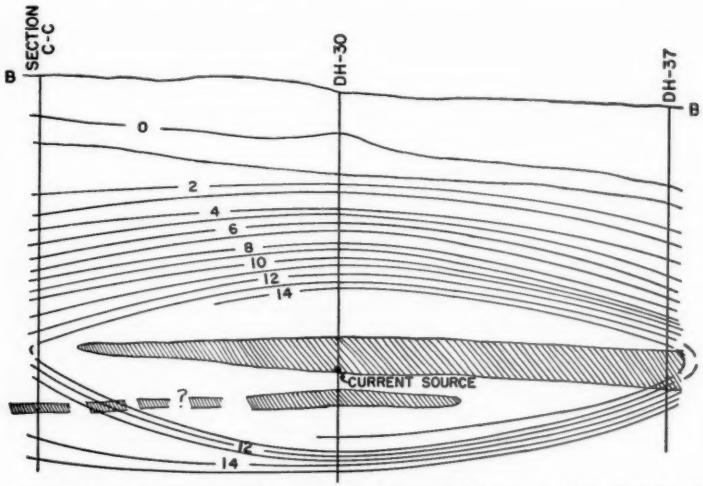

FIGURE 13.—LONGITUDINAL SECTION B-B: CURRENT SOURCE IN ORE IN HOLE 30

Pronounced ellipticity of equipotential contours shows the influence of ore in the plane of this section and its continuity between holes 30 and 37.

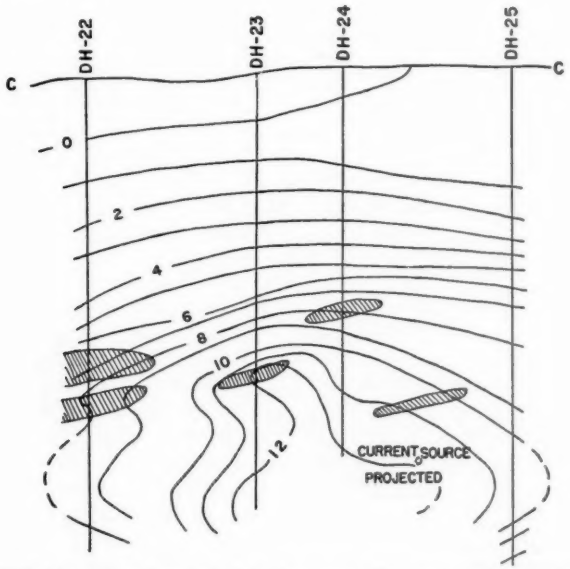

FIGURE 14.—CROSS SECTION C-C: CURRENT SOURCE IN ORE IN HOLE 29

The potential maximum lies between holes 23 and 25 and below the bottom of hole 24. None of the ore found on this section with the possible exception of that in hole 23 is connected electrically with the ore of the current source in hole 29.

the bedding planes is less than the resistivity along axes normal to the bedding. This situation is in conformity with the physical symmetry of a stratified section. The variation of resistivity in the plane of the bedding which we encounter here is of great interest.

Geological evidence indicates that the direction of minimum resistivity coincides with the

long axes of the mineralized bodies. It is believed that, in the absence of mineralization, the barren rock would have been biaxially anisotropic but that the process of mineralization established the direction of minimum resistivity.

supported by the elongated contours in the longitudinal section (Fig. 8) through holes 16, 17, and 20. Continuity at least as far as hole 16 is indicated.

With the current source in the high resistivity

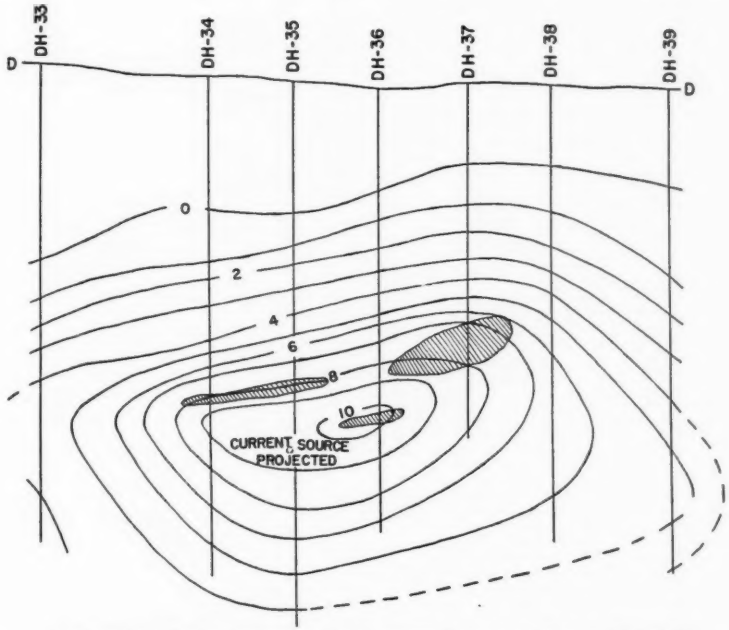

FIGURE 15.—CROSS SECTION D-D: CURRENT SOURCE IN ORE IN HOLE 29

Potential peak in hole 36 shows continuity of hole 29 ore. Larger ore in hole 37 does not have electrical continuity with hole 29 ore.

Figures 4–8 illustrate two field cases utilizing current sources placed at two levels in the same drill hole (No. 17). The locations of the drill holes are shown by Figure 4. These surveys involve the same body of rock; the only difference is in the environment of the point of electrification. Figures 5 and 7 illustrate data associated with the upper source, located in a high-resistivity zone. Figures 6 and 8 apply to data associated with the lower source, located in an excellent conductor.

In the transverse section containing holes 18 to 21 (Fig. 6), it is significant that, with the current source in the low-resistivity zone, the potential maximum focuses over a thin but highly conductive zone in drill hole 20. This suggests that the conductors in drill holes 17 and 20 are connected. This interpretation is zone (Figs. 5, 7), elongation of the contours is much less pronounced, particularly in the longitudinal section (Fig. 7), than was the case for the current electrode in the low-resistivity zone. This suggests that the electrified conductor (mineralized body) greatly influences the potential distribution. The importance of locating the current electrode in the conductor is demonstrated by these figures.

In a case in which drilling had disclosed two adjacent mineralized horizons of low resistivity, it was desired to obtain information on possible strike extension, to discover whether the two mineralized horizons were connected and to deduce any other information relative to their habits of occurrence.

The location map (Fig. 9) illustrates the arrangement of drill holes in the area of interest.

Hole 29 penetrated the lower, and hole 30 the upper mineralized horizon. Accordingly these holes were chosen as sites for the current electrodes.

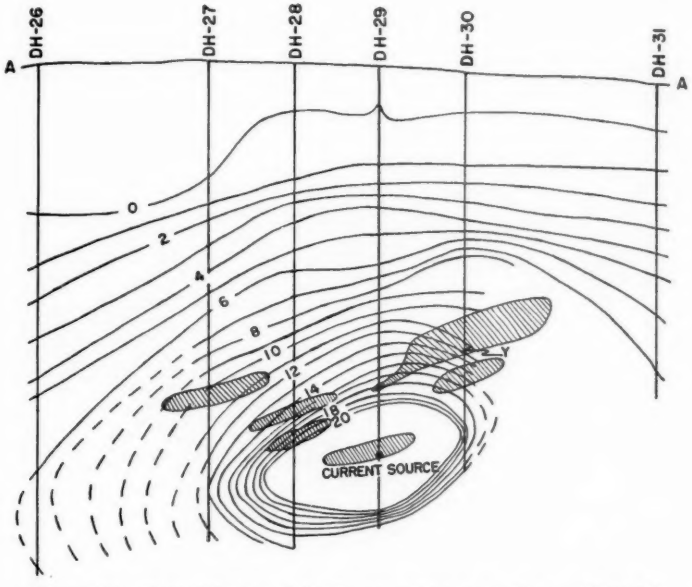

FIGURE 16.—CROSS SECTION A-A: CURRENT SOURCE IN ORE IN HOLE 29

Lack of electrical continuity between holes 29 and 30 ore is shown by intervening zone of high-potential gradient. Similar steep gradients show discrete nature of other ore lenses in holes 27 and 28.

Figure 10 illustrates contoured data obtained in the vertical section containing drill holes 22–25 for a current source in the ore in hole 30. Figure 11 covers the section containing holes 33–39, for the same current source location.

The locations of the equipotential maxima in both sections do not coincide with projections of the source upon the two sections. Instead they are shifted laterally in opposite directions in such a manner as to place them both essentially on a straight line through the current source. This line has the direction B-B (Fig. 9). This is the direction of the maximum elongation of the equipotential surfaces which surround the current source.

Figures 12 and 13 present two other sections surveyed with the same current source in drill hole 30. Figure 12 pertains to the section containing holes 26–31. Figure 13 contains the line B-B to which our attention was already directed.

The bedding-plane elongation is more extreme in section B-B than in the section containing holes 26–31. Section B-B contains the axis of minimum resistivity which is an expression of the long axis of the mineralized body.

In Figure 12, point X in drill hole 29 marks the level at which the lower mineralized horizon occurs. It appears as an area of low potential gradient. Between the hole 29 and hole 30 conductors is a zone of abnormally high potential gradient. This indicates that no close connection exists between the two mineralized zones. This interpretation is important since the geological evidence is ambiguous relative to whether a connection exists between the conductors in the two drill holes.

Figures 14 and 15 cover data obtained in the two transverse sections containing holes 22–25 and 33–39, with the current source in the deeper conductor in drill hole 29.

In Figure 14, the potential maximum lies

between drill holes 23 and 25 and is probably close to but below the bottom of hole 24. In Figure 15, the potential peak falls near hole 36. Again the two areas of potential maxima region of low potential gradient. The data support the earlier conclusion that the conductors in holes 29 and 30 are not related in this section.

The potential gradient in the plane of the

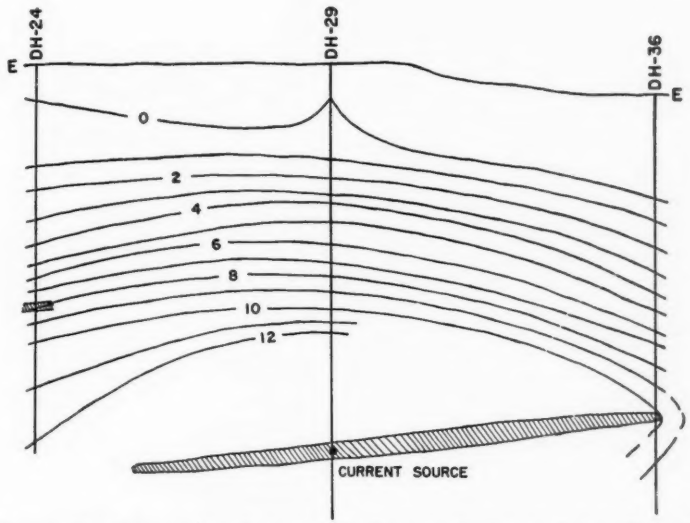

FIGURE 17.—LONGITUDINAL SECTION E-E: CURRENT SOURCE IN ORE IN HOLE 29

Probable continuity of hole 29 ore with that in hole 36 is illustrated by long axis of equipotential ellipse and location of potential peak about the ore in hole 36.

shown on these figures are very nearly on a straight line containing the current source. Axis E-E (Fig. 9) defines the horizontal component of this line. It parallels line B-B, indicating that the direction of minimum resistivity coincides in the two cases. The data of Figure 14 indicate that hole 24 stops short of the ore horizon.

Figures 16 and 17 cover data obtained in the sections containing holes 26–31 and 24, 29, and 36; the current source still being located in drill hole 29.

The tendency for the equipotential contours to be stretched out along the bedding is again in evidence as is the fact that the resistivity varies with direction in the bedding. The situation is like that of the data associated with the source in drill hole 30. The data of Figure 17 again indicate that hole 24 stops short of the ore horizon.

In Figure 16, Y marks the location of the ore in hole 30. The conducting zone appears as a bedding from hole 29 in the up-dip direction is steeper than in the down-dip direction (Fig. 16). This fact indicates that the mineralization of this horizon is more pronounced down-dip than it is up-dip.

Finally, let us compare Figures 13 and 17. The elongation of the equipotential contours while extreme in both cases is outstanding in the case of the source in the drill hole 30 conductor (Fig. 13). This suggests that the mineralization associated with the drill hole 30 conductor may be more important in its longitudinal development than the mineralization with which the hole 29 conductor is associated.

APPENDIX

The formula used to calculate the potential distribution about an isolated source embedded below the surface of an anisotropic medium in which the bedding is horizontal is as follows:

$$\frac{\phi}{I} = \frac{\sqrt{\rho_x \rho_y \rho_z}}{4\pi} \left[\frac{1}{\sqrt{\rho_x x^2 + \rho_y y^2 + \rho_z (Z - d)^2}} + \frac{1}{\sqrt{\rho_x x^2 + \rho_y y^2 + \rho_z (z + d)^2}} \right]$$

where d is the depth of the source

x and y are the horizontal co-ordinates, and z the depth co-ordinate of the point at which the potential is calculated. The origin of the co-ordinate system is the surface point above the source.

ρ_z is the resistivity along the vertical axis.

ρ_x, ρ_y are resistivities along the horizontal axes of minimum and maximum bedding plane resistivity.

I is the current flowing from the source in amperes.

ϕ is the potential at the point x, y, z, in volts referred to an infinitely distant potential reference.

When the distances used in the calculations are in feet, resistivities must be expressed in ohm-feet. When distances are in centimeters, resistivities must be expressed in ohm-centimeters.

The potential is made up of contributions from a real source located at o, o, d, and of an image source located at o, o, $-d$. The image source takes care of the effect of the air-earth boundary on the current flow.

When the resistivities are equal, the formula reduces to the case of an isolated current source embedded in an isotropic medium.

References Cited

Brown, W. H., 1935, Quantitative study of ore zoning, Austinville Mine, Wythe County, Virginia: Econ. Geology, v. 30 p. 425–433

Currier, L. W., 1935, zinc and lead region of Southwestern Virginia: Va. Geol. Survey Bull. 43, 122 p.

New Jersey Zinc Co., Palmerton, Pa.; New Jersey Zinc Co., Jefferson, Tenn.

Manuscript Received by the Secretary of the Society, February, 21, 1955

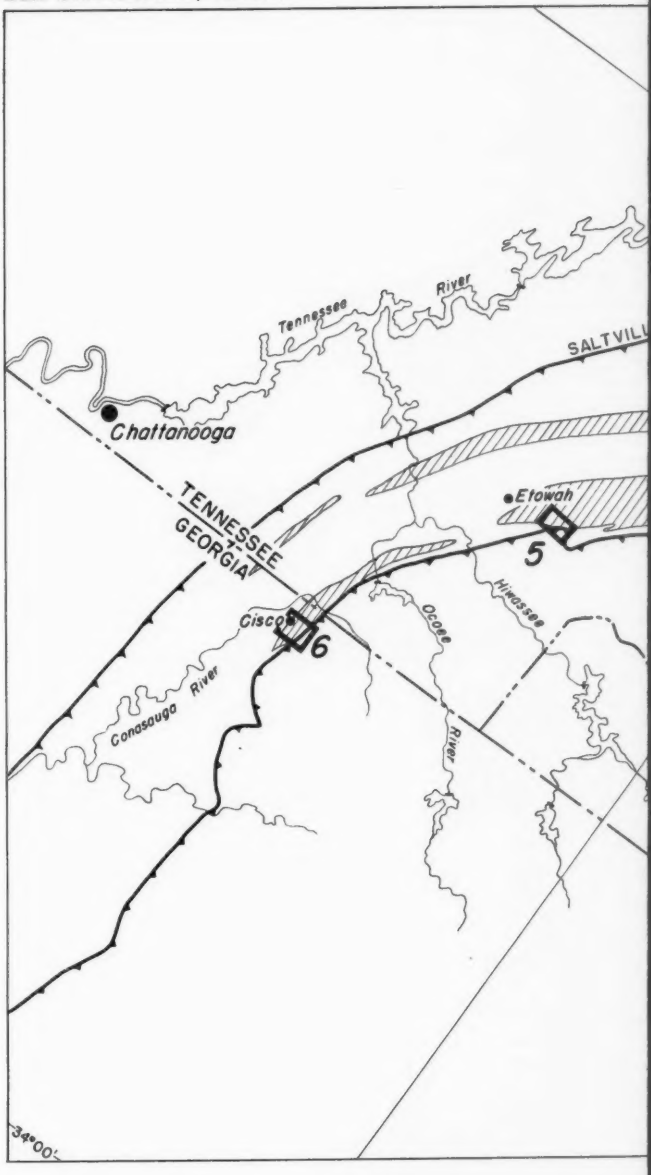

EXPLAN

– Outcrop area of coarse conglomerates.

– Outcrop area of Blount sedimentary rocks on the Pulaski and Saltville thrust sheets.

– Major overthrust faults.

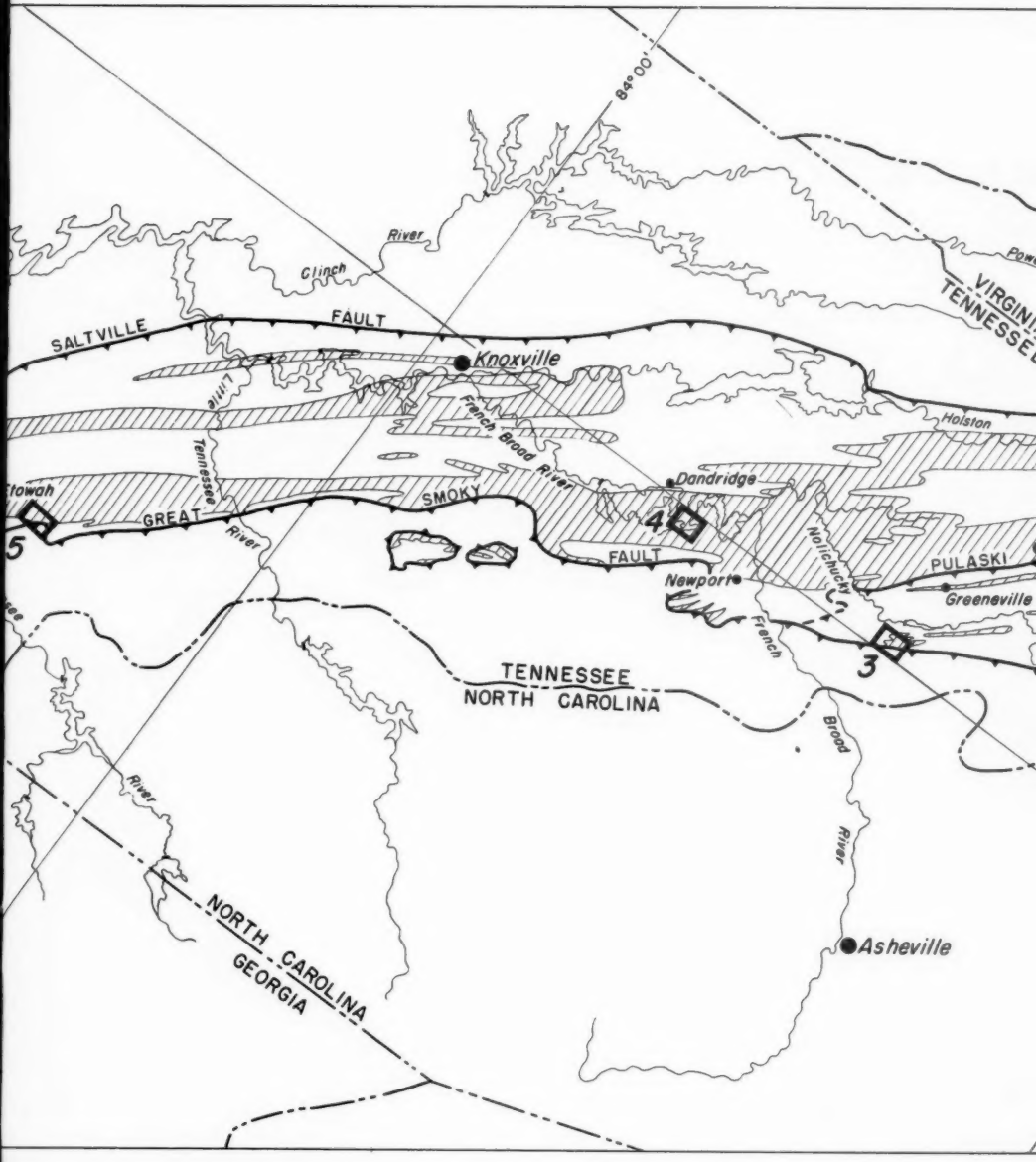

EXPLANATION

NOTE:
Geology adapted from Virginia Geological Survey Bulletin 42, Tennessee Division of Geology Bulletin 58, and Georgia Geological Survey Bulletin 54.

COARSE CONGLOMER
IN THE SOUT

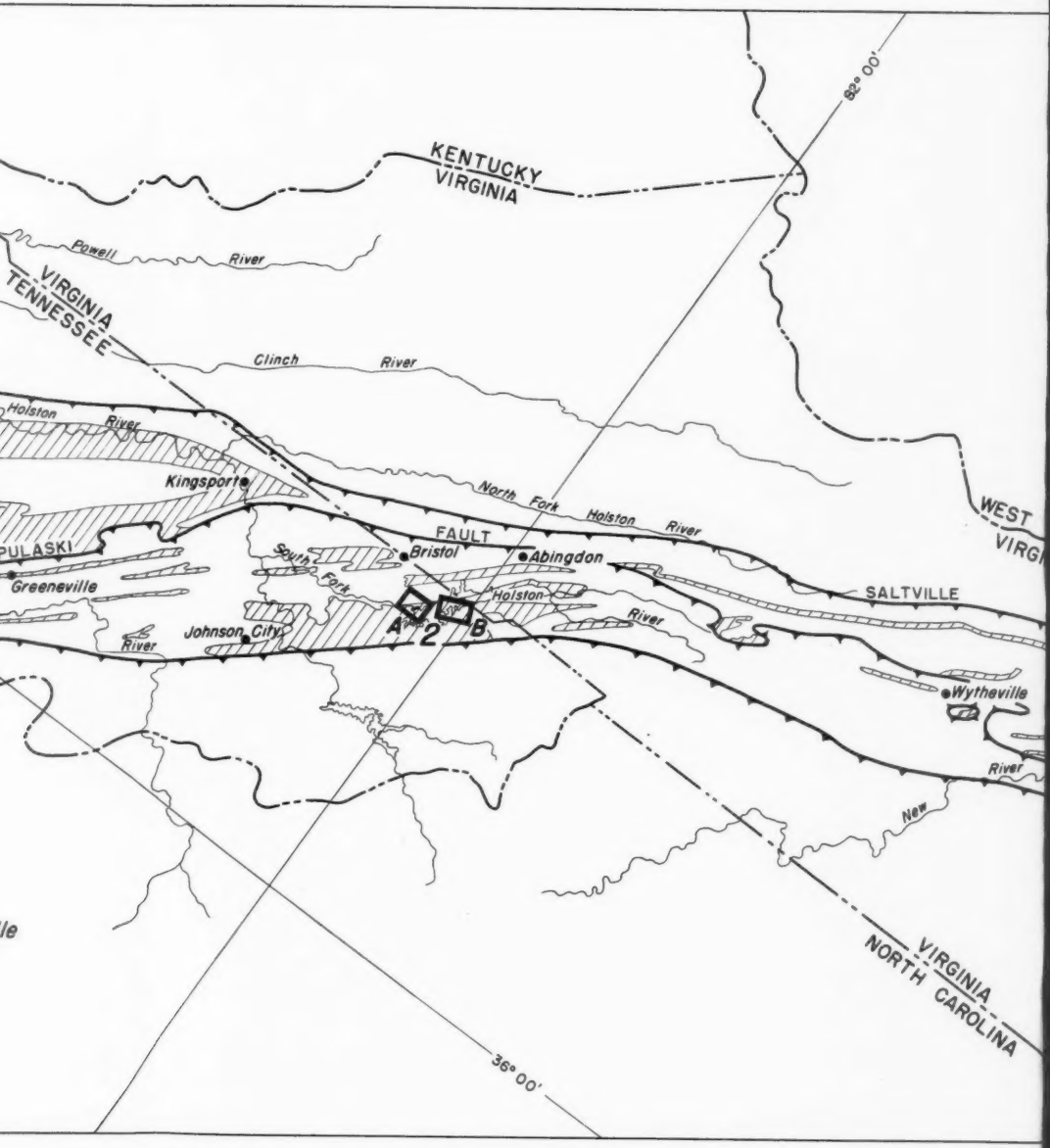

SCALE

0 10 20 30 40 50 MILES

LOMERATES OF THE MIDDLE ORDOVICIAN
SOUTHERN APPALACHIAN VALLEY

1 - Fin

2 - Sou
A-
B-

3 - Gre

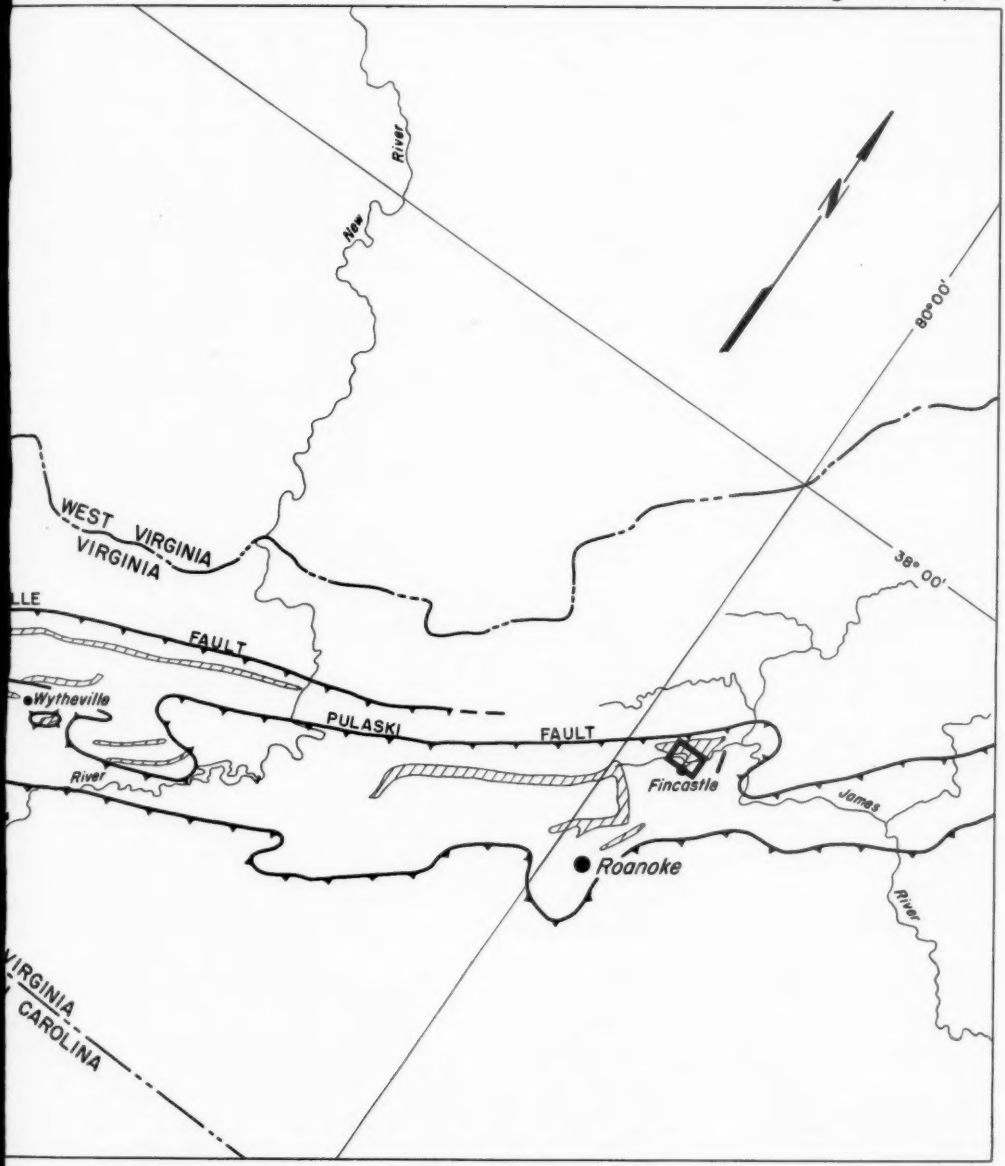

LOCATION

1 - Fincastle, Virginia Area.

2 - South Holston, Tennessee Area.
A - South Holston Dam.
B - South Holston Reservoir

3 - Greeneville, Tennessee Area.

4 - Douglas Reservoir, Tennessee Area.

5 - Etowah, Tennessee Area.

6 - Cisco, Georgia Area.

BULLETIN OF THE GEOLOGICAL SOCIETY OF AMERICA
VOL. 67, PP. 697-716, 8 FIGS., 3 PLS. JUNE 1956

COARSE CONGLOMERATES OF THE MIDDLE ORDOVICIAN IN THE SOUTHERN APPALACHIAN VALLEY

BY JOHN M. KELLBERG AND LELAND F. GRANT

ABSTRACT

Middle Ordovician conglomerates at about the same stratigraphic position have been studied in six areas along the southeastern margin of the Valley and Ridge Province for 325 miles from Fincastle, Virginia, through eastern Tennessee to northern Georgia.

Pebbles and cobbles in the conglomerates are mainly limestone derived from the Upper Cambrian and Lower Ordovician, but many are quartzite, sandstone, or siltstone from the Middle and Lower Cambrian.

Studies of the rounding of pebbles and cobbles and the distribution of the coarser beds show that the source area lay to the southeast. These conglomerates are interpreted as deposits laid down in a subsiding trough near discharge points of major streams draining recently uplifted highlands to the southeast. The conglomerates record early pulsations of the orogenic disturbance which affected the southern Appalachians from Chazy to early Trenton time.

CONTENTS

TEXT

	Page
Introduction	697
Acknowledgments	698
Scope of work	698
Previous work	698
General geologic relationships	698
Description of known deposits	698
Fincastle area	698
South Holston area	700
Greeneville area	705
Douglas Reservoir area	707
Etowah area	710
Cisco area	712
Other possible localities	714
Common characteristics of deposits	714
Conclusions	715
References cited	716

ILLUSTRATIONS

Figure	Page
1. Geologic map and section, Fincastle	699
2. Geologic map and section, South Holston Dam	701
3. Isometric section, aggregate quarry, South Holston Dam	703
4. Geologic map and sections, South Holston Reservoir	703
5. Geologic map and section, Greeneville	706
6. Geologic map and section, Douglas Reservoir	707
7. Geologic map and sections, Etowah	711
8. Geologic map and section, Cisco	713

Plate	Facing page
1. Location map of Middle Ordovician conglomerate deposits in the southern Appalachian Valley	697
2. Conglomerates, Fincastle, South Holston, and Greeneville areas	708
3. Conglomerates, Douglas Reservoir, Etowah, and Cisco areas	709

INTRODUCTION

The wedgelike Middle Ordovician clastic rocks in the southern Appalachian Valley were named the Blount group (Ulrich, 1911, Pl. 27). They are thickest along an axis between Knoxville and Bristol, Tennessee, and thin northeastward and southwestward along the strike and northwestward across the dip as they grade laterally into limestone of equivalent age. Overriding thrust sheets of the Blue Ridge Front hide the southeastward extension. This paper describes conglomerates in these clastic rocks from Fincastle, Virginia, to Cisco, Georgia (Pl. 1). Some of these deposits have been mentioned or described previously as isolated occurrences (Safford, 1869; Campbell, 1899; Keith, 1905; Stow and

Bierer, 1937; Butts, 1940, p. 159, 164; Butts and Gildersleeve, 1948, p. 29; Decker, 1952, p. 60–64), but recognition of their interrelated significance should aid in interpreting the origin of this wedge.

Acknowledgments

Information in this paper was collected by the writers as members of the geologic staff of the Tennessee Valley Authority and is published with the approval of the Authority. The writers are especially indebted to Mr. Berlen C. Moneymaker, Chief Geologist of the Tennessee Valley Authority, for the guidance, encouragement, and criticisms that he offered while the work was in progress. For many helpful suggestions and criticisms while reviewing this paper the authors wish to thank Messrs. Benjamin Gildersleeve, Warren B. Hamilton, Philip B. King, Robert A. Laurence, Robert B. Neuman, and John Rodgers. To their colleagues in the Geologic Branch of the Tennessee Valley Authority and to other geologists in the area with whom this problem was discussed the writers are grateful for their viewpoints and for their criticisms of the ideas presented. The fossils from the Douglas Reservoir and Etowah localities were identified by Messrs. G. Arthur Cooper and Robert B. Neuman.

Scope of Work

The writers first saw these Middle Ordovician conglomerates while doing geologic work on the South Holston Dam, 7 miles southeast of Bristol, Tennessee. Geologic investigations disclosed conglomerate lenses interbedded with Middle Ordovician shales and sandstones. Field examinations from Virginia to Georgia revealed six areas in the southern Appalachian Valley where conglomerate lenses occur in Middle Ordovician rocks. Presumably not all such deposits in the region have been discovered, for this would require detailed mapping of a belt 350 miles long and 20–30 miles wide; however, those found shed light on Middle Ordovician orogenic disturbances in the southern Appalachians.

Previous Work

Keith, Hayes, and Campbell did much of the original geologic mapping of the southern Appalachian Valley. Butts (1933; 1940) mapped in more detail the portion of the valley in Virginia. Data available on the Tennessee portion to 1950 were published as the Geologic Map of East Tennessee (Rodgers, 1953). Butts and Gildersleeve (1948) described the area underlain by Paleozoic rocks in northwest Georgia.

General Geologic Relationships

In this paper the southern Appalachian Valley is that portion of the Valley and Ridge Province southwest of the James River. The geologic structure is characterized by numerous southeastward-dipping, low-angle thrust faults, which define relatively narrow, linear belts of outcrop trending northeast. In some places facies changes, especially in the Ordovician rocks, from one fault sheet to the next make correlation difficult.

The clastic sediments of early Middle Ordovician age are confined to the southeasternmost thrust sheets of the Valley and Ridge Province. In three of the six areas studied, the conglomerates crop out within a mile of the thrust marking the northwestern boundary of the Blue Ridge Front.

Keith (1895) gave the name Tellico sandstone to the calcareous sandstones and shales overlying the Athens shale in the belt of outcrops southeast of Knoxville in Blount and Sevier counties, Tennessee. Butts (1940, p. 170) states that the Tellico is absent in Virginia but recognizes the thick sequence of interbedded sandstones and shales which he places in the top of the Athens at the stratigraphic position Keith defined as the Tellico. Rodgers (1953) distributes these coarser clastics among three map units—Athens, Holston, and Sevier. While recognizing the lack of agreement in the correlation of the Tellico formation (Twenhofel, 1954, p. 285, Figs. 1, 2), the authors believe that in the belts of outcrop where the conglomerates occur the name is justified for the conglomerate, sandstone, and shale overlying the Athens.

Description of Known Deposits

Fincastle Area

LOCATION AND GEOLOGIC SETTING: Probably the best-known conglomerate occurrences

are in road cuts along U. S. Highway 220, 1.5 miles north of Fincastle, Botetourt County, Virginia (Fig. 1). This locality was described by Stow and Bierer (1937, p. 71), by Butts (1940, p. 159), and by Decker (1952, p. 60–64). Here the Athens and Tellico exposures in a synclinal basin extend 9 miles along the strike and are 3½ miles in maximum width. The major portion of this outcrop belt is the Athens shale, and a small area on the southern border is underlain by Tellico. These deposits lie on a northeast salient of the Pulaski thrust sheet (Pl. 1).

Immediately south of this locality the Tellico and Athens are overridden by a minor thrust sheet of Chepultepec and Beekmantown limestone and dolomite (Fig. 1). The major overthrust marking the northwest front of the Blue Ridge lies 11 miles southeast of Fincastle.

DESCRIPTION OF OCCURRENCE: Beds of conglomerate crop out along the east side of the road 1–1½ miles north of Fincastle (Fig. 1). A 2300-foot exposure of Tellico extends from the thrust fault on the southeast to the flood plain of Catawba Creek on the northwest. The following section from southeast to northwest was measured in 1950:

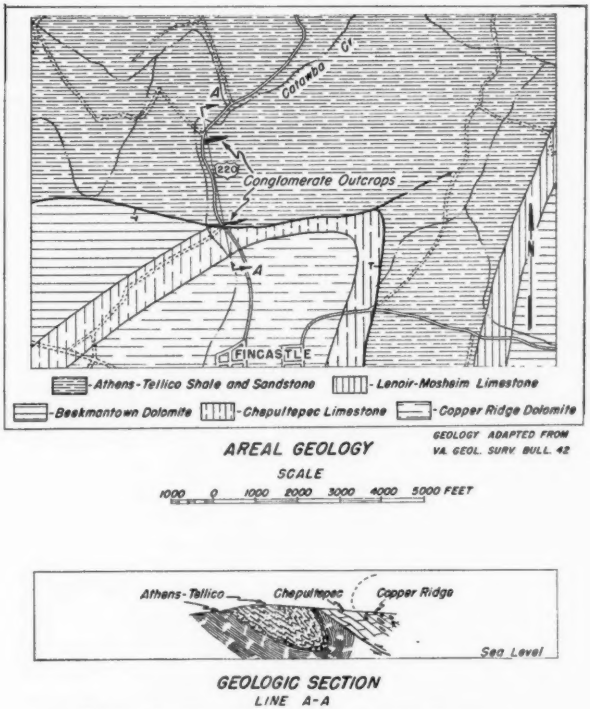

FIGURE 1.—GEOLOGIC MAP AND SECTION, FINCASTLE

Description of unit	Outcrop width feet
Chepultepec in hanging wall of fault	
Contorted shale with thin sandstone beds	50
Coarse conglomerate with sandy matrix, dip 65° SE.	25
Gradational zone with a preponderance of sandstone on southeast grading to mostly shale on northwest	225
Mostly concealed, but some exposures show indications of complex structures	1150
Shale—folded and contorted	150
Shale—containing a few small folds, average dip 60° SE.	560
Gradational zone, grading from predominantly shale on southeast to sandstone on northwest	75
Sandstone with shaly partings	5
Coarse conglomerate with sandy matrix	2
Massive sandstone	15

Description of unit	Outcrop width feet
Interbedded coarse conglomerate and sandstone; some conglomerate with a sandy matrix and some with a shaly matrix, dip 45° SE.	55
Total	2312

Although more than half the section is concealed and correlation of individual beds between the limbs of the fold is impossible, the structure is believed to be an overturned syncline whose axial plane dips southeast. This interpretation is indicated by the two gradational zones which show a general decrease in grain size toward the center of the structure and by the fact that in the regional geologic structure of the southern Appalachians overturned synclines commonly develop in the footwall of thrust faults.

Except for the exposures along U. S. Route 220 outcrops are meager in this belt. In the hills northeast of the highway bedrock is mantled by residuum, and no outcrops of conglomerate were seen. In the section exposed along the county road 5000 feet east there is no indication of conglomerate beds. Limited areal extent is characteristic of these deposits.

LITHOLOGIC ANALYSIS: Fourteen samples obtained for lithologic analysis included specimens of the coarse conglomerate, average pebble size larger than 1 inch, and the fine conglomerate, average pebble size from half to a quarter of an inch. The coarser phase makes up the bulk of the conglomerate; the finer-grained conglomerates occur as small lenses usually near the top or the bottom of the coarser beds (Pl. 2, fig. 1).

The same rock types are in both the coarse and the fine conglomerates; but the percentages differ as indicated by analyses based on a count of 2127 individual pebbles and cobbles:

Coarse Conglomerate Rock type	Per cent	Fine conglomerate Rock type	Per cent
Limestone	38.6	Limestone	9.0
Quartzite	29.0	Quartzite	9.0
Vein quartz	22.1	Vein quartz	62.7
Sandstone	4.1	Sandstone	1.2
Chert	3.7	Chert	16.9
Siltstone	1.6	Siltstone	1.2
Other	0.9	Other	0.0
Total	100.0	Total	100.0

"Other" includes rock types present in small amounts, such as greenstone and calcite.

It is possible to identify certain formations that contributed some of the pebbles and cobbles in the conglomerate. Among the limestone pebbles are fragments of fine-grained limestone conglomerate typical of those in the Elbrook formation (Middle Cambrian); pebbles of sandy limestone and of limestone with siliceous laminae typical of the Conococheague formation (Upper Cambrian); pebbles of dark gray-blue, finely crystalline limestone typical of the Chepultepec formation (Lower Ordovician); and pebbles of aphanitic, gray limestone typical of the Beekmantown formation. No limestone pebbles could be assigned to the Shady formation (Lower Cambrian) or the Rome formation (Lower Cambrian), although these formations probably are represented. Most quartzite pebbles are dark-green, arkosic, conglomeratic types common in the basal Cambrian Unicoi formation, although a few pebbles are grayish-white, clean quartzite typical of the Erwin formation (Lower Cambrian). Two distinct types of vein quartz are present in approximately equal amounts: (1) clear to milky quartz devoid of inclusions, and (2) milky quartz containing many inclusions of chlorite and limonite pseudomorphs after pyrite. The vein quartz could have been derived either from erosion of conglomerates in the Unicoi or possibly from the basement complex southeast of the Blue Ridge Front. Most of the sandstone pebbles are reddish brown and fine-grained, similar to those in the Rome formation from which they probably were derived. The majority of the chert is dense and black, typical of chert nodules in the Lenoir limestone. The limited amount of dark-green, dense, jasperoid chert is probably derived from the Shady formation. The brown siltstones probably originated from the Rome or the Hampton formation (Lower Cambrian). The greenstones could represent either the amygdaloidal basalt flows in the Unicoi or the greenstones, such as the Catoctin, farther east.

South Holston Area

LOCATION AND GEOLOGIC SETTING: Middle Ordovician clastic rocks are thickest in a belt

extending for 40 miles from Johnson City, Tennessee, to northeast of Abingdon, Virginia. South Holston Dam and Reservoir lie in the central section of this belt.

estimated to be as thick as 10,000 feet in this vicinity (Butts, 1940, p. 165), but the writers believe this is high. As no complete section is exposed an accurate measurement of the

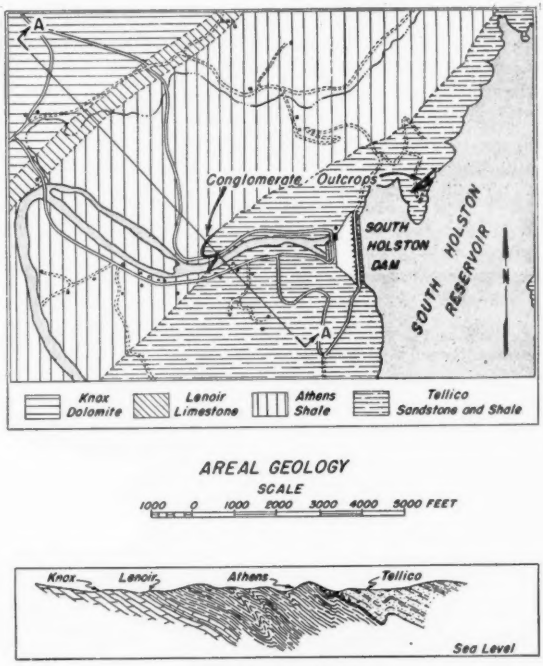

FIGURE 2.—GEOLOGIC MAP AND SECTION, SOUTH HOLSTON DAM

The Athens shale and Tellico formation crop out in the South Holston area in three belts striking northeast occupying the troughs of one broad syncline on the southeast and two narrower synclines to the northwest. The southeast limb of the largest syncline is truncated by the Holston Mountain fault along which the Unicoi quartzite is thrust over sandstones and shales of the Tellico and Athens.

Coarse conglomerates occur only in the southeasternmost outcrop belt of the Tellico formation. In the two synclines to the northwest the Tellico consists of interbedded shale and sandstone. The conglomerates are not confined to one stratigraphic position but are distributed at intervals throughout the exposed thickness of the Tellico formation.

The combined Athens and Tellico have been

thickness is impossible; however, considering the repetition by folding and faulting and the lenticular character of the beds, a thickness of not less than 5000 feet nor more than 8000 feet seems probable.

The lithology of the Tellico changes within short distances both laterally and vertically. Along the axis of South Holston Dam a continuous section 1700 feet in length, based on cores and exposures, showed lithologic variations which made difficult the detailed correlation of cores recovered from holes spaced on 12-foot centers. A gray, medium-grained, calcareous sandstone and a black, fissile, arenaceous shale account for approximately 85 per cent of the formation. The remaining 15 per cent consists of argillaceous shale, shaly sandstone, and conglomerate.

DESCRIPTION OF OCCURRENCES: Because the

Tellico is thicker in this area and because the writers have done more detailed work here, more specific information on coarse conglomerates is available from the South Holston area than from any other.

During the construction of the dam an aggregate quarry was opened in the hillside on the right bank of the river half a mile downstream from the dam (Fig. 3). The structure in the southeast flank of the hill is a warped and plunging syncline containing the basal beds of the Tellico underlain by the Athens shale. At the southwest end of the quarry a lens of coarse conglomerate 30 feet thick is the basal member of the Tellico. This lens gradually thins northeastward and is absent at the end of the quarry, 300 yards to the northeast where a 10-foot bed of medium-grained sandstone lies directly on the Athens. The only indication that this sandstone is equivalent to the conglomerate is some included widely scattered quartzite cobbles up to a foot across.

A section showing the interfingering of the sandstone and conglomerate was measured in core from exploratory holes drilled normal to the dip near the center of the quarry.

Description of unit	Thickness in feet
Medium-grained sandstone with shaly partings	29.6
Conglomerate, maximum pebble size 1 inch	0.4
Medium-grained sandstone with shaly partings	83.6
Conglomerate, maximum pebble size 1 inch	3.4
Medium-grained sandstone with shaly partings	1.9
Conglomerate, maximum pebble size 1 inch	1.9
Medium-grained sandstone with shaly partings	12.4
Conglomerate, maximum pebble size 2 inch	3.2
Conglomerate, maximum pebble size 8 inch	13.1
Athens shale; black, calcareous, pyritiferous	

Most of the rock fill for South Holston Dam was obtained from a quarry about 900 feet upstream from the dam on the right bank of the river (Fig. 2). A continuous section was measured from the Athens-Tellico contact 2000 feet northwest of the quarry to the highest beds exposed in the quarrying operations. Here the lower 100 feet of Tellico consists of thick-bedded sandstone devoid of conglomerate lenses. Succeeding this is 860 feet of interbedded shaly sandstone and sandy shale. Finally there is 340 feet of sandstone containing conglomerate lenses and a few thin shale beds.

Detailed measurements from exploratory drill holes and observations of the strata exposed in the quarry faces shows the following sequence:

Description of unit	Thickness in feet
Sandy shale—highest beds exposed	13
Fine-grained sandstone with a few shaly partings	34
Sandy shale	14
Medium-grained sandstone with a few shaly partings	13
Coarse conglomerate with shaly matrix	7
Medium-grained sandstone with a few shaly partings	31
Sandy shale	3
Medium-grained sandstone	5
Coarse conglomerate with shaly matrix	3
Medium-grained sandstone	4
Sandy shale	9
Fine-grained sandstone with shaly partings	17
Sandy shale	12
Fine-grained sandstone with a few shaly partings	24
Sandy shale	8
Medium- to fine-grained sandstone	54
Coarse conglomerate with shaly matrix	12
Medium-grained sandstone	31
Sandy shale	11
Fine-grained sandstone with shaly partings	35
Total	340

Prior to quarrying the conglomerate beds were continuous throughout the quarry, cropping out on both limbs and around the nose of a syncline. Examination of these zones where their projection along the strike intersects the axis of the dam showed medium- to coarse-grained sandstones, not conglomerates.

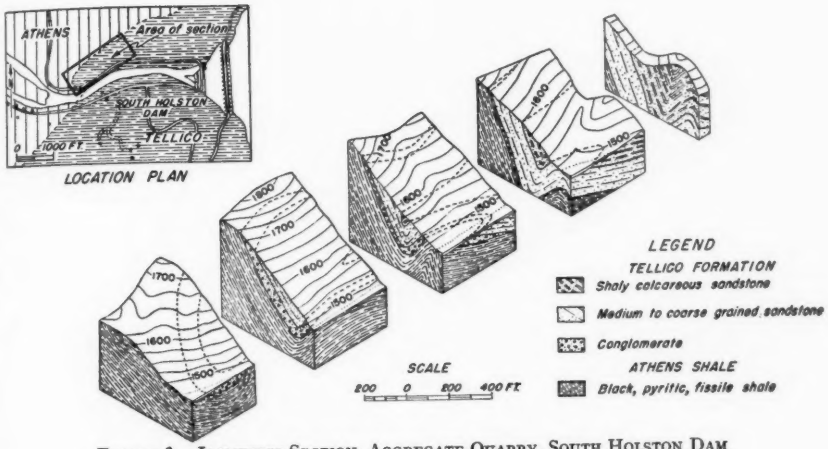

FIGURE 3.—ISOMETRIC SECTION, AGGREGATE QUARRY, SOUTH HOLSTON DAM

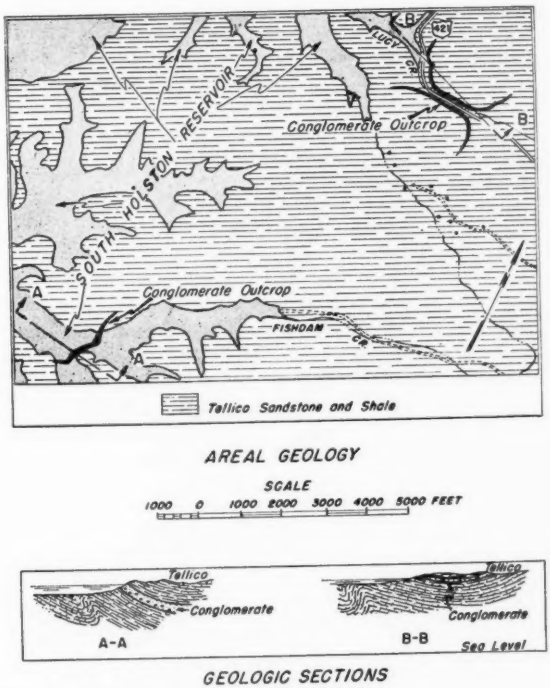

FIGURE 4.—GEOLOGIC MAP AND SECTIONS, SOUTH HOLSTON RESERVOIR

Several beds of coarse conglomerate are exposed in a small road-metal quarry on Sulphur Spring Branch of Fishdam Creek 3 miles east of South Holston Dam and in cuts along an old road 100 yards to the northeast (Fig. 4). These exposures are submerged by South Holston Lake except when the water level is below elevation 1640, a drawdown of 90 feet from normal full pool.

At this locality a zone of sandstone and conglomerate 500 feet wide strikes N. 40° E. and dips 30° SE. These strata are overlain and underlain by sandy shales and shaly sandstones. Because of complex geologic structure the exact stratigraphic position of this zone relative to the top of the Athens shale is not known; however, from all indications it is several thousand feet stratigraphically above the top of the Athens.

In the road-metal quarry features of the 70-foot exposure indicate preconsolidation slump, rapid change of grain size, and thickening and thinning of individual beds. A section was measured across the quarry face.

Description of unit	Thickness in feet
Thin-bedded, fine-grained sandstone with shaly partings showing preconsolidation slump and contortion and containing discontinuous beds of medium-grained sandstone	14
Thick-bedded, medium- to coarse-grained sandstone containing a few small lenses of fine-grained conglomerate near base	7
Coarse conglomerate in a medium-grained sandy matrix having a random sorting of pebbles ranging in size from 12 inches to one-fourth of an inch	10
Thick-bedded, medium- to coarse-grained sandstone containing a few thin lenses of fine-grained conglomerate near top	7½
Thin-bedded, fine-grained sandstone with shaly partings	3
Thick-bedded, medium- to coarse-grained sandstone	6½
Medium-bedded, fine-grained sandstone	3
Dark gray, sandy shale	2½
Thin-bedded, fine-grained sandstone with shaly partings	9
Coarse conglomerate in medium-grained sandy matrix, pebble size ranging from 6 to ¼ inch	4½
Medium-bedded, fine-grained sandstone	3
Total	70

These beds can be traced northeast along the strike to a conglomerate exposure in cuts along an abandoned road. This exposure contains the largest fragment found in the conglomerates, a conglomeratic quartzite boulder 18 inches in maximum dimension. Farther northeast the conglomerates pinch out on a slope on the right bank of Fishdam Creek.

Geologic investigations coincident with the relocation of portions of U. S. Highway 421 disclosed one subsurface and one surface occurrence of coarse conglomerates.

Exploratory drilling at the main river pier of the highway bridge crossing the reservoir disclosed a bed of coarse conglomerate 7 feet thick striking N. 40° E. and dipping 55° SE. This conglomerate contains the usual assemblage of pebbles up to 6 inches in maximum dimension embedded in a medium- to coarse-grained sandstone matrix. Exposures in the highway cuts and information from the exploratory drilling permitted measurement of a continuous section from the top of the Athens shale to this bed. The conglomerate is 1500 feet above the Athens-Tellico contact.

Along the valley of Lucy Creek, 2¼ miles southeast of the reservoir crossing, traces of coarse conglomerates crop out in cuts along the roadside. A 10-foot sandstone bed in a shallow syncline apparently is an extension of the zone exposed at the Fishdam Creek locality (Fig. 4). This bed contains scattered small rock fragments and well-rounded limestone and quartzite cobbles and shows contorted laminae and lenses indicative of preconsolidation slumping. From all indications this deposit represents the marginal fringe of a larger conglomerate deposit now hidden or removed.

Conglomerates are exposed in cuts along the relocated Virginia State Highway 672 half a mile southeast of Avens Bridge. On the southwest side of the highway seven beds of medium- to fine-grained conglomerate are interbedded with sandstones and shales. The extremely coarse conglomerates characteristic of other exposures in the South Holston area are absent. Nearly all pebbles at this locality are smaller than 2 inches in maximum dimension. From exploratory drilling at the Avens

Bridge site and from the road cuts it has been determined that the Athens shale is 2300 feet thick and that the conglomerates occur 700 feet above the Athens-Tellico contact.

It is likely that removal of residual cover by scouring action along the shore line will uncover other conglomerate outcrops.

LITHOLOGIC ANALYSIS: Where unweathered the conglomerate matrix is gray-green slightly calcareous sandstone or gray-green calcareous shale. Usually the unweathered quartzite and limestone pebbles are nearly the same color, and it is difficult to differentiate between pebbles and matrix in a fresh specimen. Slightly weathered the matrix is brownish, limestone pebbles have a gray patina, and the green quartzites are unchanged. Thus in slightly weathered rock the contrast between the matrix and the enclosed pebbles is marked (Pl. 2, figs. 2, 3). In advanced stages of weathering the quartzite pebbles protrude from the matrix, and the dissolved limestone pebbles are represented by voids.

Fifteen representative samples of conglomerate from the South Holston area were selected for lithologic analysis. The specimens show poor sorting. Most of the samples were the coarser conglomerates, average pebble size exceeding 1 inch, for the finer-grained phase makes up only a small portion. Percentages of rock types represented in the 1924 pebbles counted are:

Rock type	Per cent
Limestone	80.9
Quartzite	10.2
Sandstone	1.1
Siltstone	3.2
Vein quartz	2.6
Chert	1.9
Other	0.1
Total	100.0

The majority of the quartzite pebbles are medium-grained, dark green, and somewhat feldspathic, typical of the lower members of the Unicoi formation. Other quartzites are fine- to medium-grained, white to light gray, and well sorted, typical of the Erwin formation. Fine-grained red and green sandstones identical to those in the Rome formation occur sparsely throughout the samples as do brown siltstones apparently derived from either the Rome or the Nolichucky. The greatest variation is in the types of limestone pebbles, which include intraformational conglomerate pebbles from the Honaker; sandy, medium-grained limestones typical of the Conococheague; fine-grained to aphanitic limestones from the upper Knox; and fine-grained, argillaceous, and fossiliferous limestones from the Lenoir. Many limestone pebbles, however, have no characteristic which identifies them with a formation. Black aphanitic chert typical of the Lenoir and red and green jasperoid cherts probably from the Shady are prominent. The vein quartz is dominantly milky white without megascopic inclusions, but a few pieces of relatively clear vein quartz occur. Among the minor constituents making up about 0.1 per cent of the pebbles are greenstones probably derived from the amygdaloidal lavas in the Unicoi formation and rhyolites from the Mt. Rogers volcanic group.

Greeneville Area

LOCATION AND GEOLOGIC SETTING: Coarse conglomerates occur in the Tellico formation 45 miles southwest of South Holston Dam and 8½ miles south of Greeneville, Tennessee (Pl. 1). They are best exposed 8000 feet south of the junction of Tennessee highways 70 and 107 (Fig. 5).

In this vicinity the Athens shale and Tellico formation crop out in a distorted syncline. The belt of outcrop extends 6½ miles along the strike (N. 60° E.) and has a maximum width of 2½ miles. The southeast flank is truncated by the overthrust marking the northwestern margin of the Blue Ridge. Most of the area is underlain by the Athens shale, the overlying Tellico is exposed in the higher hills where erosional remnants are preserved in the troughs of minor synclines. Keith (1905) gives an estimated thickness of 1000 feet for the Athens and a maximum exposed thickness of 200 feet for the Tellico. Considering the intricate structure more refined measurements are not warranted.

DESCRIPTION OF OCCURRENCE: Keith (1905) in his description of the Athens shale mentions the occurrence of a thin limestone conglomerate

associated with sandy beds in the upper part of the formation east of Limestone Springs. There is little doubt that this is the conglomerate lens investigated by the authors with sandstone and sandy shale from the crest of the ridge down the southeast flank. The thicknesses of individual conglomerate beds range from 1 to 5 feet, and the zone

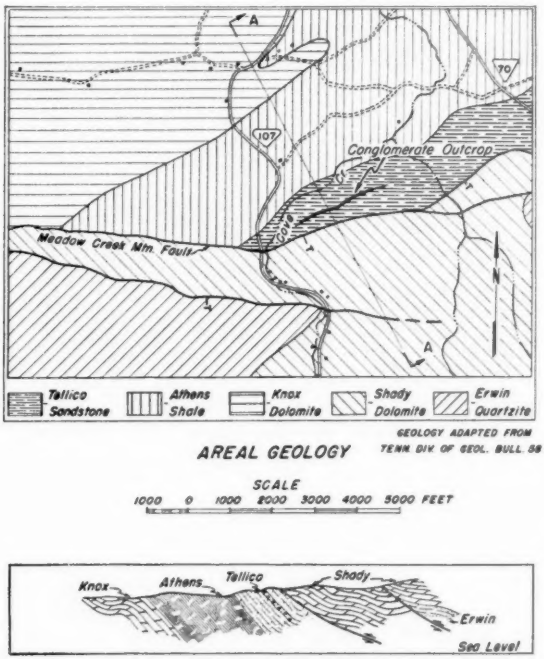

FIGURE 5.—GEOLOGIC MAP AND SECTION, GREENEVILLE

and that here Keith did not separate the Tellico from the Athens. The deposit was brought to the writers' attention by H. W. Ferguson. Earlier it was referred to in a general way by Safford (1869, p. 511).

The conglomerate lens can be traced along discontinuous outcrops in wooded terrain for slightly more than 2000 feet along the strike, N. 70° E., on the ridge southeast of Cove Creek (Fig. 5). The sandy shales, sandstones, and conglomerates of the Tellico make the ridge; the flood plain of Cove Creek to the northwest is underlain by Athens shale; the saddle and the next hill to the southeast are underlain by Shady dolomite in the hanging wall of the Meadow Creek Mountain fault.

Outcrops of conglomerate are interbedded has a maximum thickness of 80 feet. The beds thin and grade into sandstone at both ends of the outcrop belt.

Details of the structure are obscure because of the lack of continuous outcrops and the proximity to the major overthrust on the southeast. The average dip of the strata is 70° SE. It is believed that this Tellico outcrop is on the northwest limb of a minor syncline the southeast limb of which is overridden by the Meadow Creek Mountain fault block (Fig. 5).

LITHOLOGIC ANALYSIS. The coarse conglomerates at the Greeneville locality are composed primarily of limestone pebbles and cobbles averaging 3–4 inches in greatest dimension and ranging from 12 inches to one-eighth of

an inch (Pl. 2, figs. 4, 5, 6). The matrix is dominantly medium-grained, slightly calcareous, quartzose sandstone, but in a few beds the cement is argillaceous rather than arenaceous. Percentages of rock types in the 614 pebbles and cobbles counted are:

Rock type	Per cent
Limestone	79.2
Quartzite	7.9
Chert	6.2
Sandstone	4.1
Siltstone	2.2
Vein quartz	0.4
Total	100.0

In the limestone fraction several source formations could be identified: sandy limestone typical of the eastern belts of the Knox; darker, bluish-gray, slightly mottled limestone from the Shady; banded limestone and intraformational limestone conglomerate from the Honaker; and fine-grained to aphanitic, fossiliferous limestone from the Lenoir. The siltstone is identical to that in the Nolichucky and Rome formations. The fine-grained, red sandstone is typical of the Rome formation. The medium-grained, white quartzite was probably derived from the Erwin, and the arkosic, conglomeratic quartzite is typical of the Unicoi formation. The few small vein-quartz pebbles probably were derived from the conglomeratic beds in the Unicoi.

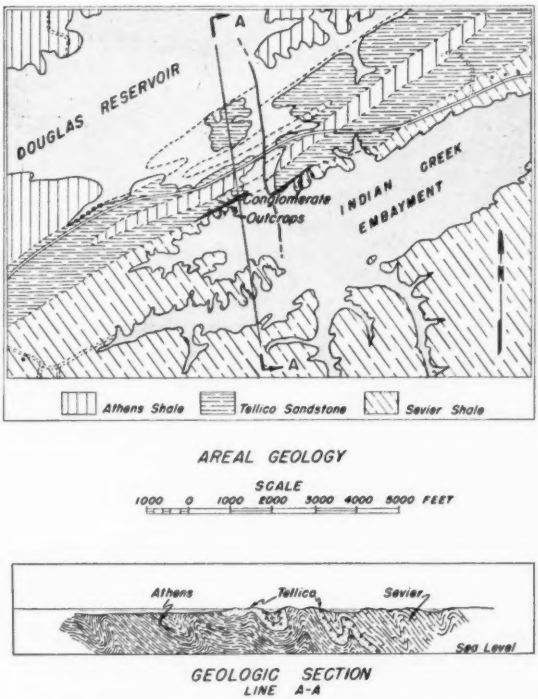

FIGURE 6.—GEOLOGIC MAP AND SECTION, DOUGLAS RESERVOIR

Douglas Reservoir Area

LOCATION AND GEOLOGIC SETTING: The first three areas described lie on the Pulaski thrust sheet; this area and the two succeeding ones lie on the Saltville thrust sheet. The Pulaski thrust either disappears under the Blue Ridge Front or dies out about 15 miles southwest of the Greeneville locality (Pl. 1). Most Middle Ordovician rocks on the Saltville

thrust sheet occur in the Bays Mountain syncline, which extends for more than 145 miles from Kingsport, Tennessee, to Etowah, Tennessee. From Kingsport to southwest of Greeneville, Tennessee, this structure is overridden on the southeast by the Pulaski thrust sheet; its extension southwestward is truncated on the southeast by the thrusts marking the northwestern boundary of the Blue Ridge Front. Only on the portion of the Saltville sheet overridden by the thrusts of the Blue Ridge Front do the coarse conglomerates occur. The outcrop belt of Middle Ordovician rocks decreases in width from 15 miles near Greeneville to 8 miles near Douglas Reservoir. The narrowing is due to minor folds and faults.

Douglas Reservoir is underlain mostly by the Athens and Sevier shales. In this area the Athens and Sevier are complexly interfolded and faulted so that their outcrop patterns appear as narrow interfingering belts striking northeast. In one belt, near the center of the reservoir, 4 miles southeast of Dandridge, Tennessee (Pl. 1), the contact between Athens and overlying Sevier is marked intermittently for 6 miles along the strike by the coarser Tellico facies, a maximum 125 feet of interbedded sandstone and shale with a few conglomeratic lenses. The best exposures of the Tellico in this area are in cuts along the county highway adjacent to the Indian Creek embayment of the reservoir and along the shore line of the embayment (Fig. 6). In the reservoir area the Athens is about 800 feet thick; the Tellico is as much as 125 feet thick; and the overlying Sevier is about 1000 feet thick. The thicknesses of the Athens and Sevier are necessarily approximate because no complete sections are exposed.

DESCRIPTION OF OCCURRENCE: In 1942 and 1943 two small quarries were opened in sandstone and conglomeratic beds near Indian Creek. Wedow (Unpublished report, Tenn. Valley Authority, 1943) delineated the zone in which these sandstones and associated conglomerates occur and noted its apparent stratigraphic position between the Athens and Sevier. Since the mapping was done wave action removing much of the residual mantle along the shore line has uncovered outcrops that show more details of the structural complexities.

In the area of the Indian Creek embayment the Tellico sandstones and conglomerates are repeated several times by folding and faulting. In cutting a gap through the ridge Indian Creek apparently followed a zone of weakness developed along a tear fault which strikes N. 10° W. This fault is indicated by divergent strikes and offsets of the strata (Fig. 6) Southwest of Indian Creek the average strike

---

PLATE 2.—CONGLOMERATES, FINCASTLE, SOUTH HOLSTON, AND GREENEVILLE AREAS

FIGURE 1.—COARSE CONGLOMERATE, FINCASTLE AREA

Typical appearance of an unweathered surface. Note the general lack of contrast between the limestone and quartzite pebbles and the unweathered matrix.

FIGURE 2.—COARSE CONGLOMERATE, FISHDAM CREEK, SOUTH HOLSTON AREA

Slightly weathered surface showing the contrast between the limestone pebbles and the matrix.

FIGURE 3.—CONGLOMERATE EXPOSURE AT SOUTH HOLSTON DAM AGGREGATE QUARRY

Moderately weathered outcrop showing poor sorting of pebbles and cobbles and faint traces of stratification. Length of scale is six inches.

FIGURE 4.—OUTCROP OF EXTREMELY COARSE CONGLOMERATE, GREENEVILLE AREA

This outcrop near the center of the conglomerate lens shows a concentration of larger than average cobbles. Note, however, the adjacent pocket composed of much smaller pebbles at the bottom of the picture.

FIGURE 5.—PARTIALLY WEATHERED BOULDER OF STRATIFIED CONGLOMERATE, GREENEVILLE AREA

Though poorly sorted, this outcrop shows more pronounced stratification than the average. The protruding dark chert pebbles indicate the amount of weathering.

FIGURE 6.—CONGLOMERATE OUTCROP SHOWING RUDE SORTING, GREENEVILLE AREA

This outcrop shows bands of rude sorting roughly parallel to the axis of the Brunton compass. Note concentration of cobbles at the bottom of the outcrop, overlain by a zone of smaller pebbles, which in turn is overlain by a zone of medium-sized pebbles, and finally another zone of cobbles in the upper right corner.

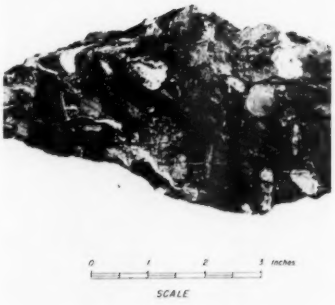

FIGURE 1

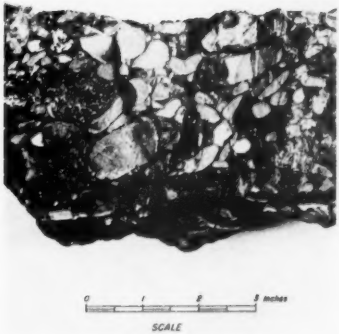

FIGURE 2

FIGURE 3

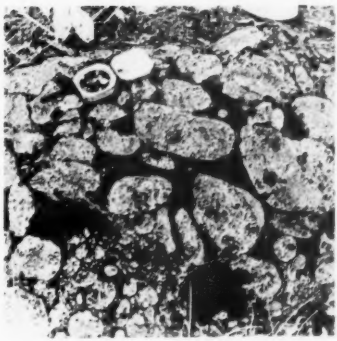

FIGURE 4

FIGURE 5

FIGURE 6

CONGLOMERATES, FINCASTLE, SOUTH HOLSTON, AND GREENEVILLE AREAS

FIGURE 1

FIGURE 2

FIGURE 3

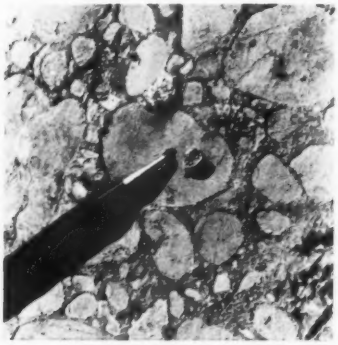

FIGURE 4

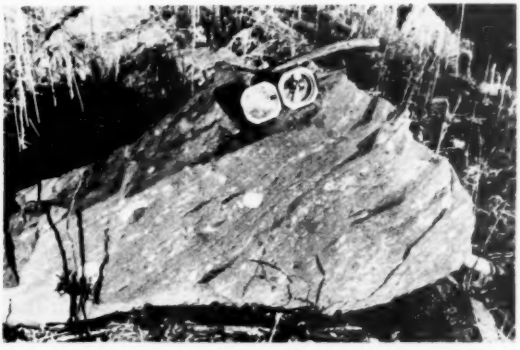

FIGURE 5

CONGLOMERATES, DOUGLAS RESERVOIR, ETOWAH, AND CISCO AREAS

is N. 60° E.; to the northeast it is N. 40° E. Repetition by folding results in three outcrop belts of Tellico on both sides of the creek. Because of the offsetting the belts are not continuous from one side of the creek to the other. The folds are asymmetrical with southeastward-dipping limbs.

The Tellico in this area differs from that at other localities. It consists of 125 feet of interbedded sandstones and shales in which the basal sandstone beds contain scattered pebbles and cobbles of limestone and quartzite and small lenses of fine-grained conglomerate, normally less than 2 feet in length and less than 1 foot thick. Brachiopods occur in the fine-grained conglomerate lenses and sandstone beds, and graptolites in the shale interbeds.

A fossil collection from the quarry on the right bank of Indian Creek was identified by G. Arthur Cooper of the U. S. National Museum, (Personal communication), who reports:

"The collection of brachiopods contained the following:

Doleroides sp.
Rostricellula sp.
Eoplectodonta aff. *E. Alternata* (Butts)
Pionodema sp.
Opikina sp.
'*Spyoceras*' sp.

"The presence of *Doleroides* and *Pionodema* indicates a level at about Cooper's Witten formation. The presence of *Eoplectodonta* in this fauna may indicate a somewhat higher horizon but that genus might be expected anywhere in the sequence. *Pionodema* on the other hand has not yet been found below the Witten.

"I am unable to be very helpful with the graptolites which are not too well preserved. The lower zone abounds in *Climacograptus* and also a dendroid suggesting *Desmograptus* aff. *D. textilis* Ruedemann. The upper graptolite zone contained only *Climacograptus*. The species of *Climacograptus* are possible *bicornis* (Hall) and/or *caudatus* Lapworth. In any case the graptolites suggest a position fairly high in the early middle Ordovician and one that is in harmony with the brachiopods."

This deposit is interpreted as representing the northwest margin of more extensive coarse clastics deposited to the southeast; the main mass has been eroded or hidden by folding and faulting. Environmental conditions during the deposition of conglomerates would not be conducive to life or the preservation of remains. Only around the margins of such areas of deposition might traces of a fauna be expected. This marginal zone seems to be represented by the Douglas Reservoir deposit.

The stratigraphic position of this deposit indicated by the faunal assemblage is somewhat higher than the position indicated by lithologic relationships. The apparent disparity may be resolved by detailed structural studies in the area. This occurrence may represent a later orogenic pulsation than other deposits.

LITHOLOGIC ANALYSIS: This deposit contains no typical beds of coarse conglomerate. Well-rounded pebbles and cobbles of limestone and quartzite up to a maximum dimension of 8 inches are scattered throughout the coarse-grained basal sandstone beds (Pl. 3, fig. 1). The sparseness and random scattering of these

---

PLATE 3.—CONGLOMERATES, DOUGLAS RESERVOIR, ETOWAH, AND CISCO AREAS

FIGURE 1.—CONGLOMERATE EXPOSURE, DOUGLAS RESERVOIR AREA

This outcrop of weathered conglomeratic sandstone is typical of the exposures at this locality. The majority of the limestone pebbles have been dissolved completely and are represented by small cavities in the sandstone.

FIGURE 2.—INTERFINGERING OF CONGLOMERATE AND SANDSTONE, ETOWAH AREA

This exposure shows typical conditions near the margin of the lens. Length of scale is six inches.

FIGURE 3.—SMALL LIMESTONE BOULDER IN CONGLOMERATE, ETOWAH AREA

The six-inch scale lies on a rounded boulder of mottled limestone which is surrounded by the usual ill-sorted assemblage of smaller pebbles and cobbles. This outcrop is near the middle of the conglomerate lens.

FIGURE 4.—FOSSILIFEROUS LIMESTONE PEBBLE, ETOWAH AREA

A silicified crinoid stem protrudes from the partially weathered limestone pebble. Note the angularity of the smallest limestone pebbles.

FIGURE 5.—TYPICAL STRATIFIED CONGLOMERATE BOULDER, CISCO AREA

This boulder shows the concentration of the pebbles parallel to the bedding, as well as the usual lack of sorting of the pebbles.

pebbles is further evidence of marginal deposition.

The pebbles and cobbles are too few for a reliable statistical count of the rock types. The quartzites are typical of the basal Cambrian Chilhowee group. Some larger limestone pebbles, aphanitic, light gray, and fossiliferous, correspond in lithology to the Mosheim member of the Lenoir in this area. In the fine-grained conglomerate lenses the majority of the pebbles are well rounded limestone with a minor admixture of subangular vein-quartz fragments. In these lenses the pebbles are too small to permit identification of the source rocks.

Etowah Area

LOCATION AND GEOLOGIC SETTING: Near the southwestern end of the Bays Mountain syncline, about 85 miles southwest of the Douglas Reservoir locality and 6 miles east of Etowah, Tennessee, is the fifth area where coarse conglomerates of Middle Ordovician age have been found (Pl. 1). At two localities near Mecca on the Etowah-Tellico Plains road lenses of coarse conglomerate are interbedded with calcareous shales and sandstones near the base of the Tellico formation (Fig. 7). In this area the Athens shale and Tellico formation crop out in a broad syncline whose southeast flank is overridden by the Great Smoky fault block. Most of the outcrop area is underlain by the Athens shale, apparently more than 4000 feet thick, in which beds of sandstone and conglomerate represent the Tellico.

DESCRIPTION OF OCCURRENCES: The first locality where conglomerate beds are exposed is 3½ miles east of Etowah along the Etowah-Tellico Plains road, 1400 feet west of the first crossing of Conasauga Creek. The second locality is 2½ miles farther northeast along the same road, one-tenth of a mile west of the McMinn County-Monroe County line (Fig. 7).

The westernmost deposit occurs in a 400-foot cut along the north side of the road west of the Conasauga Creek crossing. Three hundred feet of shales and sandstones containing two conglomerate beds are exposed in a cut at the base of a prominent ridge. The average strike of the strata is N. 70° E. and the average dip is 70° NW. The lower 200 feet of the section is fissile, calcareous shale. Succeeding this is a zone 25 feet thick of medium- to thick-bedded calcareous argillite and sandstone in which the conglomerates occur. The upper 75 feet is fissile, calcareous shale similar to that in the lower portion. Residual mantle on adjacent slopes and the terrace and alluvial cover on the flood plain of Conasauga Creek obscure other possible outcrops. In the thicker-bedded middle portion of the section two conglomerate beds occur. The lower bed, 5 feet thick, contains limestone pebbles and cobbles in an argillaceous matrix; the second bed, 2 feet thick and 10 feet higher in the section, contains limestone pebbles in a sandy matrix.

In the lower conglomerate bed brachiopods, bryozoa, and crinoid and trilobite fragments occur in the matrix. A small collection of these fossils was submitted to the U. S. Geological Survey. The report by Robert B. Neuman of the Survey Staff (Personal communication) states:

> "The following identifications were made from this collection:
>
> Brachiopods:
>
> *Multicostella* sp.
>
> *Sowerbyella negrita* (Willard)
>
> *Strophomena* sp.
>
> Bryozoan:
>
> *Rhinidictya* sp.
>
> "In addition there are fragmental, unidentifiable remains of isotelid trilobites, crinoids and an ostracode.
>
> "Positive correlation cannot be made on this small and fragmental collection. The forms identified, however, are known from the Tellico formation between the Little Tennessee River and the Chapman Highway."

The area mentioned by Neuman includes the outcrop belt of the Tellico formation southeast of Knoxville, Tennessee, from which the formation was originally described by Keith (1895).

In this deposit, as in the Douglas Reservoir deposit, the pebbles make up less than 30 per cent of the total rock mass; in other more typical deposits the pebbles make up from 70 to 80 or more per cent of the total. The decrease in the volume of the pebbles and the presence of fossils seem indicative of deposition around the periphery of a more typical deposit.

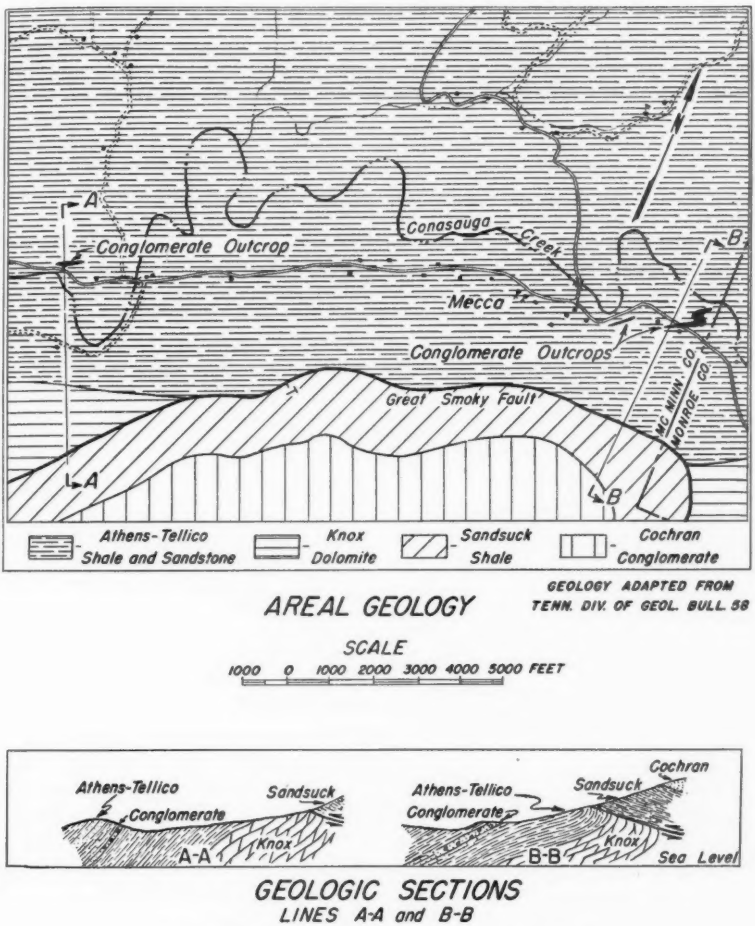

FIGURE 7.—GEOLOGIC MAP AND SECTIONS, ETOWAH

The second locality in this area is 2½ miles farther to the northeast along the Etowah-Tellico Plains road one-tenth of a mile west of the McMinn County-Monroe County line (Fig. 7). From all indications the beds exposed here are about 1500 feet lower stratigraphically than the deposit at the first locality. These conglomerates have been traced by discontinuous outcrops for more than half a mile along the strike (N. 60° E.). The average dip is 30° NW. Near the southwest end of the outcrop area sandstone containing a few beds of conglomerate less than 2 feet thick is exposed in road cuts and in an old road-metal quarry on the left bank of Conasauga Creek. Farther northeast along the road and about 250 feet lower stratigraphically the main conglomerate crops out. The lens is 75 feet thick at the road and is made up of conglomerate with thin sandstone partings (Pl. 3, fig. 2). Farther northeast and southwest the amount of sandstone increases at the expense of the conglomerate until finally there are no conglomerate beds.

LITHOLOGIC ANALYSIS: The coarse fraction of the conglomerate at both localities in the

Etowah area is dominantly limestone pebbles and cobbles with minor admixtures of quartzite, sandstone, siltstone, chert, and vein quartz. At the first locality the pebbles and cobbles are too sparsely scattered for a reliable statistical count of the rock types. At the second locality the pebbles and cobbles average more than 80 per cent of the total mass. A lithologic count of 926 pebbles on exposures of conglomerate at the second locality showed the following percentages of rock types:

Rock type	Per cent
Limestone	89.0
Quartzite	4.1
Chert	3.6
Vein quartz	1.4
Sandstone	1.5
Siltstone	0.3
Other	0.1
Total	100.0

The pebbles and cobbles range from 10 inches in greatest dimension to less than one-quarter of an inch (Pl. 3, fig. 3). The materials in the deposit are poorly sorted. In most exposures the matrix is a medium-grained, slightly calcareous, quartzose sandstone. However, in one bed the pebbles and cobbles are embedded in an argillaceous matrix.

The source rocks of some fragments can be determined. In the limestone fraction the most distinctive are the fossiliferous pebbles from the Lenoir (Pl. 3, fig. 4) and the coarsely crystalline, clastic limestones called marble in the southern Appalachian region. In addition there are sandy limestones and oölitic limestones typical of the Knox and intraformational conglomerates similar to those found in the Conasauga. The quartzites apparently were derived from the Great Smoky formation or other parts of the Ocoee group and from the quartzites of the Chilhowee group. Red and green fine-grained sandstones similar to those in the Rome are scattered throughout the deposit. Some of the tan to brown siltstones apparently were derived from the Conasauga or Rome formations, and the gray banded siltstones are typical of the finer-grained members of the Ocoee group such as the Pigeon siltstone member.

Cisco Area

LOCATION AND GEOLOGIC SETTING: The southwesternmost point at which Middle Ordovician coarse conglomerate deposits have been found is in Georgia, along State Highway 2, half a mile southeast of Cisco. This is about 33 miles southwest of the Etowah area (Pl. 1).

A syncline containing Middle Ordovician rocks extends from just south of the Hiwassee River in Tennessee 28 miles southwestward into Georgia. Thrust faults define the southeastern margin of this outcrop belt. In the central section the major overthrust marking the Blue Ridge Front is the southeastern limit of the belt for 8 miles. To the northeast and southwest the southeastern boundary is marked by thrusts which are subsidiary to the major thrust.

No accurate measurements of the thickness of Middle Ordovician rocks have been made in this area. Hayes (1895) gives a thickness of 2500 feet for the northern part of the belt in Tennessee, and Butts estimates 3500 feet for the southern part in Georgia (Butts and Gildersleeve, 1948, p. 29).

DESCRIPTION OF OCCURRENCE: In the Cisco area coarse conglomerate crops out as a single lens for about 1000 feet along the strike. The best exposure is at the northeastern end of the lens where the maximum 25-foot thickness is exposed in a bluff above the road on the southwest side of a small stream (Fig. 8). Northeast of the stream the conglomerate is absent, and the sequence is interbedded sandstone and shale. The conglomerate lens is traceable by discontinuous outcrops about 1000 feet along the strike (S. 35° W.) until it finally feathers out into sandstones and shales.

Except for the exposure at the northeastern end of the lens, rock outcrops are scarce in the area. On the basis of the limited information available the outcrop belt underlain by the sandstones and shales of the Tellico is about 3500 feet wide. The rocks strike N. 35° E. and apparently have a uniform dip of 35° SE. There is no indication of minor folding. To the northwest the Tellico conformably overlies the sandy, calcareous Athens shale; to the southeast it is overridden along most of its

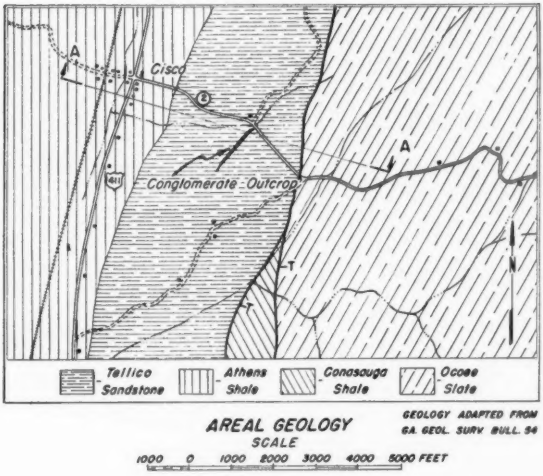

FIGURE 8.—GEOLOGIC MAP AND SECTION, CISCO

outcrop by the major thrust sheet marking the northwestern boundary of the Blue Ridge Front (Fig. 8). As calculated from the dip the Tellico is 2000 feet thick. The structure of the exposed portion of the belt is interpreted as the northwest limb of a syncline, the southeast limb of which has been overridden by the thrust sheet. The conglomerate lens occurs near the middle of the Tellico formation and is not a basal conglomerate as stated by Butts (Butts and Gildersleeve, 1948, p. 29).

A unique feature of this deposit is the dominant red color of the matrix and of the overlying and underlying beds when unweathered. At the other localities the unweathered conglomerates and associated sandstones and shales are gray or greenish gray.

LITHOLOGIC ANALYSIS: A statistical count of rock types of 848 pebbles seen on the outcrop surfaces and in small samples showed the following percentages:

Rock type	Per cent
Limestone	77.7
Sandstone	10.2
Quartzite	3.8
Chert	2.6
Siltstone	2.2
Vein quartz	2.0
Dolomite	1.5
Total	100.0

The pebble size at this locality ranges from 4 inches to one-eighth of an inch, and the average size is 1½ inches (Pl. 3, fig. 5). The matrix is a red, slightly calcareous, quartzose, medium-grained sandstone which makes up from 30 to 50 per cent of the rock.

Some of the source formations can be determined. In the limestone fraction, pebbles of aphanitic light-gray limestone typical of the eastern belts of the Knox are prevalent; the oölitic limestone pebbles could have been derived either from the Knox or from lime-

stone beds in the Conasauga. The green and gray, fine-grained sandstones are identical to those in the Rome. There are numerous fragments of reddish-brown, fine- to medium-grained sandstone which are generally larger than the average pebbles and less rounded. These seemingly were derived from the lower beds of the Tellico in the immediate area. A few quartzite pebbles are white to light gray, medium-grained, and vitreous like those in the Chilhowee group and in the Weisner quartzite. The majority of the quartzite pebbles, however, are dark gray, arkosic, and conglomeratic, similar to those in the Ocoee series. The chert is the jasperoid variety typical of that associated with the Shady dolomite.

This is the only deposit in which dolomite or dolomitic limestone pebbles were noted. In one outcrop pebbles of bluish-gray, medium-grained slightly banded and mottled dolomite are sparsely scattered through the exposure. These dolomite pebbles more nearly resemble the dolomites in the Shady in this area than those in the Knox, and presumably the Shady is the source formation.

Other Possible Localities

The writers do not presume that all Middle Ordovician coarse conglomerates in the southern Appalachian Valley have been found and studied. Some potentially favorable areas examined showed negative results; others have not been visited. Studies indicate that the coarse conglomerates are likely to occur only on the major thrust sheet immediately northwest of the Blue Ridge Front; therefore northeast of 36° N. Lat., 83° W. Long. the potentialities are limited to the Pulaski thrust sheet, southwest of this point to the Saltville thrust sheet.

Common Characteristics of Deposits

All the conglomerates studied have certain features which, despite the wide areal distribution, indicate a common mode of origin.

The most apparent features are the lenticular nature and the limited areal extent of each deposit. The largest lens of conglomerate studied has a maximum thickness of 75 feet and a maximum length of 800 yards. More typically the deposits are composed of 1–10 conglomerate lenses that range from 1 to 30 feet in thickness and from 10 to 100 yards in length interbedded with sandstone and sandy shale.

There is considerable variation in the stratigraphic position of the conglomerate lenses in the Middle Ordovician section. Only at one locality is conglomerate the basal Tellico unit resting directly on the Athens shale (Fig. 3). The maximum interval measured between a conglomerate lens and the Athens-Tellico contact is 1500 feet. Several other deposits appear to be higher in the section, but the geologic structure in those areas is so complicated that accurate measurements of position are not possible.

Another characteristic common to all conglomerate lenses studied is the poor sorting of the pebbles and cobbles. Commonly cobbles 6–8 inches long are found surrounded by pebbles whose maximum size is half an inch. In some places cobbles 4–12 inches in maximum dimension are sparsely scattered through beds of medium-grained sandstone devoid of smaller cobbles and pebbles.

A marked similarity is evident in the degree of rounding exhibited by the pebbles and cobbles in the conglomerate deposits. Among cobbles larger than 3 inches the quartzites are well rounded, and the limestones, sandstones, and siltstones are rounded to subrounded. Of the smallest pebbles, less than half an inch in maximum dimension, the quartzite and vein-quartz fragments are subrounded, and the limestone fragments are subangular. In the intermediate sizes the quartzite and vein-quartz pebbles are generally well rounded, and the limestone pebbles are subrounded to tabular.

The percentages of rock types represented further indicate the common origin of the deposits. In all conglomerates studied the percentage of limestone pebbles was higher than the percentage of any other rock type. Except for the Fincastle deposit, limestone makes up about 80 per cent of the pebbles and cobbles; quartzite is the next most prevalent rock type; then chert, sandstone, siltstone, and vein quartz. In the Fincastle deposit, limestone

and quartzite are first and second, then vein quartz, sandstone, chert, and siltstone.

All exposures of conglomerates examined are cut by two sets of filled veinlets which apparently represent two generations of joints. In one group the veinlets are confined to individual pebbles. These are generally quartz-filled and obviously developed in the source rock prior to the erosion, transport, and redeposition. The second group of veinlets, usually calcite-filled, transect the pebbles and matrix indiscriminately and obviously have been formed since the deposition and lithification of the conglomerate.

Conclusions

During this investigation many questions arose which cannot be answered. Much detailed work must be done before the relationships of the Middle Ordovician rocks in this region are known fully, but the results of this study lead to certain conclusions.

Four of the six areas are adjacent to the overthrust marking the northwestern boundary of the Blue Ridge Front. The other two areas are on the first fault sheet northwest of the Front. The Fincastle, South Holston, and Greeneville deposits are on the Pulaski thrust sheet, and the Douglas, Etowah, and Cisco deposits are on the Saltville thrust sheet, which in northeastern Tennessee and southwestern Virginia is overridden on the southeast by the Pulaski thrust. The geologic relationships in the area east of Newport, Tennessee, where the Pulaski fault approaches the mountain front (Pl. 1) have not been worked out in detail. Rodgers (1953, p. 138–139) initimates that the Pulaski fault sheet has been overridden and hidden by the Great Smoky fault sheet and may reappear at points farther southwest. If this is correct, the deposits of conglomerate southwest of Newport would probably be concealed under the Great Smoky fault sheet. This is not found to be true. It seems more probable that the Pulaski fault dies out in the wide shale belt near Newport, Tennessee, and from there southwestward the Saltville thrust sheet is the most southeasterly of the major thrust sheets of the Valley and Ridge Province.

Dolomite and dolomitic limestone fragments were found only in one conglomerate body. All calcareous fragments counted were tested with weak hydrochloric acid and all effervesced freely, even though many had megascopic characteristics typical of dolomites from formations in the region. Previous work in the southern Appalachian Valley (Butts, 1940; King *et al.*, 1944; Rodgers, 1953) shows that the Knox group becomes less dolomitic to the north and east and that the Middle Cambrian formations represented by the Conasauga, Honaker, and Elbrook become more dolomitic to the north and east. The Lower Cambrian Shady dolomite is predominantly dolomitic. On this basis dolomite and dolomitic limestone pebbles and cobbles should be abundant in all conglomerate exposures. A likely explanation is that the calcareous fragments were derived from limestone portions of these formations in an area farther east now overridden and concealed by the thrust sheets of the Blue Ridge Province.

It is evident that the Lower Cambrian clastics were altered from sandstone to vitreous quartzite prior to their erosion and the redeposition of fragments in the conglomerate lenses. Also the Cambrian and Lower Ordovician limestones were thoroughly indurated and had been subjected to some structural deformation prior to inclusion of their fragments in the conglomerates. This is evidenced by the quartz- and calcite-filled veinlets in the pebbles and cobbles. These veinlets are limited to individual pebbles and cobbles and do not extend into the surrounding matrix.

The decrease in the quantity and the grain size of coarse clastic material from the southeast to the northwest indicates that the source area of the conglomerates lay to the southeast.

Comparison of the rounding of the pebbles and cobbles of different rock types indicates the relative positions of the source formations during the period of erosional activity. The fragments derived from the older rocks, dominantly quartzite and vein quartz, are invariably more rounded than those of comparable size derived from the younger formations, mostly limestone, sandstone, and siltstone. This indicates a longer travel distance for the fragments derived from the older forma-

tions and supports the conclusion that these formations were exposed farther southeast.

Chemical analyses and petrographic studies show that the composition of the coarse conglomerate deposits does not differ radically from that of surrounding and accompanying sandstones and shales. Sandstones and shales from the South Holston and Douglas Reservoir areas are relatively calcite-rich—the average of five sandstone samples shows 32 per cent $CaCO_3$, and the average of six shale samples shows 26 per cent $CaCO_3$. The silica content of these samples is respectively 52 and 48 per cent. Petrographic studies by W. B. Hamilton of the U. S. Geological Survey (Personal communication) indicate that the matrix of the conglomerates from the South Holston area and the associated sandstones are almost identical. Both consist dominantly of quartz sand and sand-sized limestone fragments embedded in calcite, chlorite, sericite, and argillaceous material. On the basis of the chemical and physical data it is concluded that the conglomerates are extreme textural variants of the sediments in which they occur.

The conglomerates occur in widely separated areas at approximately the same stratigraphic position. In intervening areas the clastic rocks of the same age are fine-grained sandstones and shales. The areas containing conglomerate deposits are interpreted as representing points where streams draining recently uplifted highlands to the southeast discharged into the sea. Possibly these deposits were first laid down near the shore, later moved down slope, and redeposited on the floor of the trough of deposition.

The occurrence of conglomerate deposits at about the same stratigraphic position over a 325-mile distance is further evidence of the orogenic disturbance which affected this region in the Middle Ordovician. This orogeny, called the Blountian by Kay (1942, p. 1632) and the Blountian phase of the Taconian orogeny by Rodgers (1953, p. 94), apparently started in Chazy time and culminated in early Trenton time (Rodgers, 1953). The deposition of the conglomerates represents pulsations of this orogenic movement.

References Cited

Butts, Charles, 1933, Geologic map of the Appalachian Valley of Virginia with explanatory text: Va. Geol. Survey Bull. 42, 56 p.

—— 1940, Geology of the Appalachian Valley in Virginia: Va. Geol. Survey Bull. 52, pt. 1, 568 p.

Butts, Charles, and Gildersleeve, Benjamin, 1948, Geology and mineral resources of the Paleozoic area in northwest Georgia: Ga. Geol. Survey Bull. 54, 176 p.

Campbell, Marius R., 1899, Description of the Bristol quadrangle: U. S. Geol. Survey Geol. Atlas, folio 59

Decker, Charles E., 1952, Stratigraphic significance of graptolites of Athens shale: Am. Assoc. Petroleum Geologists Bull., v. 36, p. 1–145

Hayes, C. W., 1895, Description of the Cleveland quadrangle: U. S. Geol. Survey Geol. Atlas, folio 20

Kay, G. Marshall, 1942, Development of the northern Allegheny synclinorium and adjoining region: Geol. Soc. America Bull., v. 53, p. 1601–1658

Keith, Arthur, 1895, Description of the Knoxville quadrangle: U. S. Geol. Survey Geol. Atlas, folio 16

—— 1905, Description of the Greeneville quadrangle: U. S. Geol. Survey Geol. Atlas, folio 118

King, Philip B., 1950, Tectonic framework of the southeastern United States: Am. Assoc. Petroleum Geologists Bull., v. 34, p. 653–671

King, Philip B., Ferguson, H. W., Craig, L. C., and Rodgers, John, 1944, Geology and manganese deposits of northeastern Tennessee: Tenn. Geol. Survey Bull. 52, 275 p.

Rodgers, John, 1953, Geologic map of east Tennessee with explanatory text: Tenn. Geol. Survey Bull. 58, pt. 2, 168 p.

Safford, James M., 1869, Geology of Tennessee: S. C. Mercer, Printer to the State, Nashville.

Stow, M. H., and Bierer, J. C., 1937, Some significance of an Athens conglomerate near Fincastle, Virginia (abstract): Va. Acad. Sci. Proc., 1936–1937, p. 71

Twenhofel, W. H., Chairman Ordovician Subcommittee, 1954, Correlation of the Ordovician formations of North America: Geol. Soc. America Bull., v. 65, p. 247–298

Ulrich, E. O., 1911, Revision of the Paleozoic systems: Geol. Soc. America Bull., v. 22, p. 281–680

Tennessee Valley Authority, 510 Union Building, Knoxville, Tennessee

Manuscript Received by the Secretary of the Society, May 23, 1955

Publication Authorized by the Tennessee Valley Authority

BULLETIN OF THE GEOLOGICAL SOCIETY OF AMERICA
VOL. 67, PP. 717-738, 7 FIGS. JUNE 1956

HEMPHILLIAN MAMMALIAN ASSEMBLAGE FROM NORTHEASTERN OREGON

BY J. ARNOLD SHOTWELL

ABSTRACT

The Hemphillian McKay Reservoir, Oregon, local fauna is correlated with the Paote and Ertemte faunas of North China and Montpellier fauna of France. Study of these faunas shows an important North China-North America faunal interchange. The highest degree of interchange is among the carnivores, and the lowest in the edentates, primates, and artiodactyls. Several mammals fail to migrate successfully at this time because of the presence of ecologically equivalent mammals in the new area.

The local habitat of the major community represented at McKay Reservoir is that of a pond-bank association. Grassland and woodland elements from bordering communities are also recognized. New genera described are: *Hydroscapheus*, *Prosomys*, and *Leptodontomys*. New species described are: *Citellus* (*Otospermophilus*) *wilsoni*, *Ochotona spangelei*, *Hypolagus oregonensis*, *Citellus* (*Citellus*) *mckayensis*, *Perognathus sargenti*, *Canis condoni*, *Felis longignathus*, and *Prosthennops brachirostris*.

CONTENTS

TEXT

	Page
Introduction	717
Acknowledgments	717
Occurrence	718
Field technique	718
Faunal list	718
Age and correlation	719
Intercontinental faunal relationships	721
Paleoecology	724
Systematic descriptions	724
References cited	737

ILLUSTRATIONS

Figure	Page
1. Proportion of total genera of mammals in faunal exchange in the Hemphillian	722
2. Distribution of families grouped by superfamilies in the Hemphillian in North China and North America	723
3. Time and direction of migration of several late Cenozoic mammals	723
4. Insectivores and chiropterid	725
5. Lagomorphs and rodents	729
6. Lagomorphs, rodents, and carnivores	734
7. Perissodactyls and artiodactyls	736

INTRODUCTION

From 1949 to 1953 a vertebrate fauna was collected from sediments exposed by wave erosion on the east bank of McKay Reservoir (McKī), 5 miles south of Pendleton in northeast Oregon. Mr. Ray Spangle of Pendleton discovered the site in 1949, and field parties from the Museum of Natural History of the University of Oregon are still working there.

Some taxonomic groups represented at this locality were not previously known in Hemphillian faunas of North America. The McKay Reservoir locality is the Hemphillian site nearest the Eurasia-North America bridge. Several forms in the fauna are congeneric with Eurasian fossil mammals. The McKay Reservoir fauna provides a basis for study of intercontinental correlation, faunal resemblance, direction of migration, and factors preventing migration.

ACKNOWLEDGMENTS

This study was financed by grants-in-aid from the general research committee of the University of Oregon and by field funds of the Museum of Natural History of that institution. Mrs. Genevieve Shotwell assisted with the field work. Mr. and Mrs. John S. Venable cooperated in every way and made the field parties as comfortable as possible.

Many institutions lent material for com-

parison: Museum of Paleontology, University of California; California Institute of Technology; Museum of Paleontology, University of Michigan; Peabody Museum, Yale University; Museum of Natural History, University of Kansas; British Museum; and the U. S. National Museum.

Occurrence

The specimens occur in a tuffaceous sandstone and overlying conglomerate which rest on Columbia River basalt. In much of their distribution the beds are covered by younger silts. At McKay Reservoir the sandstone is at least 200 feet thick (the base is below water level), and the conglomerate is 3–5 feet thick. At other places the conglomerate is thicker, and the sandstone much thinner. This unnamed and undescribed lithologic unit may represent part of the Shutler formation.

Although some vertebrate specimens were collected from the conglomerate, most came from the upper 10–15 feet of the sandstone. The lower part of the section is apparently barren. The uppermost sandstone beds are fine-grained and tend to be platy or fissile. They are dark gray to black when wet. A coarser-grained brown bed just below these gray-black members yielded the majority of the specimens.

Few specimens showed signs of abrasion. Most small specimens are well preserved, but some large ones, especially near the surface, were weathered by frost cracking, wetting, and drying. Temperature at the site ranges from −30°F to over 110°F, and the site is often under water from 3 to 4 months each year.

To date only one articulated skeleton has been found in the deposit, a large portion of the skeleton of a ground squirrel. Apparently the deposit is a normal accumulation in a depression. Lack of abrasion of bones and the type of enclosing sediment suggest that the fossils were not transported a great distance.

Field Technique

A 500-foot offset grid system was used to show the exact position of specimens. Care was taken to collect all fragments and float.

Several small pits started were discontinued, and work was concentrated on pit 270. Small blocks of sandstone are removed with 1-inch steel chisels and 2-pound sledges. When wet, the blocks are easily broken by hand. Contrasting colors of bone and rock allow high percentage of recovery of small specimens. In order that the fauna could be studied quantitatively, all specimens and fragments were retained.

Faunal List

Arthropoda
- Crustacea
  - crayfish

Chordata
- Amphibia
  - ranid
- Reptilia
  - Testudinata
- Aves
  - Anatidae
  - Tetraonidae
- Mammalia
  - Insectivora
    - *Scapanus* sp.
    - *Hydroscapheus americanus* n. gen., n. sp.
  - Chiroptera
    - Family indeterminate
  - Lagomorpha
    - *Ochotona spangelei* n. sp.
    - *Hypolagus oregonensis* n. sp.
  - Rodentia
    - *Liodontia* sp.
    - *Mylagaulus* sp.
    - *Marmota oregonensis* n. sp.
    - *Citellus* (*Otospermophilus*) *wilsoni* n. sp.
    - *Citellus* (*Citellus*) *mckayensis* n. sp.
    - *Pliosaccomys dubius* Wilson
    - *Perognathus sargenti* n. sp.
    - *Leptodontomys oregonensis* n. gen., n. sp.
    - *Dipoides smithi* Shotwell
    - *Castor* sp.
    - *Prosomys mimmus* n. gen., n. sp.
    - *Pliozapus solus* Wilson
  - Carnivora
    - *Canis condoni* n. sp.
    - *Osteoborus* sp.
    - *Plesiogulo* sp.
    - *Pliotaxidea* sp.
    - *Felis longignathus* n. sp.
    - *Machairodus* sp.
  - Proboscidea
    - ?Family Mammutidae
  - Perissodactyla
    - *Hipparion* sp.
    - *?Neohipparion* sp.
    - *Teleoceras* sp.
  - Artiodactyla
    - *Prosthennops brachirostris* n. sp.
    - *Procamelus* or *Pliauchenia* sp.
    - *Paracamelus* sp.

Age and Correlation

The McKay Reservoir fauna is Hemphillian, as defined by Wood *et al.* (1941). This is indicated by the presence of *Dipoides* and *Plesiogulo*. In North America the first appearance of *Machairodus* and the last appearance of *Osteoborus*, *Prosthennops*, and *Teleoceras* are in the Hemphillian faunas. Genera common but not restricted to Hemphillian faunas, such as *Hypolagus* and *Neohipparion*, also appear at McKay Reservoir.

Table 1.—Genera of Mammals Common to North America, North China, and Europe in the Hemphillian

	North America					North China		Europe			
Genera	Optima	McKay	Kern River	Rome	Rattlesnake	Paote	Ertemte	Montpellier	Pikermi	Polgardi	Salmendingen
Ochotona	..	×	..	..	..	..	×	..	..	..	..
Dipoides	×	×	..	×	×	×	×	×	..	..	×
Castor	..	×	..	×	..	×	..	..	..	..	..
Plesiogulo	..	×	..	..	..	×	..	×	..	..	..
Eomellivora	..	..	×	..	..	×	..	..	..	..	..
Felis	×	×	..	..	..	..	×	..	..	..	×
Indarctos	..	..	..	..	×	×	..	..	×	..	..
Hipparion	..	×	..	..	×	×	×	×	×	×	..
Machairodus	×	×	..	..	..	×	..	..	..	×	..
Agriotherium	×	..	..	..	..	..	..	×	..	..	..

The subage relation of the McKay Reservoir fauna to other Hemphillian faunas is difficult to determine. Criteria for correlation below the level of provincial age are unavailable; the stage of evolution of various species is often used, but superpositional occurrences of these species are inadequate for reliable correlation. Error may result where this method is applied to faunas that occur in different environmental provinces. Small specific differences attributed to age may be ecological. Temporal value of stage of evolution is uncertain at the species level where superpositional occurrence cannot be demonstrated. Remarks on the relative position of various Hemphillian faunas seem unjustified or at least highly subjective.

Many genera in the McKay Reservoir fauna and other North American Hemphillian faunas occur also in Eurasia (Table 1). It is assumed in this study that faunas containing an association of many of these genera, especially those with restricted ranges, are broadly age equivalents. The level of refinement in correlation then is of age magnitude.

North China faunas which would be considered equivalents within the limits of an age include the Paote (loc. 30, especially) and Ertemte. Teilhard and Leroy (1942) refer to the Paote as Pontian (stage) and the Ertemte as middle Pliocene. Interpretation of the various North China assemblages is complicated because they were studied as taxonomic groups, not faunas; hence various taxonomic groups in a fauna may have anomalous age determinations. Pontian and middle Pliocene forms have been identified from the same fauna. Some difficulty here may be the differences in groups represented in these faunas; for instance, Ertemte has a large well-known rodent, Insectivora, chiropteran, and small carnivore representation, whereas Paote contains almost entirely the large herbivorous forms. Kurtén (1952) equates Paote and Ertemte, which is also the conclusion of this study.

A European fauna, Montpellier, contains *Dipoides* and *Plesiogulo*, genera which typify the Hemphillian in North America. Montpellier is referred to Plaisancian by most European workers. Another European fauna, Pikermi, contains both *Hipparion* and *Machairodus*, two genera found in the Hemphillian of North America. These genera were apparently long-lived in Eurasia and are of little value in intercontinental correlation. With criteria used here it is difficult to show the relationship of the Pikermi fauna to North American faunas. However, many genera occurring at Pikermi (Pontian) occur also at Paote, and on this basis the Paote and the Pikermi have been correlated. Faunas referred to Pontian or Plaisancian are equated to the same fauna, Paote. This may indicate some overlap in the Pontian and Plaisancian time. Paleontologists are dependent on European workers for the proper application of stratigraphic control in assigning faunas to European type sections.

Until stratigraphic positions of European faunas are better established, it is possible only to correlate with faunas and await their assignment into the type sections. Apparently North American Hemphillian is broadly equivalent in

TABLE 2.—CONTEMPORARY SUBFAMILIES AND GENERA OF NORTH CHINA AND NORTH AMERICAN MAMMALS DURING HEMPHILLIAN

Classification	North America	North China	Common Genera	Common Subfamily
Insectivora				
Talpinae	.....	*Scaptochirus*		
Scalopinae	*Scapanus*	.....		
Erinaceinae	.....	*Erinaceus*		
Soricinae	.....	*Neomys*		
Desmaninae	*Hydroscapheus*	.....		
Crocidurinae	.....	*Crocidura*		
Lagomorpha				
Ochotonidae	*Ochotona*	*Ochotona*	X	X
Palaeolaginae	*Hypolagus*	.....		
	Notolagus	.....		
Leporinae	*Caprolagus*	.....		
Primates	.....	*Pliopithicus*		
Edentata	*Sinclairia*	.....		
Rodentia				
Aplodontidae	*Liodontia*	.....		
	.....	*Pseudaplodon*		
Mylagaulidae	*Mylagaulus*	.....		
Eomyidae	*Kansasimys*	.....		
	Leptodontomys	.....		
Sciurinae	*Sciurus*	.....		
	Citellus	.....		
	Marmota	.....		
Geomyinae	*Thomomys*	.....		
	Pliosaccomys	.....		
Perognathinae	*Perognathus*	.....		
Dipodomyinae	*Cupidinimus*	.....		
	Prodipodomys	.....		
Heteromyinae	*Diprionomys*	.....		
Castorinae	*Castor*	*Castor*	X	X
	.....	*Palaeomys*		
Castoroidinae	*Dipoides*	*Dipoides*	X	X
Cricetinae	*Peromyscus*	.....		
	.....	*Anatolomys*		
	.....	*Pseudomeriomes*		X
	.....	*Lophocricetus*		
	.....	*Cricetulus*		
	.....	*Microtodon*		
	.....	*Nannocricetus*		
	.....	*Sinocricetus*		
	.....	*Prosiphenus*		
Microtinae	*Prosomys*	.....		
	Goniodontomys	.....		
Rhyzomyidae	.....	*Pararhyzomys*		
Murinae	.....	*Progonomys*		
	.....	*Mus*		
	.....	*Parapodemus*		
	.....	*Stephanomys*		
Sicistinae	.....	*Heterosminthus*		
Zapodinae	*Pliozapus*	.....		
Dipodinae	.....	*Brachyscirteles*		
	.....	*Paralactaga*		
	.....	*Sminthoides*		

TABLE 2.—CONTINUED

Classification	North America	North China	Common Genera	Common Subfamily
Carnivora				
Caninae	*Canis*	.....		
	Vulpes	*Vulpes*	X	X
Amphicyoninae	.....	*Amphicyon*		
Simocyoninae	.....	*Simocyon*		X
	Araeocyon	.....		
Borophaginae	*Osteoborus*	.....		
Ursidae	*Plionarctos*	.....		
	Agriotherium	*Agriotherium*	X	X
	Indarctos	*Indarctos*	X	
Procyoninae	*Bassariscus*	.....		
Mustelinae	*Plesiogulo*	*Plesiogulo*	X	X
	Martes	*Martes*	X	
	.....	*Sinictis*		
	.....	*Propulorius*		
	Mustela	*Mustela*	X	
	Brachypsalis	.....		
	Cernictis	.....		
Mellivorinae	*Eomellivora*	*Eomellivora*	X	X
Melinae	.....	*Parataxidea*		X
	Pliotaxidea	.....		
	.....	*Melodon*		
	.....	*Meles*		
	.....	*Trochictis*		
Mephitinae	.....	*Promephitis*		
Lutrinae	.....	*Lutra*		
	Lutravus	.....		X
Hyaenidae	.....	*Ictitherium*		
	.....	*Hyaena*		
	.....	*Lycyaena*		
Nimravinae	*Pseudaelurus*	.....		
	.....	*Metailurus*		X
Felinae	*Felis*	*Felis*	X	X
Machairodontinae	*Machairodus*	*Machairodus*	X	X
Proboscidia				
Gomphotherinae	.....	*Serridentinus*		
	Tetralophodon	*Tetralophodon*	X	X
Mammutidae	*Mammut*	*Mammut*	X	X
Platybelodontinae	*Amebelodon*	.....		
Stegodontinae	.....	*Stegolophodon*		
	.....	*Stegodon*		
Perissodactyla				
Equinae	*Hipparion*	*Hipparion*	X	X
	Neohipparion	.....		
	Nannippus	.....		
	Pliohippus	.....		
Aceratheriinae	.....	*Chilotherium*		
Caenopinae	*Aphelops*	.....		
Teleoceratinae	*Teleoceras*	.....		
Dicerorhininae	.....	*Dicerorhinus*		
Elasmotherinae	.....	*Sinotherium*		
Artiodactyla				
Suidae	.....	*Chleuastochoerus*		
	.....	?*Propotamochoerus*		
Tayassuidae	*Prosthennops*	.....		
Camelinae	*Procamelus*	.....		
	Pliauchenia	.....		
	Paracamelus	.....		

TABLE 2.—CONTINUED

Classification	North America	North China	Common Genera	Common Subfamily
Alticamelinae	*Alticamelus*	.....	..	..
Cervinae	.....	*Cervocerus*	..	..
	.....	*Axis*	..	..
Odocoileinae	.....	*Procapreolus*	..	..
Paleomerycinae	*Pediomeryx*	.....	..	..
	Blastomeryx	.....	..	..
Dromomerycinae	*Cranioceras*	.....	..	..
Palaeotraginae	.....	*Palaeotragus*	..	..
	.....	*Samotherium*	..	..
Antilocaprinae	*Capromeryx*	.....	..	..
	Ilingoceros	.....	..	..
	Sphenophalos	.....	..	..
Hippotraginae	.....	*Paraprotoryx*	..	..
	.....	*?Protoryx*	..	..
	.....	*Sinotragus*	..	..
	.....	*Tragoceras*	..	..
Antilopinae	.....	*Gazella*	..	..
Caprinae	.....	*Plesiaddax*	..	..
	.....	*Urmatherium*	..	..

age to such European faunas as that represented at Montpellier and to North China faunas characterized by Paote and Ertemte.

INTERCONTINENTAL FAUNAL RELATIONSHIPS

Table 2 lists the orders, subfamilies, and genera of mammals known from the North American Hemphillian and North China deposits of equivalent age. Undoubtedly there are omissions from the lists, and some items may appear in error, although care was taken to avoid this. The data on North China faunas are based largely on Teilhard and Leroy (1942). Genera and subfamilies which occur on both continents are indicated. The appearance of a genus in the faunas of two continents indicates migration between those two continents.

Table 2 lists genera common to the faunas of North America and North China during the Hemphillian. The relative importance of this migration can be seen only by comparison with faunal interchanges of other periods. Simpson (1947) studied the faunal interchanges of the Cenozoic and shows that interchange was greater in Middle than in the Early Pliocene but not so great as in the Pleistocene. As shown by Simpson the most important interchanges are those of the early Cenozoic.

It is of interest to note which mammals migrate and what factors allow or impede migration at a particular time. Data in Table 2 are

TABLE 3.—NUMBER OF GENERA OF MAMMALS IN NORTH CHINA AND NORTH AMERICA AND COMMON TO BOTH CONTINENTS IN HEMPHILLIAN

Order	North America	North China	Genera in common
Insectivores	2	4	0
Lagomorphs	4	1	1
Primates	0	1	0
Edentates	1	0	0
Rodents	20	21	2
Carnivores	19	23	9
Proboscidians	3	5	2
Perissodactyls	6	4	1
Artiodactyls	11	14	0

presented graphically in Figure 1 to show the proportional amount of migration within various orders of mammals during the Hemphillian. The heavy bar through the middle of the illustration represents the area of interchange between North China and North America; breaks in this bar indicate migration. The size of the break is proportional to the number of genera of the order noted found on both continents in the Hemphillian. The cross-hatched areas indicate the additional proportion of families of each order found on both continents. Primates and Edentata do not appear on the illustration since they have no Hemphillian taxonomic categories common to the two continents. Figure 1 shows that the proportion of genera involved in migration varies greatly from order to order—a high proportion of Carnivora genera migrated in the Hemphillian, while no Artiodactyla genera did. Some orders have families but no genera, or a greater proportion of families than genera, common to the two regions. This apparently represents migration, subsequent isolation, and independent evolution or extinction of the genera once common to the two continents.

Several major factors may affect the success of migration in a particular taxonomic group: (1) the topographic conditions of the inter-

change area may be such that only particularly adapted mammals can make the move, (2) the climatic conditions of the interchange area may

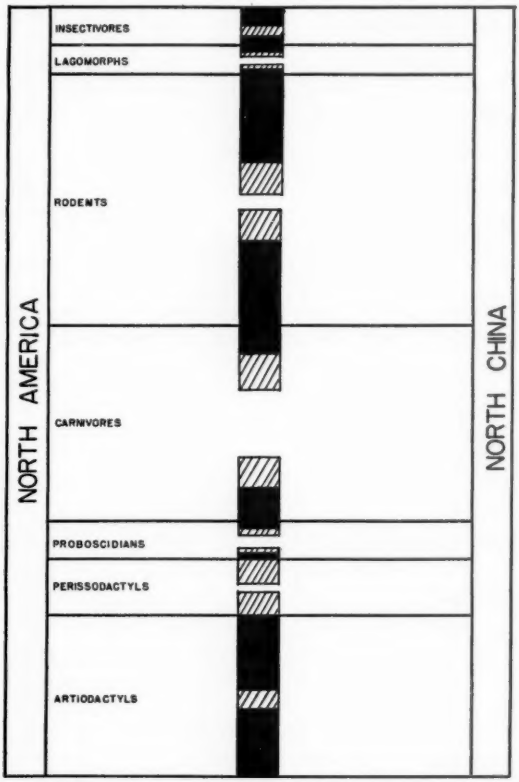

FIGURE 1.—PROPORTION OF TOTAL GENERA OF MAMMALS IN FAUNAL EXCHANGE IN THE HEMPHILLIAN
Shaded areas represent proportion of families found in common to the two areas.

be such that mammals adapted for other situations and thus not living adjacent to the area of interchange could not make use of it, and (3) the invader may find mammals of similar habitat and niche requirements already living in the new area and thus cannot establish himself.

It is unlikely that any one of these factors can explain all instances of nonmigration at a particular interval. However, one may be more important at one interval. In the Hemphillian, topographic conditions of the interchange area apparently are unimportant since such diversely adapted forms as mastodonts, pikas, beavers, and horses intermigrate. Simpson (1947) emphasized the effect of climatic conditions of the interchange area in that "warm adapted forms" are prevented from using a cool area of interchange. This undoubtedly is important in the restriction of some mammals. However, examination of the faunas of the two regions indicates that competition of similarly adapted mammals for a particular niche is a more important factor in the Hemphillian.

In the classification of mammals, members of a superfamily are usually similarly adapted except where isolation results in local adaptive radiation (hystricomorphs in South America). Families of mammals in North America and North China during the Hemphillian are shown in Figure 2; families are grouped in superfami-

lies and orders. In groups which experienced interchange, families are the same on both continents and appear as continuous bars across the chart. Of particular interest are the families

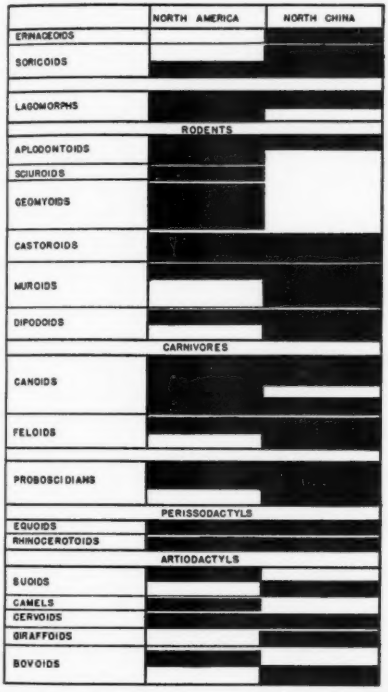

FIGURE 2.—DISTRIBUTION OF FAMILIES GROUPED BY SUPERFAMILIES IN THE HEMPHILLIAN IN NORTH CHINA AND NORTH AMERICA

of orders and superfamilies which had little interchange, the artiodactyls for instance. The families of various superfamilies of artiodactyls balance each other in checkerboard fashion on the chart. The pigs of North China are matched by the peccaries of North America. The giraffoids and a family of bovoids of North China are matched by the camels and another family of bovoids in North America. At the subfamily level the pairing of groups of nonmigrants becomes even more striking. None of the five subfamilies of rhinos on the two continents during the Hemphillian migrated. Two of the families are North American, and three are found in North China.

The carnivores had a high interchange. The Hyaenidae of the Feloidea were not present in North America in Hemphillian; however, hyaenoid dogs were abundant.

None of the Geomyoidea (gophers, pocket

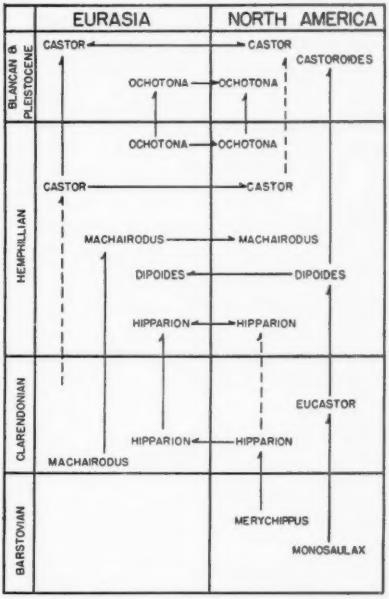

FIGURE 3.—TIME AND DIRECTION OF MIGRATION OF SEVERAL LATE CENOZOIC MAMMALS

mice, and kangaroo rats) of North America had family representatives in North China (Fig. 2). The Muroidea of North China, except for one family, have no North American representation. The Rhyzomyidae (bamboo rats) of the Muroidea are similar in adaptations to the pocket gophers of North America. The Dipodinae are similar to the kangaroo rats in adaptation. Although the geomyids are restricted to North America, probable ecological equivalents are the Rhyzomidae of the Muroidea and the Dipodinae of the Dipodoidea from the mid-Pliocene of North China. Superfamily Sciuroidea (Fig. 2) has no apparent ecological equivalent in North China, but, soon after mid-Pliocene, squirrels invaded this area.

Many nonmigrants of the Hemphillian appear to have had ecological equivalents in the region being successfully entered by other animals. This is considered to be a major factor

in their inability to migrate successfully. The appearance of similarly adapted but distantly related groups is to be expected after a period of little or no interchange between two areas. Interchange during the lower Pliocene was very low. A few North American Hemphillian mammals which did not migrate can be considered "warm adapted": the Primates, sloths, and possibly the procyonids. The sloths, however, appear in the Hemphillian faunas of Oregon, an area certainly not warm at that time. Pleistocene sloths occur as far north as Alaska.

The direction of migration of a particular genus of mammal, to or from North America, is not always evident. In order to determine the immediate source area of a migrant form it is necessary to have available data on the distribution of its ancestral group. If a long-lived form such as *Machairodus* has an earlier history in one area, this is probably the immediate source area. *Machairodus* is therefore considered to have moved to North America. Figure 3 illustrates later Cenozoic history and distribution of several Hemphillian genera for which there are at least some data on direction of migration. For *Castor*, *Ochotona*, and *Hipparion*, more than one migration is indicated. The infrequent occurrence of *Hipparion* in the Hemphillian of North America may indicate either a return from North China or a holdover from the Clarendonian in some areas. *Ochotona* is known from only one Hemphillian fauna (McKay Reservoir) and does not appear generally in North American faunas until the Quaternary. *Castor* is similar in distribution but is known from several Hemphillian faunas in the Pacific Northwest. These instances may be explained by limited distribution of forms at particular times and/or by separate migrations. Evidence does not indicate which is more likely.

Paleoecology of the Fauna

The McKay Reservoir fauna was used as an example in a discussion of methods in mammalian paleoecology (Shotwell, 1955b). At least three communities were recognized in material from the quarry: a pond-bank association, a grassland, and a woodland. The pond-bank was the major community, and the others represented bordering communities.

Systematic Descriptions[1]

Phylum ARTHROPODA

Class CRUSTACEA

Grinding disks of crayfish are abundant at McKay Reservoir.

Phylum CHORDATA

Class AMPHIBIA

Several tibia-fibulae in the fauna probably are those of a ranid, possibly *Rana*.

Class REPTILIA

Numerous turtle carapace fragments have not yet been assigned to a genus.

Class AVES

Specimens of Anatidae and Tetraonidae in the fauna will be described in a subsequent report.

Class MAMMALIA

Order INSECTIVORA

Family Talpidae

Subfamily Talpinae

Scapanus sp.

A humerus UOMNH F-3506 and a scapula UOMNH F-3508, both incomplete, represent *Scapanus*. The humerus is not notably different from that of living species (*Scapanus townsendi*); on the scapula the infraspinous fossa extends anteriorly farther than on living species. It may represent another talpid.

Subfamily Desmaninae

Hydroscapheus americanus n.gen.n.sp.

(Figure 4)

Type: Humerus UOMNH F-4101.

Paratypes: Femur UOMNH F-2698, tibia-fibulae UOMNH F-3792, F-2456, clavicle UOMNH F-3206.

[1] Abbreviations used in this study are: UOMNH—University of Oregon, Museum of Natural History; UCMP—University of California, Museum of Paleontology; USNM—United States National Museum; UKMNH—University of Kansas, Museum of Natural History; UMNP—University of Michigan, Museum of Paleontology; and BM—British Museum.

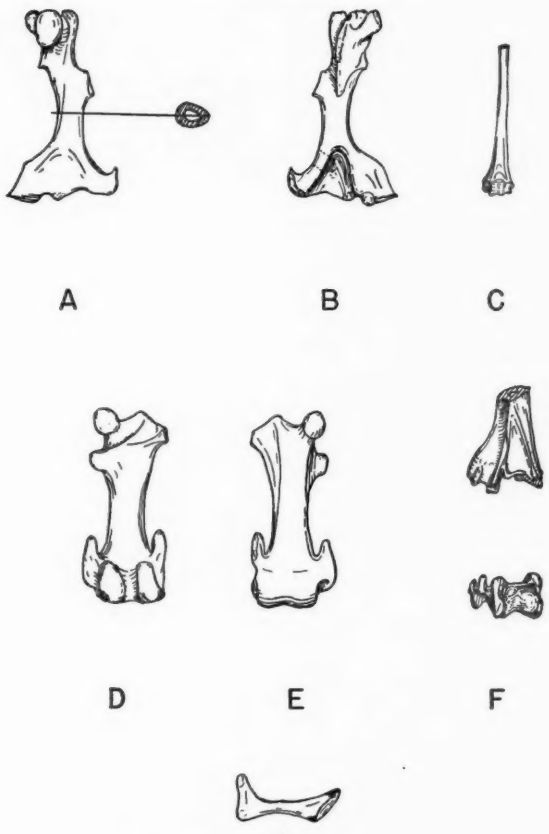

FIGURE 4.—INSECTIVORES AND CHIROPTERID
A.—*Hydroscapheus americanus*, type, F-4101, humerus, ×1.5
B.—*Hydroscapheus americanus*, humerus, ×1.5
C.—Chiropterid, humerus, ×1.5
D.—*Hydroscapheus americanus*, F-2698, femur, ×1.5
E.—*Hydroscapheus americanus*, femur, ×1.5
F.—*Hydroscapheus americanus*, F-3792, tibia-fibular, ×1.5
G.—*Hydroscapheus americanus*, F-3206, clavicle, ×1.5

Type Locality: McKay Reservoir, Oregon

Diagnosis—A desman water mole about four-fifths the size of living *Desmana*. Humerus lacks bicipital tunnel; has rounded head; no pit or fossa for origin of great ligament of *M. flexor digitorum profundus*. Femur has ovoid head and well-developed fused sesamoids on epicondyles.

Description—The material has been compared with *Galemys pyrenaicus* (USNM 172374) and *Desmana moshata* (BM 1919.7.7.2313). Only illustrations were available of the fossil desmans. The technique of measurement is that used by Reed (1951).

Humerus, Figure 4 A, B
Length—18.1 mm
Proximal width—4.8 mm
Distal width—10.2 mm
Head thickness—4.1 mm
Shaft width—2.8 mm
Shaft thickness—2.2 mm

Humerus is apparently about one-third larger than those of *Mygalinia* and *Galemys* and about four-fifths the size of that of *Desmana*. Head of the humerus is rounded. There is no indication of elongation of head to ovoid outline as in other desmans. According to Dr. Charles Reed (Personal

communication), who examined the material, the only other talpid with a rounded head on the humerus is the Asiatic shrew mole *Uropsilus*. The head of the *Hydroscapheus* humerus is not separated from the lesser tuberosity as in *Desmana* and *Galemys*. The lesser tuberosity is smaller than in *Desmana*. Bicipital groove is not covered to form a tunnel as in living desmans and is rather shallow. It is not known whether or not *Mygalinia* has a covered bicipital groove. Orientation of pectoral ridge is similar to *Desmana*. Prominent deltoid process is farther posterior than in *Desmana*. Small ridge runs from deltoid process to neck of the humerus head in *Hydroscapheus*. The short teres tubercle is set off from the ovoid shaft of humerus (Fig. 4 A).

Distal end of humerus is broadly flattened as in other desmans. Entepicondylar foramen opens into deep fossa on anterior side as in *Desmana*. Indistinct olecranon fossa is shallower than in *Desmana*. No fossa for origin of great ligament of *M. flexor digitorum profundus*. This fossa or pit is well developed in *Desmana*. In *Hydroscapheus* a flat surface directed anteriorly may have acted as an area of attachment for great ligament of *M. flexor digitorum profundus*.

Clavicle, Figure 4 G
Length—8.4 mm
Height—1.0 mm
Thickness—0.8 mm

Clavicle is generally similar in outline to that of *Desmana* but differs in lesser details. Proximal end of *Hydroscapheus* clavicle is broader and flatter than those of *Desmana* and *Galemys*. The distal articular surface is different from that of *Desmana*. In *Desmana* posteriorly directed surface of distal end is ovoid in outline. Articular area is flattened, and surface is irregular. In *Hydroscapheus* articular surface, directed posteriorly, is long and narrow and has an irregular face.

Femur, Figure 4 D, E
Length—19.7 mm
Breadth of shaft—3.0 mm
Proximal breadth—7.9 mm
Distal breadth—condyles—6.4 mm
Thickness of shaft—1.9 mm

Femur of *Hydroscapheus* resembles other desmans in outline. It has the same size relationship to the femur of *Desmana* as the humerus. Shaft appears to be more slender than in *Desmana*, but this may be largely the effect of different arrangement of the third trochanter. It is more proximal in *Hydroscapheus* than in *Desmana* and is not well separated from the greater trochanter. The third trochanter and greater trochanter of the new genus form a long, narrow, rugose attachment area instead of separate attachment areas as in *Desmana* and *Galemys*. Head of femur in *Hydroscapheus* is ovoid, not rounded as in *Desmana* and *Galemys*. It has the appearance of being directed more anteriorly than in *Desmana*, but the relative position of ligamental attachment seems to be the same. Patellar surface of femur of *Hydroscapheus* is nearly at right angles to shaft; in *Desmana* the angle is less than 90°. Sesamoids of epicondyles in the new species are larger than those of *Desmana*.

Tibia-fibula, Figure 4 F
Distal breadth—6.4 mm

Tibia-fibula of *Hydroscapheus* is known only from distal fragments. The two bones are well fused. Posteriorly the tibia-fibula has three distinct grooves; *Desmana* has two. Articular surface for astragulus of *Hydroscapheus* is broader and shallower than that of *Desmana*.

Caudal vertebrae are similar to those of *Desmana* and indicate a long, heavy, fleshy, flattened tail.

The overall similarity of the skeletal elements of *Hydroscapheus* to living desmans indicates its position in the Desmaninae. The rounded head of the humerus suggests that movement is not so restricted as in other talpids, indicating that *Hydroscapheus* was not as good a burrower as many talpids. However this does not restrict it from burrowing. The fleshy tail and the broad distal area of the humerus made *Hydroscapheus* a good swimmer, thus the name *Hydroscapheus* (water-digger).

The appearance in North America of a mammal whose subfamily is not known outside Europe indicates how little is known of the historical biogeography of smaller mammals.

Order CHIROPTERA

A distal fragment of a humerus is referable to the Chiroptera, UOMNH F-2517, Figure 4 C. The proximal end is missing which makes family designation uncertain.

Order LAGOMORPHA

Family OCHOTONIDAE

Ochotona spanglei n.sp.

(Figures 5, 6)

Type: Left lower jaw with P3-M3, UOMNH F-4083, Figures 5 A, 6 F, 6 G.

Type Locality: McKay Reservoir.

Diagnosis—A pike about the size of the living North American species. The character of the $P\bar{4}$-$M\bar{3}$ is similar, but there is a rounded external lobe on $P\bar{3}$. Posterior and anterior faces of this tooth

are straight. Named in honor of Ray Spangle who discovered the McKay Reservoir locality.

Description—$P\bar{3}$ is triangular in outline with two external re-entrant angles, posterior one is slightly deeper. A re-entrant on the anterior face of the tooth forms an anterior external rounded loop. There is a lesser groove on the anterior internal face of the tooth. Fossettids are apparently lacking. Cement is present. $P\bar{4}$-$M\bar{3}$ are not distinct from living North American pikas. This species differs from others in the rounded anterior external lobe and straight anterior and posterior faces of the $P\bar{3}$.

Discussion—This occurrence of the genus *Ochotona* is the earliest known in North America. The family is recorded from both North America and Eurasia prior to this appearance. *Ochotona* apparently appears on both continents at the same time. Since this is the only record in North America in the Hemphillian and there are apparently no others until the Pleistocene, the present record may possibly represent an unsuccessful immigration.

Family LEPORIDAE

Hypolagus oregoneneis n.sp.

(Figures 5, 6)

Type: Left lower jaw with P3-M3, UOMNH F-4094, Figures 5 B, 6 B, 6 C, 6 E.

Paratypes: Lower jaws, UOMNH F-2702, F-2907, F-4037, F-4036, F-2906, F-3064, F-2908, F-2063, F-3663; right maxilla fragment with P2, UOMNH F-4099.

Additional material: 4 $P\underline{2}$, 52 $\underline{M}$'s, 13 $\underline{I}$, 17 $\bar{I}$, 13 $P\bar{3}$, 10 $\bar{M}$'s, 7 astragali, 21 calcanea, 11 humerus fragments, 1 femur fregment, 13 tibia fragments, 2 ulna fragments, 2 radius fragments, 3 scapula fragments, 1 pelvis fragment, and 3 trapesia.

Diagnosis—A large *Hypolagus* with grooves and striations on the anterior face of the lower P3. There are two grooves on the face of the upper P2 but only one re-entrant angle opening on the anterior face. Larger than *H. vetus* (Kellogg).

Description—Lowers: Outline of P3 is more semicircular than triangular, but the internal border is terminated by a distinct crest at the widest point. Posterior external re-entrant angle is L-shaped with open base; it extends about halfway across the tooth. There is a small lake lingual to the end of the re-entrant. This lake often has a line of small lakes entering each column of the tooth. Anterior re-entrant angle is an open V and is about one-third as long as the posterior. Anterior face often has three grooves running the full length; the deepest is at the antero-labial edge of the tooth, one is just anterior to the widest point of the tooth, and the third is about halfway between. All these grooves are not always present. Several smaller grooves, also characteristic of the anterior face, give a corrugated effect.

The molariform teeth P4-M2 are similar to *Hypolagus vetus* (Kellogg) and have a small lake in each column. In many specimens a string of tiny lakes extends from this lake to the exterior edge of the tooth.

M3 is smaller and shorter than the other teeth. Anterior column is crescentic, and posterior one, a rounded triangle; each column has a small lake.

Uppers—Outline of P2 is ovoid. A single re-entrant angle opens near lingual border of anterior face. There is a distinct groove in the tooth face at this point. About halfway to the labial edge of the anterior face is another prominent groove, a notch or sometimes a gentle curve in the enamel pattern. These grooves are filled with cement.

Comparisons—*Hypolagus oregonensis* is a large form comparable in size to *Lepus californicus californicus* Gray. The lower jaw and skeleton do not differ noticeably from *Lepus*. The new species is larger than known *Hypolagus* species. Grooving of the anterior face of the $P\bar{3}$ and $P\underline{2}$ is peculiar to this species.

Measurements—Type UOMNH F-4094.
Diastema—17.1 mm
Depth of lower jaw below P4—12.5 mm
$P\bar{3}$-$M\bar{3}$—alveoli—16.9 mm
$P\bar{3}$-$M\bar{3}$—occlusal—14.4 mm

	Antero-posterior (*mm*)	Transverse (*mm*)
$P\bar{3}$	3.2	2.8
$P\bar{4}$	3.0	3.5
$M\bar{1}$	2.9	3.4
$M\bar{2}$	2.7	3.3
$M\bar{3}$	1.9	2.1
Paratype UOMNH F-4099		
$P\underline{2}$	1.6	2.9

Order RODENTIA

Suborder SCIUROMORPHA

Superfamily APLODONTOIDEA

Family APLODONTIDAE

Liodontia sp.

A single molar, UOMNH F-3632, is referable to this genus.

Family MYLAGAULIDAE

Mylagaulus sp.

(Figure 6 D)

A single lower fourth premolar, representing *Mylagaulus* in this fauna is comparable to specimens

from the Rome, Oregon fauna. There are nine lakes. Anterior-posterior measurement is 14.3 mm, and the transverse is 6.6 mm. This is slightly larger than the largest specimens from Rome.

Superfamily SCIUROIDEA

Family SCIURIDAE

Citellus (Otospermophilus) wilsoni n.sp.

(Figure 5)

Type: A complete right lower jaw with P4-M3; incisor missing. UOMNH F-4097, Figure 5 C, C1.

Paratypes: Crushed skull and lower jaws, fore- and hindfeet, radii and ulna, distal end of tibia, UOMNH F-3596.

Type Locality: McKay Reservoir.

Diagnosis—The differences in height of trigonid and talonid and the length of the tooth row are similar to the living *Citellus beechyi*. All lower-dentition teeth are at least as wide as long. Metalophid becomes progressively shorter from M1-M3. Upper P4-M3 are subquadrate in shape. Lophs are nearly parallel on the uppers. Metaloph does not connect to the protocone until late wear. Named in honor of Dr. R. W. Wilson.

Description—Lower Dentition: Hypoconid of P4 is large at the base, giving the tooth a trapezoidal outline. The protoconid and hypoconid are separate in unworn specimens but join with wear. There is no metalophid. Protolophid and protoconid form a small projecting (lingual anteriorly) crest not connected to the parametaconid. Posteriolophid is not connected to hypoconid in unworn specimens but connects with wear. Hypoconid is present in unworn specimens. Small entoconid appears as a serration in posterioloph in unworn material but is more prominent in worn specimens. Ectolophid is reduced.

M1-M2 are about as wide as long. Talonid basin is smooth. Protolophid connects the parametaconid and protoconid. Metalophid does not reach the parametaconid but descends into the talonid basin just short of it. Trigonid basin then opens into the talonid basin. Posterolophid is smooth in unworn specimens, mesostylid and entoconid are reduced. Posterolophid is broadly connected to the hypoconid.

M3 is as wide as long and nearly a right triangle in occlusal outline. Protoconid is in the position of the right angle. Metalophid is short and descends directly to the talonid basin. Posterolophid connects smoothly to the hypoconid. The talonid basin floor has slight rugosities but is smooth overall. Ectostylid is reduced.

Upper Dentition: P3 is small (1 mm in diameter) with single cusp and root.

Metaloph of P4-M2 does not connect to the protocone until late stages of wear. Hypocone forms a distinct projection on the side of each tooth. Mesostyle is present. Teeth are subquadrate. Lophs are nearly parallel. The metaconule is at the end of the metaloph. Protoloph and posterior cingulum form a U. Protoloph and metaloph are about the same height and a little higher than the posterior and anterior cingulum. Parastyle is prominent and as high as the protoloph and metaloph.

M3 is not much larger than M2. Metaloph is absent. Posterior cingulum curves more than in M2 but is directed posteriorly. The tooth is almost heart-shaped. Apex is the protocone.

Comparisons—The new species is about one-fifth larger than *C.* (*Otospermophilus*) *gidleyi* Merriam, Stock, and Moody. The trigonid basin in *O. gidleyi* is complete in M1-M3 but not in *O. wilsoni*. The metalophid does not enter the talonid basin in the M2 or M3 as in *O. wilsoni*. The difference in height of crown between talonid and trigonid is similar in the two species. The uppers of *O. gidleyi* are not known.

C. (*Otospermophilus*) *argonatus* Stirton and Goertz is also a small species closer in size to *O. gidleyi* than to *O. wilsoni*. The trigonid of *O. argonatus* is curved posteriorly rather abruptly in contrast to the other two species. The $P\underline{4}$-$M\underline{1}$ are the only known teeth of *O. argonatus*.

An otospermophilid in the Thousand Creek fauna is closer to *O. argonatus* or *O. gidleyi* than to *O. wilsoni*.

Citellus rexroadensis Hibbard differs from the above species in having the protoconid and parametaconid widely separated.

On the skull of *C.* (*Otospermophilus*) *wilsoni* the infraorbital foramen is semicircular. The posterior border of the base of the zygomatic arch is opposite the M1. The masseteric tubercles are well developed. Tooth row of uppers is 11.6 mm in UOMNH F-3835.

Measurements—Type UOMNH F-4097

	Antero-posterior (*mm*)	Transverse (*mm*)
$P\underline{4}$	1.9	2.2
$M\underline{1}$	1.9	2.7
$M\underline{2}$	2.4	2.7
$M\underline{3}$	3.1	2.9

Citellus (Citellus) mckayensis n.sp.

(Figure 5)

Type: Left lower jaw fragment, UOMNH F-3627, Figure 5 D, D1.

Type Locality: McKay Reservoir.

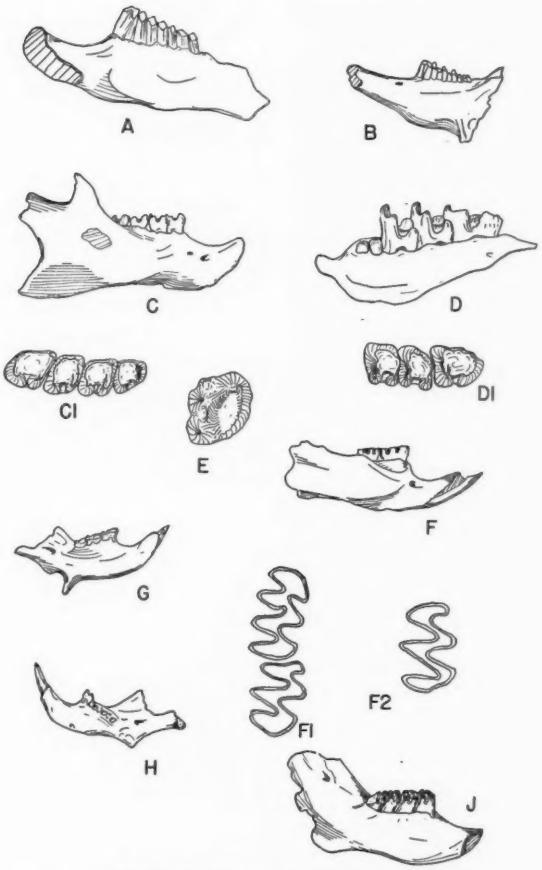

FIGURE 5.—LAGOMORPHS AND RODENTS

A.—*Ochotona spangeli*, type, F-4083, left lower jaw, ×2.1
B.—*Hypolagus oregonensis*, type, F-4094, left lower jaw, ×0.54
C.—*Citellus* (*Otospermophilus*) *wilsoni*, type, F-4097, right lower jaw, ×1.1
C1.—*Citellus* (*Otospermophilus*) *wilsoni*, occlusal view lower dentition, ×2.1
D.—*Citellus* (*Citellus*) *mckayensis*, type, F-3627, left lower jaw fragment, ×2.1
D1.—*Citellus* (*Citellus*) *mckayensis*, occlusal view lower M1–M3, ×2.1
E.—*Marmota oregonensis*, type, F-3625, left lower M1, occlusal view, ×2.1
F.—*Prosomys mimus*, type, F-3667, right lower jaw, ×2.1
F1.—*Prosomys mimus*, type, lower M1–M2, occlusal view, ×7.1
F2.—*Prosomys mimus*, F-3638, upper M1, occlusal view, ×7.1
G.—*Pliozapus solus*, F-2480, left lower jaw, ×2.1
H.—*Leptodontomys oregonensis*, F-3633, type, right lower jaw, ×2.1
J.—*Perognathus sargenti*, F-3637 ,type, left lower jaw, ×2.1

Diagnosis—Molars increase in size from $\overline{M}1$–$\overline{M}3$. A species about the size of living *C.* (*Citellus*) *columbianus*. Trigonid is much higher than talonid on all the molars. A distinct notch is present between posteriolophid and parametaconid. Metalophid connects progressively farther down on parametaconid from $\overline{M}1$ to $\overline{M}3$. $\overline{M}1$ and $\overline{M}2$ are wider than long; $\overline{M}3$ is longer than wide.

Description—M1 is slightly wider than long. Trigonid is much higher than talonid. Hypoconid is lower than posterolophid. Parametaconid is much higher than protoconid. Posterolophid is separated by a distinct notch from the parametaconid. Trigonid basin is complete and formed by the protolophid and metalophid.

M2 is similar to M1. Metalophid does not con-

nect as high on the parametaconid as in M1. Trigonid basin is complete.

M3 is longer than wide and much larger than the M2. Occlusal outline is a modified obtuse triangle, obtuse angle at the protoconid. Metalophid connects at base of parametaconid. A prominent entoconid forms a lophid which projects into the talonid basin and is directed towards the hypoconid. There is a small notch in the occlusal outline where this lophid leaves the posterolophid. Hypoconid is large and not bifurcated as in many living species. As on other molars a prominent notch separates the posteriolophid and the parametaconid.

Comparisons—Citellus (*Citellus*) *mckayensis* is the earliest known ground squirrel referable to the subgenus *Citellus*. Its presence with otospermophilid ground squirrels shows that the genus *Citellus* had already radiated into its several subgenera by Hemphillian time. Mandibles tentatively referred to this species are comparable to those of living species, but reference is somewhat tenuous because they do not contain teeth. Similarity in size between the *C. wilsoni* and *C. Mckayensis* makes differentiation of skeletal postcranial elements impossible.

Measurements—Type UOMNH F-3627.
M1-M3 7.5 mm

	Antero-posterior (*mm*)	Transverse (*mm*)
M$\bar{1}$	1.8	2.3
M$\bar{2}$	2.0	2.6
M$\bar{3}$	3.5	2.0

Marmota oregonensis n.sp.

(Figure 5)

Type: unworn left M$\bar{1}$, UOMNH F-3625, Figure 5 E.

Paratype: Little worn right M$\bar{1}$, UOMNH F-3626.

Type Locality: McKay Reservoir.

Diagnosis—A marmot about the size of the living *M. monax*. Has a large trigonid basin. Floor of talonid basin has several ridges or rugosities similar to those in *M. nevadensis* Kellogg.

Description—Protoconid and parametaconid of M$\bar{1}$ are well separated making the occlusal outline of the tooth quadrate. Protolophid is strongly connected to protoconid and parametaconid. The complete metalophid forms a relatively large trigonid basin in the unworn tooth. A protoconulid is present. Entoconid is distinct but small and connected to the posterolophid only at the base. Mesostylid is small but distinct. An ectolophid is also present. Posterolophid is partly separated from the hypoconid by a small hypoconulid. Talonid basin has a rugose floor with a deep groove extending around the antero-lateral border. This groove is bridged by one of the rugosities at the entolophid.

Comparisons—Marmota oregonensis is much larger than *M. minor* and much smaller than *M. nevadensis*. Its characters are like those of *M. nevadensis*. It is also smaller than *M. mexicana* Wilson from the Yeopmera fauna (Rincon fauna).

Measurements—Type UOMNH F-3625.

	Antero-posterior (*mm*)	Transverse (*mm*)
M$\bar{1}$	4.8	5.1

Family CASTORIDAE

Subfamily CASTOROIDINAE

Dipoides smithi Shotwell

The small beaver *Dipoides* is common in this fauna. The specimens from McKay Reservoir are described elsewhere (Shotwell, 1955a).

Subfamily CASTORIDINAE

Castor sp.

A fragment of a large upper incisor UOMNH F-4071 is the only evidence of *Castor* in the fauna. The tooth is 9.9 mm wide and 8.4 mm anteroposteriorly. Enamel is restricted to the flat anterior face. The specimen is larger than living *Castor* of North America and slightly larger than specimens referred to *C. californicus* Kellogg. *Castor* has been described previously from the Hemphillian Rome fauna of Oregon by Wilson (1937).

Superfamily GEOMYOIDEA

Family GEOMYIDAE

Pliosaccomys dubius Wilson 1936

A complete left lower jaw UOMNH F-3631 and several mandible fragments are present. The ascending ramus is not higher than that in the modern *Geomys*, from which it differs in the absence of the pit at the internal base of the coronoid process. These characters were not distinguishable in the type of *Pliosaccomys*.

Family HETEROMYIDAE

Perognathus sargenti n.sp.

(Figures, 5 6)

Type: Left lower jaw with damanged ascending ramus, broken incisor, and P4-M3, UOMNH F-3637, Figures 5J, 6A.

Type Locality: McKay Reservoir.

Diagnosis—Premolar very molariform with suggestion of six cusps. A large form with molars much like the living *Perognathus hispidus*.

Named in honor of Mr. and Mrs. S. Sargent who contributed much of their time in the early collecting at the type locality.

Description—Lower jaw more massive than modern forms. Although broken, the ascending ramus appears to have been higher than that of modern species. The proximal end of the incisor is well above the dental foramina as in living species. Anterior external cingulum is prominent in the P4, M1, and M2 and is part of the occlusal surface of the tooth in the state of wear of the type material. Anterior external cingulum is reduced in the $\bar{M}3$. Two anterior cusps are well separated in the $\bar{P}4$ with a groove extending down the anterior face of tooth, probably not being removed by wear. Anterior cusps of the molars are partly separated on their posterior side as in the living species. Posterior cusps of the P4 are partly separated by a valley on anterior side. Those of the molars are separated on the posterior side. Posterior external (stylar cusp) is attached to the posterior internal cusp in the stage of wear exhibited in the type material. Probably it is separate in unworn or less-worn teeth.

Unlike other forms of *Perognathus* the two lophs of the molars are connected by a small ridge twinned on the P4. *Perognathus sargenti* differs from other species in its progression towards a sexituberculate pattern. This gives the premolar a molariform appearance. The new species might be given generic status since only four cusps are described for the premolar in the generic diagnosis of *Perognathus*. The fact that many living species of *Perognathus* exhibit well-developed cingular cusps in the milk premolars, however, indicates that the new species should be included in this genus.

Measurements—P4-M3—4.6 mm.

	Antero-posterior (*mm*)	Transverse (*mm*)
P4	0.8	1.0
M1	1.1	1.4
M2	1.3	1.5
M3	1.0	1.1

Family EOMYIDAE

Leptodontomys oregonensis n.gen., n.sp.

(Figures 5, 6)

Type: A complete right lower jaw with incisor and P4, UOMNH F-3633, Figures 5H, 6H.

Type Locality: McKay Reservoir.

Diagnosis—Anterior and posterior cingula complete but not as high as the prominent cusps and did not take part in early wear of the tooth. Wear pattern is E-shaped. Molars apparently little if any larger than the premolar.

Description—$\bar{P}4$ measures 0.8 mm transversely and 0.7 mm antero-posteriorly. It is low-crowned and has two roots. Posterior and anterior cingula are not as high as occlusal surface in little-worn tooth. Protoconid and metaconid connected by a single metalophid. Mesoconid, the smallest cusp, is triangular in outline and joins the protoconid and hypoconid by an ectolophid. Section of ectolophid from mesoconid to hypoconid is shorter than that from mesoconid to protoconid. Lingual valley is large and Y-shaped. Labial valley is nearly straight, trending anteriorly. Alveoli for M1-M3 indicate three rooted molars. M1 and M2 the two anterior root alveoli are small, the posterior one large (nearly twice as big as anterior ones. M3 roots have similar equilateral triangle arrangement, but the posterior root is not much larger than the anterior ones.

Characters of the lower jaw: there is no pit or depression between M3 and coronoid process. Small foramina are numerous on the lingual side; one just outside the anterior lip of the dental foramen, one just below the dental foramen, and a small foramen posterior to the M3. There are also small foramina below the P2, M1, and M2. There is a prominent tuberosity near the ventral border of the mandible on the lingual side directly below the anterior edge of the P4. Condylar process is directed posteriorly. Angle is slightly inflected. There is no masseteric crest. Masseteric fossa is rather flat. The upper border curves up to meet it in a sharp point just below the P4. Mental foramen is in line with the upper border of the masseteric fossa on the labial side of the mandible about halfway between the incisor and P4. Incisor face is rounded. Cross-section outline is ovoid. Enamel is restricted to the antero-labial sides. Incisor crosses the tooth row near the middle. Angle between the tooth row and incisor is small, 8° to 10°. The diastem is nearly as long as the tooth row.

Comparisons and taxonomic position—*Leptodontomys* does not compare with any modern families of rodents or with any known Pliocene family. The tooth pattern, the shape of the masseteric fossa, the peculiar arrangement of molar roots, and shape of the incisor are like the Oligocene *Adjidaumo*. It differs from this genus by having a poorly developed posterior cingulum, a smaller mesoconid, and widely separated protoconid and metaconid on P4. P4 of *Leptodontomys* is more molariform than P4 of *Adjidaumo*. Resemblance is of family magnitude; therefore, this new genus is placed in the family Eomyidae. Another middle-

Pliocene form similar but much larger than *Leptodontomys* is *Kansasimys* Wood (1936). This genus is strikingly like various eomyids but has four roots on the molars. Wood does not compare it with members of this family. He describes the masseteric fossa as ending in a sharp angle, and this character is apparent in eomyids. There seems to be no immediate need for a new family for either of these two genera, although skull characters may require such a distinction.

Measurements—Tooth-row alveoli P4-M3—2.9 mm.

Greatest length lower-jaw incisor to coronoid—11 mm.

Suborder MYOMORPHA

Superfamily MUROIDEA

Family CRICETIDAE

Subfamily MICROTINAE

Prosomys mimus n.gen. n.sp.

(Figure 5)

Type: Right lower jaw with incisor and M1-M2, ascending ramus broken just above level of tooth row, UOMNH F-3667, Figure 5 F, F1.

Paratypes: Right maxilla fragment with M1, UOMNH F-3638, Figure 5 F2.

Type Locality: McKay Reservoir.

Diagnosis—Teeth rooted and low-crowned. Re-entrant angles open and without cement. Smaller than living *Arvicola*, to which it is closely related. Lower M1 with straight-sided re-entrant angles, anterior loop semicircular with flat base, adjacent re-entrant angles meet directly, others alternate with three alternating triangles. Upper M1 has anterior loop and four alternating triangles.

Description—Lower dentition: $\underline{M1}$ has 2 roots; not as high-crowned as *Mimomys*. There is a posterior loop, three alternating triangles, and an anterior loop. Anterior loop is semicircular and smooth, much as in *Ondatra*. There is no indication of an additional re-entrant angle. Posterior border of anterior loop is straight, the two adjacent angles *d* and *e* meet squarely. Anterior border of middle internal re-entrant angle *c* has a slight distal notch. Other re-entrant angles are straight-sided. All re-entrants are broadly open, V-shaped. There is no cement. Internal triangles are higher than exterior triangles, but the bases of both are about equal size.

M2 has a posterior loop and four alternating triangles. Re-entrant-angle borders are straight; angles V-shaped. There is no cement. Fourth triangle has a rounded anterior border. Internal triangles are larger than external triangles. M2 is smaller than M1, but difference is not as great as in *Mimomys*.

Upper Dentition: M1 has one anterior and two posterior roots, anterior loop, and four alternating triangles. Borders are straight; internal re-entrants are U-shaped, and external ones are V-shaped. Internal triangles are smaller, and their apices are more rounded.

Alveoli of M2 indicate two anterior roots.

Characters of the mandible: shallow groove between the tooth row and coronoid process. There is a foramen at base of groove opposite M3. Incisor is round-faced, passes under the tooth row below M3, and extends on above occlusal surfaces. Dental foramen is below anterior root of $\underline{M1}$.

Comparisons—The only other Hemphillian microtine known is *Goniodontomys* from the Rome fauna. It differs from *Prosomys* in that the triangles of the teeth are opposite instead of alternating. *Goniodontomys* may be related to *Microtoscoptes* Schaub from the upper Pliocene of Asia. This genus also has the triangles opposite. *Mimomys* of the Blancan of North America and the Villafranchian of Europe and Asia is the form most closely related to *Prosomys*. *Mimomys* differs from *Prosomys* by having an additional re-entrant angle in the $\underline{M1}$ which is not as long in relation to the height of crown as the other re-entrant angles. This additional re-entrant wears to a lake. The shape of the posterior border of the anterior loop is an inflected chevron, not straight as in *Prosomys*. *Mimomys* is a much larger form. The anterior borders of the re-entrant angles are not straight as in *Prosomys* but have a distinct notch distally as in the modern *Ondatra*. The re-entrants are more closed than in *Prosomys*. The close relationship of *Mimomys* to the genus is evident by the incomplete additional re-entrant angle, the low-crowned rooted teeth, lack of cement, and similarity in the $\underline{M2}$'s and $\underline{M1}$'s. The step from *Prosomys* to *Mimomys* is apparently a phylogenetic one.

Discovery of this early microtine, which is closely related to the modern voles and lemmings, allows some speculation as to phylogenetic relationships of these rodents. There are many possible progressions from a basic type suggested by *Prosomys*: increase in size, increase in height of crown, addition of triangles, and complication of the borders of the re-entrant angle. Several segregated groups show that such progressions are usually combinations of several of the features listed, one being more predominant than others. Listed below are the groups suggested.

(1) Increase in size, some addition of triangles, but remaining rooted and moderately low-crowned. Represented by *Ondatra*.

(2) Moderate increase of number of triangles, some increase in size, but still rooted. *Prosomys, Mimomys, Ogmodontomys, Arvicola.*

(3) Addition of many triangles, little increase in size, and rooted at some time in ontogeny. *Pliophenacomys, Phenacomys.*

(4) Great increase in height of crown and in number of triangles and loss of roots. *Microtus.*

This does not include all known genera but shows certain examples. These groups are largely evident in M1. Other teeth maintain the same general arrangement of triangles in all forms. M2-M3 become relatively smaller.

Measurements—M1-M3 aveoli, 5.4 mm.

	Antero-posterior (*mm*)	Transverse (*mm*)
M1	1.9	1.1
M2	1.5	1.3
M1	2.0	1.2

Superfamily DIPODOIDEA

Family ZAPODIDAE

Subfamily ZAPODINAE

Pliozapus solus Wilson 1936

(Figure 5)

A left lower jaw complete with incisor and M1-M3, UOMNH F-2480, is in the collection from McKay Reservoir. The teeth are at about the same stage of wear as the type material. M1-M3, 3.7 mm.

Order CARNIVORA

Family CANIDAE

Subfamily BOROPHAGINAE

Osteoborus sp.

(Figure 6)

Osteoborus is represented by a distal fragment of a humerus, occipital bone with condyles, calcaneum, astragalus, and a single upper fourth premolar, UOMNH F-4093. P4 has a vestigial protocone similar to that of *O. littoralis* VanderHoof. Metacone has three deep serrations. Paracone is more rounded than in *O. diabloensis* Richey. P4 cannot be definitely referred to any known species for which upper teeth are known.

Subfamily CANINAE

Canis condoni n.sp.

(Figure 6)

Type Lower jaw with M2, UOMNH F-3241, Figure: 6 K.

Type Locality: McKay Reservoir.

Diagnosis—A small dog about the size of *Vulpes fulva*. Lower M2 transitional between *Tomarctus* and *Canis* in the development of the paraconid.

Description—Lower dentition: hypoconid and entoconid of M1 connected by a ridge (Fig. 6 L, N). There is a small but well-developed accessory cusp between the entoconid and metaconid.

M2, paraconid present, small and separated somewhat from the protoconid by a minute valley. Protoconid and metaconid about equal size and opposite. A small crest connects metaconid to anterior edge of the tooth and reaches the paraconid, resulting in a closed trigonid basin. There is a prominent anterior labial cingulum. Hypoconid is large. Entoconid is represented by a low ridge, running around the heel from hypoconid to metaconid.

Upper Dentition: protocone of P4 distinct with a small high single cusp (Fig. 6 M). Blade of metacone is flat-topped in outline. Paracone is high and pointed. There is a slight internal cingulum on the metacone.

Taxonomic Position—The ridge connecting the hypoconid and entoconid in the M1 and the complete trigonid of the M2 suggests a primitive *Canis*. These characters rarely appear in *Vulpes*. Slenderness of the lower jaw is foxlike, but a logarithmic graph of living and fossil dogs and foxes shows that slenderness of foxes is a function of size.

Comparisons—Small and sometimes indistinct paraconid of the M2 distinguishes this species from others of *Canis*.

Family MUSTELIDAE

Subfamily MUSTELINAE

Pliotaxidea sp.

A fragmental ramus UOMNH F-3243 with a well-worn M1 in place is referable to the genus *Pliotaxidea*. A specific designation cannot be made with available material.

Plesiogulo sp.

(Figure 6)

A maxilla fragment containing P4-M1, UOMNH F-3656, and a fragmental M1, UOMNH F-2441, both from the right side, represent *Plesiogulo* in the fauna. Their position in the deposit and occlusion suggest they are from the same individual (Fig. 6 P, Q). Three species of *Plesiogulo* are recognized, *P. monspessulans* Viret from Montpellier, France,

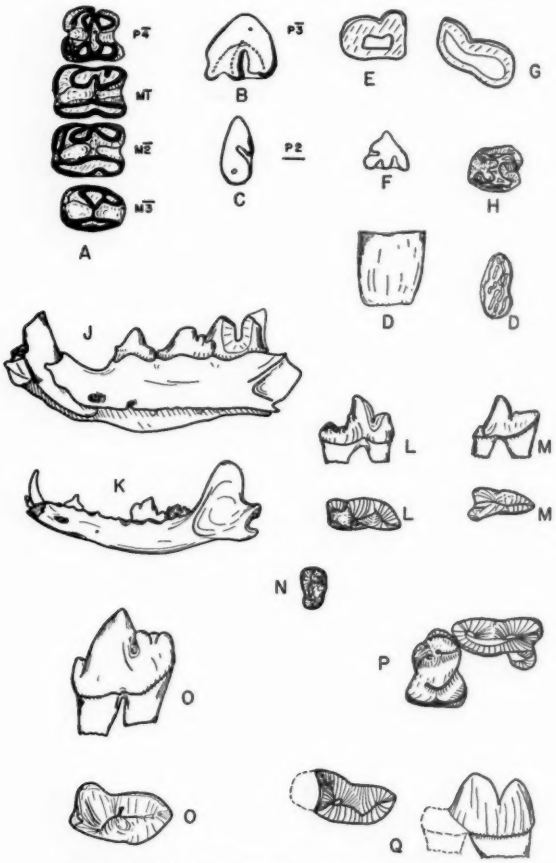

FIGURE 6.—LAGOMORPHS, RODENTS, AND CARNIVORES

A.—*Perognathus sargenti*, occlusal view lower dentition, ×2.1
B.—*Hypolagus oregonensis*, lower right P3, occlusal view, ×3.6
C.—*Hypolagus oregonensis*, upper P2, occlusal view, ×3.6
D.—*Mylagaulus sp.*, lower P4, occlusal and side views, ×0.71
E.—*Hypolagus oregonensis*, cross-section of upper incisor, ×3.6
F.—*Ochotona spangeli*, right lower P3, occlusal view, ×3.6
G.—*Ochotona spangeli*, cross-section, upper incisor, ×7.1
H.—*Leptodontomys oregonensis*, lower P4, occlusal view, ×7.1
J.—*Felis longignathus*, type F-2628, left lower jaw, ×0.71
K.—*Canis condoni*, type, F-3241, left lower jaw, unshaded teeth not part of type, ×0.36
L.—*Canis condoni*, lower M1, occlusal and side views, ×0.71
M.—*Canis condoni*, upper P4, occlusal and side views, ×0.71
N.—*Canis condoni*, lower M1, occlusal view, ×0.71
O.—*Osteoborus sp.*, upper P4, occlusal and side views, ×0.71
P.—*Plesiogulo sp.*, occlusal view upper P4-M1, ×0.71
Q.—*Plesiogulo sp.*, occlusal view lower M1 and side view, ×0.71

P. brachygnathus (Schlosser) from Paote, North China, and *P. marshalli* (Martin) from the Edson Quarry, Kansas. Zdansky (1924) illustrated the variation of P4-M1 outline within the genus. Comparison of the type and referred specimen of *P. marshalli* with casts of Zdansky's illustrated specimens does not reveal any differences which can be used to separate the two forms. The material from McKay Reservoir shows a flatter and possibly more expanded protocone in the upper M1. No species designation for the McKay material is warranted at present.

Family FELIDAE

Subfamily FELINAE

Felis longignathus n.sp.

(Figure 6)

Type: Incomplete left lower jaw with broken canine, P3, P4, M1. M1 with damaged talonid, three small incisor alveoli. UOMNH F-2628, Figure 6 J.

Type Locality: McKay Reservoir.

Diagnosis—A cat about the same size as the ocelot, with a long diastem between canine and $P\bar{3}$. No $P\bar{2}$ present; a much reduced talonid on the M1, and a deep open notch between paraconid and protoconid of $M\bar{1}$.

Description—Mandible with relatively long diastem, two mental foramina, one directly below the middle of the diastem, the other below the $P\bar{3}$. Anterior one is larger. Lower jaw rather deep, the exact depth cannot be determined from the specimen.

Alveoli for three small nearly equal-sized incisors are present in the type.

Canine is rather straight, damaged.

$P\bar{3}$ is about same height as $P\bar{4}$ and $M\bar{1}$. Paraconid and metaconid, about equal size. A small cingulum surrounds the metaconid.

$P\bar{4}$ is larger than P3; has a distinct talonid. Metaconid is distinct from protoconid.

$M\bar{1}$ has paraconid and protoconid separated by a deep open notch. Lingual valley filled by a bulbous cusp not evident in other cats. Posterior side of protoconid is broken away so that exact characters of talonid and metaconid cannot be determined. Discernable characters suggest a much reduced talonid and probably no metaconid.

Taxonomic Position—It is difficult to determine generic identity of Pliocene cats with reduced talonids on the $M\bar{1}$ because of the gradual transition of *Pseudaelurus* to *Felis*. Stock (1934), following Matthew (1910), distinguished *Pseudaelurus* by the three lower premolars. But Simpson (1945) includes Hibbard's *Pratifelis* and *Adelphailurus* under *Pseudaelurus*. Both genera have only two premolars. The genus *Metailurus* of Zdansky (1924) is described by Matthew (1929) as being transitional from *Pseudaelurus* to *Felis*. Matthew (1910) did not consider *Metailurus* separable from *Pseudaelurus*. Stock (1934) maintains that the genus *Metailurus* is distinct and typifies it in part as having two lower premolars.

The new species is smaller than known species of *Pseudaelurus* or *Metailurus*. It has no indication of a $P\bar{2}$. Canine is rather straight. The deep open notch between the protoconid and paraconid is like that in the living lynx and more open than in *Felis palaeosinensis* Zdansky from China. It is referred to *Felis* here because of the reduced talonid of the $M\bar{1}$ and the deep protoconid-paraconid notch in that tooth. Skull material may make such a designation unjustified.

Comparisons—The new species closely resembles *Felis proterolyncis* Savage (1941) from the Optima fauna of Oklahoma. *F. longignatha* is slightly larger and apparently has a proportionately longer diastem. The mandible is not as deep in *F. proterolyncis*. Characters of the teeth are similar in the two species. The bulbous cusp in the lingual valley of the M1 of *F. longignatha* is not present in *F. proterolyncis*.

Subfamily MACHAIRODONTINAE

Machairodus sp.

A proximal fragment of a femur, a metapodial, and the serrated edge of a Saber canine tooth are referred to *Machairodus*.

Order PERISSODACTYLA

Family EQUIDAE

Subfamily EQUINAE

Hipparion sp.

(Figure 7)

Material referable to *Hipparion* consists of a fragmentary upper milk dentition, an upper premolar, metatarsals and metacarpals, an astragalus, and other foot elements (Fig. 7 E, G). Premolar has an ovoid protocone. Hypoconal groove is isolated at the present state of wear. Anterior border of prefossette is without re-entrants. Posterior border has four regular loops exteriorly, followed by a large loop with two re-entrants and a kidney-shaped loop between them. Internal edge of the posterior border is marked by a large bifurcated re-entrant. Postfossette anterior border has a large external loop broken into several small loops. This is followed by a series of three radially arranged re-entrants at internal edge. Posterior border has a single bifurcated re-entrant. Plicaballin is twinned. Shape of protocone is most like *H. anthonyi* Merriam among North American hipparions but is somewhat rounded. Hypoconal groove is closed at an earlier stage of wear in the McKay species than in any other North American horses of this genus. The styles do not rise abruptly from the ectoloph but are molded into it. This gives a semicircular cross section between styles instead of the more or less rectangular one of most species. The McKay species is larger than other known North American forms

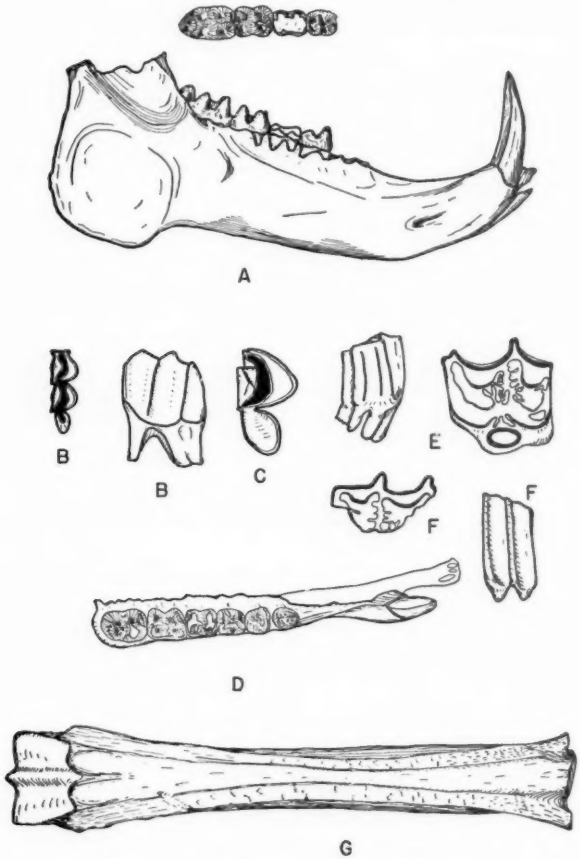

FIGURE 7.—PERISSODACTYLS AND ARTIODACTYLS
A.—*Prosthennops brachirostris*, F-3585, mandible and occlusal view P4-M3, ×0.36
B.—*Procamelus sp.*, lower M3, ×0.36
C.—*Paracamelus sp.*, lower M3 fragment, ×0.36
D.—*Prosthennops brachirostris*, type, F-2767, upper dentition, occlusal view, ×0.36
E.—*Hipparion sp.*, upper premolar, occlusal view, ×2, side view, ×0.36
F.—*?Neohipparion sp.*, upper ?molar occlusal view, ×2, side view, ×0.36
G.—*Hipparion sp.*, metapodial, ×0.36

and is comparable in size with specimens of *H. gracile* Kaup from Pikermi, Greece. In simplicity of the anterior border of the postfossette, complexity of enamel pattern of posterior and anterior border of these fossettes, roundness of the protocone, and mode of style attachment the McKay species is similar to *H. gracile*. It differs from *gracile* in the character of the hypoconal groove and the flatter lingual side of the protocone. The characters of this tooth are apparently a mixture of those seen in North American and Eurasian hipparions. The milk teeth UOMNH F-2763 are similar to those of *gracile* but differ in shape and attachment of the styles.

Metacarpals and metatarsals and astragalus are like *H. gracile* both in size and character.

?Neohipparion sp.

(Figure 7)

Styles and fragments of the fossettes of an upper-cheek tooth in the material from McKay Reservoir are similar to species of *Neohipparion*, but reference to a species is not possible (Fig. 7 F).

Family RHINOCEROTIDAE

Teleoceras sp.

This rhinoceros is common in the McKay sediments, but no skull material is known. A few teeth are present including an incisor, M1, M2, damaged upper and lower molars, and canines. Appendicular skeletal elements are numerous: complete and fragmental specimens of five femora, three humeri, five radii, two pelvi, several hind- and forefoot elements, plus many fragmentary pieces. The taxonomic situation in this genus as described by Stirton (Matthew, 1932, p. 390) makes specific designation of this material valueless.

Order PROBOSCIDIA

A proboscidian is represented in the fauna by a centrum fragment. No generic or family assignment can be made.

Order ARTIODACTYLA

Family TAYASSUIDAE

Prosthennops brachirostris n.sp.

(Figure 7)

Type: Restored palate with canines and complete cheek-tooth series, UOMNH F-2767, Figure 7 D.

Type Locality: McKay Reservoir.

Paratypes: Lower jaw complete except for incisors and P2's and P3's, UOMNH F-3585, Figure 7 A.

Diagnosis—A peccary with a short diastem. No internal cingulum on lower-cheek teeth, and only a slight external one. Upper P2 is triangular with three cusps and a slight external cingulum.

Description—Upper-jaw teeth are little-worn in the type. P2 is triangular with three cusps and a slight external cingulum. P3 is more quadrate and bears four cusps. P4 has a posterior and anterior cingulum. There is also a posterior accessory cusp. M1-M3 have a slight internal cingula and strong external ones. There are accessory cusps in the valleys. M3 is rectangular and tends to widen anteriorly.

Lower-jaw canines are large and well developed. No cingulum on interior side of cheek-tooth series, and a slight one externally. Valleys are generally clean of accessory cusps.

Comparison with other species—*P. oregonensis* Colbert differs from the new species in the lack of a strong external cingulum on the upper-cheek teeth and a much longer diastem. Both *P. longirostris* Thorpe and *P. serus* (Cope) differ in their much greater diastem. *P. serus* also tends to have numerous cuspids. The new species is apparently larger and has squarer teeth than *P. niobrarensis* Colbert. Other species of *Prosthennops* differ in these same characters.

Family CAMELIDAE

At least two species of camels are represented in the fauna; one is large, about the size of *Paracamelus*, the other is small, near the size of *Procamelus*.

The large species (Fig. 7 C) is known from a fragmental lower right third molar, distal end of a humerus, tibia, phalanges, astragalus, pelvis, and metapodial fragments. The smaller species (Fig. 7 B) is represented by lower right M3, M2, two well-worn upper M3's, and a metapodial. Styles of the lower third molar are slightly more prominent than in *Procamelus coartatus* Stirton, while in other characters it closely resembles that species. A lower M3 from Thousand Creek figured and described by Merriam (1911, Fig. 50 A, B, UC No. 12765) is close to the McKay Reservoir species. The material known makes it necessary to designate the small species as probably representing *Procamelus* or *Pliauchenia* and the larger one as representing *?Paracamelus*.

REFERENCES CITED

Kurtén, B., 1952, The Chinese Hipparion fauna: Soc. Sci. Fennica, Comm. Biol., tome 13, no. 4, 82 p.

Matthew, W. D., 1910, The phylogeny of the Felidae: Am. Mus. Nat. History Bull. 28, p. 289–316

—— 1929, Critical observations upon Siwalik mammals, Am. Mus. Nat. History Bull. 61, p. 437–560

—— 1932, A review of the rhinoceroses with a description of Aphelops material from the Pliocene of Texas: Calif. Univ. Dept. Geol. Sci. Bull., v. 20, p. 411–480

Merriam, J. C., 1911, Tertiary mammal beds of Virgin Valley and Thousand Creek in northwestern Nevada, Pt. II, Vertebrate faunas: Calif. Univ. Dept. Geol. Sci. Bull., v. 6, p. 199–304

Reed, C. A., 1951, Locomotion and apendicular anatomy in three soricoid insectivores: Am. Midland Naturalist, v. 45, p. 513–671

Savage, D. E., 1941, Two new middle Pliocene carnivores from Oklahoma, with notes on the Optima fauna: Am. Midland Naturalist, v. 25, p. 692–710

Shotwell, J. A., 1955a, A review of the Pliocene beaver *Dipoides*: Jour. Paleontology, v. 29, p. 129–144

—— 1955b, An approach to the paleoecology of mammals: Ecology, v. 36, p. 327–337

Simpson, G. G., 1945, The principles of classification and a classification of mammals: Am. Mus. Nat. History Bull., v. 85, 350 p.

—— 1947, Holarctic mammalian faunas and continental relationships during the Cenozoic: Geol. Soc. America Bull., v. 58, p. 613–688

Stock, C., 1934, Skull and dentition of the Miocene cat, *Pseudaelurus*: Geol. Soc. America Bull., v. 45, p. 1051–1058

Teilhard, P., and Leroy P., 1942, Chinese fossil mammals: Inst. Geobiol. Pekin, no. 8, 142 p.

Wilson, R. W., 1936, A Pliocene rodent fauna from Smiths Valley, Nevada: Carnegie Inst. Wash. Pub. 473, p. 15–34

—— 1937, New middle Pliocene rodent and lagomorph faunas from Oregon and California: Carnegie Inst. Wash. Pub. 487, p. 1–19

Wood, A. E., 1936, A new rodent from the Pliocene of Kansas: Jour. Paleontology, v. 10, p. 392–394

Wood, H. E., *et al.*, 1941, Nomenclature and correlation of the North American continental Tertiary: Geol. Soc. America Bull., v. 52, p. 1–48

Zdansky, O., 1924, Jungtertiare carnivoren Chinas: Paleontologica Sinica, II, fas. 1, p. 1–155

Museum of Natural History, University of Oregon, Eugene, Oregon

Manuscript Received by the Secretary of the Society, January 10, 1955

BULLETIN OF THE GEOLOGICAL SOCIETY OF AMERICA
VOL. 67, PP. 739-762, 7 FIGS. JUNE 1956

STATISTICAL ANALYSIS OF LOW-LEVEL RADIOACTIVITY OF PENNSYLVANIAN BLACK FISSILE SHALE IN ILLINOIS

BY W. C. KRUMBEIN AND H. A. SLACK

ABSTRACT

Black fissile shale in Pennsylvanian cyclothems in the western part of the Illinois Basin shows low-level radioactivity as measured by alpha-particle emission. Preliminary analysis showed a ten-fold variability in radioactivity among closely spaced samples, with no apparent concentration in particular zones of the thin shale units. These relations favored design of a sampling experiment for evaluation of average radioactivity of the shale and for detection of regional radioactivity gradients.

Interlocked regional and local sampling designs were set up and provided 176 samples for a regional study and 32 samples for a local study, including evaluation of the experimental error. The interlocked designs furnished data for estimating stratigraphic variability of samples spaced from about 1 foot to 18 miles apart.

Strip mines, mine dumps, and some well cores provided regional samples of the 3-foot black fissile shale bed overlying Coal No. 6 in an area about 200 miles long and 20 miles wide. The local samples were collected from four localities within a single mine. In both sampling designs the maximum variability occurred at the lowest sampling level, indicative of a "spotty" distribution of radioactivity in the black shale. Neither the geological evidence nor the statistical analysis suggested any strong regional gradient in radioactivity over the area studied. Both the geological and statistical data support the inference that the radioactive material was associated with the depositional environment, rather than introduced by wholly diagenetic processes.

CONTENTS

TEXT

	Page
Introduction	740
Purpose of the study	740
Acknowledgments	740
Stratigraphic relations of black fissile shale	740
Areal distribution of black fissile Brereton shale	741
Radioactivity of black fissile shales	742
Design of sampling plan	743
General statement	743
Regional sampling design	744
Local sampling design	746
Analysis of the samples	747
Procedure	747
Statistical treatment of the data	747
Radioactivity maps	749
Environment of black fissile shale deposition	751
Conclusion	753
Appendix	753
Statistical model	753
Graphic representation of the hierarchial model	756
Confidence limits on mean radioactivity	757
Statistical tests of significance	758
Application of cost function to sampling data	760
References cited	760

ILLUSTRATIONS

Figure	Page
1. Isopach map of black fissile Brereton shale, southwestern Illinois	742
2. Township and supertownship layout for regional sampling plan	745
3. Radioactivity map of black fissile Brereton shale	750
4. Statistical model for regional sampling hierarchy	754
5. Statistical model for local sampling hierarchy	755
6. Variance components estimated by models of Figures 4 and 5	756
7. Graphical presentation of hierarchical model, illustrated by Sample 1 of Mine *a*, Township I of Supertownship F	757

TABLES

Table	Page
1. Average spacing of sample locations	746
2. Radioactivity of black fissile Brereton shale (regional samples)	747
3. Radioactivity of black fissile Brereton shale (local data)	748
4. Analysis of variance and variance components (regional samples)	748
5. Analysis of variance and variance components (local samples)	749
6. Tests of hypotheses (relative variability, regional and local data)	759
7. Tests of hypotheses (homogeneity of individual sampling levels, regional and local data)	760

Introduction

A conspicuous member of many western Illinois Pennsylvanian cyclothems is a black fissile shale a few feet thick that occurs above the coal in the upper half of the cyclothem. The shale is relatively massive in the subsurface, but on exposure it develops roughly rectangular blocks with a high degree of fissility. The weathered shale splits easily into paper-thin sheets parallel to the bedding.

The shale commonly grades upward to gray calcareous shale, or into a harder black shale that weathers into small flakes. Downward the fissile shale locally grades into black carbonaceous lumpy shale. In some cyclothems the uppermost shale member may also be black, but it has a soapy feel and weathers into ellipsoidal masses. This paper is concerned with only the thin black fissile shale member of the cyclothem.

The senior author has been interested for some years in areal variations among black fissile shales. Applications of conventional particle-size and mineral analysis are hindered, however, by the fine grain size, the difficulty of disaggregation, and the flocculating effects of ferrous ions and organic matter. Within the past few years interest was reawakened by recognition that the low-level radioactivity of the shales is susceptible of accurate measurement. Thus, alpha-particle emission may be used to study the areal variation in at least one attribute of the shale apparently related to the depositional environment.

Purpose of the Study

Preliminary sampling experiments described in a later section show that radioactivity of cyclothemic black fissile shale varies widely among closely spaced samples without displaying any consistently higher values at the top or bottom of the unit. In a statistical sense these findings suggest that the black fissile shale can be treated as a single homogeneous sampling stratum. It was accordingly decided to apply statistical design to the problem of estimating average radioactivity over an extensive area, as well as to detect the presence of any significant regional gradients in the radioactivity.

The present paper illustrates a statistical design believed to be applicable to a variety of sampling problems in geology. The thin black fissile shale, averaging about 3 feet in thickness, is treated as a single sampling unit, but the design can be extended to thicker shales having several zones of concentration or change. Such extension involves mainly the superposition of additional sampling strata on the basic plan. Some of the design elements in more elaborate sampling plans are touched upon later.

Acknowledgments

The writers are indebted to J. A. Simon, Head of the Coal Division of the Illinois Geological Survey, for making available much information on the black Brereton shale and for co-operation in selection of sampling localities. Dr. Paul E. Potter of the Illinois Geological Survey was most helpful in the design of the sampling plan. The writers are indebted to Dr. W. H. Clatworthy, formerly at the Statistical Engineering Laboratory of the National Bureau of Standards, for advice and friendly criticism of the first draft of the statistical treatment. The writers are solely responsible for any departures from statistical rigor in this paper, however. Colleagues in the Department of Geology at Northwestern were helpful in discussing geological implications of the statistical data. The Graduate School of Northwestern University supported the study with research grants, which are gratefully acknowledged.

Stratigraphic Relations of Black Fissile Shale

Black fissile shale is member number 8 in Weller's "ideal cyclothem" of western Illinois (Weller, unpublished 1933 ms.; *see* also William and Payne, 1942, p. 86). Coal is member number 5, and in the ideal cyclothem the black shale is separated from the coal by gray shale and argillaceous marine limestone. In most western Illinois cyclothems these two members are missing, and the black fissile shale (if present) lies directly above the coal.

Extensive mapping of cyclothems by Weller and Wanless (Weller, 1930; Wanless, 1931;

Wanless and Weller, 1932) has shown that the black fissile shale is one of the most persistent members of those cyclothems in which it occurs. The shale is usually relatively thin, seldom exceeding several feet in thickness, and more commonly averaging 3 feet or less. The distinctive characteristics of the shale, and its association with a particular set of beds in a cyclothem permits easy correlation over wide areas.

The senior author's experience with Pennsylvanian black shales has been mainly with lower Desmoinesian cyclothems in western Illinois and parts of Missouri, Kansas, and Oklahoma. In selecting a black shale for the present study, it was desirable to find one that could be sampled over a large area. At the suggestion of J. A. Simon, Head of the Coal Division of the Illinois State Geological Survey, the black shale overlying the Herrin (No. 6) coal of western and southern Illinois was selected. Mr. Simon made available a large amount of subsurface data and gave every aid in location of suitable sampling localities.

Coal No. 6 occurs in the Brereton cyclothem (Wanless, 1931) which straddles the McLeansboro-Carbondale contact in earlier stratigraphic classification. The cyclothem occupies a position near the top of the Desmoinesian (Moore *et al.*, 1944), and its limestone member is equivalent in part to the Fort Scott Limestone of the mid-continent.

The Brereton cyclothem varies somewhat in character along its outcrop belt in Illinois. In north-central Illinois the basal member is the Vermilionville sandstone. Coal No. 6 is prominently developed and extensively mined, and the black fissile shale occurs at some distance above the coal, separated from it by gray shale and thin sandstone. The Brereton limestone lies above the black shale.

In western Illinois the basal sandstone of the Brereton cyclothem locally develops into a channel sand, the coal is somewhat thinner than it is farther north, and the black fissile shale lies immediately above the coal. In southwestern Illinois the basal sandstone is missing, the coal is well developed and extensively mined, and the black fissile shale lies directly on the coal, with a well-developed marine limestone above.

Areal Distribution of Black Fissile Brereton Shale

Although the black fissile shale is a persistent member in the Brereton cyclothem, it is not everywhere equally well developed. In some mines the black shale in the roof is irregularly interrupted by patches of gray shale or by local areas in which the overlying limestone forms the coal roof. Instances are known in which small lenses of gray shale lie between the coal and the black shale, so that when seen in the mine roof, the black shale is missing. There are other instances where gray shale occupies the position between coal and limestone in mines and boreholes. In western Illinois the Brereton black shale commonly seen in outcrop is absent locally (Wanless, 1931).

The occurrence of several kinds of black shale in parts of the Brereton cyclothem also makes it difficult to interpret subsurface bore-hole data unless cores are available. Driller's logs may record 20 feet or more of black shale overlying Coal No. 6, but later information shows that only a few feet are fissile in the sense used here. The Illinois State Geological Survey files contain thousands of borehole records, and this information was summarized on a township basis through the courtesy of J. A. Simon. The records were interpreted in the light of Mr. Simon's experience and probably provide the best set of thickness data now available.

The data compiled by Mr. Simon were arranged into an isopach map by the writers (Fig. 1). The number of observations ranged from one or two to more than 50 per township, but because of the questionable value of some of the records and the great variability in adjacent boreholes the map was prepared as a generalization of the maximum thickness encountered in each of the more than 150 townships for which data were available. The average thickness is less than 3 feet.

The regional maximum-thickness pattern of the black fissile Brereton shale is patchy and irregular, although several east-west belts of thicker and thinner shale may be seen. There is no marked thickness gradient along or across the map, since the range from 0 to 5 feet occurs over the whole map area. The areas of zero thickness have patches of shale, but these are

too small and irregular to be shown on the map. Similar irregularities occur in other thickness areas, and a large-scale map would show greater spottiness.

No evidence was found that the upper or lower portions of the fissile shale were consistently more radioactive than the samples taken from interior points.

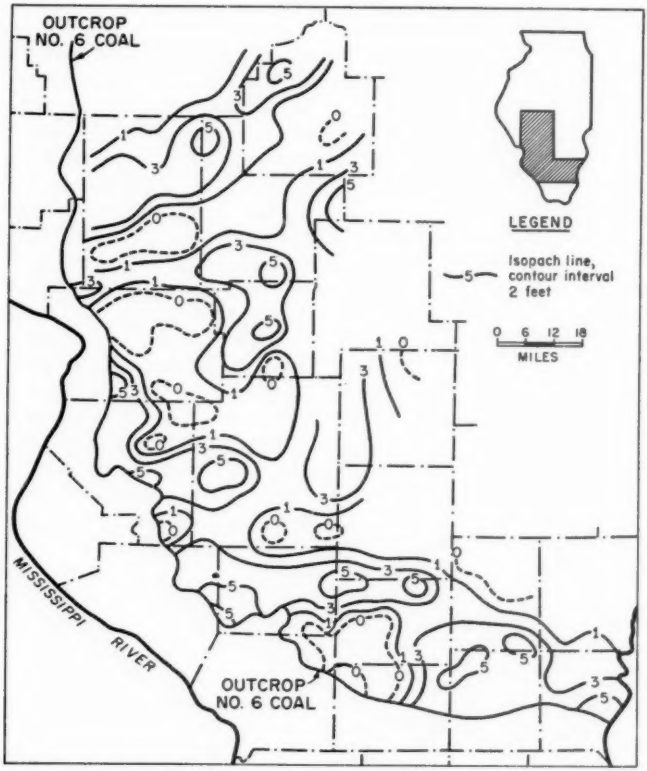

FIGURE 1.—ISOPACH MAP OF BLACK FISSILE BRERETON SHALE, SOUTHWESTERN ILLINOIS
Contours indicate maximum thickness encountered in outcrops and boreholes. Dashed lines enclose areas of essentially no black fissile shale.

RADIOACTIVITY OF BLACK FISSILE SHALES

Black fissile shales of cyclothems display a low level of radioactivity. In 1952, the writers conducted experiments on scattered samples obtained in large part from the Illinois State Geological Survey. The writers noted a ten-fold variation in alpha-particle emission and conducted preliminary sampling experiments to determine whether the fissile shale is uniform in its radioactivity. Samples from the top and bottom contacts in several areas were compared with samples from within the shale, and the radioactivity was highly variable throughout.

A formal experiment of this type is reported elsewhere (Slack and Krumbein, 1955). Four vertical sections were taken through the 20-inch bed of black fissile shale above Coal No. 6 in a strip mine in southern Illinois (Saline County). The first section was randomized along the mine wall and the other sections laid off at 10-foot intervals. Each vertical section was divided into four sampling strata consisting of the top and bottom 2 inches and two central zones each 8 inches thick. Four samples were taken at random in each sampling zone. In this experiment probability samples were used to provide a more rigorous test, although the

samples were continuous through the top and bottom sampling zones, varying only slightly in their horizontal placement. Half of the 64 samples were thus collected within 2 inches of the top or bottom contacts, and the interior samples covered substantially the complete 16 inch thickness of the central sampling zones.

A statistical hypothesis was set up to the effect that no significant differences were present between the four vertical sections along the shale bed or between the four sampling zones within the bed. Analysis of variance showed no significant differences in either direction at the conventional 5 per cent significance level. From this and other experiments it was inferred that the black fissile shale has no significantly high radioactivity concentration near the contacts and no interior zones of significantly higher radioactivity over the area sampled. In a sampling sense this implies that all samples in each grid could have been drawn from a single homogeneous radioactivity population. The practical application is that the thin black fissile shale may be treated as a single sampling stratum. Had there been evidence of a higher concentration of radioactivity at the top, for example, the black fissile shale could have been divided into two or more sampling strata, each subject to its own sampling plan.

The radioactivity of the black fissile shale was measured with a Radiation Counter Laboratory alpha scintillometer containing a 1.5-inch diameter activated zinc sulphide phosphor. The samples were powdered and placed in a source dish of the same diameter as the phosphor, to a depth sufficient to be considered infinitely thick for alpha-ray emission. Counts were recorded by a conventional scaling device. Additional details of the collection and analysis of the count data are given in Slack and Krumbein (1955).

A sample of the black shale was analyzed for its uranium content through courtesy of T. F. Bates. This analysis provides a conversion factor from alpha counts to uranium content. Under the experimental conditions used, 1 alpha particle per minute per 1.5-inch diameter circle of powdered shale is equivalent to 0.0031 per cent of uranium. Although these analytical data provide a basis for relating the alpha-particle counts to uranium content of the shale, the treatment in this paper is based on the alpha-particle data.

Design of Sampling Plan

General Statement

The small-scale sampling experiments on the black fissile Brereton shale led to the conclusion that the unit could be treated as a single sampling stratum. Where this condition holds, the design of a sampling scheme is greatly simplified. However, where the study concerns thicker shales in which color, fissility, radioactivity, texture, or other characteristics vary from top to bottom, an important element in the sampling design is the division of the total shale thickness into natural sampling strata on the basis of the observed properties. Each sampling stratum would then be equivalent to the single sampling stratum of this study.

Subdivision of thick rock bodies into thinner, more homogeneous units for sampling represents the statistical process of "stratification". Stratified sampling in such cases carries the advantage that the variability within any stratum is less than the total variability that would be encountered if the samples were distributed over the whole major unit. Selection of the thin black fissile shale above Coal No. 6 involved stratification of the total population of all black shales to the particular subpopulation of black fissile shale in a specific cyclothem. Moreover, restriction of the sampling to unaltered portions of the shale represents additional stratification within the sampling unit. Stratification may be carried further, but with each extension the inferences drawn from a stratum become increasingly restricted to that part of the total population.

Although the black shale unit is here considered as a single homogeneous sampling stratum, the ten-fold variability in radioactivity requires closely spaced samples on the one hand to obtain necessary local detail, and widely spaced samples on the other to include the broader regional effects. The problem is similar to many other geological investigations in which a knowledge of the detailed section is required at the outcrop level, and yet the outcrop (or well) data must be fitted together to provide an adequate regional picture.

Several choices are available in the specific method of sampling thin stratigraphic units. Channel samples extend through the total thickness, but unless each thin layer is analyzed separately, the variability within the unit is averaged out. Moreover, the number of localities where complete channel samples could be collected was limited, and their use would severely limit the areal scope of the study. Reliance was accordingly placed on hand-specimen sized samples collected on a probability basis (Cochran, Mosteller, and Tukey, 1954) to provide a larger area for study and to permit estimation of sample-to-sample variability in the unit. It was felt that the risk of missing thin highly radioactive layers was slight on the basis of the preliminary sampling experiments. Unless such layers were relatively numerous and widespread it seems doubtful that they would do more than affect the regional mean slightly and inflate the variability at local or intermediate sample spacings. If the layers were numerous, probability sampling should pick them up on the average in proportion to their relative frequency of occurrence.

Any sampling design which covers an entire area with closely spaced samples would entail prohibitive time and cost. Fortunately, the problem may be approached by an adaptation of multilevel (hierarchical) sampling. This type of sampling was introduced into geology by Olson and Potter (1954) and Potter and Olson (1954) in connection with a regional study of cross-bedding in basal Pennsylvanian sands. Potter and Siever (1955) extended the method to a four-level study of local and regional variability in basal Pennsylvanian and upper Chester sediments.

Multilevel sampling may be designed to include as many sampling levels as desired. It is possible to start with large units as the top sampling level, and "nest" successively smaller sampling units within the large units until samples about a foot apart are obtained. Such a complete hierarchical design would require a large number of samples. It was decided to separate the master design into a regional part and a local part, the latter including a laboratory subsampling level. This modification of standard hierarchical sampling provides widely spaced samples in the regional design and closely spaced samples in the local design and furnishes data on the accuracy of the laboratory measurements. It also reduces the number of samples that would be required for a single hierarchy having the same number of sampling levels.

Regional Sampling Design

Multilevel sampling requires selection of a master sampling unit of such size that preferably 10 or more master units will cover the area to be studied. The present area is about 200 miles long and 20 miles wide. This was divided into 11 master units, each 3 by 3 townships on edge. Potter and Siever (1955) refer to such units as "supertownships", and the term is retained here, although the master blocks need not have 9 townships in every application of the design.

Once the largest units are selected, smaller units may be nested within them. In the present design two townships were nested in each supertownship, two mines were nested in each selected township, and four samples were collected at each selected mine. The regional design thus has four sampling levels.

The manner of selecting townships, mines, and samples deserves comment. The statistical model is a randomized block design in which townships, mines, and samples are selected at random. The largest units are laid out with the problem in mind and constitute the major blocks used in this study. In some studies the major blocks may be selected at random from a larger population of blocks.

Collecting samples at random is considered questionable by some geologists. This view is justified if the samples are taken with no regard to the geological requirements of the study. Actually, randomization is a systematic process involving some mechanical means, such as a random-number table, coins, dice, or a deck of cards. The purpose of randomization is to insure that no personal bias enters the sampling plan. Before the randomizing process is applied, the subject-matter problem is set up so that samples can be drawn without invalidating later subject-matter decisions or inferences.

As pointed out, the writers concluded that the thin black fissile shale could be treated as a

single sampling stratum. Hence, to provide that all parts of the shale have an equal chance of entering the sample, a mechanical process may be used to eliminate subjective decisions regarding the exact points at which samples are to be taken. Restriction of the sampling sites to mines, wells, or other localities which provide unaltered samples places some restraints on complete randomization. When cost, physical difficulty of taking samples, or other considerations limit complete randomization, various weighting schemes are available for adjusting the data. These added complexities are treated in Cochran, Mosteller, and Tukey's discussion of probability and nonprobability sampling (1954).

In laying out the regional sampling design all known underground and strip mines, active or inactive, were indicated on a work map of the mining area for Coal No. 6 in southwestern and southern Illinois. The area was divided into 11 major sampling units (supertownships) consisting of nine townships each (Fig. 2). In theory two townships are selected at random from each supertownship, and two mines selected at random in each chosen township. It was found that some townships were blank and occasional townships had only a single mine. Random numbers were drawn, and if one fell on a blank township, another drawing was made. This practice probably introduced a slight bias into the population variability at the level affected.

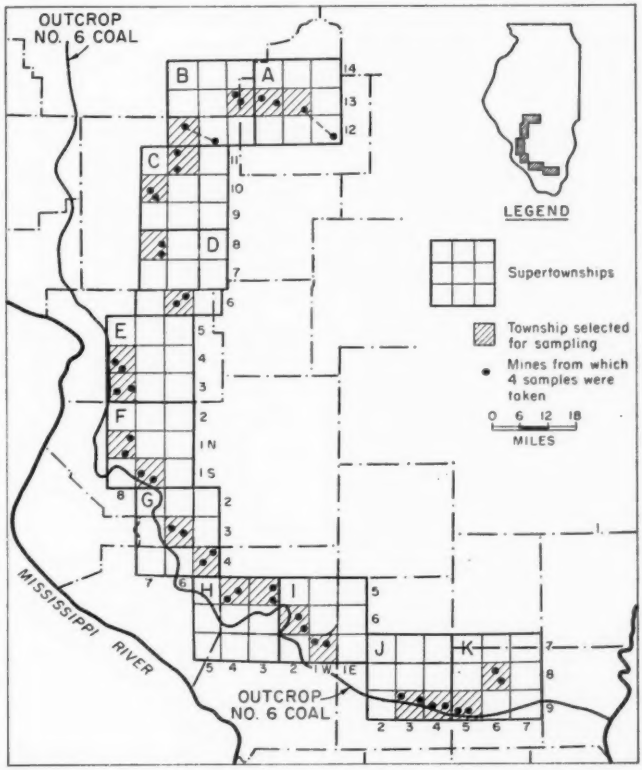

FIGURE 2.—TOWNSHIP AND SUPERTOWNSHIP LAYOUT FOR REGIONAL SAMPLING PLAN

As the sampling proceeded north along the supertownships, no special difficulties were encountered until supertownships A and B were reached. In these only one township in each had two or more mines. It was necessary either

to modify the sampling design by introducing subsamples of unequal size or to obtain two mines from adjacent townships. The latter was chosen because it seemed preferable to introduce a slight bias into the variability at this sampling level rather than complicate the model by introducing an unequal number of subsamples.

A decision also had to be made regarding the manner of collecting samples from each mine. Many of the underground mines and some of the strip mines were inactive. Thus it was not feasible to obtain samples directly from walls or roof in most townships. Accordingly, four randomized positions were taken on mine dumps or spoil heaps where necessary, and samples were taken from the most recently excavated blocks of black fissile shale at each site.

No other black fissile shale could be present in the mine dumps, and they provided a much larger choice of sampling localities. Comparison of mine-dump samples with others collected from known locations in strip mines showed no significant difference between the variances of the two groups (Dixon and Massey, 1951, p. 88). It is believed that this sampling procedure did not strongly influence the results of the study.

Experience showed that samples within a single strip mine ranged from about 0.1 to 1.5 miles apart. Assuming that the same order of distance applies to samples from mine dumps, the regional sampling design provides samples on its lowest level about half to three-quarters of a mile apart on the average. To extend the sampling design to the local outcrop level, one of the supertownships with active strip mines was selected at random beforehand for a local sampling hierarchy.

Local Sampling Design

United Electric Fidelity Mine No. 11 (Duquoin County, Illinois) was selected in supertownship I to provide a local hierarchy based on four detailed sampling grids. The grids were randomized in the mine and ranged from 0.25 to 2 miles apart, with an average spacing of about 0.7 miles. Hence, the top level of the local hierarchy provided about the same spacing as the lowest level of the regional hierarchy.

The black fissile Brereton shale averaged about 40 inches thick in the grids. Each grid area was divided into four major rectangles 20 inches by 5 feet, and each major rectangle was subdivided into four minor rectangles, each 10 inches by 2.5 feet. (*See* Fig. 5, Appendix.) In each case the position of the first vertical was randomized on the exposure. All exposures were recent and unweathered.

TABLE 1.—AVERAGE SPACING OF SAMPLE LOCATIONS

(a) *Regional Design*	
Between adjacent supertownships (center to center)	18.0 miles
Between townships within supertownships	9.3 miles
Between mines within townships	3.1 miles
Between samples within mines	0.5 miles
(b) *Detailed (Local) Design*	
Between grids within a mine	0.7 miles
Between major units within grids	4.6 feet
Between minor units within major units	2.2 feet
Between samples within minor units	0.5 feet
Between replicates within samples	(subsamples split from powdered material)

In sampling from the grids, two major rectangles were selected at random in each grid, two minor rectangles were selected at random in the chosen major rectangles, and two samples were taken at random from the selected minor rectangles. The samples within the minor rectangles averaged less than a foot apart.

The local grids provide data for estimates of within-mine variability at several sampling levels. Table 1 indicates how the regional and local hierarchies tie together to provide seven levels of sampling, ranging from points less than a foot apart within a mine to locations about 18 miles apart between adjacent supertownships. In addition, an eighth level is provided for estimating the laboratory error from duplicate analyses of the grid samples.

If a single hierarchy were used to collect samples spaced from 18 miles to half a foot

apart, it would have been necessary to prepare four grids at each mine and in essence repeat the local grid 44 times, yielding a total of 44 by 32, or 1408 samples. By separating the master hierarchy into two parts at the samples-within-mines level, the project required only 176 regional and 32 local samples, roughly 15 per cent of those required by the complete design. This modification of standard hierarchical designs thus has some advantages over complete designs where considerations of time or cost are involved.

There is a risk involved in combining two hierarchies in this manner, inasmuch as the single randomly selected mine could depart widely from the average regional radioactivity. It was anticipated from the preliminary studies, however, that no strong radioactivity gradient is present regionally, so that although the two hierarchies do not yield identical numerical results, the complete data provide estimates of sampling variability of the entire range of sample spacing.

TABLE 2.—RADIOACTIVITY OF BLACK FISSILE BRERETON SHALE
(Alpha particles per minute, regional samples)

Townships	Mines	Samples	Supertownships										
			A	B	C	D	E	F	G	H	I	J	K
I	a	1	1.20	2.97	1.04	2.30	1.17	5.10	2.08	2.79	2.07	3.77	4.89
		2	1.46	1.76	1.04	4.38	0.92	2.17	3.67	1.05	2.22	2.10	1.60
		3	1.63	1.82	1.59	3.85	1.24	1.38	0.86	1.60	1.14	4.48	2.27
		4	3.17	2.23	1.99	3.50	1.33	1.73	1.15	1.29	3.67	2.82	1.73
	b	1	1.70	3.47	3.47	3.87	8.67	3.05	1.12	1.21	0.83	1.85	2.00
		2	1.34	5.77	2.71	1.04	3.97	4.57	4.90	0.87	1.36	1.61	7.23
		3	1.55	2.57	3.30	3.33	1.68	0.99	1.80	1.30	2.93	1.63	2.18
		4	2.50	3.15	3.13	3.37	3.40	1.43	1.27	3.17	1.58	3.05	2.10
II	a	1	2.33	2.33	2.62	1.11	1.68	1.34	1.33	1.51	1.24	2.93	1.40
		2	0.90	1.24	2.73	1.19	1.26	4.43	3.33	8.25	1.29	2.91	1.81
		3	2.68	1.52	2.57	4.37	1.53	6.62	5.97	2.70	1.23	1.16	1.21
		4	2.48	2.00	2.62	6.13	1.92	3.33	1.07	1.78	0.88	2.43	1.97
	b	1	3.03	1.98	1.19	5.47	1.22	3.10	1.02	3.70	0.95	2.08	1.58
		2	3.30	1.41	3.83	2.22	1.06	5.63	0.99	1.37	1.02	1.73	1.37
		3	2.93	1.38	7.47	4.00	1.20	3.47	4.00	0.98	0.84	1.19	1.19
		4	4.68	1.96	1.42	2.48	1.58	1.06	1.43	2.20	0.84	2.23	4.60

ANALYSIS OF THE SAMPLES

Procedure

The field samples were crushed through a ⅛-mm screen in a Raymond Laboratory Hammer Mill. Subsamples of the powdered material were then withdrawn for measurement in the alpha scintillometer. The time required for 100 alpha particles was recorded and the data expressed as alpha particles per minute per 1.5-inch diameter circle of powder. The samples were measured in random order to avoid any possible bias from using the same order as used in the field collection.

Statistical Treatment of the Data

The observational data for the regional samples are listed in Table 2 and for the local samples in Table 3. Observations based on counts represent samples drawn from a Poisson distribution (Slack and Krumbein, 1955) and as such the spread of the distribution (variance) is equal to the mean value. A square-root transformation is appropriate for statistical analysis in such cases (Bartlett, 1947; Kempthorne, 1952, p. 153). This transformation stabilizes the variance and permits probability statements to be made about the results. Tests for variance stability are given in Dixon and Massey (1951, p. 147) and were applied in the preliminary studies. Statistical analysis in this paper is based on the square roots of the values in Tables 2 and 3.

The average value of the radioactivity for the complete set of regional samples was 2.42 alpha particles per minute per 1.5-inch circle of powdered shale. This represents the grand mean of the raw data, and it is equivalent to a mean uranium content of 0.0075 per cent. Confidence limits may be placed around the grand mean by using the corresponding mean of the square-root transformed data and converting the limits to the raw-data equivalent. Computations are shown in the Appendix and indicate that the grand mean of the raw data has (to a first approximation) a 95 per cent probability of lying between 1.96 and 2.50 alpha particles per minute per 1.5-inch circle of powdered shale. The equivalent uranium values are 0.006 to 0.008 per cent.

TABLE 3.—RADIOACTIVITY OF BLACK FISSILE BRERETON SHALE

(Alpha particles per minute, local data)

Major units	Minor units	Samples	Replicates	Grids			
				1	2	3	4
I	A	1	a	1.20	1.02	1.70	1.52
			b	1.13	1.21	2.01	0.95
		2	a	1.12	2.97	0.93	1.20
			b	1.21	3.03	0.84	1.09
	B	1	a	1.20	2.50	0.92	2.97
			b	1.13	2.65	0.91	3.14
		2	a	3.93	1.54	1.18	2.72
			b	3.96	1.93	1.02	3.19
II	A	1	a	0.98	1.28	2.90	1.48
			b	0.88	1.40	3.00	1.38
		2	a	1.20	0.98	2.73	1.24
			b	1.01	1.02	2.57	1.36
	B	1	a	1.57	0.86	0.84	0.98
			b	1.27	0.71	0.80	0.84
		2	a	1.36	0.82	0.85	1.03
			b	1.03	0.91	0.93	0.88

A single observation in any multilevel sampling design is subject to variations associated with each level of the hierarchy, and these variations need to be isolated to evaluate the data. The specific model used in the present design is described in the Appendix to this paper. The statistical treatment of the transformed data consists of estimating the variance contribution associated with each sampling level. The method used is analysis of variance, and the standard procedures are given in Anderson and Bancroft (1952, p. 325), Olson and Potter (1954), Potter and Olson (1954), Cochran (1953, Chap. 10), Bennett and Franklin (1954, p. 358), and Potter and Siever (1955).

TABLE 4.—ANALYSIS OF VARIANCE AND VARIANCE COMPONENTS

(Regional samples)

(a) Analysis of Variance

Source	Sum of squares	Degrees of freedom	Mean square
Between supertownships	3.7479	10	0.3748
Between townships within supertownships	3.5079	11	0.3189
Between mines within townships	4.5989	22	0.2090
Between samples within mines	21.3174	132	0.1615

(b) Variance Components

Level	Difference	"Sample size"	Component
Supertownships	0.0559	16	0.0035
Townships	0.1099	8	0.0137
Mines	0.0475	4	0.0119
Samples	0.1615	1	0.1615

Table 4 shows the results of the statistical analysis for the regional data. The upper part of the table lists the mean squares in the last column, and these are used as a basis for the estimates of variance components shown in the last column of the lower part of the table. It is apparent from the relative values that the variance "pay-off" is at the lowest regional sampling level. This means that most of the fluctuations among the observations in Table 2 occur between samples within mines. This large contribution to the total variability may be further analyzed by using the data from the local sampling design.

Table 5 shows the analysis of variance and variance components for the local hierarchy. The experimental data suggest that there is no real variance contribution at the grid level, which is equivalent to the sample level in the

regional design. The main variance contributions occur at the minor unit level and at the closely spaced samples-within-minor-units level, which represent sample spacings of about 2 feet and half a foot, respectively (Table 1). The much lower variance contribution of the replicates within samples (duplicate analyses) is evidence of the lack of appreciable laboratory error in the study.

TABLE 5.—ANALYSIS OF VARIANCE AND VARIANCE COMPONENTS

(Local samples)

(a) Analysis of Variance

Source	Sum of squares	Degrees of freedom	Mean square
Between grids (within a mine)	0.0264	3	0.0088
Between major units within grids	1.6359	4	0.4090
Between minor units within major units	2.5948	8	0.3244
Between samples within minor units	1.6013	16	0.1001
Between replicates within samples	0.1210	32	0.0038

(b) Variance Components

Level	Difference	"Sample size"	Component
Grids	−0.4002	16	0.0000
Major units	0.0846	8	0.0106
Minor units	0.2243	4	0.0561
Samples	0.0963	2	0.0482
Replicates	0.0038	1	0.0038

As far as the levels in the local hierarchy are concerned, the variance pay-off is about evenly split between the closely spaced sampling level and the next higher level. It would be possible to attach a third hierarchy of sampling, with samples a few inches or centimeters apart. It is anticipated that the variance contribution of 0.0482 at the sample level in Table 5 would be spread over several additional levels, inasmuch as laboratory studies of black-shale radioactivity (Bates, 1953) have shown that the radioactivity varies strongly on a single microscope slide. On this basis, it would appear that the largest variance component is contributed at the minor-unit-within-grids level in the local hierarchy, and at the township and mine levels in the regional hierarchy.

These estimates of the relative importance of variance components at the sampling levels carry certain implications about optimum spacing of samples. Assuming that the original inference of a single homogeneous sampling stratum is justified, the results indicate that samples need not be collected closer than about 2 feet apart along single outcrops in order to estimate local mean radioactivity values. Similarly, on a regional basis, either the mine or the township may be used as an appropriate sampling level to study regional variations.

In part, sample spacing depends upon the uses to be made of the data. These uses are of two general kinds. One is to estimate mean values at different sampling levels, and the other is to study areal variations in the measured attribute. In most geological problems the regional mean value is of less importance than an evaluation of the regional variation in radioactivity. Such areal variation is best shown on maps, and the sample spacing would be chosen at that level which most effectively brings out the regional trends.

The mean squares in Tables 4 and 5 may be used to test certain statistical hypotheses about the homogeneity of the black-shale radioactivity locally and regionally. Several such hypotheses are illustrated in the Appendix.

RADIOACTIVITY MAPS

The discussion in the preceding section, and the results of the statistical tests in the Appendix indicate that regional maps of black fissile Brereton shale radioactivity may be based either on townships or mines as appropriate sampling levels. Several working maps were prepared by using (1) the average of 16 sample values in each supertownship, (2) the average of 8 sample values in each sampled township, and (3) the average of 4 sample values from each mine. The maps all showed essentially the same pattern, with increasing smoothness of contours and a somewhat lessened range of values as additional samples were included in

the averages. Figure 3, based on 4 samples per mine, is shown here as an example. The control points are the mines shown in Figure 2.

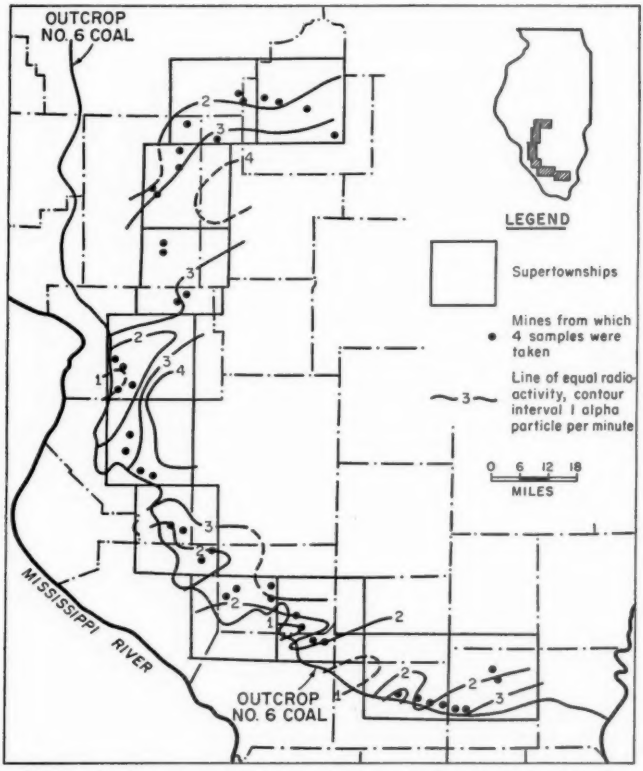

FIGURE 3.—RADIOACTIVITY MAP OF BLACK FISSILE BRERETON SHALE

The radioactivity map shows no marked over-all regional gradient from north to south, although a band of higher values trends across supertownships C and D and a high area lies in E and F, whereas lower values dominate in supertownships H, I, and J. Statistical tests described in the Appendix suggest that at the supertownship level there is some regional heterogeneity in radioactivity, which becomes more marked at the township and mine levels.

The radioactivity map is similar in some respects to the isopach map (Fig. 1), and comparison of the maps suggests that high radioactivity values may be associated with smaller shale thicknesses, as in super-townships C and D. Although a scatter diagram on a township basis showed no significant correlation, there may in fact be a genetic basis for an inverse relationship between shale thickness and radioactivity. The writers are indebted to Dr. John L. Rich of the University of Cincinnati (Personal communication) for suggesting that the more bituminous parts of the shale, presumably richer in radioactivity than other parts with less organic (kerogen) content, would be subject to greater compaction after burial than those parts with higher silt and clay content. By this process the areas where silt and clay are most abundant relative to kerogen would now have, relatively, the thickest shale and lowest radioactivity per unit, whereas where the kerogen content was greatest the shale thickness would be relatively least and the radioactivity per unit would be highest.

The selection of the mine or township level

as the basis for regional radioactivity mapping in this study implies collection of more than a single sample at each control point. Figure 3 is based on means of four individual values and hence averages out the local extremes that may occur in individual samples. The use of averages for regional mapping has a bearing on facies mapping of stratigraphic units. Most facies maps use single wells or outcrops as control points. A design which permits averaging of several wells at each regional control point would smooth the facies lines in the same manner as in the radioactivity map. In facies mapping the problem is complicated by the wide spacing of wildcat wells in some areas. Commonly a decision must be made between the advantage of using averages and the risk of failure to detect significant facies changes if individual values are combined. Potter and Siever (1955) discuss some of the implications of control-point spacing in their study of basal Pennsylvanian and Upper Chester sandstones and limestones.

Multilevel designs provide irregularly spaced control points for contour mapping (Fig. 3). Composite models that extend the multilevel design to include data for estimating regional gradients in rows and columns of major sampling units are discussed elsewhere (Krumbein, 1955). These composite models may be supplemented with evenly spaced control points to provide a more uniform basis for mapping.

Environment of Black Fissile Shale Deposition

The thickness map (Fig. 1) carries several implications regarding the environment in which the Brereton black fissile shale was deposited. There is no evidence of an erosional break between the shale and the overlying marine limestone. This suggests that the original conditions of accumulation were irregular, such as would occur if the shale were deposited on an essentially flat plain with minor surface irregularities transgressed by marine or brackish waters.

Moore (1929) presented an analysis of probable environmental conditions during the Pennsylvanian period:

> "The uniformity and very great extent of many of the Pennsylvanian coal beds and immediately associated strata can mean only that a featureless swampy plain extended throughout the area of coal deposition. The plain was not necessarily horizontal, for a slope sufficiently low to make movement of water sluggish would, in a nearly flat humid region, permit development of broad swamps. It is conceivable, indeed, that any slight existing drainage may have been so ill organized that open waterways were practically nonexistent, the water moving as an extremely sluggish sheet flow."

Inasmuch as the Brereton black fissile shale lies immediately above Coal No. 6, the coal swamps were probably invaded by marine waters which may have spread slowly over the essentially horizontal surface. Such marine invasions may occur without substantial wave action (Keulegan and Krumbein, 1949), thus permitting deposition of marine sediments above the coal with essentially no widespread or intensive reworking of the older deposits.

Variations of water depth in the swamps and irregularities in the peaty surface, as well as broad shallow channels in the swamp would provide a pattern of distribution of the initial invading sea water similar to that in Figure 1. Normal open circulation of the water was effectively restricted, as attested by the properties of the black shale.

The shale contains abundant organic matter and yields oily fumes on heating. It may locally grade laterally into canneloid shale or cannel coal. Fossils in the shale include phosphatic brachiopods, (linguloids and discinids), small articulate brachiopods (*Ambocoelia*), thin-shelled depauperate pelecypods, occasional ammonoids, some fish remains, conodonts, and spores. The fossils are crushed nearly flat.

The fissile shale is relatively rich in iron sulphide, present as pyrite in disseminated grains, nodules, and fossil replacements. Phosphatic nodules may occur, and sideritic concretions, many of which are large, are common in the black fissile shales of some cyclothems. The clay minerals in the black shale are commonly dominantly illitic.

The presence of organic matter, pyrite, phosphatic nodules, siderite, and an aberrant fauna with few calcareous representatives implies a depositional environment of low oxygen content (negative Eh) and mildly alkaline or slightly acidic conditions (pH between 6.9 and 7.8).

These are the characteristics of a humid restricted (euxinic) environment (Fleming and Revelle, 1939; Krumbein and Garrels, 1952). Moore (1929) suggested a combination of extreme shallowness providing too little depth for open circulation or effective wave agitation, and sufficient sunlight to promote abundant plant growth and partial decay as important features of the environment required for quiet undisturbed accumulation of a humous or bituminous muck.

Possibly, the marginal phases of the invading sea carried the black shale environment with them as the sea advanced eastward or northeastward across Illinois. The partially stagnant conditions set up by the initial shallow marine waters as they invaded the coal swamp would be succeeded by open circulation conditions accompanied by Brereton limestone deposition as the water deepened and cleared. Alternatively, if the black shale was deposited simultaneously over its whole area of occurrence, subsequent limestone deposition would require removal of the restrictions to provide normal marine open-circulation conditions.

The local occurrence of gray clay shale directly above the coal suggests that open circulation conditions prevailed here and there during the initial stages, permitting deposition of normal fine-grained detrital sediments. The absence of black shale in local areas where the Brereton limestone lies directly on the coa- suggests that these areas were not covered by the initial marine invasion, but became sites of deposition as the water deepened and permitted normal marine accumulation of carbonates.

The crushed fossils in the black shale support the inference that the material accumulated as a humous or bituminous muck with several times its own volume of water. Subsequent compaction squeezed out the water and crushed the fossils. This process probably also accounts for development of the laminae. Pettijohn (1949, p. 459) suggests that the initial volume of the sediment was perhaps five times its present thickness. The present average thickness of the Brereton black shale ranges from about 18 to 36 inches, so that the colloidal muck could be about 7 to 15 feet thick.

Studies by Bates and co-workers (1953) show that uranium in the Chattanooga black shale is associated with the pyrite-organic-clay complex, apparently very finely disseminated through the rock. The writers believe that the spotty dissemination of radioactivity in the black fissile Brereton shale represents substantially the same kind of distribution of uranium as in the Chattanooga. Marine plants and other organisms probably played a part in extracting and fixing uranium ions from the sea water (McKelvey and Nelson, 1950). The ions would be disseminated through the partially decayed colloidal muck and could have become associated with iron sulphide formed in the restricted environment as well as with accumulating detrital clay.

The absence of high radioactivity at the black fissile shale contacts and of any unusual radioactive "hotspots" in local areas of the region mapped support the inference that the uranium was associated with the depositional environment, rather than having been introduced by wholly diagenetic processes. Diagenetic changes would be concentrated at contacts or in localized areas where structural, ground water, or other conditions favored secondary concentration.

Some of the statistical tests described in the Appendix (Table 6) support the inference of primary environmental control. The tests fail to show that the variation in radioactivity between sampling units of any size is significantly greater than that between the next smaller units nested within them. This means that although the townships, for example, may differ among themselves in their radioactivity, there is no tendency for them to show greater variability in radioactivity than is shown by the mines within them. This relative uniformity at successive levels extends through the hierarchy until individual samples within a local grid are reached.

The results of these tests, which show no evidence of secondary concentration of radioactivity such as would be likely to occur if diagenetic changes were operative in some parts of the map area, suggest that the over-all spottiness of radioactivity is characteristic of the entire sampling hierarchy. The use of about 200 samples, from six sampling levels at spacings of 6 inches to 18 miles, with samples col-

lected on a probability basis, from an inferred homogeneous sampling stratum about 3 feet thick, is believed by the writers to include a wide enough range of areal units to have picked up secondary concentration if it were present.

Conclusion

Increasing emphasis on regional analysis during recent years poses numerous problems on the amount of detail to be included in a study. Choice has to be made between two extremes: examining every well and outcrop, or selecting relatively widely spaced control points which it is hoped will provide an adequate regional picture. Statistical design, especially with multilevel sampling models, can play a large part in this choice of alternative sampling plans.

The present study, based on a thin stratigraphic unit that can be correlated with confidence, and apparently free from any serious sample stratification problems, seemed to offer an opportunity for application of a standard sampling model. The use of two interlocked hierarchies represents a modification of the standard multilevel design and illustrates one way estimates of variability for closely spaced samples can be made from a reasonable number of observations at one or a few localities in the region. In regional terms it was seen that sample spacing based on mines in a township (about 3 miles apart) or on townships within a supertownship (about 9 miles apart) provide adequate data for regional mapping of black fissile Brereton shale radioactivity. If a map is the primary objective, the sampling localities would presumably be laid on a grid, with several samples averaged for each control point.

Sampling designs can be applied to geological problems more effectively if the stratigraphic unit is first "stratified" into relatively homogeneous sampling strata. Each stratum may then be sampled as a unit in its own right, and the data from each stratum can later be combined for estimates affecting the total unit. Cochran (1953) treats stratified sampling in some detail. Where desired, it is possible to adjust the sample spacing in each stratum to obtain equally reliable estimates for each stratum mean. Potter and Siever (1955) discuss this aspect of the sampling problem.

Application of probability sampling in geology deserves detailed consideration. To the extent that probability samples can be taken, the geologist shifts some of the responsibility for valid statistical inferences to the statistician. Samples within a stratum need not be taken completely at random for this purpose; various designs are available (Cochran, 1953) for using systematic samples, cluster samples, grid samples, and others, each having some mechanical means of randomization. Problems associated with nonavailability of samples (covered intervals, lack of outcrops, absence of boreholes) are troublesome in geology, but they have their counterparts in other sampling fields, and adjustments can be made for such situations (Cochran, Mosteller, and Tukey, 1954).

The increasing tendency to use standard statistical designs in geology suggests that the specific model used in this study be made explicit to the reader. The following Appendix contains this technical material plus some discussion of confidence intervals, statistical tests, and cost functions as applied in the present study.

Appendix

Statistical Model

The statistical model used in this study is a standard hierarchical design, described by Cochran (1953, p. 215), Anderson and Bancroft (1952, p. 325), Bennett and Franklin (1954, p. 358), Olson and Potter (1954), and Potter and Olson (1954). The sample layout for the regional design is shown in Figure 4. The random variable X_{ijkm} represents a single observation on an individual sample in the design. The value of the random variable depends on the grand mean μ, plus a contribution α from the i-th supertownship, plus a contribution β from the j-th township in the i-th supertownship, plus a contribution γ from the k-th mine in the j-th township of the i-th supertownship, plus a contribution ∂ from the m-th sample from the k-th mine in the j-th township of the i-th supertownship. The contributions α_i, $\cdots$, ∂_{ijkm} are all considered random variables with mean zero and variances as indicated in the lower left lines of Figure 4. The population mean μ is considered a fixed constant.

The sample layout for a grid in the local hierarchy is shown in Figure 5. Here the random variable X_{rstuv} represents a single observation on a laboratory

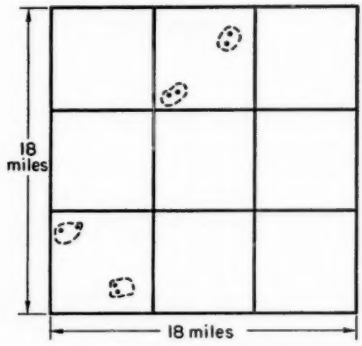

$$X_{ijkm} = \mu + \alpha_i + \beta_{ij} + \gamma_{ijk} + \partial_{ijkm}$$

ANALYSIS OF VARIANCE

SOURCE	SUM OF SQUARES	DEGREES OF FREEDOM	MEAN SQUARE
BETWEEN SUPERTOWNSHIPS	$SS_1 = \frac{\Sigma_i(\Sigma_{jkm}X_{ijkm})^2}{bcd} - \frac{(\Sigma_{ijkm}X_{ijkm})^2}{abcd=n}$	a-1	$V_1 = \frac{SS_1}{a-1}$
BETWEEN TOWNSHIPS WITHIN SUPERTOWNSHIPS	$SS_2 = \frac{\Sigma_{ij}(\Sigma_{km}X_{ijkm})^2}{cd} - \frac{\Sigma_i(\Sigma_{jkm}X_{ijkm})^2}{bcd}$	a(b-1)	$V_2 = \frac{SS_2}{a(b-1)}$
BETWEEN MINES WITHIN TOWNSHIPS	$SS_3 = \frac{\Sigma_{ijk}(\Sigma_m X_{ijkm})^2}{d} - \frac{\Sigma_{ij}(\Sigma_{km}X_{ijkm})^2}{cd}$	ab(c-1)	$V_3 = \frac{SS_3}{ab(c-1)}$
BETWEEN SAMPLES WITHIN MINES	$SS_4 = \Sigma_{ijkm}(X_{ijkm})^2 - \frac{\Sigma_{ijk}(\Sigma_m X_{ijkm})^2}{d}$	abc(d-1)	$V_4 = \frac{SS_4}{abc(d-1)}$
TOTAL	$\Sigma_{ijkm}(X_{ijkm})^2 - \frac{(\Sigma_{ijkm}X_{ijkm})^2}{abcd=n}$	abcd-1	

ESTIMATION OF VARIANCE COMPONENTS

LEVELS	DIFFERENCE	SAMPLE SIZE	VARIANCE COMPONENT
SUPERTOWNSHIPS	$V_1 - V_2$	bcd	$S^2_\alpha = \frac{V_1 - V_2}{bcd}$
TOWNSHIPS	$V_2 - V_3$	cd	$S^2_\beta = \frac{V_2 - V_3}{cd}$
MINES	$V_3 - V_4$	d	$S^2_\gamma = \frac{V_3 - V_4}{d}$
SAMPLES	V_4	1	$S^2_\partial = V_4$

EXPLANATION OF SYMBOLS:

X_{ijkm} = a single observation.
μ = grand mean.
α_i = comp. due to supertwp. i.
β_{ij} = comp. due to twp. j, within supertwp i.
γ_{ijk} = comp. due to mine k, within twp. j, within supertwp. i.
∂_{ijkm} = comp. due to sample m, within mine k, within twp. j within supertwp. i.
$\alpha_i, \beta_{ij}, \gamma_{ijk}$ & ∂_{ijkm} are independent with Mean 0 and variances $S^2_\alpha, S^2_\beta, S^2_\gamma$ & S^2_∂ respectively.

i varies from 1 to a
j varies from 1 to b
k varies from 1 to c
m varies from 1 to d

where
a = number of supertwps.
b = number of twps./supertwp.
c = number of mines/twp.
d = number of samples/mine
n = abcd = total samples collected.

FIGURE 4.—STATISTICAL MODEL FOR REGIONAL SAMPLING HIERARCHY

For convenience of notation and comparison with the mean squares in the analysis of variance table, all variances are shown as S^2. More rigorously the theoretical variances should be shown as σ^2 in the lower left part of this figure.

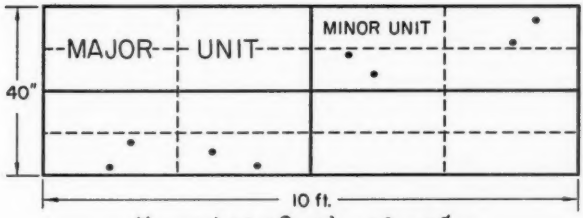

$$X_{rstuv} = \nu + \epsilon_r + \Theta_{rs} + \lambda_{rst} + \rho_{rstu} + \phi_{rstuv}$$

ANALYSIS OF VARIANCE

SOURCE	SUM OF SQUARES	DEGREES OF FREEDOM	MEAN SQUARE
BETWEEN GRIDS WITHIN A MINE	$SS_5 = \frac{\Sigma_r(\Sigma_{stuv}X_{rstuv})^2}{fghp} - \frac{(\Sigma_{rstuv}X_{rstuv})^2}{efghp=N}$	e-1	$V_5 = \frac{SS_5}{e-1} \doteq S^2_\theta$
BETWEEN MAJOR UNITS WITHIN GRIDS	$SS_6 = \frac{\Sigma_{rs}(\Sigma_{tuv}X_{rstuv})^2}{ghp} - \frac{\Sigma_r(\Sigma_{stuv}X_{rstuv})^2}{fghp}$	e(f-1)	$V_6 = \frac{SS_6}{e(f-1)}$
BETWEEN MINOR UNITS WITHIN MAJOR UNITS	$SS_7 = \frac{\Sigma_{rst}(\Sigma_{uv}X_{rstuv})^2}{hp} - \frac{\Sigma_{rs}(\Sigma_{tuv}X_{rstuv})^2}{ghp}$	ef(g-1)	$V_7 = \frac{SS_7}{ef(g-1)}$
BETWEEN SAMPLES WITHIN MINOR UNITS	$SS_8 = \frac{\Sigma_{rstu}(\Sigma_vX_{rstuv})^2}{p} - \frac{\Sigma_{rst}(\Sigma_{uv}X_{rstuv})^2}{hp}$	efg(h-1)	$V_8 = \frac{SS_8}{efg(h-1)}$
BETWEEN REPLICATES WITHIN SAMPLES	$SS_9 = \Sigma_{rstuv}(X_{rstuv})^2 - \frac{(\Sigma_{rstuv}X_{rstuv})^2}{p}$	efgh(p-1)	$V_9 = \frac{SS_9}{efgh(p-1)}$
TOTAL	$\Sigma_{rstuv}(X_{rstuv})^2 - \frac{(\Sigma_{rstuv}X_{rstuv})^2}{efghp=N}$	efghp-1	

ESTIMATION OF VARIANCE COMPONENTS

LEVELS	DIFFERENCE	SAMPLE SIZE	VARIANCE COMPONENT
GRIDS	$V_5 - V_6$	fghp.	$S^2_\epsilon = \frac{V_5 - V_6}{fghp}$
MAJOR UNITS	$V_6 - V_7$	ghp	$S^2_\theta = \frac{V_6 - V_7}{ghp}$
MINOR UNITS	$V_7 - V_8$	hp	$S^2_\lambda = \frac{V_7 - V_8}{hp}$
SAMPLES	$V_8 - V_9$	p	$S^2_\rho = \frac{V_8 - V_9}{p}$
REPLICATES	V_9	1	$S^2_\phi = V_9$

EXPLANATION OF SYMBOLS:

X_{rstuv} = a single observation.
ν = grand mean for mine.
ϵ_r = comp. due to grid r.
Θ_{rs} = comp. due to major units, within r.
λ_{rst} = comp. due to minor unit t, within s, within r.
ρ_{rstu} = comp. due to sample u, within t, within s, within r.
ϕ_{rstuv} = comp. due to replicate v within u, within t, within s, within r.
$\epsilon_r, \Theta_{rs}, \lambda_{rst}, \rho_{rstu}$ & ϕ_{rstuv} are independent with mean 0 and variances $S^2_\epsilon, S^2_\theta, S^2_\lambda, S^2_\rho$ & S^2_ϕ respectively.

r varies from 1 to e
s varies from 1 to f
t varies from 1 to g
u varies from 1 to h
v varies from 1 to p
where
e = no. of grids/mine
f = no. of major units/grid
g = no. of minor units/maj. unit
h = no. of samples/minor unit
p = no. of replicates/sample
N = efghp = total samples collected.

FIGURE 5.—STATISTICAL MODEL FOR LOCAL SAMPLING HIERARCHY
See comment in caption of Figure 4 regarding use of S^2 in this model.

the averages. Figure 3, based on 4 samples per mine, is shown here as an example. The control points are the mines shown in Figure 2.

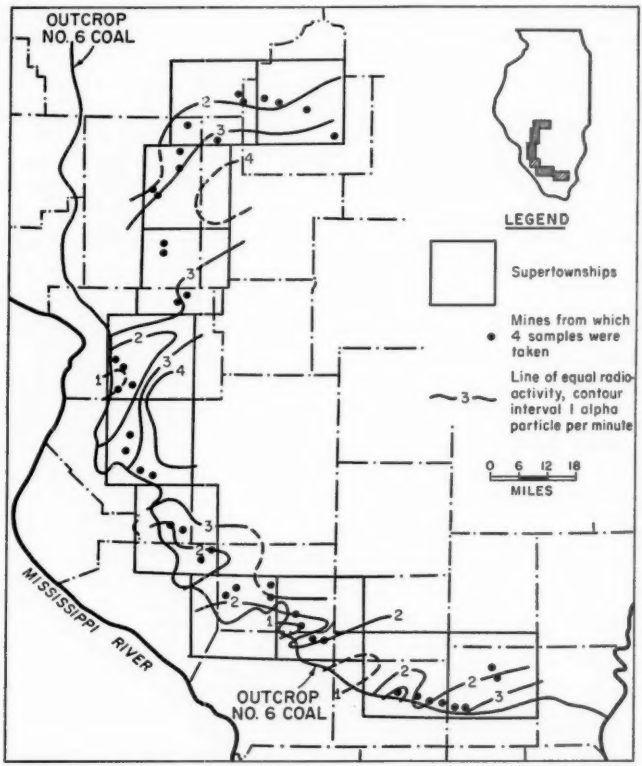

FIGURE 3.—RADIOACTIVITY MAP OF BLACK FISSILE BRERETON SHALE

The radioactivity map shows no marked over-all regional gradient from north to south, although a band of higher values trends across supertownships C and D and a high area lies in E and F, whereas lower values dominate in supertownships H, I, and J. Statistical tests described in the Appendix suggest that at the supertownship level there is some regional heterogeneity in radioactivity, which becomes more marked at the township and mine levels.

The radioactivity map is similar in some respects to the isopach map (Fig. 1), and comparison of the maps suggests that high radioactivity values may be associated with smaller shale thicknesses, as in super-townships C and D. Although a scatter diagram on a township basis showed no significant correlation, there may in fact be a genetic basis for an inverse relationship between shale thickness and radioactivity. The writers are indebted to Dr. John L. Rich of the University of Cincinnati (Personal communication) for suggesting that the more bituminous parts of the shale, presumably richer in radioactivity than other parts with less organic (kerogen) content, would be subject to greater compaction after burial than those parts with higher silt and clay content. By this process the areas where silt and clay are most abundant relative to kerogen would now have, relatively, the thickest shale and lowest radioactivity per unit, whereas where the kerogen content was greatest the shale thickness would be relatively least and the radioactivity per unit would be highest.

The selection of the mine or township level

as the basis for regional radioactivity mapping in this study implies collection of more than a single sample at each control point. Figure 3 is based on means of four individual values and hence averages out the local extremes that may occur in individual samples. The use of averages for regional mapping has a bearing on facies mapping of stratigraphic units. Most facies maps use single wells or outcrops as control points. A design which permits averaging of several wells at each regional control point would smooth the facies lines in the same manner as in the radioactivity map. In facies mapping the problem is complicated by the wide spacing of wildcat wells in some areas. Commonly a decision must be made between the advantage of using averages and the risk of failure to detect significant facies changes if individual values are combined. Potter and Siever (1955) discuss some of the implications of control-point spacing in their study of basal Pennsylvanian and Upper Chester sandstones and limestones.

Multilevel designs provide irregularly spaced control points for contour mapping (Fig. 3). Composite models that extend the multilevel design to include data for estimating regional gradients in rows and columns of major sampling units are discussed elsewhere (Krumbein, 1955). These composite models may be supplemented with evenly spaced control points to provide a more uniform basis for mapping.

Environment of Black Fissile Shale Deposition

The thickness map (Fig. 1) carries several implications regarding the environment in which the Brereton black fissile shale was deposited. There is no evidence of an erosional break between the shale and the overlying marine limestone. This suggests that the original conditions of accumulation were irregular, such as would occur if the shale were deposited on an essentially flat plain with minor surface irregularities transgressed by marine or brackish waters.

Moore (1929) presented an analysis of probable environmental conditions during the Pennsylvanian period:

> "The uniformity and very great extent of many of the Pennsylvanian coal beds and immediately associated strata can mean only that a featureless swampy plain extended throughout the area of coal deposition. The plain was not necessarily horizontal, for a slope sufficiently low to make movement of water sluggish would, in a nearly flat humid region, permit development of broad swamps. It is conceivable, indeed, that any slight existing drainage may have been so ill organized that open waterways were practically nonexistent, the water moving as an extremely sluggish sheet flow."

Inasmuch as the Brereton black fissile shale lies immediately above Coal No. 6, the coal swamps were probably invaded by marine waters which may have spread slowly over the essentially horizontal surface. Such marine invasions may occur without substantial wave action (Keulegan and Krumbein, 1949), thus permitting deposition of marine sediments above the coal with essentially no widespread or intensive reworking of the older deposits.

Variations of water depth in the swamps and irregularities in the peaty surface, as well as broad shallow channels in the swamp would provide a pattern of distribution of the initial invading sea water similar to that in Figure 1. Normal open circulation of the water was effectively restricted, as attested by the properties of the black shale.

The shale contains abundant organic matter and yields oily fumes on heating. It may locally grade laterally into canneloid shale or cannel coal. Fossils in the shale include phosphatic brachiopods, (linguloids and discinids), small articulate brachiopods (*Ambocoelia*), thin-shelled depauperate pelecypods, occasional ammonoids, some fish remains, conodonts, and spores. The fossils are crushed nearly flat.

The fissile shale is relatively rich in iron sulphide, present as pyrite in disseminated grains, nodules, and fossil replacements. Phosphatic nodules may occur, and sideritic concretions, many of which are large, are common in the black fissile shales of some cyclothems. The clay minerals in the black shale are commonly dominantly illitic.

The presence of organic matter, pyrite, phosphatic nodules, siderite, and an aberrant fauna with few calcareous representatives implies a depositional environment of low oxygen content (negative Eh) and mildly alkaline or slightly acidic conditions (pH between 6.9 and 7.8).

These are the characteristics of a humid restricted (euxinic) environment (Fleming and Revelle, 1939; Krumbein and Garrels, 1952). Moore (1929) suggested a combination of extreme shallowness providing too little depth for open circulation or effective wave agitation, and sufficient sunlight to promote abundant plant growth and partial decay as important features of the environment required for quiet undisturbed accumulation of a humous or bituminous muck.

Possibly, the marginal phases of the invading sea carried the black shale environment with them as the sea advanced eastward or northeastward across Illinois. The partially stagnant conditions set up by the initial shallow marine waters as they invaded the coal swamp would be succeeded by open circulation conditions accompanied by Brereton limestone deposition as the water deepened and cleared. Alternatively, if the black shale was deposited simultaneously over its whole area of occurrence, subsequent limestone deposition would require removal of the restrictions to provide normal marine open-circulation conditions.

The local occurrence of gray clay shale directly above the coal suggests that open circulation conditions prevailed here and there during the initial stages, permitting deposition of normal fine-grained detrital sediments. The absence of black shale in local areas where the Brereton limestone lies directly on the coa- suggests that these areas were not covered by the initial marine invasion, but became sites of deposition as the water deepened and permitted normal marine accumulation of carbonates.

The crushed fossils in the black shale support the inference that the material accumulated as a humous or bituminous muck with several times its own volume of water. Subsequent compaction squeezed out the water and crushed the fossils. This process probably also accounts for development of the laminae. Pettijohn (1949, p. 459) suggests that the initial volume of the sediment was perhaps five times its present thickness. The present average thickness of the Brereton black shale ranges from about 18 to 36 inches, so that the colloidal muck could be about 7 to 15 feet thick.

Studies by Bates and co-workers (1953) show that uranium in the Chattanooga black shale is associated with the pyrite-organic-clay complex, apparently very finely disseminated through the rock. The writers believe that the spotty dissemination of radioactivity in the black fissile Brereton shale represents substantially the same kind of distribution of uranium as in the Chattanooga. Marine plants and other organisms probably played a part in extracting and fixing uranium ions from the sea water (McKelvey and Nelson, 1950). The ions would be disseminated through the partially decayed colloidal muck and could have become associated with iron sulphide formed in the restricted environment as well as with accumulating detrital clay.

The absence of high radioactivity at the black fissile shale contacts and of any unusual radioactive "hotspots" in local areas of the region mapped support the inference that the uranium was associated with the depositional environment, rather than having been introduced by wholly diagenetic processes. Diagenetic changes would be concentrated at contacts or in localized areas where structural, ground water, or other conditions favored secondary concentration.

Some of the statistical tests described in the Appendix (Table 6) support the inference of primary environmental control. The tests fail to show that the variation in radioactivity between sampling units of any size is significantly greater than that between the next smaller units nested within them. This means that although the townships, for example, may differ among themselves in their radioactivity, there is no tendency for them to show greater variability in radioactivity than is shown by the mines within them. This relative uniformity at successive levels extends through the hierarchy until individual samples within a local grid are reached.

The results of these tests, which show no evidence of secondary concentration of radioactivity such as would be likely to occur if diagenetic changes were operative in some parts of the map area, suggest that the over-all spottiness of radioactivity is characteristic of the entire sampling hierarchy. The use of about 200 samples, from six sampling levels at spacings of 6 inches to 18 miles, with samples col-

lected on a probability basis, from an inferred homogeneous sampling stratum about 3 feet thick, is believed by the writers to include a wide enough range of areal units to have picked up secondary concentration if it were present.

Conclusion

Increasing emphasis on regional analysis during recent years poses numerous problems on the amount of detail to be included in a study. Choice has to be made between two extremes: examining every well and outcrop, or selecting relatively widely spaced control points which it is hoped will provide an adequate regional picture. Statistical design, especially with multilevel sampling models, can play a large part in this choice of alternative sampling plans.

The present study, based on a thin stratigraphic unit that can be correlated with confidence, and apparently free from any serious sample stratification problems, seemed to offer an opportunity for application of a standard sampling model. The use of two interlocked hierarchies represents a modification of the standard multilevel design and illustrates one way estimates of variability for closely spaced samples can be made from a reasonable number of observations at one or a few localities in the region. In regional terms it was seen that sample spacing based on mines in a township (about 3 miles apart) or on townships within a supertownship (about 9 miles apart) provide adequate data for regional mapping of black fissile Brereton shale radioactivity. If a map is the primary objective, the sampling localities would presumably be laid on a grid, with several samples averaged for each control point.

Sampling designs can be applied to geological problems more effectively if the stratigraphic unit is first "stratified" into relatively homogeneous sampling strata. Each stratum may then be sampled as a unit in its own right, and the data from each stratum can later be combined for estimates affecting the total unit. Cochran (1953) treats stratified sampling in some detail. Where desired, it is possible to adjust the sample spacing in each stratum to obtain equally reliable estimates for each stratum mean. Potter and Siever (1955) discuss this aspect of the sampling problem.

Application of probability sampling in geology deserves detailed consideration. To the extent that probability samples can be taken, the geologist shifts some of the responsibility for valid statistical inferences to the statistician. Samples within a stratum need not be taken completely at random for this purpose; various designs are available (Cochran, 1953) for using systematic samples, cluster samples, grid samples, and others, each having some mechanical means of randomization. Problems associated with nonavailability of samples (covered intervals, lack of outcrops, absence of boreholes) are troublesome in geology, but they have their counterparts in other sampling fields, and adjustments can be made for such situations (Cochran, Mosteller, and Tukey, 1954).

The increasing tendency to use standard statistical designs in geology suggests that the specific model used in this study be made explicit to the reader. The following Appendix contains this technical material plus some discussion of confidence intervals, statistical tests, and cost functions as applied in the present study.

Appendix

Statistical Model

The statistical model used in this study is a standard hierarchical design, described by Cochran (1953, p. 215), Anderson and Bancroft (1952, p. 325), Bennett and Franklin (1954, p. 358), Olson and Potter (1954), and Potter and Olson (1954). The sample layout for the regional design is shown in Figure 4. The random variable X_{ijkm} represents a single observation on an individual sample in the design. The value of the random variable depends on the grand mean μ, plus a contribution α from the i-th supertownship, plus a contribution β from the j-th township in the i-th supertownship, plus a contribution γ from the k-th mine in the j-th township of the i-th supertownship, plus a contribution ∂ from the m-th sample from the k-th mine in the j-th township of the i-th supertownship. The contributions $\alpha_i, \cdots, \partial_{ijkm}$ are all considered random variables with mean zero and variances as indicated in the lower left lines of Figure 4. The population mean μ is considered a fixed constant.

The sample layout for a grid in the local hierarchy is shown in Figure 5. Here the random variable X_{rstuv} represents a single observation on a laboratory

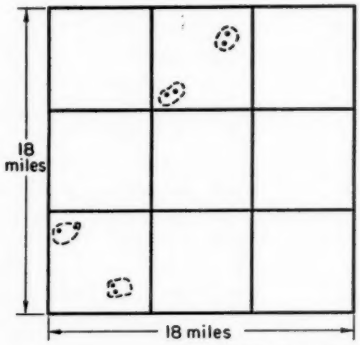

$$X_{ijkm} = \mu + \alpha_i + \beta_{ij} + \gamma_{ijk} + \partial_{ijkm}$$

ANALYSIS OF VARIANCE

SOURCE	SUM OF SQUARES	DEGREES OF FREEDOM	MEAN SQUARE
BETWEEN SUPERTOWNSHIPS	$SS_1 = \frac{\Sigma_i(\Sigma_{jkm}X_{ijkm})^2}{bcd} - \frac{(\Sigma_{ijkm}X_{ijkm})^2}{abcd=n}$	$a-1$	$V_1 = \frac{SS_1}{a-1}$
BETWEEN TOWNSHIPS WITHIN SUPERTOWNSHIPS	$SS_2 = \frac{\Sigma_{ij}(\Sigma_{km}X_{ijkm})^2}{cd} - \frac{\Sigma_i(\Sigma_{jkm}X_{ijkm})^2}{bcd}$	$a(b-1)$	$V_2 = \frac{SS_2}{a(b-1)}$
BETWEEN MINES WITHIN TOWNSHIPS	$SS_3 = \frac{\Sigma_{ijk}(\Sigma_m X_{ijkm})^2}{d} - \frac{\Sigma_{ij}(\Sigma_{km}X_{ijkm})^2}{cd}$	$ab(c-1)$	$V_3 = \frac{SS_3}{ab(c-1)}$
BETWEEN SAMPLES WITHIN MINES	$SS_4 = \Sigma_{ijkm}(X_{ijkm})^2 - \frac{\Sigma_{ijk}(\Sigma_m X_{ijkm})^2}{d}$	$abc(d-1)$	$V_4 = \frac{SS_4}{abc(d-1)}$
TOTAL	$\Sigma_{ijkm}(X_{ijkm})^2 - \frac{(\Sigma_{ijkm}X_{ijkm})^2}{abcd=n}$	$abcd-1$	

ESTIMATION OF VARIANCE COMPONENTS

LEVELS	DIFFERENCE	SAMPLE SIZE	VARIANCE COMPONENT
SUPERTOWNSHIPS	$V_1 - V_2$	bcd	$S^2_\alpha = \frac{V_1 - V_2}{bcd}$
TOWNSHIPS	$V_2 - V_3$	cd	$S^2_\beta = \frac{V_2 - V_3}{cd}$
MINES	$V_3 - V_4$	d	$S^2_\gamma = \frac{V_3 - V_4}{d}$
SAMPLES	V_4	1	$S^2_\partial = V_4$

EXPLANATION OF SYMBOLS:

X_{ijkm} = a single observation.
μ = grand mean.
α_i = comp. due to supertwp. i.
β_{ij} = comp. due to twp. j, within supertwp i.
γ_{ijk} = comp. due to mine k, within twp. j, within supertwp. i.
∂_{ijkm} = comp. due to sample m, within mine k, within twp. j within supertwp. i.
$\alpha_i, \beta_{ij}, \gamma_{ijk}$ & ∂_{ijkm} are independent with Mean 0 and variances $S^2_\alpha, S^2_\beta, S^2_\gamma$ & S^2_∂ respectively.

i varies from 1 to a
j varies from 1 to b
k varies from 1 to c
m varies from 1 to d

where
a = number of supertwps.
b = number of twps./supertwp.
c = number of mines/twp.
d = number of samples/mine
n = abcd = total samples collected.

FIGURE 4.—STATISTICAL MODEL FOR REGIONAL SAMPLING HIERARCHY

For convenience of notation and comparison with the mean squares in the analysis of variance table, all variances are shown as S^2. More rigorously the theoretical variances should be shown as σ^2 in the lower left part of this figure.

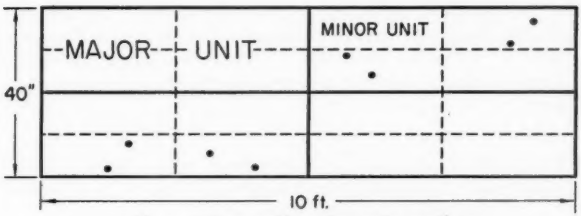

$$X_{rstuv} = \nu + \epsilon_r + \Theta_{rs} + \lambda_{rst} + \rho_{rstu} + \phi_{rstuv}$$

ANALYSIS OF VARIANCE

SOURCE	SUM OF SQUARES	DEGREES OF FREEDOM	MEAN SQUARE
BETWEEN GRIDS WITHIN A MINE	$SS_5 = \frac{\Sigma_r(\Sigma_{stuv}X_{rstuv})^2}{fghp} - \frac{(\Sigma_{rstuv}X_{rstuv})^2}{efghp=N}$	e-1	$V_5 = \frac{SS_5}{e-1} \doteq S^2_\phi$
BETWEEN MAJOR UNITS WITHIN GRIDS	$SS_6 = \frac{\Sigma_{rs}(\Sigma_{tuv}X_{rstuv})^2}{ghp} - \frac{\Sigma_r(\Sigma_{stuv}X_{rstuv})^2}{fghp}$	e(f-1)	$V_6 = \frac{SS_6}{e(f-1)}$
BETWEEN MINOR UNITS WITHIN MAJOR UNITS	$SS_7 = \frac{\Sigma_{rst}(\Sigma_{uv}X_{rstuv})^2}{hp} - \frac{\Sigma_{rs}(\Sigma_{tuv}X_{rstuv})^2}{ghp}$	ef(g-1)	$V_7 = \frac{SS_7}{ef(g-1)}$
BETWEEN SAMPLES WITHIN MINOR UNITS	$SS_8 = \frac{\Sigma_{rstu}(\Sigma_vX_{rstuv})^2}{p} - \frac{\Sigma_{rst}(\Sigma_{uv}X_{rstuv})^2}{hp}$	efg(h-1)	$V_8 = \frac{SS_8}{efg(h-1)}$
BETWEEN REPLICATES WITHIN SAMPLES	$SS_9 = \Sigma_{rstuv}(X_{rstuv})^2 - \frac{(\Sigma_{rstuv}X_{rstuv})^2}{p}$	efgh (p-1)	$V_9 = \frac{SS_9}{efgh(p-1)}$
TOTAL	$\Sigma_{rstuv}(X_{rstuv})^2 - \frac{(\Sigma_{rstuv}X_{rstuv})^2}{efghp=N}$	efghp-1	

ESTIMATION OF VARIANCE COMPONENTS

LEVELS	DIFFERENCE	SAMPLE SIZE	VARIANCE COMPONENT
GRIDS	$V_5 - V_6$	fghp	$S^2_\epsilon = \frac{V_5 - V_6}{fghp}$
MAJOR UNITS	$V_6 - V_7$	ghp	$S^2_\theta = \frac{V_6 - V_7}{ghp}$
MINOR UNITS	$V_7 - V_8$	hp	$S^2_\lambda = \frac{V_7 - V_8}{hp}$
SAMPLES	$V_8 - V_9$	p	$S^2_\rho = \frac{V_8 - V_9}{p}$
REPLICATES	V_9	1	$S^2_\phi = V_9$

EXPLANATION OF SYMBOLS:

X_{rstuv} = a single observation.
ν = grand mean for mine.
ϵ_r = comp. due to grid r.
Θ_{rs} = comp. due to major units, within r.
λ_{rst} = comp. due to minor unit t, within s, within r.
ρ_{rstu} = comp. due to sample u, within t, within s, within r.
ϕ_{rstuv} = comp. due to replicate v within u, within t, within s, within r.
$\epsilon_r, \Theta_{rs}, \lambda_{rst}, \rho_{rstu}$ & ϕ_{rstuv} are independent with mean 0 and variances $S^2_\epsilon, S^2_\theta, S^2_\lambda, S^2_\rho$ & S^2_ϕ respectively.

r varies from 1 to e
s varies from 1 to f
t varies from 1 to g
u varies from 1 to h
v varies from 1 to p
where
e = no. of grids/mine
f = no. of major units/grid
g = no. of minor units/maj. unit
h = no. of samples/minor unit
p = no. of replicates/sample
N = efghp = total samples collected.

FIGURE 5.—STATISTICAL MODEL FOR LOCAL SAMPLING HIERARCHY
See comment in caption of Figure 4 regarding use of S^2 in this model.

subsample. The value of the random variable depends on a grand mean ν (which may or may not be the same as μ, depending on whether or not a regional radioactivity gradient is present), plus a contribution ϵ from the r-th grid, plus a contribution

In the "estimation of variance components" section of Figures 4 and 5 the algebraic process of separating the components is shown in two stages. The first is the subtraction of the mean squares, and the resulting difference is then divided by the

VARIANCE COMPONENTS FOR HIERARCHICAL MODELS

SOURCE	DEGREES OF FREEDOM	MEAN SQUARE	MEAN SQUARE IS ESTIMATE OF
BTWN. SUPERTWPS.	a − 1	V_1	$S_\partial^2 + dS_\delta^2 + cdS_\beta^2 + bcdS_\alpha^2$
BTWN. TOWNSHIPS	a(b − 1)	V_2	$S_\partial^2 + dS_\delta^2 + cdS_\beta^2$
BTWN. MINES	ab(c − 1)	V_3	$S_\partial^2 + dS_\delta^2$
BTWN. SAMPLES	abc(d − 1)	V_4	S_∂^2
BTWN. GRIDS	e − 1	V_5	$S_\theta^2 + pS_\rho^2 + hpS_\lambda^2 + ghpS_\theta^2 + fghpS_\epsilon^2$
BTWN. MAJOR UNITS	e(f − 1)	V_6	$S_\theta^2 + pS_\rho^2 + hpS_\lambda^2 + ghpS_\theta^2$
BTWN. MINOR UNITS	ef(g − 1)	V_7	$S_\theta^2 + pS_\rho^2 + hpS_\lambda^2$
BTWN. SAMPLES	efg(h − 1)	V_8	$S_\theta^2 + pS_\rho^2$
BTWN. REPLICATES	efgh(p − 1)	V_9	S_θ^2

FIGURE 6.—VARIANCE COMPONENTS ESTIMATED BY MODELS OF FIGURES 4 AND 5
See comment in caption of Figure 4 regarding use of S^2 in this model.

θ from the s-th major unit in the r-th grid, plus a contribution λ from the t-th minor unit in the s-th major unit of the r-th grid, plus a contribution ρ from the u-th sample in the t-th minor unit of the s-th major unit of the r-th grid, plus a contribution ϕ from the v-th replicate (laboratory subsample) of the u-th sample of the t-th minor unit of the s-th major unit of the r-th grid. The contributions $\epsilon_r, \cdots, \phi_{rstuv}$ are all considered random variables, as in the preceding paragraph for α to ∂.

Analysis of variance is used to separate the total variability of X_{ijkm} and X_{rstuv} into mean squares associated with each hierarchical level. The mean squares represent estimates of the total variability at the corresponding sampling levels. As such they contain contributions from variabilities introduced at each lower level nested in the design. The manner in which these contributions from successively lower levels combine to give the mean square associated with the uppermost level is shown in Figure 6. The mean square at the lowest level of the regional hierarchy, V_4, contains only S_∂^2, whereas at the next higher level V_3 contains contributions from both S_∂^2 and S_γ^2. By subtracting V_4 from V_3 and dividing by d, the component S_γ^2 may be isolated:

$$[(S_\partial^2 + dS_\gamma^2) - S_\partial^2]/d = S_\gamma^2.$$

"sample size" which represents the number of times the component is present. Thus, subtraction of V_4 from V_3 for the regional experiment in the upper part of Table 4 yields 0.2090 − 0.1615 = 0.0475 as shown in the lower left of Table 4. The "between-mines" level is present $d = 4$ times, so that the variance component is recorded as 0.0119.

The first subtraction ($V_2 - V_1$) in Table 5 yields a negative number: 0.0088 − 0.4090 = −0.4002. This suggests that there is no component of variance contributed by the uppermost level in the local sampling hierarchy. An alternative interpretation is that an unusual sampling event occurred, and that there is a small but real variance at this level. Either of these alternatives implies that the large variance component apparently associated with the lowest sampling level in the regional design is actually distributed mainly over successive levels in the local hierarchy, represented by samples spaced closer than half a mile apart.

Graphic Representation of the Hierarchical Model

The statistical model provides a convenient way of showing graphically how the contributions of each sampling level affect the value of a single observation. In the regional model of Figure 4 the α repre-

sents the departure of the supertownship mean from the grand mean, here considered the population mean for illustration. The β represents the departure of the township mean from the supertownship mean, and the component γ represents the departure of the mine mean from the township mean. Finally, the ∂ represents the departure of a single observation from its mine mean. In a sense, each of these departures represents a "kick" at the sampling level involved.

Either the raw or the transformed data may be used to illustrate the operation of the hierarchical model. Consider sample 1 of mine a of township I of supertownship F. The individual observation is shown as 5.10 alpha particles per minute (Table 2). This is X_{ijkm}, here X_{FIal} of the model in Figure 4. The mean value of supertownship F is 3.09 alpha particles per minute. The value α_F is the difference between this mean and the grand mean, $3.09 - 2.42 = +0.67$. The mean of township I of supertownship F is 2.55 alpha particles per minute. The value of β_{FI} is the difference between this and the supertownship mean, $2.55 - 3.09 = -0.54$. The mean of mine a in township I of supertownship F is 2.59 alpha particles per minute. The value of γ_{FIa} is the difference between this and the township mean, $2.59 - 2.55 = +0.04$. The individual measurement of sample 1 of this mine was 5.10, and the value of ∂_{FIal} is the difference between this and the mine mean, $5.10 - 2.59 = +2.51$.

According to the model in this specific instance, these values should combine as follows:

$$X_{FIal} = \mu + \alpha_F + \beta_{FI} + \gamma_{FIa} + \partial_{FIal}$$
$$5.10 = 2.42 + 0.67 - 0.54 + 0.04 + 2.51$$

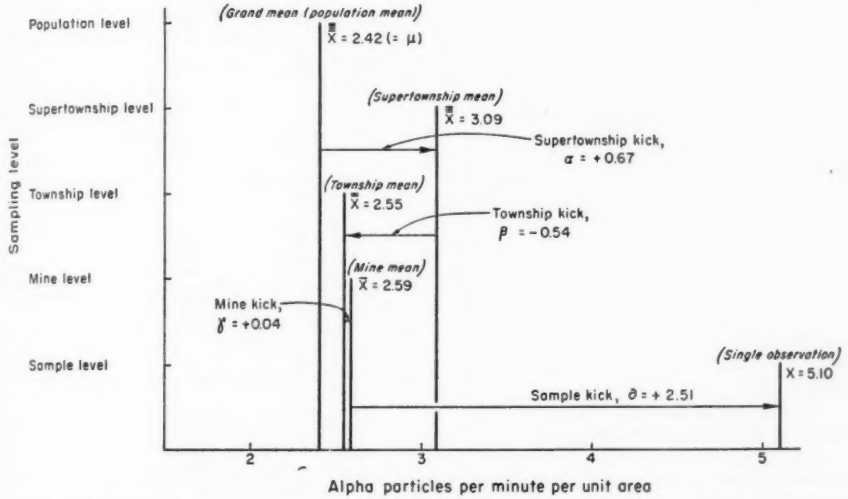

FIGURE 7.—GRAPHICAL PRESENTATION OF HIERARCHICAL MODEL, ILLUSTRATED BY SAMPLE 1 OF MINE *a*, TOWNSHIP I OF SUPERTOWNSHIP F

The figure illustrates the magnitude and direction of the departures (kicks) at each level of the hierarchy for this sample.

Figure 7 shows the example graphically. The largest kick occurs at the sample level, and the smallest occurs at the mine level. The township level is represented by a negative kick slightly less than the positive kick of the supertownship. For the general case the variance components at each level give an "average" estimate of the variability at that level. The variance components themselves can be used to estimate the variance of the mean value associated with the given level. If desired, a frequency curve can be drawn around each mean value to indicate its expected variability.

Confidence Limits on Mean Radioactivity

Confidence limits are defined as values of the variate such that the interval between the limits has a certain probability of including the population mean (Dixon and Massey, 1951, p. 73). The grand mean of the radioactivity data is an estimate of the population mean, and as such is subject to some variability.

For practical purposes the grand mean of the untransformed data, 2.42 alpha particles per minute per unit area, is a more easily visualized number

than the mean of the square-root transformed data. However, the extreme skewness of the distribution of raw data renders it difficult to make direct probability statements regarding the variability of the mean of the untransformed data. Instead, confidence limits are usually set about the mean of the transformed data and these limits are converted back to the original values by squaring them. The limits are symmetrical about the transformed mean but become unsymmetrical about the mean of the raw data.

In setting up confidence limits on means in a sampling hierarchy it is necessary to take into account the variance components at the several levels. Anderson and Bancroft (1952, p. 326), Cochran (1953, Chap. 10), Olson and Potter (1954), and Potter and Siever (1955) discuss the topic. If the sampling proportions at each level are less than 1/20, the variance of the grand mean is (Anderson and Bancroft, 1952, p. 326):

$$V(\bar{\bar{\bar{X}}}) = (S_\alpha^2/a) + (S_\beta^2/ab) + (S_\gamma^2/abc) + (S_\delta^2/abcd).$$

In the present study all 11 supertownships were used, so that a complete enumeration was made at the highest level. Under these conditions the supertownships add no variance component to the mean. Two out of nine townships in each supertownship were used, so that the proportion of townships per supertownship is $b/B = 0.22$, where $b = 2$ and $B = 9$. Similarly, if a single mine is considered as covering a substantial part of a township, a correction factor based on c/C would be needed. In the present study it is believed that the average area represented by four samples at the mines level is not significantly larger than 1/20. The number of samples that could be collected in any one mine is practically unlimited, so that correction factors are needed only at the two highest levels.

Under these conditions the variance of the grand mean becomes:

$$V(X) = \left(\frac{1}{a} - \frac{1}{A}\right) S_\alpha^2 + \left(\frac{1}{ab} - \frac{1}{AB}\right) S_\beta^2 + \left(\frac{1}{ab} - \frac{1}{AB}\right) \frac{S_\gamma^2}{c} + \left(\frac{1}{ab} - \frac{1}{AB}\right) \frac{S_\delta^2}{cd}.$$

In this equation, $a = A = 9$; $b = c = 2$; $B = 9$; $d = 4$, and the variance components are given in the lower part of Table 4. By using these data, the estimated variance of the grand mean of the transformed data is computed as 0.001408, and the estimated standard deviation is 0.038. The 67 per cent confidence limits are $1.49 \pm 0.04 = 1.45$ and 1.53. Confidence limits at the 95 per cent confidence level are computed by multiplying the standard deviation by the corresponding probability value of t for the degrees of freedom involved. At the highest level in multilevel sampling it is conventional to use $(a - 1)$ degrees of freedom rather than $(abcd - 1)$, as Anderson and Bancroft (1952, p. 326) and Potter and Siever (1955) point out. The value of t at the 95 per cent level in a two-tailed test for 10 degrees of freedom is 2.23 (Dixon and Massey, 1951, p. 307). Hence there is a 95 per cent probability that the interval $1.49 \pm (2.23)(0.38) = 1.49 \pm 0.085$ includes the population mean for the transformed data. These limits are 1.40 to 1.58.

In terms of the raw data, the confidence limits for the grand mean, 2.42, are found by squaring the transformed limits. As a first approximation, therefore, the grand population mean of the raw data has a 95 per cent probability of lying between 1.96 and 2.50 alpha particles per minute per 1.5-inch diameter circle of powdered shale, as mentioned in the earlier text.

Statistical Tests of Significance

A statistical significance test is a probability test used to determine whether a group of samples could reasonably have come from a single population, or whether a preferred interpretation is that they were derived from different populations. Bennett and Franklin (1954, p. 365) describe tests of significance for successive levels in hierarchical designs. These can be conducted directly with the mean squares associated with the several sampling levels in Tables 4 and 5.

The kind of questions that can be answered by these tests include the following: do the supertownships differ more among themselves than do the townships within them? Do the townships differ more among themselves than do the mines within them? These tests thus compare the relative variability in radioactivity associated with successive levels of the hierarchy. A second kind of statistical test can be used to determine whether the units at any level are homogeneous among themselves. This second type of question can be expressed as follows: is the variability between supertownships significantly greater than the variability within supertownships? Is the variability between townships significantly greater than the variability within townships? These tests thus compare the units at any level without regard to their relative variability with respect to other levels. The second type of test is based on the single factor analysis of variance as described in Dixon and Massey (1951, p. 121) and involves some recomputation of the mean squares in Tables 4 and 5.

The tests of relative variability at successive levels were mentioned in the text in connection with the inference of primary environmental control of radioactivity. These tests are shown in Table 6, abbreviated for convenience of presentation. The first hypothesis, stated more fully, is that, "At the 5 per cent significance level there is no greater variation in mean radioactivity between supertownships than between townships within a supertownship." In conducting the test, the mean square at the top level in Table 4 is divided by the mean square of the second level: 0.3748/0.3189 = 1.17. This ratio is the observed F value, which is less than the critical value of F at the 5 per cent level for 10, 11 degrees of freedom (tabulated in Dixon and Massey, 1951, p. 310, as 2.86). Hence, the ratio is nonsignificant (NS), and the hypothesis is not rejected.

TABLE 6.—TESTS OF HYPOTHESES† (Relative variability, regional and local data)

Hypothesis	F ratios
(1) No significant variation between supertownships compared with variation between townships in a supertownship	1.17 NS (10,11) $F_{.05} = 2.86$
(2) No significant variation between townships compared with variation between mines within a township	1.53 NS (11,22) $F_{.05} = 2.26$
(3) No significant variation between mines compared with variation between samples within a mine	1.29 NS (22,132) $F_{.05} = 1.64$
(4) No significant variation between grids compared with variation between major units within a grid	<1 NS (3,4) $F_{.05} = 6.59$
(5) No significant variation between major units compared with variation between minor units within major units	<1 NS (4,8) $F_{.05} = 3.84$
(6) No significant variation between minor units compared with variation between samples within a minor unit	3.24* (8,16) $F_{.05} = 2.59$
(7) No significant variation between samples compared with variation between replicates within a sample	26.34** (16,34) $F_{.01} = 2.58$

* Significant at 0.05 level.
** Significant at 0.01 level.
† The arrangement of the number on the right is: top line—observed F ratio; center line—degrees of freedom for test; bottom line—critical F value for d.f. involved.

As Table 6 shows, all the levels in the regional design (items 1 to 3) are homogeneous compared to the next lower level, and the same homogeneity persists through the first two levels of the local design (items 4 and 5). At the minor-units level, where the samples are spaced about 2.5 feet apart, the variation becomes significant, indicating some heterogeneity at about this scale in the relative radioactivity. The asterisks after item 7 in Table 6 indicate that the variation between samples is very significant compared with variation between duplicate samples. This last test is important in indicating that the variability introduced by laboratory errors is very small compared with the variability among samples.

Inclusion of the laboratory subsampling level in the detailed hierarchy provides replicate data for determination of the laboratory errors in the study, and hence provides a self-contained experiment (Youden, 1951, p. 72). In the present case it is seen that errors due to sample splitting, measurement, and other laboratory sources are minor compared with the differences that are of importance, *i.e.*, differences among the samples themselves.

The tests for homogeneity of individual sampling levels are shown in Table 7. The tests involve some recomputation of mean squares, accomplished by pooling the variability at all levels below the one being tested. As Table 7 shows, there is some heterogeneity at each regional level individually (items 1 to 3) indicating that the variation in radioactivity between the supertownships, for example, is greater than would be attributed to a single population. In terms of Figure 3 this implies that the trend of somewhat higher values in supertownships C and D may be significantly different from the trend of unusually low values in the western part of supertownship J. That the townships may also differ significantly among themselves is shown by the local bunching of contours in Figure 3, such that the mean radioactivity (on a mine basis) may double in some townships, but not change greatly in others.

Items 4 to 7 of Table 7 apply to the local hierarchy. Item 4 shows that variations between grids do not differ significantly from variation within grids. This supports the earlier inference that there is essentially no variance component associated with the samples-within-mines level of the regional hierarchy, and that the sample variance of 0.1615 shown as the last item in Table 4 is actually distributed over still lower levels in the detailed hierarchy of Table 5.

Items 5 and 6 of Table 7 show highly significant variations, further evidence that the occurrence of radioactivity in the black shale is very spotty among closely spaced samples. The last item in Table 7

verifies the earlier conclusion that the variability of the laboratory measurements is very small compared with the variability among samples.

TABLE 7.—TESTS OF HYPOTHESES†

(Homogeneity of individual sampling levels, regional and local data)

(1)	No significant variation between supertownships compared with variation within supertownships	2.10* (10,165) $F_{.05} = 1.87$
(2)	No significant variation between townships compared with variation within townships	2.05** (21,154) $F_{.01} = 2.00$
(3)	No significant variation between mines compared with variation within mines	1.71** (43,132) $F_{.01} = 1.69$
(4)	No significant variation between grids compared with variation within grids	<1 NS (3,60) $F_{.05} = 2.76$
(5)	No significant variation between major units compared with variation within major units	3.08** (7,56) $F_{.01} = 2.98$
(6)	No significant variation between minor units compared with variations within minor units	7.91** (15,48) $F_{.01} = 2.40$
(7)	No significant variation between samples compared with variation between replicates within a sample	49.71** (31,32) $F_{.01} = 2.34$

* Significant at 0.05 level.
** Significant at 0.01 level.
† The arrangement of the numbers on the right is: top line—observed F ratio; center line—degrees of freedom for test; bottom line—critical F value for d.f. involved.

Application of Cost Function to Sampling Data

One advantage of multilevel sampling is that it provides data for optimum allocation of sampling effort over the hierarchy. This may be especially important in redesign of a preliminary sampling plan for more detailed analysis of a stratigraphic unit. The optimum sampling and subsampling fractions are found by application of cost functions to combinations of the several variance components.

Cochran (1953, p. 225) describes a cost function which may be used in a two-level hierarchy, and Potter and Olson (1954) discuss its application to additional sampling levels. In applying the cost function, the cost (or time) required for a unit at each hierarchical level is so distributed over the hierarchy that the variance of the mean at each level is kept at a minimum.

In the present study the writers collected four samples per mine. The question may be raised whether there is some optimum number of samples to be collected per mine, assuming that the same number of mines is to be visited.

This question may be answered by use of Cochran's cost function,

$$C = C_m c + C_e cd,$$

where the total cost C is made up of a component C_m that is proportional to the number of mines (c) per township, and a component C_e that is proportional to the total number of elements (mines times samples, cd). In this example the "grand mean" of the mines is the township mean of the hierarchy, and the problem is to minimize its variance. Cochran (1953, p. 226) shows the process and derives the solution for the optimum number of samples per mine, d':

$$d' = \sqrt{(S_\delta^2/S_\gamma^2)(C_m/C_e)}.$$

In the present study the cost (time) for locating a mine in a township was approximately 50 minutes, and the time for collecting and analyzing a sample was approximately 95 minutes. The sample variance is 0.1615 and the mine variance is 0.0119 (Table 4). Hence,

$$d' = \sqrt{(0.1615/0.0119)(50/95)} = 2.7.$$

The closest whole number to 2.7 is 3, so that a total of three samples from each of two mines per township would be an optimum number.

REFERENCES CITED

Anderson, R. L., and Bancroft, T. A., 1952, Statistical theory in research: N. Y., McGraw-Hill Book Co., 399 p.

Bartlett, M. S., 1947, The use of transformations: Biometrics, v. 3, p. 39–52

Bates, T. F., 1953, An investigation of the mineralogy, petrography, and paleobotany of uranium-bearing shales and lignites: Atomic Energy Commission, Project No. E-32 (NYO-3363)

Bennett, C. A., and Franklin, N. L., 1954, Statistical analysis in chemistry and the chemical industry: N. Y., John Wiley and Sons, 724 p.

Cochran, W. G., 1953, Sampling techniques: N. Y., John Wiley and Sons, 330 p.

Cochran, W. G., Mosteller, F., and Tukey, J. W., 1954, Principles of sampling: Jour. Am. Stat. Assoc., v. 49, p. 13–35

Dixon, W. J., and Massey, F. J., 1951, Introduction to statistical analysis: N. Y., McGraw-Hill Book Co., 370 p.

Fleming, R. H., and Revelle, R., 1939, Physical processes in the ocean: *in* Recent marine sediments, P. D. Trask, *Editor*, Am. Assoc. Petroleum Geologists, Tulsa, Okla., p. 48–141

Kempthorne, O., 1952, The design and analysis of experiments: N. Y., John Wiley and Sons, 631 p.

Keulegan, G. H., and Krumbein, W. C., 1949, Stable configuration of bottom slope in a

shallow sea and its bearing on geological processes: Am. Geophys. Union Trans., v. 30, p. 855–861

Krumbein, W. C., 1955, Statistical analysis of facies maps: Jour. Geology, v. 63, p. 452–470

Krumbein, W. C., and Garrels, R. M., 1952, Origin and classification of chemical sediments in terms of pH and oxidation-reduction potentials: Jour. Geology, v. 60, p. 1–33

McKelvey, V. E., and Nelson, J. M., 1950, Characteristics of marine uranium-bearing sedimentary rocks: Econ. Geology, v. 45, p. 35–53

Moore, R. C., 1929, Environment of Pennsylvanian life in North America: Am. Assoc. Petroleum Geologists Bull., v. 13, p. 459–487

Moore, R. C., *et al.*, 1944, Correlation of Pennsylvanian formations of North America: Geol. Soc. America Bull., v. 55, p. 657–706

Olson, J. S., and Potter, P. E., 1954, Variance components of cross-bedding direction in some basal Pennsylvanian sandstones of the Eastern Interior Basin: statistical methods: Jour. Geology, v. 62, p. 26–49

Pettijohn, F. J., 1949, Sedimentary rocks: N. Y., Harper and Bros., 526 p.

Potter, P. E., and Olson, J. S., 1954, Variance components of cross-bedding direction in some basal Pennsylvanian sandstones of the Eastern Interior Basin: geological application: Jour. Geology, v. 62, p. 50–73

Potter, P. E., and Siever, R., 1955, A comparative study of upper Chester and lower Pennsylvanian stratigraphic variability: Jour. Geology, v. 63, p. 429–451

Slack, H. A., and Krumbein, W. C., 1955, Measurement and statistical evaluation of low-level radioactivity of rocks: Am. Geophys. Union Trans., v. 36, p. 460–464

Wanless, H. R., 1931, Pennsylvanian cycles in western Illinois: Ill. State Geol. Survey Bull. 60, p. 179–193

Wanless, H. R., and Weller, J. M., 1932, Correlation and extent of Pennsylvanian cyclothems: Geol. Soc. America Bull., v. 43, p. 1003–1016

Weller, J. M., 1930, Cyclical sedimentation of the Pennsylvanian period and its significance: Jour. Geology, v. 38, p. 97–135

Willman, H. B., and Payne, J. N., 1942, Geology and mineral resources of the Marseilles, Ottawa, and Streator Quadrangles: Ill. State Geol. Survey Bull. 66, 388 p.

Youden, W. J., 1951, Statistical methods for chemists: N. Y., John Wiley and Sons, 126 p.

Northwestern University, Evanston, Illinois

Manuscript Received by the Secretary of the Society, December 30, 1954

BULLETIN OF THE GEOLOGICAL SOCIETY OF AMERICA
VOL. 67, PP. 763-806, 18 FIGS., 10 PLS. JUNE 1956

STRUCTURE AND PETROLOGY OF ENCHANTED ROCK BATHOLITH, LLANO AND GILLESPIE COUNTIES, TEXAS

BY ROBERT M. HUTCHINSON

ABSTRACT

Enchanted Rock batholith is one of several moderate-sized plutons that intruded a framework of tightly folded Precambrian metamorphic rocks in Middle Precambrian time. Tectonic features within the mass and structural attitude of wall rocks indicate the northern third is phacolithic. The remainder is both discordant and concordant batholithic, although the schists show a tendency to box the compass around the batholith. The phacolithic part occupies a synclinal trough plunging 35°–40° SE.

The batholith consists of four concentric zones: (1) outer zone, medium to coarse leucogranite and granite; (2) intermediate zone, medium to coarse granite and quartz monzonite; (3) intermediate central zone, coarse quartz monzonite and alkalic granodiorite; and (4) the core, fine to medium leuco-quartz monzonite and leucogranite. Rapakivi are most abundant in zone 3. Seriate porphyritic texture prevails in all zones except the core where it is increasingly hiatal. Chilled border rocks are 10–20 feet wide and consist of leuco-quartz monzonite and quartz monzonite. Apophyses of the batholith in metamorphic wall rocks are leuco-quartz monzonite and leucogranite. Hiatal porphyritic texture prevails in chilled border and apophyses rocks.

Internal structures of the batholith and its relation to country-rock structures indicate intrusion during the late, most severe stages of regional compression. Tensile stresses along axial planes of folds exerted structural control and guided the rise of the magma, as indicated by the pear-shaped outline of the batholith. The most probable mechanism of magma generation is selective fusion (melting) of random rock material. This occurred at depth in down-buckled zones below the present position of the batholith.

Concentration of the proportions of normative constituents of individual rock zones is strikingly grouped about a composition having a 1:1:1 ratio of albite:orthoclase:quartz. Mineralogically there are systematic gradations in proportions of plagioclase, microcline, and quartz between rock zones suggesting that unmixing of sodic plagioclase from microcline was a dominant process.

Outline shape of rock zones, textural relations between plagioclase and microcline crystals, and maxima-minima concentrations of unmixed sodic plagioclase suggest migration of part of the unmixed material within the batholith during the later stages of its structural and intrusive history. Field and chemical evidence indicate that probably not more than 5 per cent of the granites of the batholith are of replacement origin.

Failure of roof rocks with partial escape of volatiles, cessation of regional tectonism, and depletion of the magma reservoir in the late stages of intrusion probably are responsible for finer grain of the core. Age determinations by the "Larsen Method" give an average age for the batholith of 815 million years.

CONTENTS

TEXT

	Page
Introduction	764
Location and scope of work	765
Previous work	765
Acknowledgments	765
Geologic setting	766
General	766
Metamorphic rocks	766
Sedimentary rocks	767
Structural setting	767
Introduction	767
Regional structure	767
Relation to country-rock structures	767
Structural petrology	769
Fabric axes	769
Linear-flow structures	769
Long dimension of microcline phenocrysts	769
Dimensional orientation of biotite	770
Dimensional orientation of quartz mosaics	770

	Page
Platy flow structures	770
Platy parallelism of phenocrysts	770
Flow layers (schlieren)	772
Parallelism of xenoliths	772
Rock "swirls"	772
Combination of linear- and platy-flow structures	772
Fracture systems	772
Cross-joints	772
a-c joints	773
a-b joints	775
Marginal fissures	775
Aplite-filled shears	777
Meaning of flow structures	777
Meaning of joints and marginal fissures	777
Summary of structure	777
Petrography	778
General	778
Gradational nature of rock zones	779
Textural variation across rock zones	780
Specific gravity of rocks	781
Composition	782
X-ray analysis of feldspars	785
Plagioclase-microcline relationships	786
Twins and zones in plagioclase	788
"Chill" border and metasomatism of wall rocks	788
Metasomatism of inclusions	791
Petrology	792
Age determinations	792
Development of rock zones	792
Significance of plagioclase-microcline relationships	794
Interpretation of compositional variation	796
Source of the granite	799
Problem of the schlieren	802
Significance of color	804
References cited	804

ILLUSTRATIONS

Figure		Page
1.	Rock zones, internal and wall-rock structures of Enchanted Rock batholith	768
2.	Relationship of fabric axes to crystallographic axes	769
3.	Relationship of fabric axes to crystallographic axes	770
4.	Petrofabric diagrams of biotite and quartz in outer zone of the batholith	771
5.	Contour diagrams of primary fractures and regional joints of the batholith	774
6.	Contour diagrams of primary fractures of the batholith filled with pegmatite and/or aplite	776
7.	Relationship of primary fractures to primary flow structures	778
8.	Rock types of Enchanted Rock batholith	779
9.	Variation of plagioclase composition in rock zones of the batholith	781
10.	Harker variation diagram of igneous rocks of central Texas	783
11.	Modal composition of plagioclase in rocks of the batholith	786
12.	Modal composition across granitized contact (schist-granite) at north part of the batholith	790
13.	Normative composition (albite + orthoclase + quartz) of rocks of Enchanted Rock batholith containing 80 per cent or more of these normative constituents	796
14.	Modal composition of rocks of Enchanted Rock batholith	797
15.	Normative composition (albite + orthoclase + quartz) of Valley Spring gneiss and Packsaddle schist, Precambrian of central Texas	800
16.	Hypotheses for occupancy of synclines by rising magma	801
17.	Zonation and anorthite content of the consecutive zones	802
18.	Rapakivi from intermediate central zone	803

Plate		Facing page
1.	Enchanted Rock batholith, Texas	763
2.	Structure sections of Enchanted Rock batholith, Texas	Following page 768
3.	Internal structures of the batholith	772
4.	Primary fractures and xenoliths	772
5.	Border-zone relationships	772
6.	Textural changes (core-rim) across Enchanted Rock batholith	772
7.	Plagioclase-microcline relationships	788
8.	Plagioclase-microcline relationships	788
9.	Plagioclase-microcline relationships	788
10.	Rapakivi and zoned plagioclase	788

TABLES

Table		Page
1.	Chemical analyses	782
2.	Modes	784
3.	Norms	785
4.	Relation between albite rims on plagioclase and microcline-plagioclase boundary in rock zones of the batholith	787
5.	Age determinations of zircons from Enchanted Rock batholith	793
6.	Chemical analyses of Valley Spring gneiss and Packsaddle schist	793

Introduction

Enchanted Rock batholith has outcrop relief of less than 700 feet; however an unusually large portion of its outcrop surface is well exposed and permits comprehensive observation and sampling.

Enchanted Rock batholith project has produced information on (1) influence of tectonic setting on processes of magma generation; (2) time relation of intrusion to general tectonics; (3) importance of structural controls in rise and emplacement of granite; and (4) process of batholith crystallization and effect of autometamorphic change on the gross textural and mineralogical properties of the rocks.

Stenzel (1936) was the first to carry out de-

tailed studies in granite tectonics in the Precambrian of central Texas when he mapped the internal and wall-rock structures of Wolf Mountain phacolith 20 miles northeast of Enchanted Rock batholith. The present investigation is part of a long-range program of detailed study in the structural and intrusive history of the Precambrian igneous rocks of the central Texas area.

Location and Scope of Work

The area is situated in the south-central part of the Llano uplift (Pl. 1). The batholith outcrops in the southwestern corner of Llano County and extends several miles south into Gillespie County.

This report is based on 7 months of field work done during the summers of 1950, 1951, and 1952. The principal purpose was to map the structure and describe the petrology of Enchanted Rock batholith and its immediate surrounding wall rocks. The entire batholith and a contact zone half a mile to a mile wide bordering the entire batholith were mapped on aerial photographs on the scale of 8 inches to the mile.

Previous Work

The first geologic map of the Llano-Burnet quadrangles was prepared by the U. S. Geological Survey in 1909 (Paige, 1911; 1912). This map, on a scale of 2 miles to the inch, serves today as an excellent field guide. It shows the outcrop pattern of the batholith and the regional structure and distribution of Packsaddle schist and Valley Spring gneiss.

Stenzel (1935) summarized the Precambrian structural conditions in the Llano region and in 1936 made a structural study of the Wolf Mountain phacolith. Keppel (1940) made a reconnaissance study of concentric patterns in the plutons of the Llano-Burnet region. He included in his report a brief survey of Enchanted Rock batholith.

Goldich (1941) critically examined physicochemical data pertaining to intrusions of the central Texas region. Two chemical analyses of rocks of the batholith were published by Barnes, Dawson, and Parkinson (1947). Barnes (1952) mapped the geology of the Crabapple Creek quadrangle which includes the southern tip of the batholith and in 1954 published geophysical data for rocks of the area. The present writer published results of a statistical study of texture of the batholith in 1952, in 1953 he summarized the petrology, and in 1954 reported on age determinations of Precambrian intrusions of the central Texas area.

Acknowledgments

Part of this report was included in the doctoral dissertation submitted to the Department of Geology, University of Texas, Austin, Texas. Members of the doctoral committee supervising the work were Professors F. M. Bullard, R. K. Deford, J. T. Lonsdale, H. P. Bybee, and S. E. Clabaugh. Doctor Lonsdale, Director of the Bureau of Economic Geology, kindly supplied aerial photographs from the Bureau files. Dr. V. E. Barnes and Dr. H. B. Stenzel also guided parts of the work. Dr. E. J. Weiss, University of Texas, furnished use of X-ray equipment made available through a grant to the Ceramic Engineering Department by the Edward Orton Jr. Ceramic Foundation. Dr. R. D. Dragsdorf, Kansas State College, ran powder-diffraction patterns.

The writer is indebted to The Geological Society of America for a grant from the Penrose Bequest for chemical analyses. Age determinations of zircons were made by H. W. Jaffe and David Gottfried under the direction of Dr. Esper S. Larsen, Jr. The University of Texas Department of Geology financed some of the thin sections.

Dr. Wm. Scott MacKenzie ran single-crystal X-ray studies and critically read the section on feldspars. Dr. Hatten S. Yoder directed the writer's attention to rims of unmixed albite at plagioclase-microcline boundary contacts. Photographs of large thin sections were made through the courtesy of Dr. G. E. Goodspeed. Prof. J. R. Chelikowsky, Department of Geology, Kansas State College, conferred on several aspects of the structural problem. Dr. O. F. Tuttle gave valuable advice.

Professors R. C. Emmons, A. F. Hagner, and S. S. Goldich read the original manuscript critically.

To the ranchers of the area is owed a debt of gratitude for making the study possible. The

author is particularly grateful to J. G. Moss, M. A. Moss, Chas. Keese, J. R. Jedlicka of Llano County and O. C. Montgomery and L. T. Schrank of the town of Llano for their hospitality and co-operation during the field work.

Geologic Setting

General

At the end of Cretaceous time the Cretaceous Sea was removed by a widespread general uplift. The Cretaceous cover was eroded to expose Paleozoic rocks as a window. Paleozoic rocks were further eroded to expose the basement of Precambrian crystallines. This basement has been less resistant to erosion than the sedimentary rocks surrounding it; thus today the Llano region is not only a topographic low and a structural high, but also a stratigraphic inlier. Cambrian and Cretaceous sedimentary rocks occur both as erosional outliers and as remnants in down-faulted blocks (Pl. 1). They overlie the basement complex with angular unconformity.

The Precambrian metamorphic rocks have been intensively intruded by igneous rocks, mostly granites with some quartz monzonite. Small intrusions include more basic rocks (granodiorite, quartz diorite, and gabbro). Pegmatites, aplites, and aplogranites accompany the larger intrusives.

In the larger intrusives three principal types of granites have been recognized by Stenzel (1934, p. 74–79) on the basis of their probable age relationship as follows:

(3) Sixmile granites; fine-grained, gray biotite granites, typically exposed in quarries near Sixmile (youngest)

(2) Oatman granites; medium-grained, gray to pink, cataclastic granites, typically exposed in Oatman Creek southeast of Llano

(1) Town Mountain granites; coarse-grained to porphyritic granites, commonly with large flesh-colored feldspars, typically exposed in the abandoned quarries on Town Mountain north of Llano (oldest)

The rocks of Enchanted Rock batholith belong to the Town Mountain type.

Metamorphic Rocks

The metamorphic rocks are divisible into two large formations, the Valley Spring gneiss and the Packsaddle schist. The Valley Spring gneiss is the older and is named after the town of Valley Spring in Llano County, Texas. The Packsaddle schist is named for Packsaddle Mountain, Llano County, Texas, where excellent exposures occur on the west side of the mountain.

VALLEY SPRING GNEISS: The base of the gneiss is not visible. A measured section (Pl. 2, Section B-B′) shows at least 6000 feet of consistently fine to medium quartzo-feldspathic gneiss of varying shades of orange pink. Biotite occurs as disseminated flakes and bands up to 6 inches in thickness. Many small-scale drag folds accompanied by local intrusion and recrystallization increase the difficulty of measuring an accurate section.

The gneiss seems to be of sedimentary origin. It contains many fine-grained, dense quartzitic lenses and shows lithologic banding that may be original stratification continuing uniformly laterally in some outcrops for several hundred to thousands of feet.

The northern tip of the batholith lies in contact with the gneiss, which 1 mile off the northeast flank of the batholith on the Luke Moss ranch, changes from thick- to thin-bedded quartzo-feldspathic gneiss becoming increasingly quartzose with some muscovite. The contact between the gneiss and Packsaddle schist is placed where a coarse, flaky muscovite-quartz-feldspar schist begins.

PACKSADDLE SCHIST: Outcrops of Packsaddle schist are mainly on the east, southeast, south, and southwest flanks of the batholith. The schist is dominantly dark gray to blackish, strongly schistose, and contains highly variable amounts of fine- to medium-grained biotite, muscovite, sericite, chlorite, glaucophane, sillimanite, tremolite, wollastonite, serpentine, talc, epidote, hornblende, quartz, feldspar, garnet, scheelite, calcite, and graphite. The original sediments, after metamorphism, became mainly schists of these types. Sandstones were altered to gneiss or gneissoid schist, and the limestones to marble or wollastonite.

A measured section of the schist (Pl. 2, Section C-C′) shows a thickness of at least 5400 feet of varied composition. Dark colors of the schists are in direct contrast with the predominant orange pink of the underlying Valley Spring gneiss. Occasional intercalated bands of

quartzo-feldspathic gneiss, similar in appearance to the Valley Spring gneiss, occur throughout the formation.

Sedimentary Rocks

The 170-square-mile area mapped includes two formations younger than Precambrian. These are incompletely exposed. The Hickory sandstone member and the Cap Mountain limestone member of the Riley formation are Upper Cambrian in age. Outcrops of these cover part of the core and west side of the area mapped (Pl. 1). The Hickory sandstone attains a thickness of 406 feet, and the Cap Mountain limestone 75 feet. The Hensell sand is Lower Cretaceous and is 18 feet thick. Outcrops are 2 miles due south of C. Keese's ranch house in the south part of the area. Quaternary terrace gravels and alluvium also occur.

Structural Setting

Introduction

Enchanted Rock batholith is a granite-quartz monzonite-granodiorite intrusion about 100 square miles in area. It is pear-shaped and has intruded a framework of tightly folded Precambrian metamorphic rocks. The batholith is named after the largest of several exfoliation domes exposed on the southeast side of the mass (Pl. 3, fig. 1).

Regional Structure

The major structural lines are anticlinal and synclinal axes striking N. 17°–30° W. and plunging 16°–45° SE. The axis of the Castell syncline plunges 35°–40° SE. directly into the northern part of the batholith. Sixmile anticline is several miles to the east, strikes N. 25° W. and plunges less than 45° SE.

The longer dimension of Enchanted Rock batholith is 15 miles and strikes N. 10°–15° W. The shorter dimension is 9 miles and strikes at right angles to the long dimension. The northern third occupies the trough of the Castell syncline, the axis striking N. 10°–15° W. and plunging 35°–40° SE. (Fig. 1); it is in contact with Valley Spring gneiss which dips inward toward the batholith. Flow structures within this part of the batholith reflect in part the dips of the wall rocks.

The southern two-thirds is in contact with the Packsaddle schist. On the west side of the batholith the Packsaddle schist is overturned steeply to the east and suggests a thrusting directed about S. 40° E. (Pl. 2, Section C-C′). This structure is believed to be fairly large and to involve the central-west side of the batholith. The schists on the southeast side of the batholith, immediately east of Enchanted Rock, reflect in their attitude the presence of the Sixmile anticline, 3 miles to the east. Strike is N. 60° W., and dips are 20°–40° SW. Strike of these units swings sharply to the north as they approach the edge of Enchanted Rock batholith and dips approach vertical.

North of the northern part of the batholith, one-eighth and one-fourth mile, respectively, an anticline and a syncline strike approximately N. 80° W. almost at right angles to the synclinal trough occupied by the intrusion (Fig. 1). The syncline is north of the anticline and dies out within a quarter of a mile to the west. It is hidden by overburden to the east. The anticline, a small-scale structure, is overturned to the north for about a mile to the southeast.

Relation to Country-Rock Structures

Along the 45 miles of its outer perimeter the contact of the batholith with metamorphic wall rocks is discordant at three places. West of House Mountain for 4 miles along the contact as far north as Berry Spring the discordance is strong; east of Hickory Creek the Valley Spring gneiss and Packsaddle schist gradually pull away from the contact, and east of Silvermine Creek discordance is sharp for about a mile. Contact of granite along the remainder of the wall rocks is concordant, although in many places wall rocks are sharply discordant 1000 feet from the granite–wall rock contact. The 3-mile distance south from Silvermine Creek on the east side of Sandy Creek illustrates this.

Considerable crowding of wall rocks is evident on the east and southeast flanks of the batholith. The gentle westerly dips of the southwest limb of the Sixmile anticline steepen rapidly and swing almost parallel to the strike of the wall of the batholith. The schists within 1000 feet of the wall rocks have been squeezed into a tight, almost isoclinal syncline. The axis of this fold strikes N. 11° E. and follows along

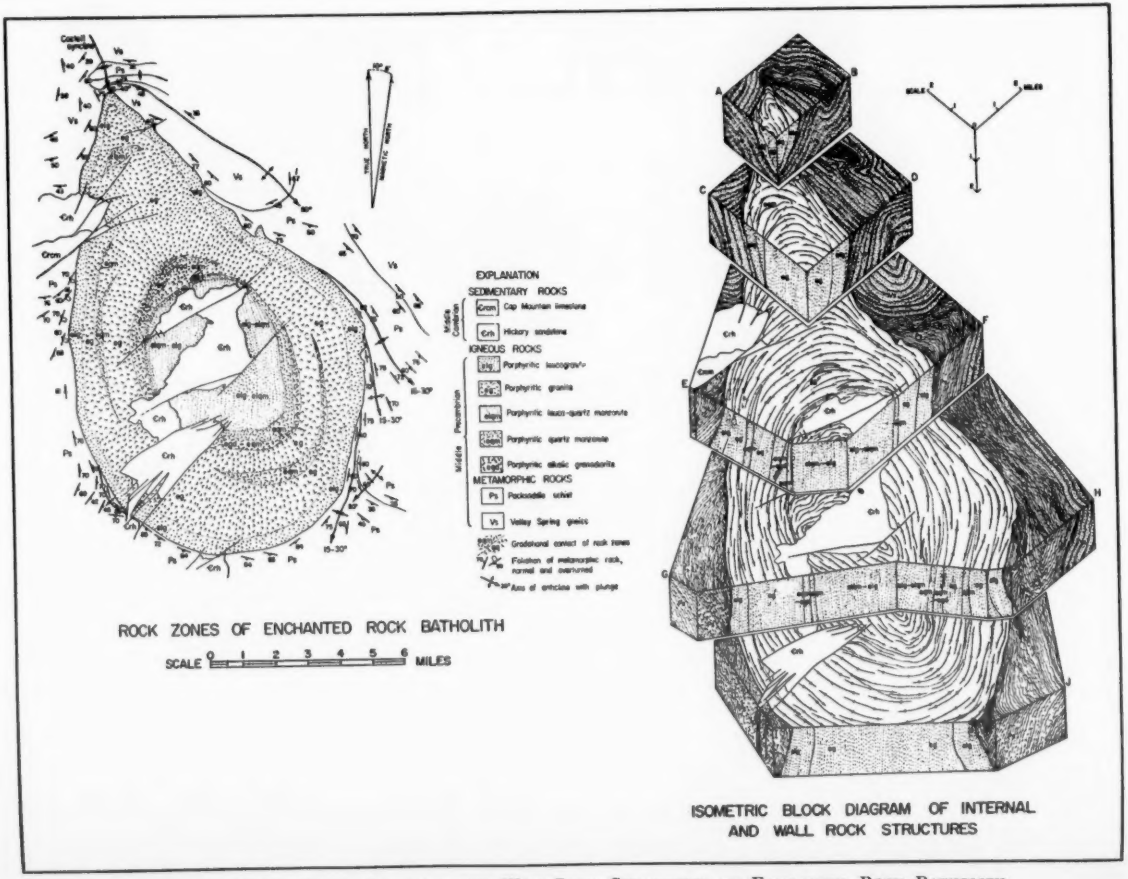

FIGURE 1.—ROCK ZONES, INTERNAL AND WALL-ROCK STRUCTURES OF ENCHANTED ROCK BATHOLITH

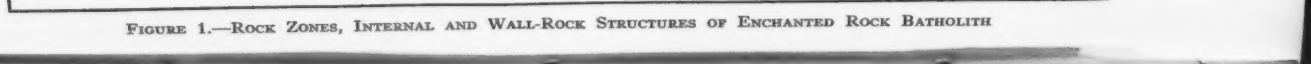

FIGURE 1.—ROCK ZONES, INTERNAL AND WALL-ROCK STRUCTURES OF ENCHANTED ROCK BATHOLITH

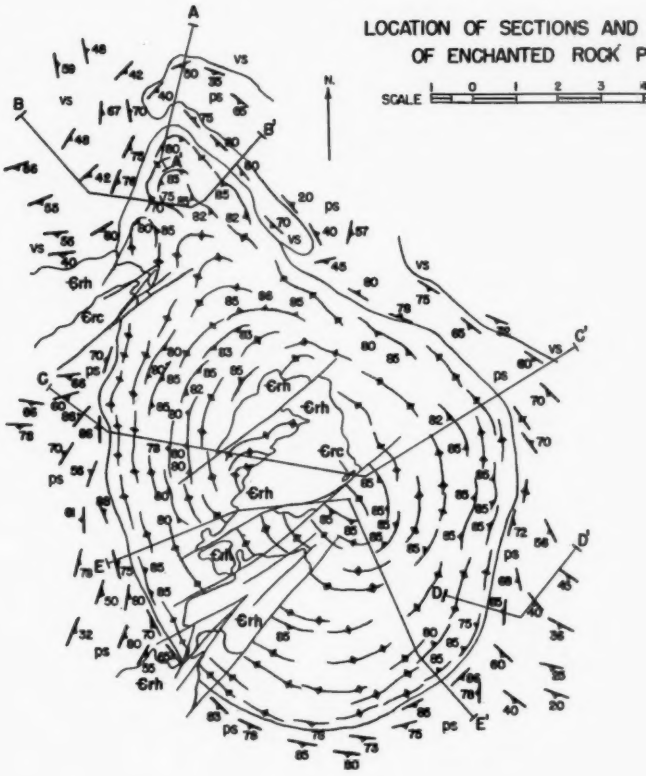
LOCATION OF SECTIONS AND
OF ENCHANTED ROCK P
SCALE
N.
A
A'
B
B'
C
C'
D
D'
E
E'
Xrh
Xrc
vs
ps

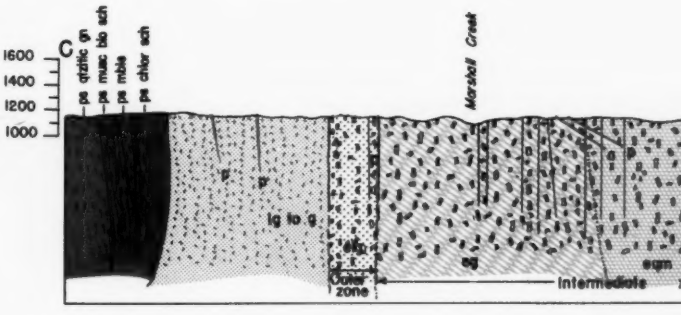
C
1600
1400
1200
1000
ps granitic gn
ps musc bio sch
ps mbls
ps chlor sch
Marshall Creek
lg to g
elg
eg
egn
Outer zone
Intermediate

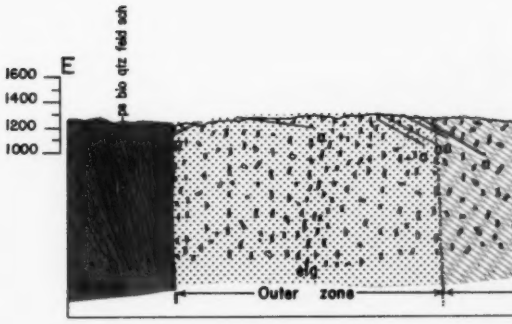
E
1600
1400
1200
1000
ps bio qtz feld sch
elg
Outer zone

AND STRUCTURE
CK PLUTON

4 5 MILES

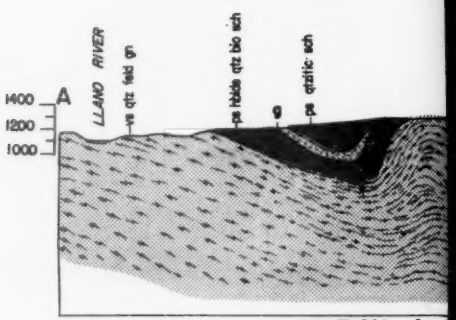

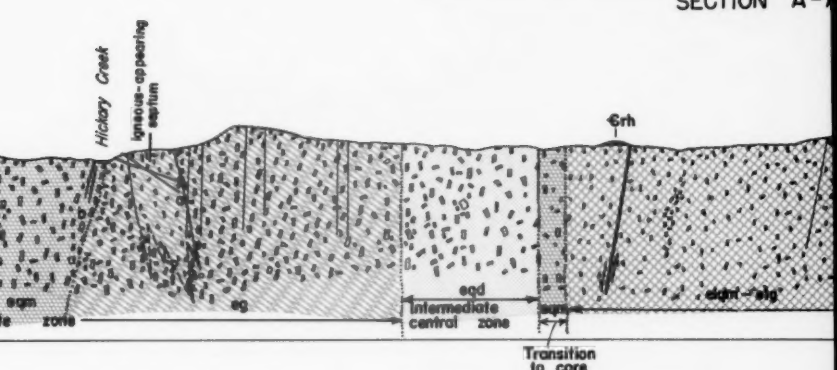

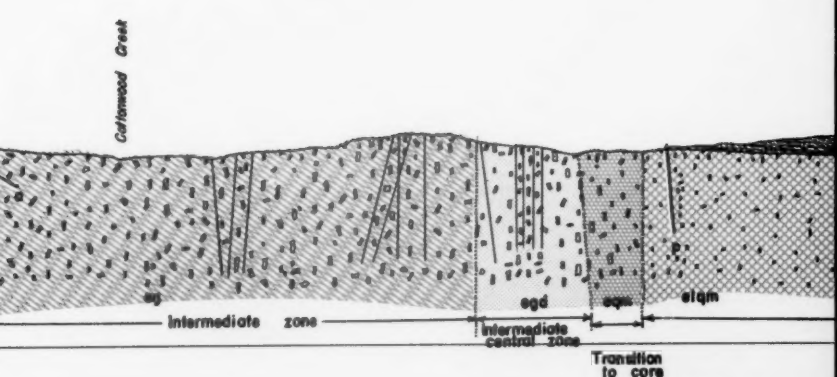

STRUCTU

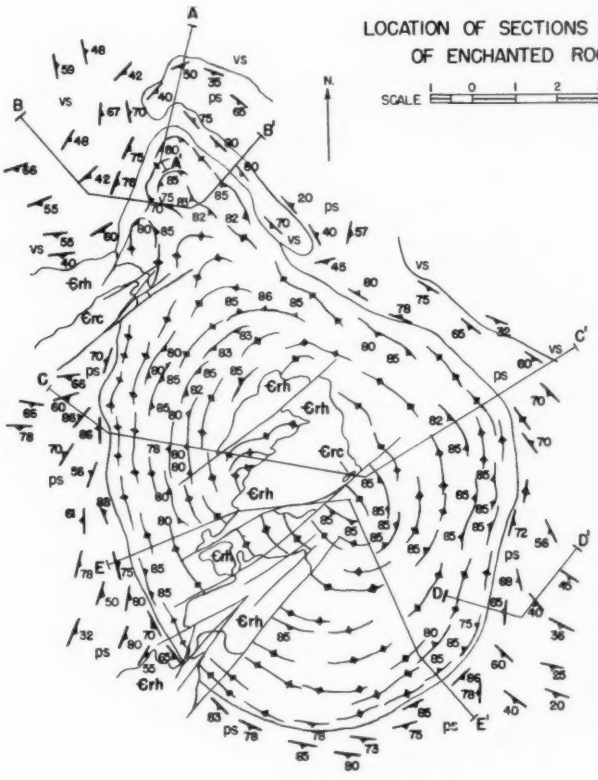
LOCATION OF SECTIONS AND S
OF ENCHANTED ROCK PL
SCALE
0 1 2 3 4
N.
A
A'
B
B'
C
C'
D
D'
E
E'
vs
ps
Crh
Crc

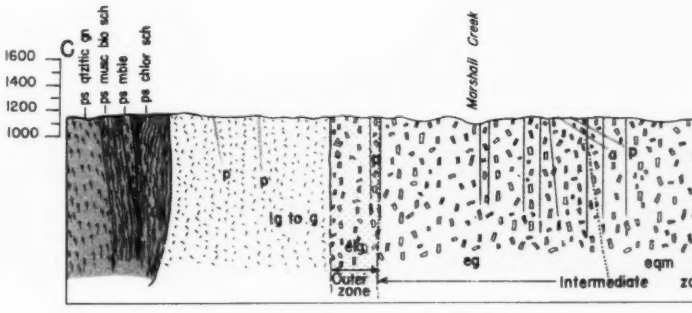
C
ps qtztic sch
ps musc bio sch
ps mbio sch
ps chlor sch
1600
1400
1200
1000
Marshall Creek
lg to g
Outer zone
Intermediate

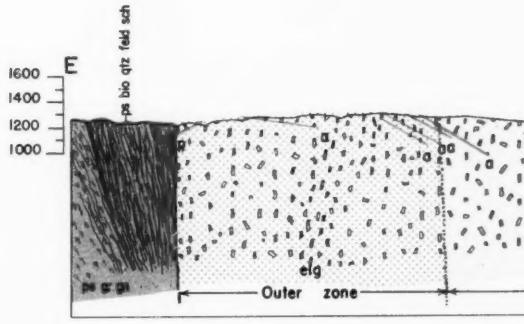
E
ps bio qtz feld sch
1600
1400
1200
1000
Outer zone

AND STRUCTURE
CK PLUTON

4 5 MILES

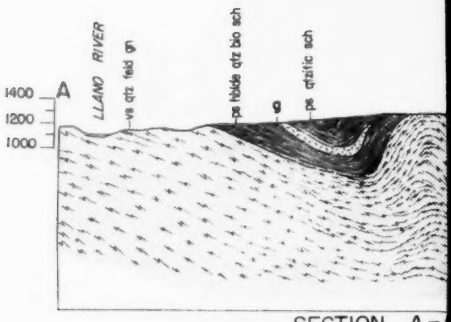

SECTION A-A

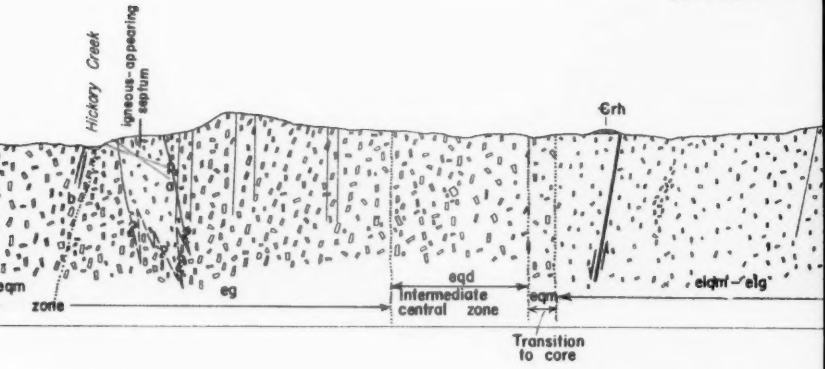

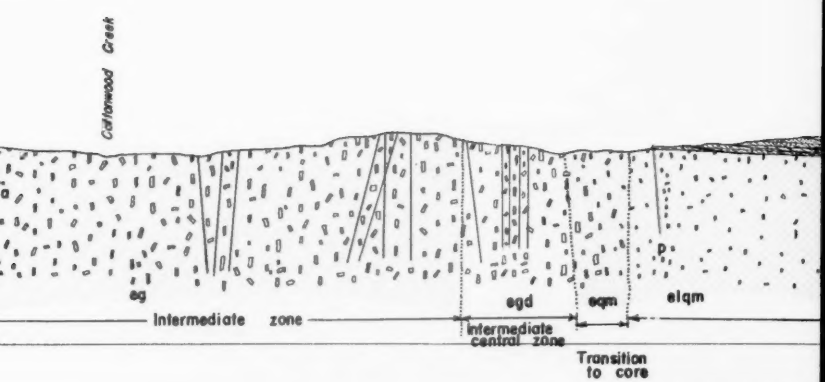

STRUCTU

UCTURE
ON
MILES

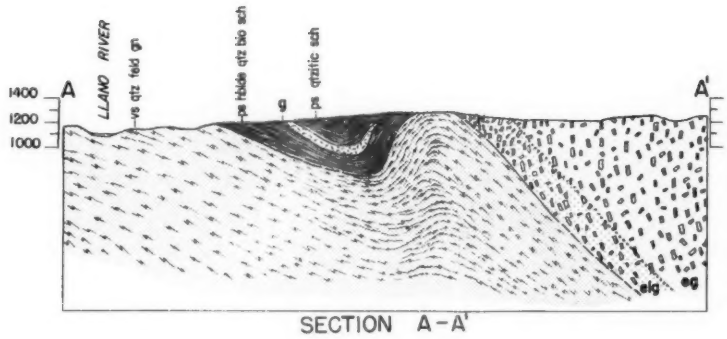

SECTION A-A'

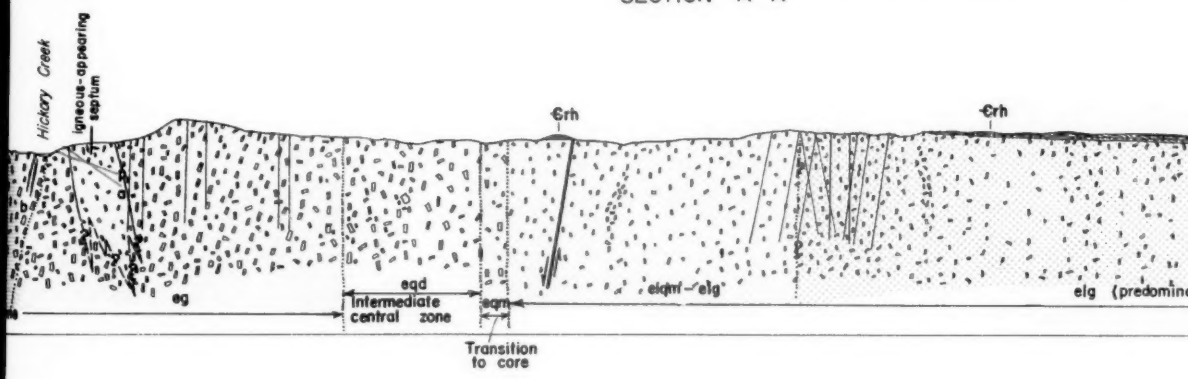

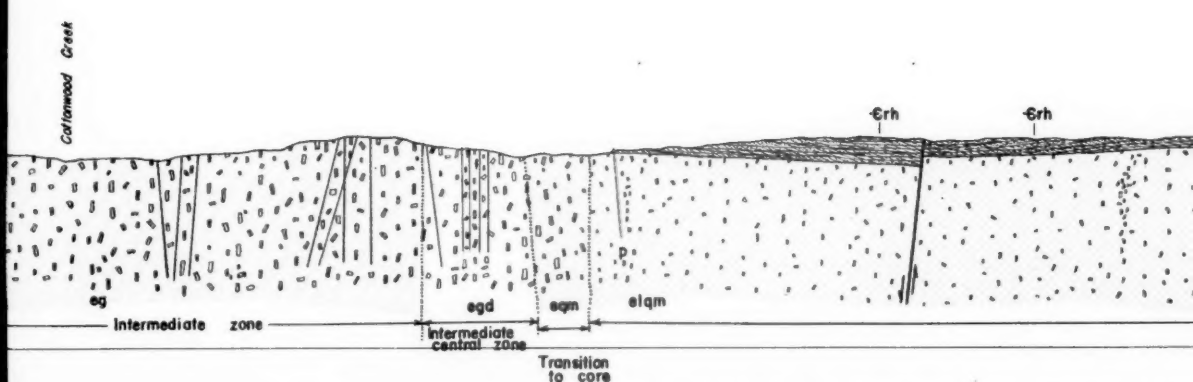

STRUCTURE SECTIONS, ENCHANT

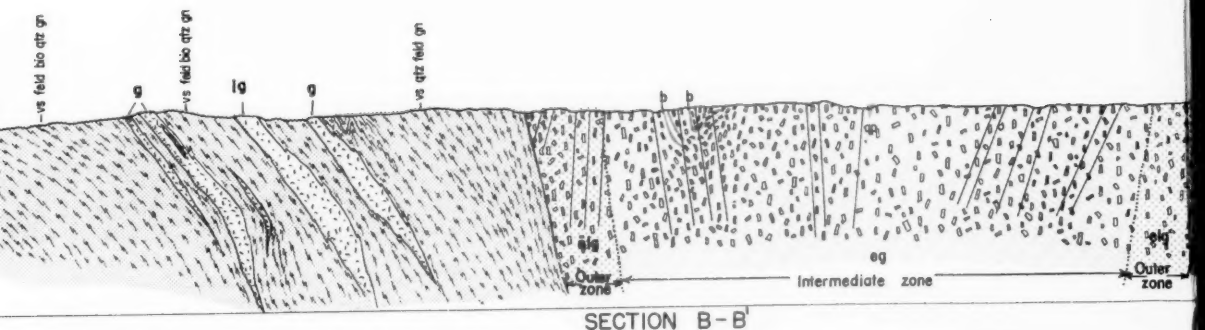

SECTION B-B'

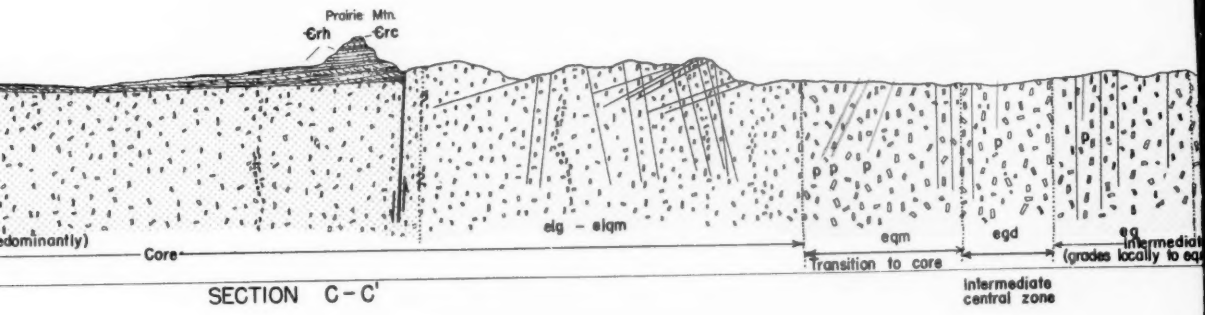

SECTION C-C'

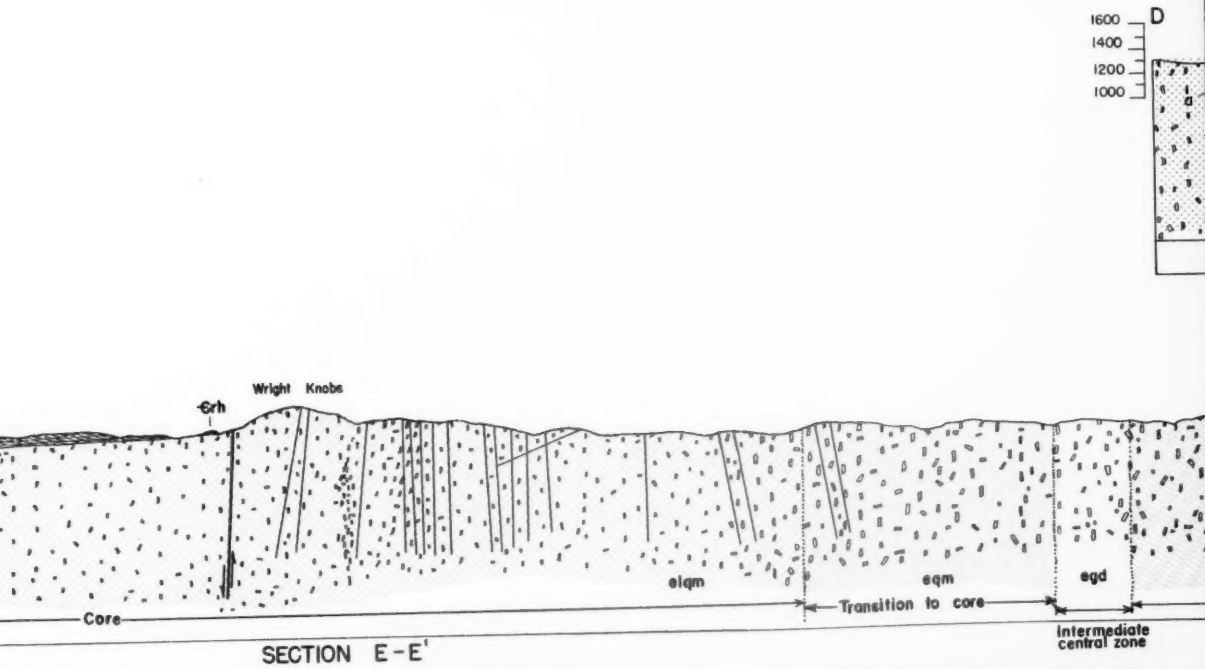

SECTION E-E'

ANTED ROCK BATHOLITH, LLANO AND GILLESPIE COUNTIES, TEXAS

See Plate 1 for explanation of symbols.

UCTURE
N
MILES

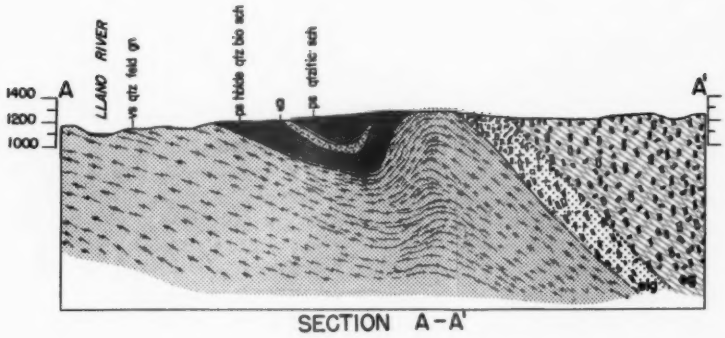

SECTION A-A'

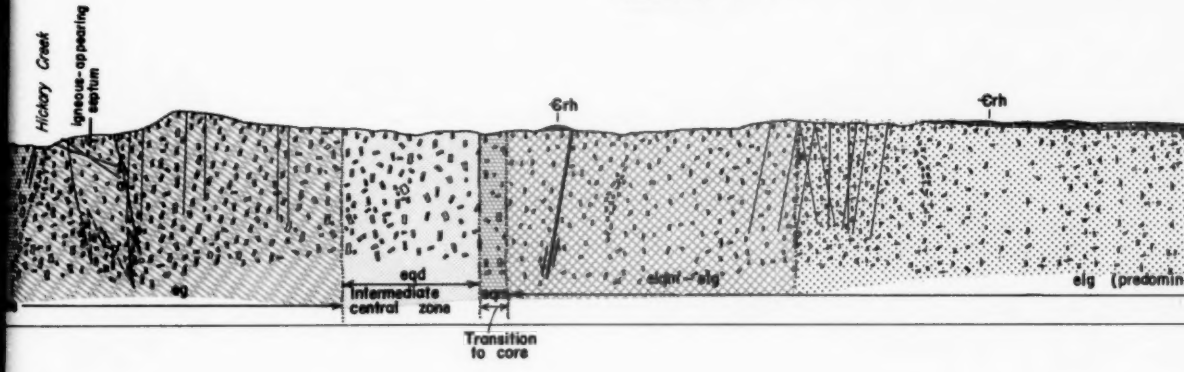

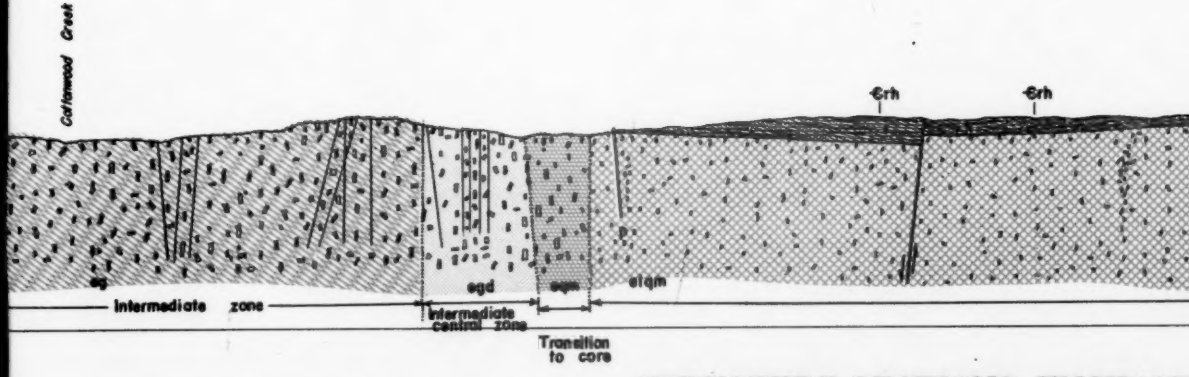

STRUCTURE SECTIONS, ENCHANT

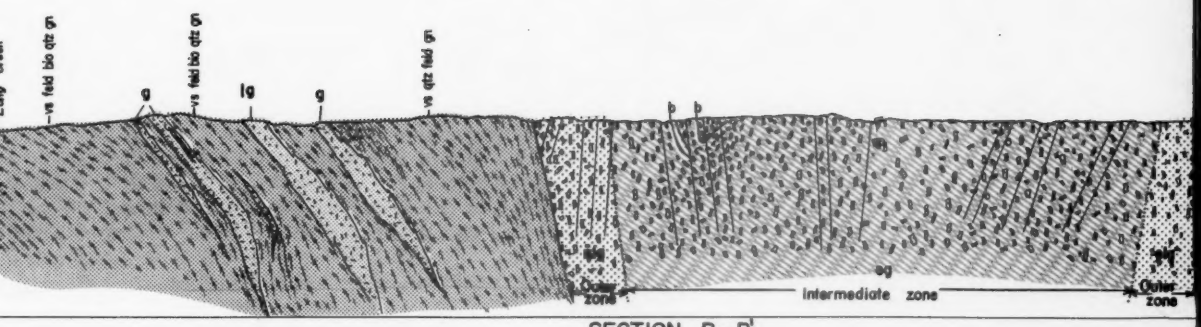

SECTION B-B'

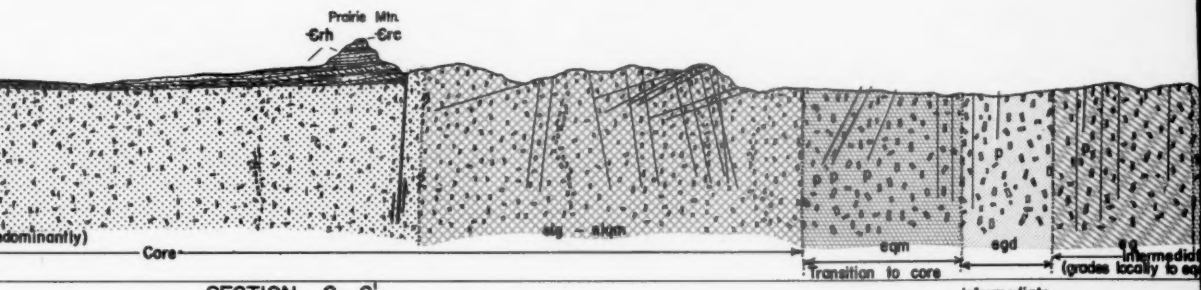

SECTION C-C'

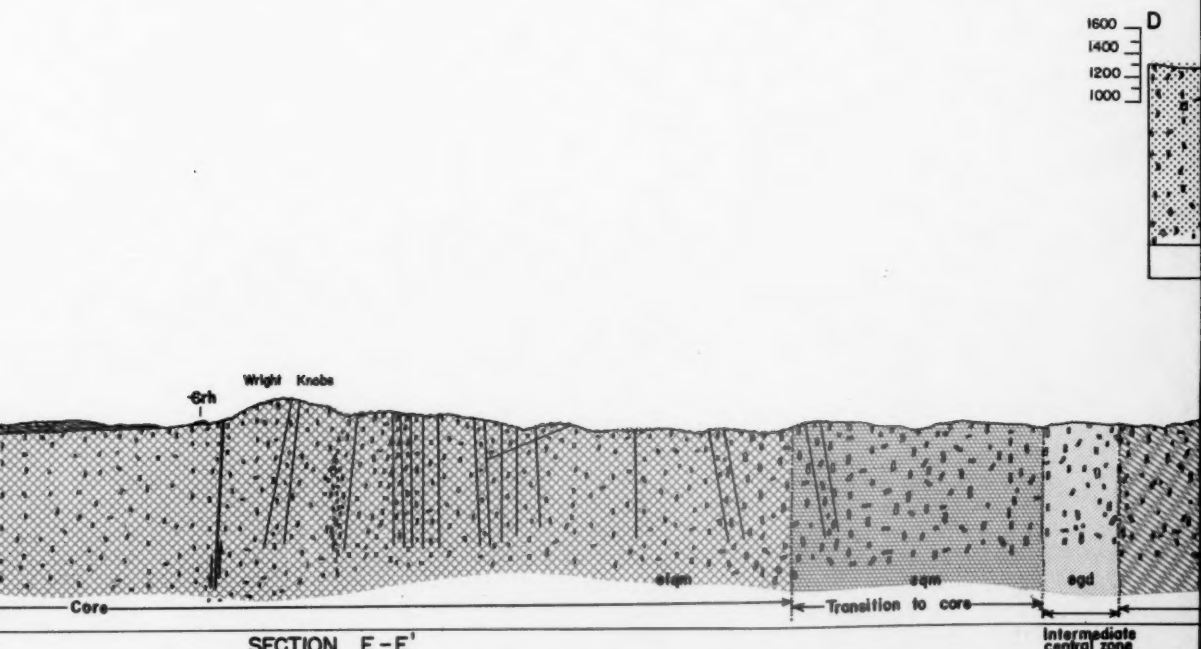

SECTION E-E'

ANTED ROCK BATHOLITH, LLANO AND GILLESPIE COUNTIES, TEXAS

See Plate 1 for explanation of symbols.

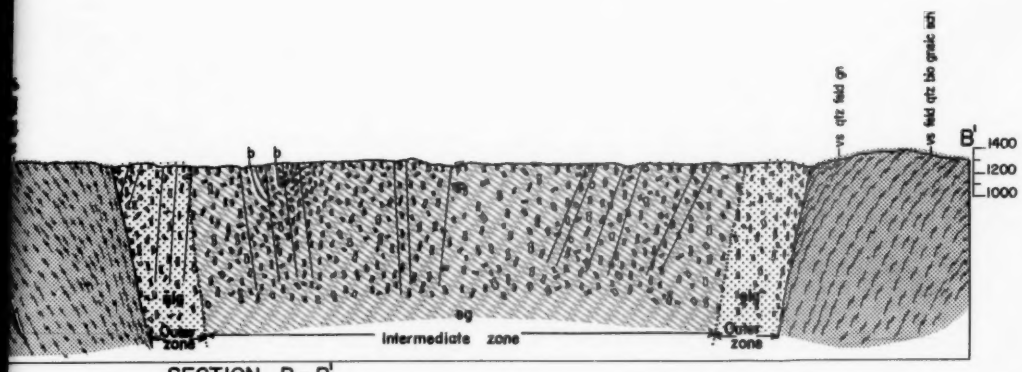

SECTION B - B'

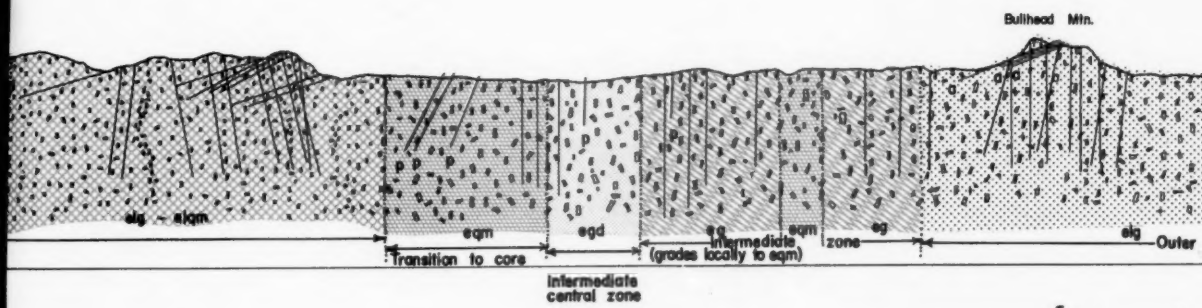

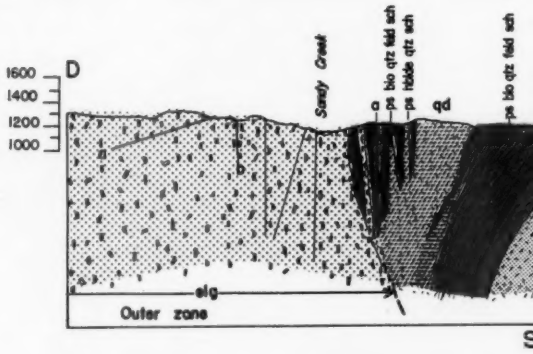

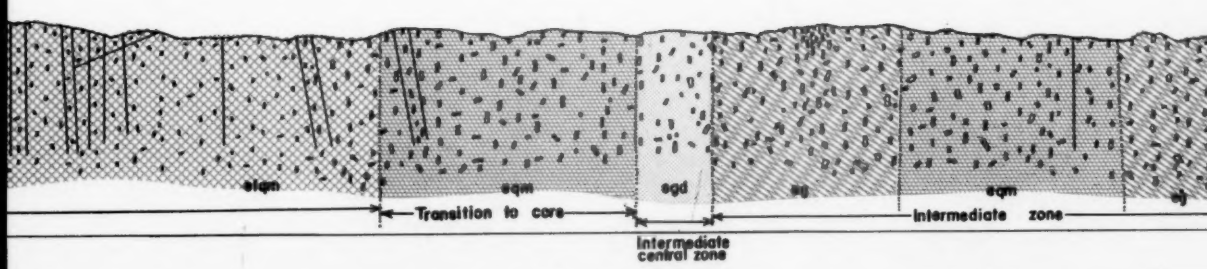

, LLANO AND GILLESPIE COUNTIES, TEXAS

f symbols.

Map of Texas with location of area

By Robert M. Hutchinson

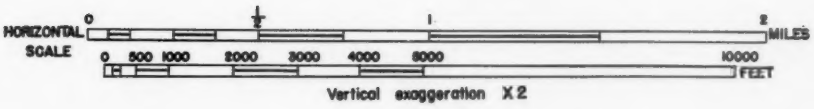

Vertical exaggeration X2

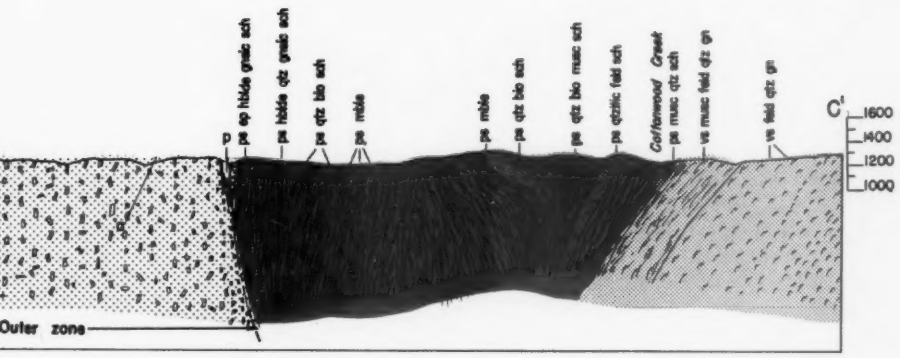

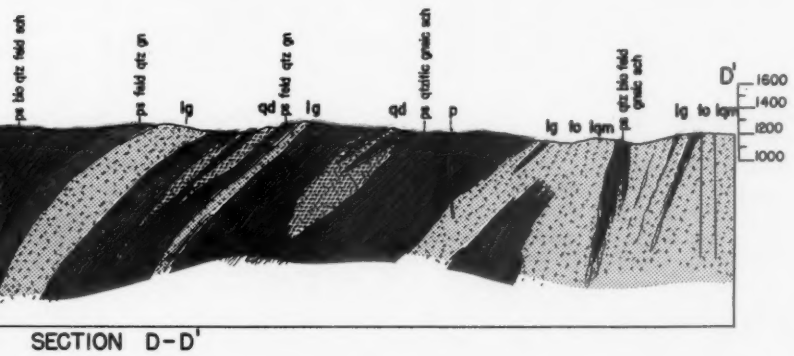

SECTION D-D'

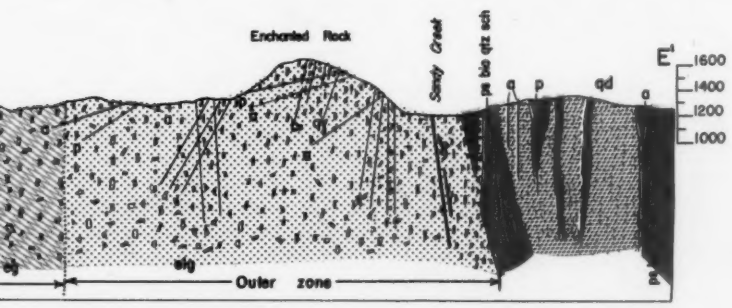

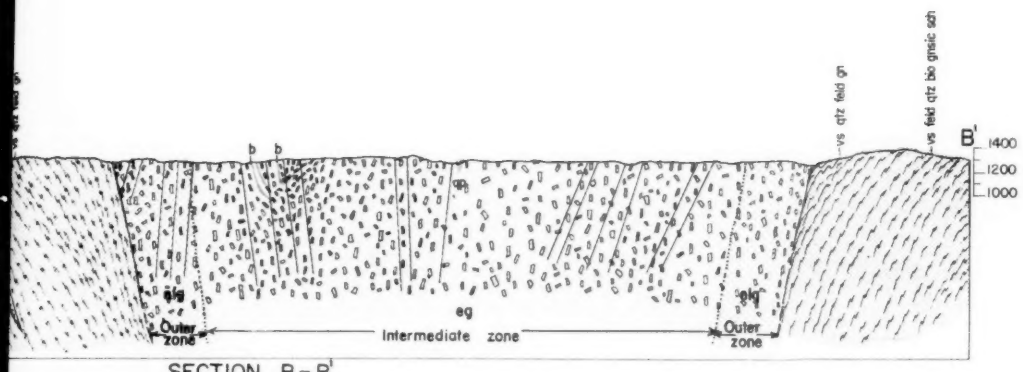

SECTION B-B'

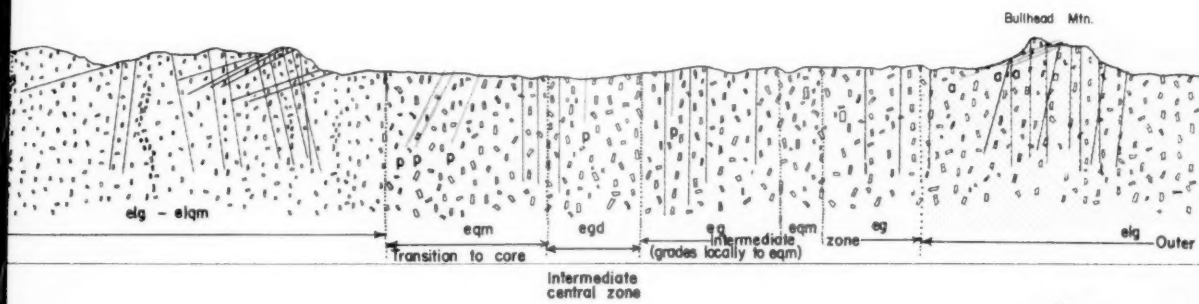

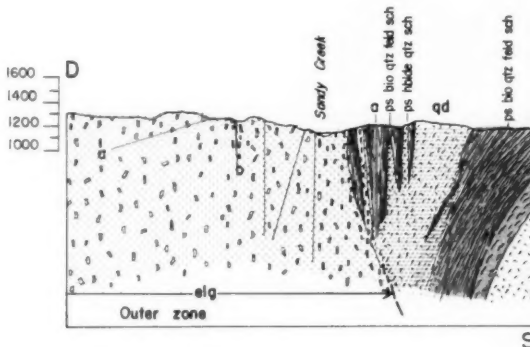

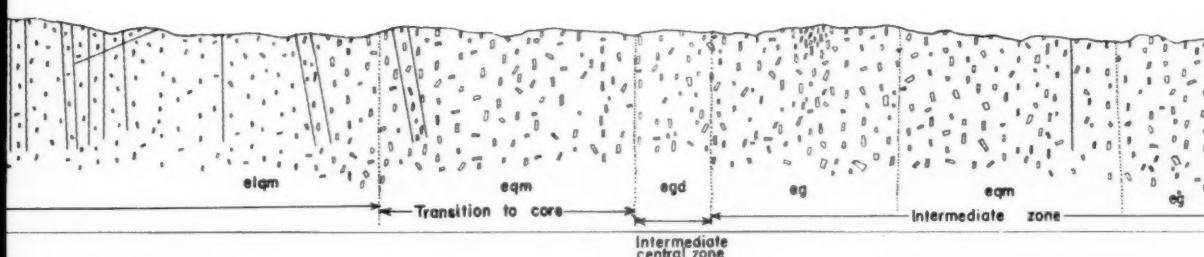

, LLANO AND GILLESPIE COUNTIES, TEXAS

f symbols.

Map of Texas with location of area

By Robert M. Hutchinson

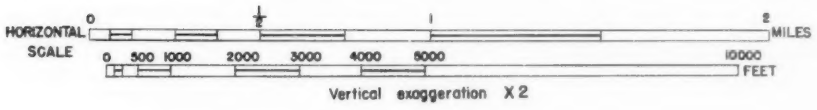

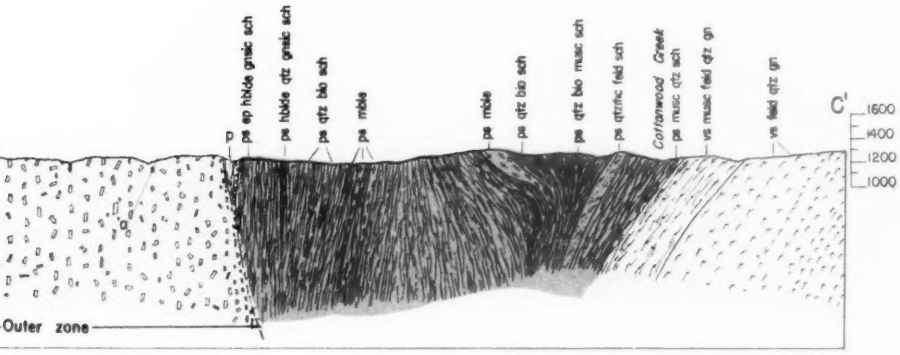

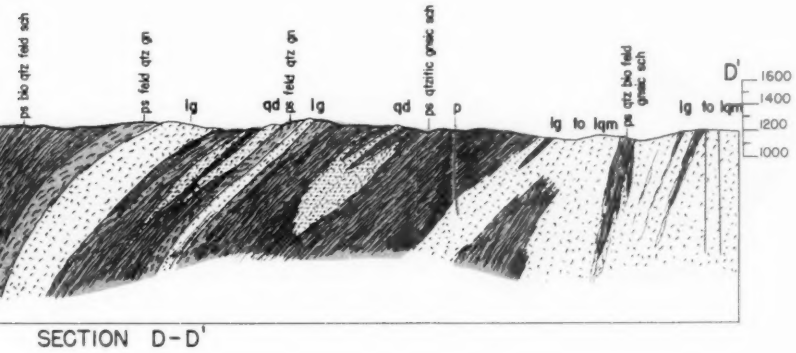

SECTION D-D'

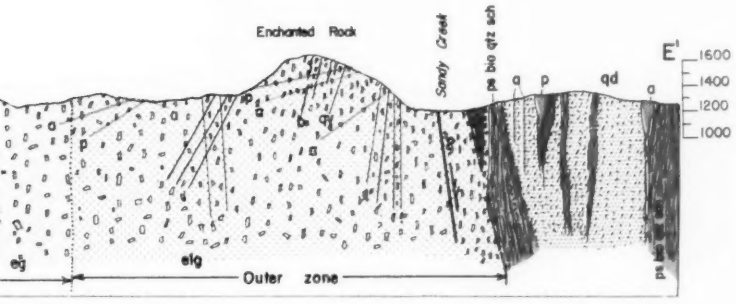

the east side of the batholith for a distance of about 4 miles, reflecting the outline of the edge of the batholith. A similar relationship, though on a smaller scale, occurs on the southwest side of the batholith.

In many places, within several hundred feet of the flank of the batholith, the schists dip steeply toward the granite, possibly suggesting by their attitude that the granite has tended to override the schists.

Structural Petrology

Fabric Axes

The fabric elements (minerals) have dimensional orientation plainly visible in the field (Pl. 3, fig. 2). The orientation is linear (linear-flow structure) and planar (planar-flow structure). The Cloos method of mapping the internal structures of igneous rocks, which is concerned almost exclusively with megascopic features that are apparent in the field, is applicable to rocks of the batholith.

Fabric axes are used in describing dimensional orientation of single-crystal fabric units. Sander's original terminology (1926, p. 328; 1930, p. 119) is applied to primary-flow structure in rocks of the batholith. The axes are referred to as *a*, *b*, and *c*. The critical axis denoting direction of transport is *a*. It may be either perpendicular or parallel to lineation. Fairbairn (1949, p. 6) defines the *b* and *c* axes as follows:

> "*b* is limited to parallelism with fold axes and is almost always associated with lineation. It is commonly perpendicular to *a*, since direction of movement in the development of a major fold is normal to its axial line. If foliation is developed, *b* lies in the foliation surface.
>
> "*c* is used to denote the normal to the plane formed by *a* and *b*, and has no independent existence as a fabric coordinate."

Linear-Flow Structures

Long dimension of microcline phenocrysts.—Orientation of the long dimension of microcline phenocrysts took place so that each crystal assumed, as nearly as possible, a minimum projection area perpendicular to the lineation. Crystal habit consists of either prisms and basal pinacoids (Fig. 2) or right- or left-handed Carlsbad twins (Fig. 3). The longest crystallographic dimension of each type of crystal corresponds to the c[1] axis, and this is parallel or subparallel to the principal flow direction, the critical axis *a*. During early stages of intrusion and crystallization the principal direction

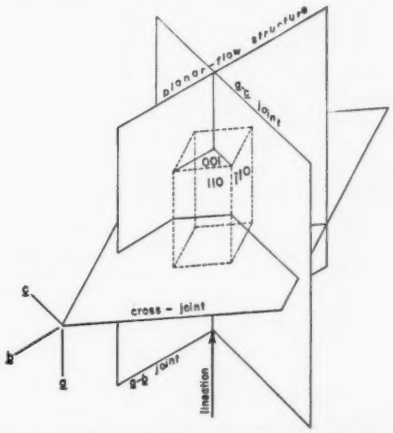

FIGURE 2.—RELATIONSHIP OF FABRIC AXES TO CRYSTALLOGRAPHIC AXES

of transport was vertical, or nearly so. Primary lineation is parallel to this direction of transport. Figures 2 and 3 show the relationship of fabric axes to crystallographic axes. Prismatic crystals are square in outline, and commonly the c axis is 2–4 times the width. Appearance of one of these (110) forms in the field is shown in Figure 2 of Plate 3.

Microcline phenocrysts are rectangular with (010) predominant over (110) and (120) forms. These are truncated by (001) and (201) forms (Fig. 3). The longest dimension is not the c axis but a diagonal axis. However, because of the tendency of the crystal to orient with minimum areal outline perpendicular to the direction of transport, the c axis lies parallel or subparallel to the *a* axis (Fig. 3).

A fairly good check on orientation of the c axis was possible in the field. On horizontal or near-horizontal outcrop surfaces accurate readings on pitch of the lineation were obtained from (1) the outlines of prism faces on twinned phenocrysts, (2) the trace of the Carlsbad twin plane, and (3) the dip of crystal faces. These

[1] Crystallographic axes designated by roman type throughout paper.

are recorded on Plate 1. This linear parallelism is considered a reliable reproduction of the direction of greatest lengthening in the rock during the period when the structure developed.

Dimensional orientation of quartz mosaics.—The petrofabric diagram of the c axis for these grains is subpolar (Fig. 4b) and subnormal to the *ac* fabric plane. A series of separate maxima

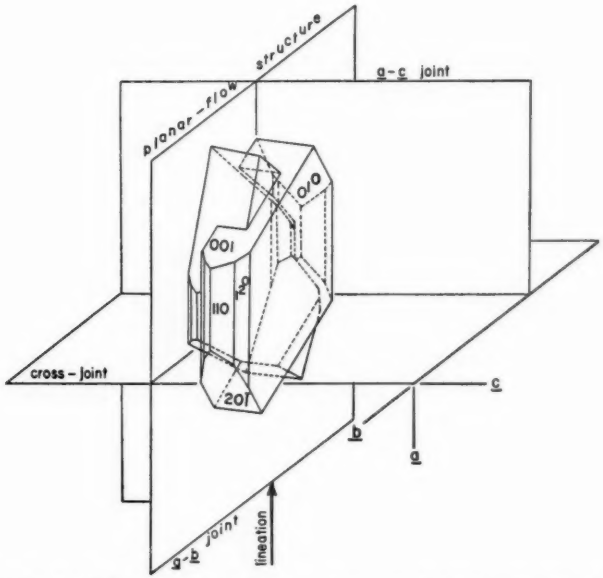

FIGURE 3.—RELATIONSHIP OF FABRIC AXES TO CRYSTALLOGRAPHIC AXES

Dimensional orientation of biotite.—Linear-tabular aggregates of 1-mm flakes have their long dimensions subparallel to the *a* fabric axis. Disseminated grains of biotite also occur but are not so abundant as the clusters. Crowding of biotite flakes between large microcline crystals often distends the clusters into narrow layers parallel to the platy flow structure in the *ab* fabric plane.

The most common maximum for the poles of cleavage flakes is at *c* with dispersion of some poles in a partial girdle parallel to *ac*. The chief maximum of the poles is inclined a few degrees to *c* (Fig. 4a). This dimensional orientation probably developed during upward movement of the granite parallel to the *a* direction at the same time it was crowded laterally toward the wall of the chamber in the *c* direction. Micas in thin section do not appear ruptured or bent. The micas with poles normal to the *ac* plane are interpreted as having grown in *a-c* tension cracks.

contained within a girdle are inclined approximately 30° to the *b* fabric axis or might be said to be subnormal to the lineation, *a*.

During movement each grain tended to rotate about its c axis in the *ab* fabric plane with the c axis tending subnormal to the *ac* fabric plane, or the *a* fabric axis.

Platy Flow Structures

Platy parallelism of phenocrysts.—Microcline phenocrysts exhibit platy parallelism (Pl. 3, fig. 2). The crystals have their largest faces (010) in parallel planes. Prism faces (110) and (120) generally are visible when the c axis parallels the *a* fabric axis. Not all crystals with (201) faces visible instead of (110) and (120) have their c axis parallel to the lineation.

The a-c plane of the rectangular-shaped phenocrysts is subparallel or parallel to the direction of dip of the *a-b* fabric plane (Fig. 2).

The degree of alignment in the outer and

FIGURE 4.—PETROFABRIC DIAGRAMS OF BIOTITE AND QUARTZ IN OUTER ZONE OF THE BATHOLITH

(a) 55 cleavage poles of biotite from outer zone of the batholith. Thin section cut normal to the platy flow structure and parallel to the lineation (*a* is lineation).

(b) 100 quartz axes from outer zone of the batholith. Thin section cut normal to the platy flow structure and parallel to the lineation (*a* is lineation).

intermediate zones is very high; an estimated 70 per cent have their a-c planes within 45° of being parallel to the *a-b* fabric plane. Automorphic plagioclase and microcline of the groundmass are similarly oriented.

Flow layers (*schlieren*).—Biotite-rich and microcline-rich layers are readily observed because of textural and color contrasts with the surrounding rock. Biotite-rich schlieren have sharp boundaries (Pl. 3, fig. 3), whereas microcline-rich schlieren tend to be more gradational (Pl. 3, fig. 4). Within individual flow layers the relative proportion of minerals is fairly constant. Thickness and length of the layers range widely. They may be straight (Pl. 3, fig. 3) or curved (Pl. 3, fig. 5). Crystals of microcline distributed within and lying up against these biotite-rich schlieren have brachypinacoids (010) parallel to the strike of the flow layers. The flow layers show marked parallelism to platy flow structure of the surrounding rock.

Concentrations of biotite-rich schlieren are restricted to the outer 1½- to 2-mile border of the batholith. Microcline-rich schlieren occur more commonly in the intermediate and intermediate central zones of the batholith.

Biotite-rich schlieren, commonly several inches thick, are straight or slightly curved and 30–200 feet in length. The relationship of the longest dimension to the direction of lineation could not be obtained from most of the outcrops. They have thus been mapped as planar flow structure and not as lineation. Arcuate schlieren are local and small scale and are restricted mostly to the outer zone.

Parallelism of xenoliths.—Slablike inclusions of metamorphic rocks are arranged in layers parallel to platy flow structure. Figure 6 of Plate 4 shows this parallelism.

Some inclusions strike 15°–30° transverse to surrounding platy flow structure and rarely are as much as 75° off strike (Pl. 4, fig. 7). It is not

---

PLATE 3.—INTERNAL STRUCTURES OF THE BATHOLITH

FIGURE 1.—Enchanted Rock and subsidiary domes on southeast side of the batholith. View looking east.

FIGURE 2.—Combination of linear and platy flow structures. Lineation plunges 70° to the left in the plane of the platy flow structure which is vertical. North tip of the batholith.

FIGURE 3.—Narrow biotite-rich schlieren parallel to platy flow structure. On exfoliation dome a quarter of a mile south of Enchanted Rock dome.

FIGURE 4.—Microcline-rich schliere subparallel to platy flow structure of enclosing porphyritic medium granite of intermediate zone. Hammer handle parallels platy flow structure.

FIGURE 5.—Symmetrically curved biotite-rich schlieren 1 mile west of House Mountain. Platy flow structure of surrounding area parallels hammer handle.

FIGURE 6.—Rock swirl 1 mile east of the Kidd ranch house

PLATE 4.—PRIMARY FRACTURES AND XENOLITHS

FIGURE 1.—Outcrops of the outer zone in the south part of the batholith show *a-c* joints and *a-b* joints. Platy flow structure trends left to right parallel to hammer handle and is vertical.

FIGURE 2.—An *a-c* joint filled with pegmatite 1 mile northwest of Enchanted Rock dome. Hammer handle parallels platy flow structure which is vertical and strikes right to left.

FIGURE 3.—Folded aplite of marginal fissure dips 17° left. Hanging wall moved up with development of freely opened space subsequently occupied by aplite. Outcrop on east side of Enchanted Rock dome. Platy flow structure parallels hammer handle.

FIGURE 4.—Aplite-filled shear on exfoliation dome a quarter of a mile south of Enchanted Rock dome. Platy flow structure within aplite subparallels walls of fissure.

FIGURE 5.—Biotite-rich schlieren cut by marginal fissure filled with pegmatite and aplite. Fissure dips 17° left. Outcrop is southwest side of Enchanted Rock dome.

FIGURE 6.—Concordant xenoliths of Packsaddle schist partly replaced by granite, 1 mile north of House Mountain.

FIGURE 7.—Discordant xenolith of Packsaddle schist in porphyritic alkalic granodiorite of intermediate central zone 3 miles northwest of Enchanted Rock dome. Long axis of xenolith strikes 70° transverse to platy flow structure of enclosing granodiorite. Microcline phenocrysts have crowded against faces of the xenolith which was probably gradually sinking prior to solidification of the magma.

FIGURE 1

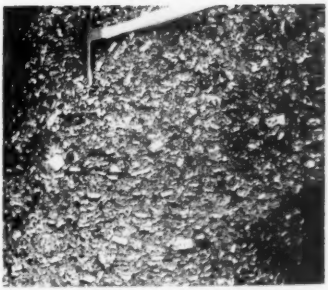

FIGURE 2

FIGURE 3

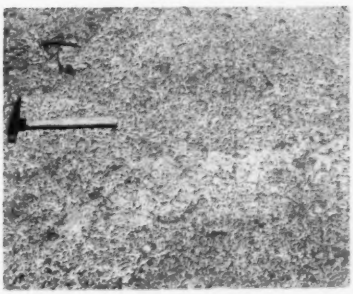

FIGURE 4

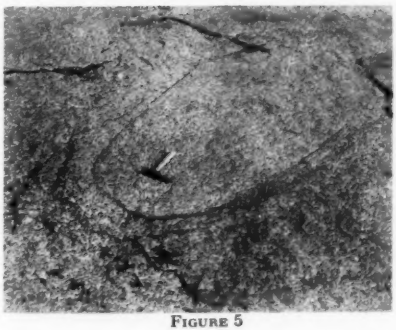

FIGURE 5

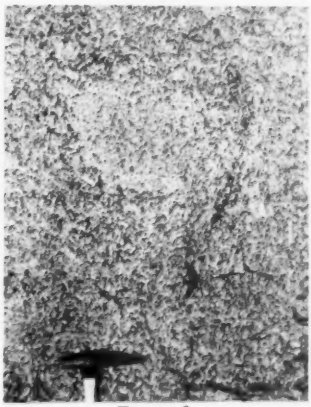

FIGURE 6

INTERNAL STRUCTURES OF THE BATHOLITH

FIGURE 1

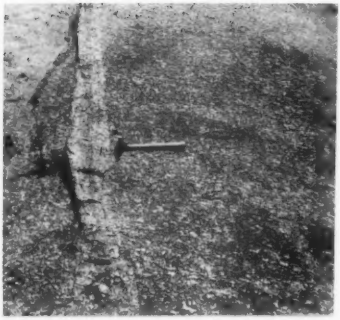

FIGURE 2

FIGURE 3

FIGURE 4

FIGURE 5

FIGURE 6

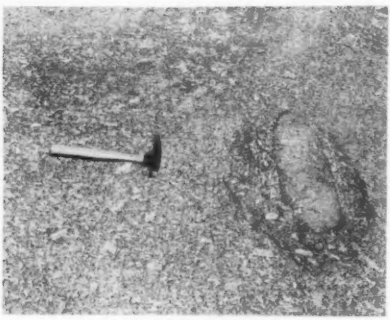

FIGURE 7

PRIMARY FRACTURES AND XENOLITHS

FIGURE 1

FIGURE 2

FIGURE 3

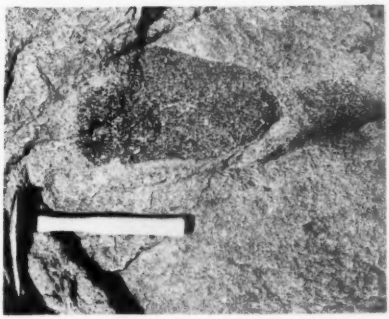

FIGURE 4

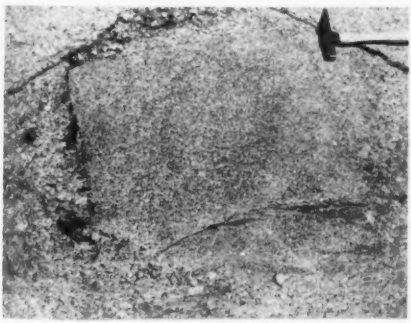

FIGURE 5

FIGURE 6

BORDER-ZONE RELATIONSHIPS

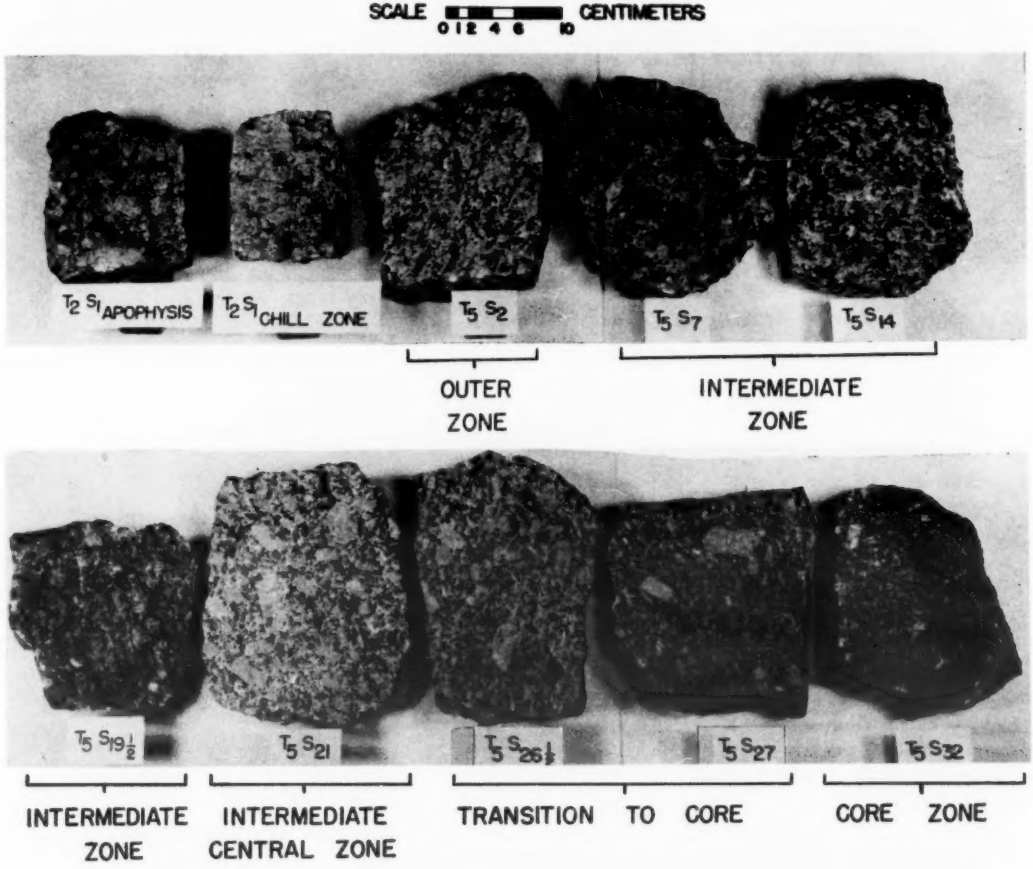

TEXTURAL CHANGES (CORE-RIM) ACROSS ENCHANTED ROCK BATHOLITH
Section along Traverses T_2 and T_5

uncommon for them to have dips considerably less than the platy flow structure. Specific gravity of a few of these ranges from 2.71 to 2.74 as compared to 2.66 to 2.70 for the enclosing igneous rock.

Xenoliths are exceedingly rare in the core of the batholith. Over the 15 square miles covered by the core rock only one xenolith was observed. With this exception the xenoliths lie outside the core within the intermediate central, intermediate, and outer zones. Of approximately 600 xenoliths mapped only 3 seemed to grade into biotite-rich schlieren.

Rock "swirls".—Circular patterns of microcline-rich concentrations were observed in two places (Pl. 3, fig. 6). No information could be gathered from the outcrop on whether these were cylindrical or spherelike. The swirl-like pattern around and including these structures suggests development by interlamellar movement of magma sheets tending to rotate microcline-rich centers.

Combination of linear- and platy-flow structure.—Linear flow structure lies within the planar flow structure and is best seen where the outcrop surface parallels the *a-b* fabric plane. On this surface the linear character of rectangular and square microcline phenocrysts is seen to best advantage. So nearly equidimensional are twinned microcline phenocrysts when viewed in the *a-b* fabric plane that lineation is barely visible. Crystals with only (110) and (001) faces developed emphasize the lineation considerably where they occur (Pl. 3, fig. 2). On one 8-mile statistical traverse with station readings at approximately 600-foot intervals, within a 100-square centimeter area at each station, the long and short dimensions of 672 microcline phenocrysts were measured on horizontal outcrop surface. Of these, 83 (12.3 per cent) showed development of (110) faces only.

Fracture Systems

Cross-joints.—Lineation is parallel to the direction of maximum elongation, and cross-joints, which are essentially tensional in origin, are perpendicular to the linear flow structure. Throughout most of the batholith lineation is close to vertical so the cross-joints are horizontal or nearly so.

Exposures of cross-joints are rare. They are best developed on House Mountain and in a series of small, steep hills extending a mile or so north of House Mountain on the east side of Hickory Creek. Joint surfaces commonly are 2–10 feet apart, fairly smooth, and devoid of any hydrothermal alteration. Cross-joints are absent from the series of exfoliation domes along the southeast side of the batholith in the vicinity of Enchanted Rock.

a-c joints.—Joints perpendicular to planar flow structure and dipping parallel to the lineation are designated *a-c* joints. Their formation is attributed to lateral or peripheral stretching taking precedence over movement in the *a* direction (Fig. 5a). Joints of this orientation occur as far as 3 miles from the rim toward the core. They may possibly occur in the core. Dips are nearly vertical, and the joints commonly extend for several hundred feet in straight, persistent lines. This is one of the more prominent of the primary fracture systems.

By use of a Schmidt equal-area net, poles normal to *a-c* joints have been plotted on the

---

PLATE 5.—BORDER-ZONE RELATIONSHIPS

FIGURE 1.—"Chill" border rock on east flank of batholith. Partial replacement of metamorphic wall rocks is visible. Main mass of batholith lies to left.

FIGURE 2.—Contact of schist wall rock and quartz monzonite of border zone, southeast side of the batholith. Contact dips 70° SW. under the batholith.

FIGURE 3.—"Basic front" of biotite-rich layers shown in Figure 12. Layers curve left and dip 25–60° to right.

FIGURE 4.—Partly replaced xenoliths of recrystallized Packsaddle schist in leuco-quartz monzonite of "chill" border zone. East side of batholith 1 mile northeast of Enchanted Rock dome along Sandy Creek.

FIGURE 5.—Block-shaped xenolith of aplite in porphyritic leucogranite of the outer zone 50 feet from chilled border zone, southeast flank of batholith.

FIGURE 6.—Apophysis of porphyritic leucogranite pinching out in Packsaddle schist. East bank of Sandy Creek half a mile northeast of Enchanted Rock dome.

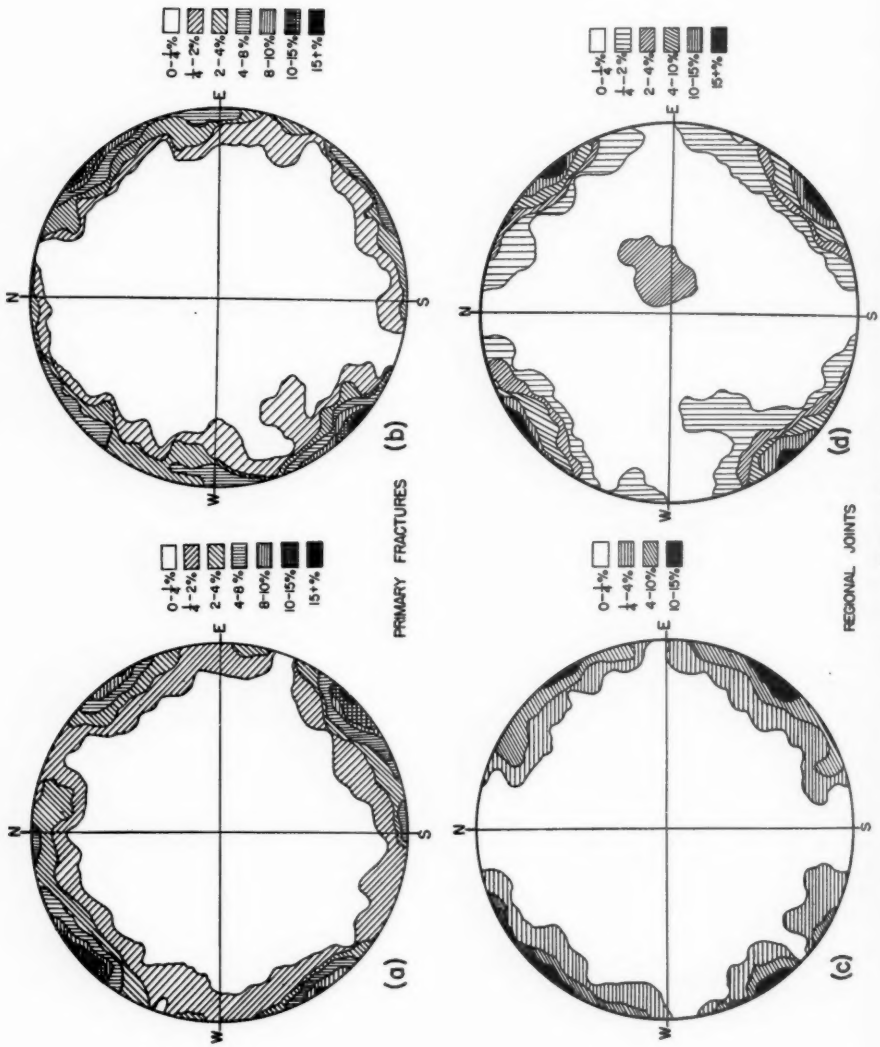
0–½%
½–2%
2–4%
4–8%
8–10%
10–15%
15+%
0–½%
½–2%
2–4%
4–10%
10–15%
15+%
0–½%
½–4%
4–10%
10–15%
N
S
E
W
(a)
(b)
(c)
(d)
PRIMARY FRACTURES
REGIONAL JOINTS

FIGURE 5

lower hemisphere and their concentration contoured. The contour diagram for 379 joints is girdle-polar (Fig. 5a). Each joint plotted on Plate 1 represents, on the average, four joints at the outcrop with similar strike and dip; hence, Figure 5a actually represents 1516 joints. The girdle distribution indicates *a-c* joints carry completely around the batholith. The nonuniform distribution of the *a-c* joints and the shape of the batholith contribute to the polar character of the diagram. Polar concentrations in the northeast–southwest and northwest–southeast corners are due mainly to similarity in strike and dip of *a-c* joints and a set of regional joints. The regional joints have a northeast and northwest strike and are close to vertical in all places. Where these coincide with the strike of the *a-c* joints the two sets are indistinguishable. In Figure 5a an effort was made to plot only the *a-c* joints in a zone about 3 miles inward toward the center from the rim of the batholith. The polar character of the contour diagram still persists and is due not only to nonuniform distribution of *a-c* joints but also to the impossibility of distinguishing the regional joints from *a-c* joints where strikes and dips are the same.

A contour diagram of what are thought to be only the regional joints in the intermediate central, intermediate, and outer zones of the batholith is given in Figure 5c. The contour diagram for 97 joints shows that these also occur throughout the outer portions of the batholith.

Strong evidence favoring a primary origin for the *a-c* joints is found in the presence of pegmatite and aplite dikes with similar strikes and dips. A contour diagram of 135 joints of the intermediate central, intermediate, and outer zones is girdle-polar (Fig. 6d). The similarity of this diagram to that for *a-c* joints is striking. It strongly suggests that those joints with similar orientations in close proximity to the ones filled with pegmatite and aplite are of primary origin (Pl. 4, fig. 2).

a-b joints.—Interlamellar shearing separated some layers parallel or nearly parallel to planar flow structure—*i.e.*, in the *a-b* plane. These are *a-b* joints (longitudinal joints) (Pl. 4, fig. 1). A contour diagram of 175 *a-b* joints in the intermediate central, intermediate, and outer zones has been prepared (Fig. 5b). The diagram is girdle polar. Here again the inability to distinguish between regional joints striking northwest and northeast and *a-b* joints with the same strike is partly responsible for the polar character of the diagram.

Pegmatite and aplite veins strongly suggest a primary origin for these joints. The contour diagram of 96 *a-b* joints filled with pegmatite and aplite is very similar to that for just the *a-b* joints (Fig. 6b). Long narrow veins 1–4 feet wide and up to a quarter of a mile in length are distributed at frequent intervals around the batholith. A contour diagram of 41 pegmatite- and aplite-filled *a-c* and *a-b* joints in the core of the batholith is girdle polar (Fig. 6a). This suggests that probably some of the joints represented as regional in Figure 5d are actually either *a-c* or *a-b* joints. The pegmatites and aplites of the core are narrower and shorter than in the other zones. Few are more than 1–5 inches wide and 25–50 feet long.

No pegmatite and aplite dikes parallel the northwest–northeast regional joints in the north, east, south, or west portions of the batholith.

Marginal fissures.—Marginal fissures are restricted to the outer mile-wide perimeter of the batholith. Dips are low, 10°–25°, and toward the center of the batholith. Pegmatite and aplite occur either singly or together and have occupied the marginal fissures. The contour diagram of 82 marginal fissures filled with peg-

FIGURE 5.—CONTOUR DIAGRAMS OF PRIMARY FRACTURES AND REGIONAL JOINTS OF THE BATHOLITH

(a) Contour diagram of 379 *a–c* joints in intermediate central, intermediate and outer zones. Plotted on lower hemisphere.

(b) Contour diagram of 175 *a–b* joints in intermediate central, intermediate and outer zones. Plotted on lower hemisphere.

(c) Contour diagram of 97 joints oblique to planar-flow structure in intermediate central, intermediate and outer zones. Plotted on lower hemisphere.

(d) Contour diagram of 327 joints oblique to planar-flow structure in core of the batholith. Plotted on lower hemisphere.

Note: Each joint measured in the field and plotted on Plate 1 represents 4 joints with similar strike and dip. Hence, Figures 5, (a), (b), (c) and (d) actually represent 1516, 700, 388 and 1308 joints, respectively.

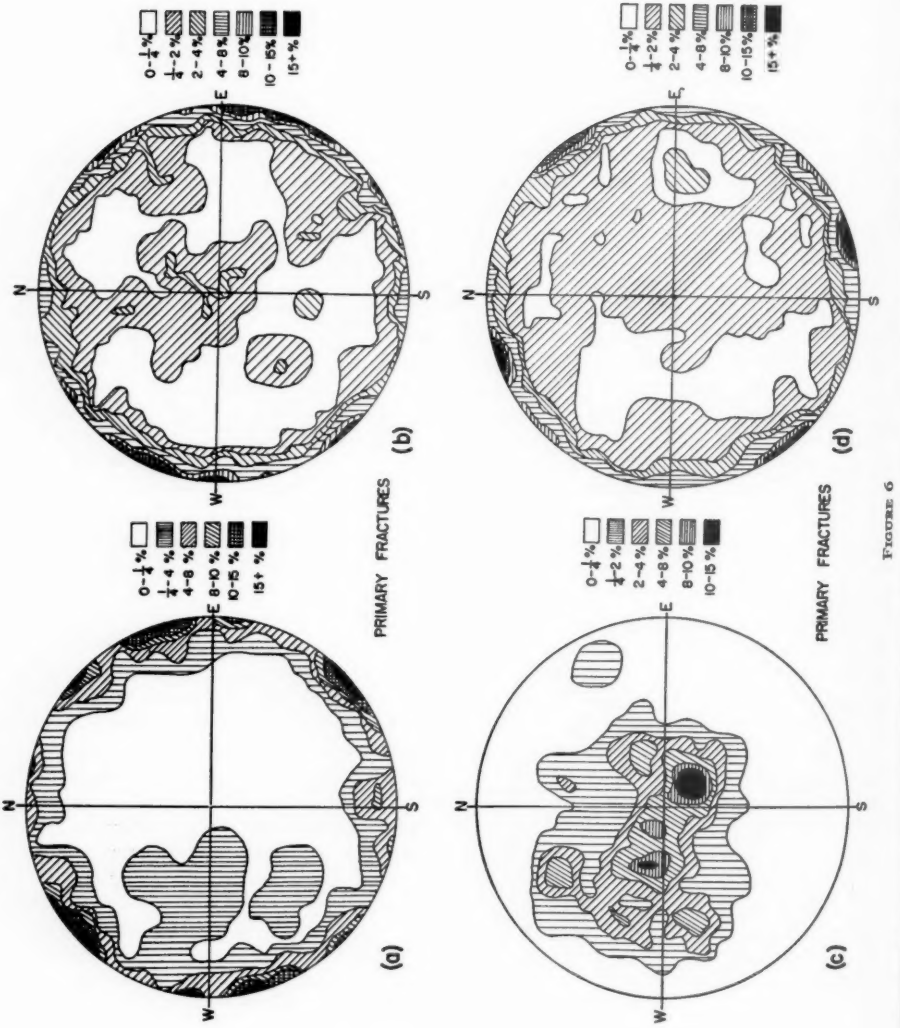

FIGURE 6

matite and/or aplite is central polar (Fig. 6c). In Figure 5 of Plate 4 biotite-rich schlieren are crosscut by pegmatite and aplite occupying a marginal fissure.

Aplite-filled shears.—Aplite-filled shears occur on the exfoliation dome immediately south of Enchanted Rock (Pl. 4, figs. 3, 4) and 1 mile west of House Mountain. Planar flow structures in aplite are subparallel to the walls of the fissures. Planar flow structure of enclosing porphyritic medium leucogranite strikes oblique to walls of the fissure.

Meaning of Flow Structures

The flow-structure pattern is circular concentric and possesses an overall continuity which reflects the shape of the chamber. In most places rock zones parallel flow structures, but in the north and south parts of the batholith flow structures cross rock boundaries where they bend or arch and are independent of them. This, combined with gradational contacts between all rock zones, suggests contemporaneity of development as well as emplacement of the granite mass as a single unit.

Flow lines parallel the contact of the batholith with the metamorphic wall rocks where it is discordant as well as concordant. A higher degree of crystal alignment exists in the rock zones successively nearer the wall-rock contact. Also the amount of interphenocrystal area decreases in rocks closer to the contact with metamorphic wall rocks (Pl. 6). Crowding of granite against wall rocks probably would aid in formation of both features.

There is much less overall continuity of flow lines in the constricted north tip and core of the batholith. A frictional or "drag" effect by the wall rock of Valley Spring gneiss as the batholith moved up the trough of the Castell syncline with a spiral motion probably caused the pattern of flow lines in the north part of the batholith.

The local discontinuity and swirl-like patterns of the flow lines in the central part of the core probably represent a slackening of the force of intrusion owing possibly to depletion of the magma reservoir.

Meaning of Joints and Marginal Fissures

The girdle-polar character of the contour diagram for *a-c* joints results from their subradial distribution at right angles to the concentrically curved flow structures. While under a peripheral tensional stress owing to continued rise of the yet-mobile core, the outer, intermediate, and intermediate central zones developed *a-c* joints. In places these opened "freely". Pegmatites and aplites consolidated in the freely opening space and have vertical to near-vertical dips. Large, steeply dipping disc-shaped bodies of aplite in the northeast part of the batholith have their longer dimension normal to the flow structures. Tensile stresses appear to have been more severe in this part of the batholith, indicated by the large number of aplite bodies present.

Restricted distribution of marginal fissures to the outer zone, their prevailingly low dips toward the core, and the central-polar character of the contour diagram seem to indicate a near-vertical rising column of granite. Continued upward motion of the core material after outer zones had stiffened placed them under vertical tension and opened marginal fissures which were filled by aplitic and pegmatitic material (Fig. 7).

Summary of the Structure

The structures of Enchanted Rock batholith and its relation to country-rock structures indi-

FIGURE 6.—CONTOUR DIAGRAMS OF PRIMARY FRACTURES OF THE BATHOLITH FILLED WITH PEGMATITE AND/OR APLITE

(a) Contour diagram of 25 *a–b* and 16 *a–c* joints of the core filled with pegmatite and/or aplite. Plotted on lower hemisphere.

(b) Contour diagram of 96 *a–b* joints filled with pegmatite and/or aplite in intermediate central, intermediate and outer zones. Plotted on lower hemisphere.

(c) Contour diagram of 82 marginal fissures filled with pegmatite and/or aplite in the outer zone. Plotted on lower hemisphere.

(d) Contour diagram of 135 *a–c* joints filled with pegmatite and/or aplite in intermediate central, intermediate and outer zones. Plotted on lower hemisphere.

cate that at the level now exposed by erosion the batholith was emplaced by forceful injection accompanied by replacement of wall rocks. and (6) the independence of rock-type boundaries from flow-structure patterns which indicates these two features formed contemporane-

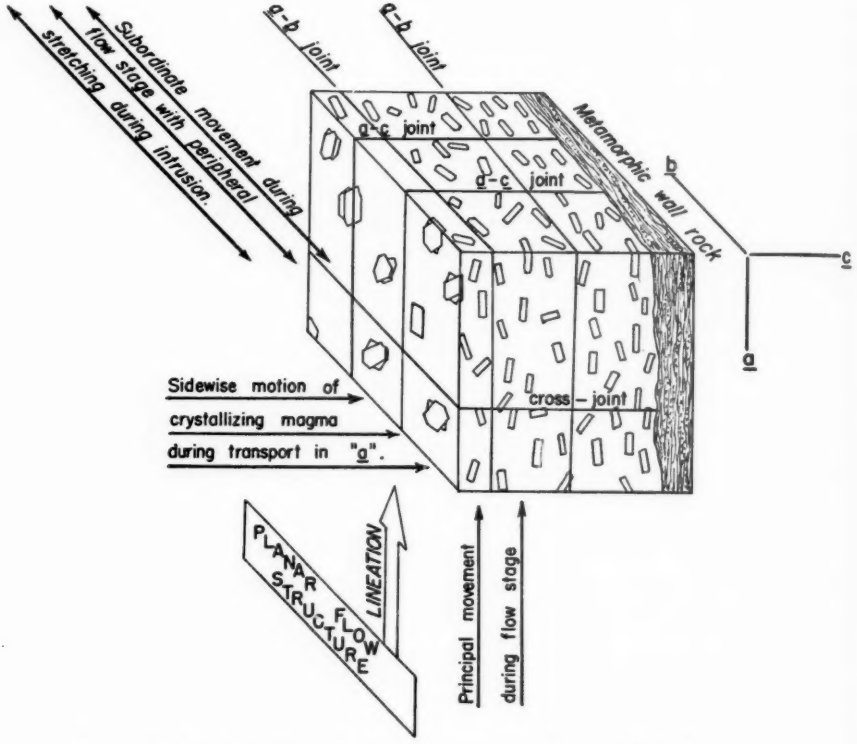

FIGURE 7.—RELATIONSHIP OF PRIMARY FRACTURES TO PRIMARY FLOW STRUCTURES

The principal lines of evidence for injection are: (1) the overall continuity and circular concentric pattern of linear and planar flow structures within the batholith; (2) the local concentric swirl-like pattern of flow structures in the north part of the batholith; (3) the presence of moved inclusions within the batholith; (4) the subradial pattern of near-vertical *a-c* joints, some of which are filled with pegmatite or aplite or both, consistent with a continued peripheral stretching caused by upward movement of the core after the outer zone had stiffened; (5) the restricted occurrence (to the outer zone) of marginal fissures which are filled with pegmatite or aplite or both, attesting further to late upward surge of the batholith's core; ously and further suggests the batholith was emplaced as a single unit without multiple intrusion.

The pear-shaped outline and internal structures of the batholith appear to have developed as the rising mass of granite assumed a position requiring minimum expenditure of energy yet maximum structural adjustment.

PETROGRAPHY

General

Enchanted Rock batholith is made up of five kinds of granitic rocks: leucogranite, granite, leuco-quartz monzonite, quartz monzonite, and alkalic granodiorite. In all these the ratio of

potash feldspar to plagioclase ranges from slightly in excess of 2:1 to 1:1. In one isolated occurrence the ratio was 3:1. The leucogranite hornblende up to 1.4 per cent, sodic andesine is rare, and soda-lime feldspar slightly exceeds potash feldspar.

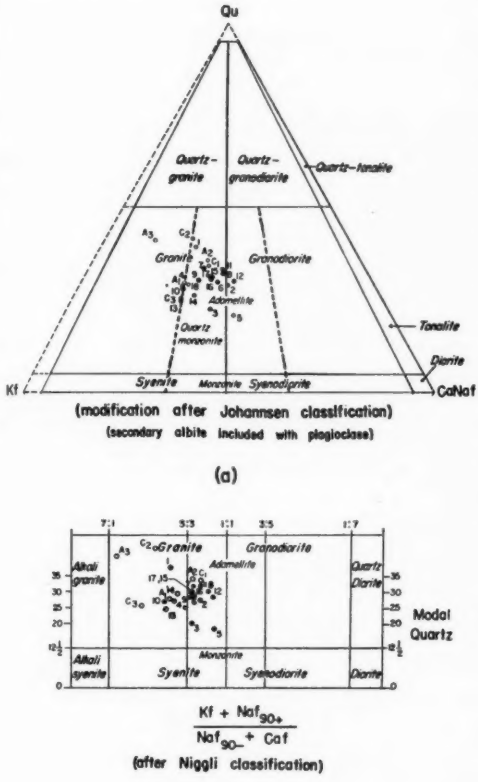

Rock Symbol on Plate I	Number used on this Fig.	Rock Zone Sampled
T_2S_{5a}	1	Outer
9-10-2	2	Intermediate
9-7-8	3	Intermediate Central
$T_3S_{19\frac{1}{2}}$	4	Intermediate
T_3S_{21}	5	Intermediate Central
T_3S_{32}	6	Core
T_1S_{37}	7	Core
T_1S_{34}	8	Core
T_1S_{33}	9	Core
T_3S_{41}	10	Core
T_3S_{39}	11	Core
9-14-2	12	Core
T_1S_{58}	13	Outer
T_1S_{16}	14	Intermediate
N. ½ CORE	15	Core
S. ½ CORE	16	Core
AVG. FOR CORE	17	Core
T_1S_3	18	Outer
C_1	C_1	"Chill" Border
C_2	C_2	"Chill" Border
C_3	C_3	"Chill" Border
A_1	A_1	Apophysis
A_2	A_2	Apophysis
A_3	A_3	Apophysis

• Rock sample from Core of batholith
• Rock sample from zones surrounding Core

FIGURE 8.—ROCK TYPES OF ENCHANTED ROCK BATHOLITH

consists of quartz, microcline, sodic andesine, calcic to sodic oligoclase, and less than 5 per cent biotite. The granite differs only in having more than 5 per cent biotite, sodic andesine is less calcic, and there is less of it. In quartz monzonite the ratio of potash feldspar to soda-lime feldspar is between 6.5:3.5 and 1:1. This terminology is used in place of the potash feldspar-rich adamellites of Johannsen. The average quartz monzonite consists essentially of quartz, microcline, sodic andesine, and calcic to sodic oligoclase with 3–10 per cent biotite. The alkalic granodiorite differs only in having

Gradational Nature of Rock Zones

The modes used for final identification of the rock types were computed by the Rosiwal method with a determined error ranging from 2 to 7 per cent, averaging about 5 per cent. This determined error is enough to affect final classification of those rocks in which ratio of potash feldspar to plagioclase is very close to 1:1. Johannsen's (1931) quantitative mineralogical classification is used with slight modifications. During the Rosiwal analyses record was kept of all albite. This consisted of microcline micro-

perthite and albite exsolution rims on plagioclase at microcline-plagioclase boundaries. It was not possible to measure all albite in the microcline microperthite, but as much as was visible was included with the exsolution rim albite and all classified as plagioclase in plotting rock types on Figure 8a. This tends to shift the plot of rock types in the direction of granodiorite, in contrast to Johannsen's classification which places all microperthite in the potash feldspars. A plot after Niggli's classification (Fig. 8b) tends to shift the plots toward granite.

Distribution of rock types exhibited laterally within the batholith corresponds to the pear-shaped outline made by the contact with the metamorphic wall rocks (Fig. 1; Pl. 1). Four roughly concentric zones occur: (1) outer zone, medium to coarse leucogranite and granite; (2) intermediate zone, medium to coarse granite and quartz monzonite; (3) intermediate central zone, coarse quartz monzonite and alkalic granodiorite; and (4) the core, fine to medium leuco-quartz monzonite and leucogranite. Between the outer zone and the metamorphic wall rocks, but not everywhere present, is a chilled border zone 10–20 feet in width consisting of porphyritic fine to medium leuco-quartz monzonite and quartz monzonite. Narrow apophyses of porphyritic leuco-quartz monzonite and leucogranite branch out into schist wall rocks from the outer zone.

Contacts between individual rock zones are all gradational and could not be mapped as lines. The color patterns of Plate 1 indicate the approximate boundaries between rock types. The least gradational contact occurs between the intermediate central and the intermediate zones. Changes in color and relative proportions of minerals are noticeable throughout a distance of 50–100 feet. Microcline phenocrysts in the alkalic granodiorite and quartz monzonite of the intermediate central zone are grayish orange pink (5YR 7/2) and are set in a groundmass of clear quartz and light-gray (N7) to very light-gray (N8) plagioclase with scattered microcline. Black (N1) biotite grains are abundantly scattered throughout the groundmass. This is in fairly sharp contrast to the porphyritic granite of the adjacent intermediate zone containing considerably more microcline phenocrysts and quartz with less plagioclase and biotite. This rock is moderate reddish orange (10R 6/6) to moderate reddish brown (10R 4/6), with light-gray (N6) plagioclase. The alkalic granodiorite and quartz monzonite of the intermediate central zone appear predominantly light gray (N7) with scattered grayish-orange-pink microcline phenocrysts, and the granite of the intermediate zone is a uniform moderate reddish orange.

Toward the core grain size decreases; plagioclase and biotite content drops over an average distance of an eighth of a mile on the west and five-eighths of a mile on the east side of the core. The rock throughout this zone is dominantly quartz monzonite but, in places, is leuco-quartz monzonite. Texturally it might be referred to as a transitional zone between the coarse alkalic granodiorite and quartz monzonite of the intermediate central zone and the fine leuco-quartz monzonite and leucogranite of the core. Fine leucogranite seems to be concentrated in the center of the core, but no contact could be established so slight are differences in rock types (Fig. 1).

The narrow arcuate ribs of quartz monzonite within the intermediate zone are discernible in the field only by the increase in plagioclase content accompanied by an increase in granularity from medium to coarse. These may be granitic in part. Contacts grade over a distance of several hundred feet. The granite of the intermediate zone and the leucogranite of the outer zone have a contact very difficult to locate more accurately than within 500 feet.

Textural Variation Across Rock Zones

Porphyritic texture prevails throughout all zones of the batholith (Pl. 6). Seriate porphyritic texture predominates in the outer, intermediate, intermediate central, and in parts of the core. Hiatal porphyritic texture occurs in rocks of the core, the chilled border, and the apophyses in the schist wall rocks.

Feldspar is the major constituent of these rocks, and the arrangement and size of the feldspar crystals generally determine the texture of the rock. Phenocrysts of microcline are set in a groundmass of smaller crystals of microcline, plagioclase, quartz, biotite, some hornblende, and accessories. Plagioclase throughout the

textural zones is restricted to the groundmass, although a few phenocrysts can be found. These are adjudged in most crystals to have once been microcline now replaced by oligoclase.

system was used. The pycnometer method was used periodically to check accuracy of the specific-gravity values obtained with the apparatus. Pycnometer values never differed by

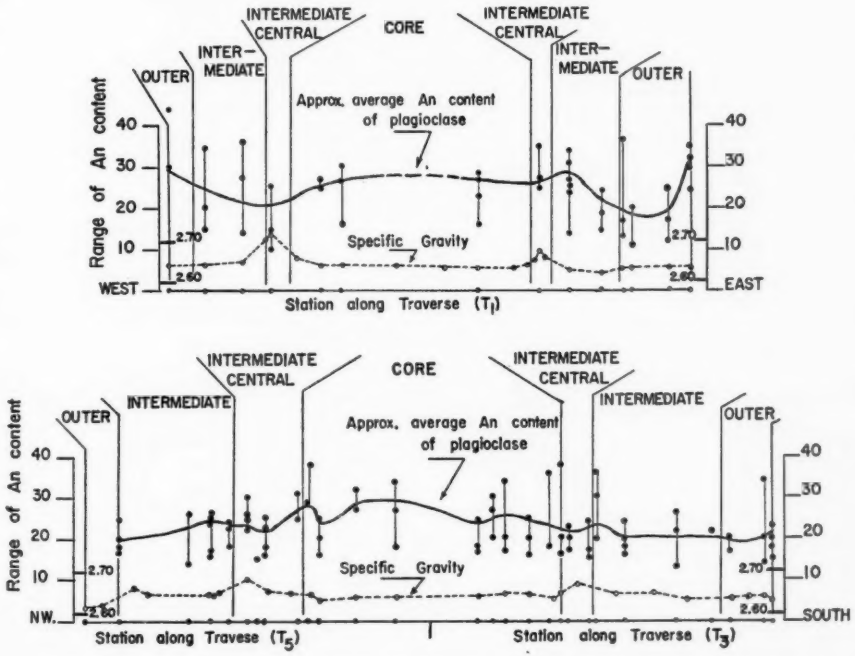

FIGURE 9.—VARIATION OF PLAGIOCLASE COMPOSITION IN ROCK ZONES OF THE BATHOLITH

Johannsen's grain-size classification has been used (1931, p. 31). Groundmass texture of the core rock is predominantly fine extending slightly into medium. The remainder of the batholith has a groundmass texture of medium to coarse. Chilled border rocks are medium to fine, and apophyses have a fine groundmass extending occasionally into medium.

Specific Gravity of the Rocks

About 150 specific-gravity determinations were made on samples collected along the same traverse lines as those used in collecting thin-section material. The pycnometer method required too much time, and a special apparatus was designed and constructed to obtain specific gravity of rough and square-cut chunks weighing 25–200 grams. The principle of immersion buoyancy combined with an air-evacuation

more than 0.4 per cent. This indicated the specific-gravity values obtained with the apparatus had an absolute limit of error of ± 0.01. At least two, sometimes three, and occasionally five determinations were made for each sample.

Inspection of data shows two sets of fairly consistent values: (1) the core rock where specific gravity ranges from 2.63 to 2.64, and (2) the intermediate zone where values range from 2.63 to 2.66 (Fig. 9). A single sharp peak ranging from 2.67 to 2.71 occurs on all curves. It coincides with the plagioclase and biotite-rich intermediate central zone identified as porphyritic alkalic granodiorite. Values of the outer zone show a tendency to drop fairly suddenly and range from 2.60 to 2.64. This is a reflection of the low plagioclase and biotite content of the rock.

The specific-gravity curves obtained are believed significant. Just as the differences in rock types are comparatively small for the batholith, so are the differences in specific gravity.

TABLE 1.—CHEMICAL ANALYSES

	Core	Intermediate central zone			Intermediate zone	Outer zone	
Sample number	6	5	5a	3	2	1	1a
SiO_2	73.65	69.59	69.56	69.46	75.21	73.90	74.76
Al_2O_3	13.42	14.43	14.74	14.59	12.86	13.61	13.16
Fe_2O_3	0.55	0.94	0.88	0.80	0.56	0.57	0.40
FeO	1.42	2.53	2.34	2.65	1.23	0.96	1.51
MgO	0.53	0.75	0.75	0.81	0.21	0.17	0.28
CaO	1.33	2.18	2.21	2.03	0.99	0.89	0.85
Na_2O	3.20	3.41	3.73	3.52	3.36	3.21	2.94
K_2O	4.70	4.75	4.66	4.57	4.70	6.01	5.67
H_2O+	0.32	0.35	0.26	0.38	0.22	0.16	0.15
H_2O-	0.08	0.01	0.04	0.07	0.01	0.01	0.04
CO_2	0.13	0.06	0.01	0.07	0.04	0.03	0.06
TiO_2	0.24	0.47	0.46	0.50	0.21	0.15	0.19
P_2O_5	0.07	0.16	0.15	0.17	0.05	0.03	0.04
MnO	0.05	0.04	0.07	0.07	0.07	0.02	0.03
BaO	n.d.	n.d.	0.08	n.d.	n.d.	n.d.	0.03
F	n.d.	n.d.	0.24	n.d.	n.d.	n.d.	0.08
S	n.d.	n.d.	0.04	n.d.	n.d.	n.d.	0.03
Total	99.69	99.67	100.22	99.69	99.72	99.72	100.22
Less O	.....	.....	0.12	.....	.....	.....	0.05
	99.69	99.67	100.10	99.69	99.72	99.72	100.17
Sp. gr.	2.652	2.685	n.d.	2.687	2.653	2.635	n.d.

1, 2, 3, 5, 6, J. A. Maxwell, analyst, 1953; 1a and 5a, R. B. Ellestad, G. Kahan, analysts, (Barnes, 1947, p. 69, 78).

Composition

The compositions of the batholith rocks are gradational. It was not possible to measure the true average composition of the plagioclase. As many measurements as possible were made on individual oscillatorily and progressively zoned crystals. Relative widths and abundance of zoning in thin sections gave an approximate average of content of plagioclase, shown by the curved line in Figure 9. Sodic andesine can be found in all rock zones, but the commonest range of composition is An_{12}–An_{30}. Secondary albite is excluded from the diagram, although it ranged from An_{10} to An_0. Extinction angles were measured on a 5-axis universal stage by the Rittmann zone method. Approximately 950 measurements were made on 75 thin sections collected along traverse lines rim-core-rim of the batholith and normal to flow structures. (Pl. 1). Results for traverses T_1, T_3, and T_5 are shown in Figure 9. Variation of An content is about the same in all rock zones.

The chemical analyses of Enchanted Rock batholith show a silica range from 69.5 to 75.2 per cent (Table 1). A plot of the analyses on a Harker variation diagram shows three bunched at one end about 69.5 per cent silica and 4 scattered, yet still bunched, from 73.7 to 75.2 per cent silica. A plot of 25 chemical analyses from 16 additional intrusions of the surrounding area of the same petrographic province provided a more suitable grouping of points through which smooth curves might be drawn and petrogenic interpretation of Enchanted

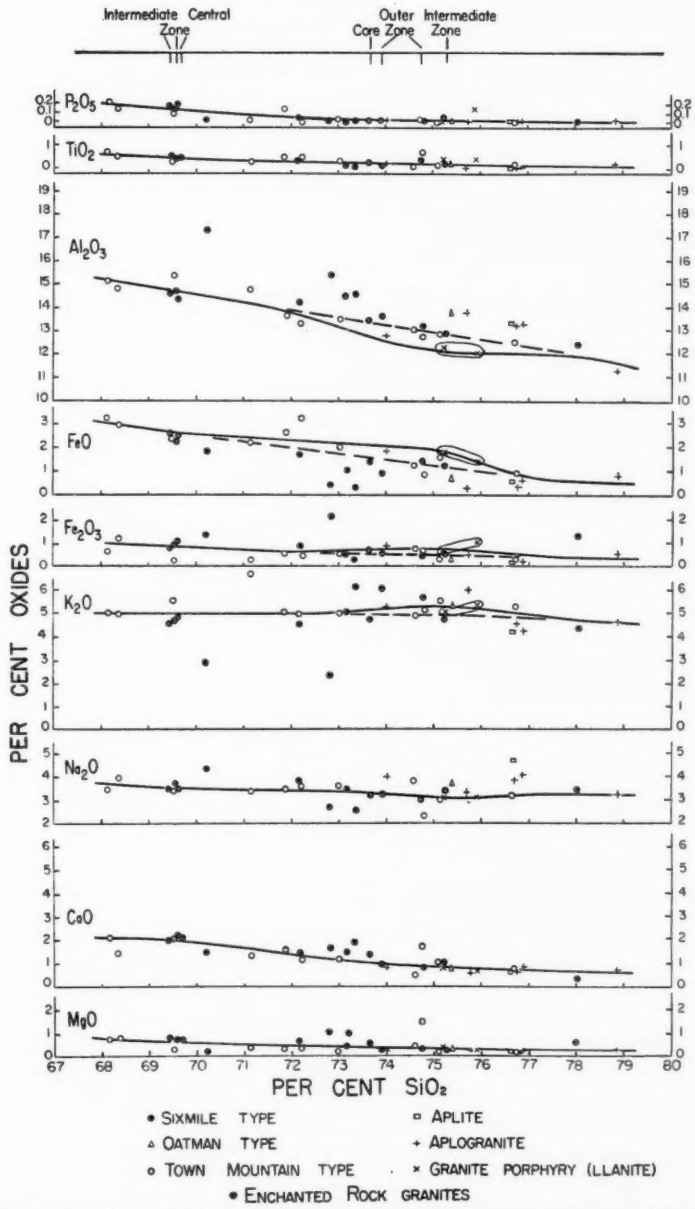

FIGURE 10.—HARKER VARIATION DIAGRAM OF IGNEOUS ROCKS OF CENTRAL TEXAS

Rock batholith attempted (Fig. 10). Geographic location of individual intrusions and full petrogenic discussion of igneous rocks of the Precambrian area is outside the scope of this paper.

The plot of the oxides for igneous rocks of the area shows a progressive chemical change, initially noted by Goldich (1941), and also brings out a grouping of the different rock

TABLE 2.—MODES

Analyses by R. M. Hutchinson

Analyses numbers refer to Fig. 8	Core (north half)				Core (south half)			Intermediate central zone		Intermediate zone		
	6	7	8	9	10	11	12	3	5	2	4	14
Quartz	28.9	32.3	30.5	28.6	27.6	32.3	28.8	20.5	18.8	27.9	27.7	29.6
Microcline	34.9	35.0	32.4	37.1	43.0	32.4	32.1	36.6	34.7	33.2	39.3	37.9
Andesine and/or oligoclase	26.6	28.1	31.3	28.3	20.0	26.6	30.4	26.3	33.6	28.0	21.8	22.5
Albite (secondary)	5.7	(included in plagioclase)			6.1	4.8	3.9	4.9	4.8	6.0	4.4	5.0
Biotite	3.9	3.8	4.9	5.2	3.1	3.3	4.6	9.5	5.3	3.9	6.0	4.2
Hornblende	0.1	....	....	....	....	tr.	....	1.2	1.4	0.2	tr.	....
Sphene	0.3	0.2	....	0.1	....	0.1	0.1	0.4	0.7	tr.	0.5	0.1
Zircon	0.1	0.1	0.3	0.1	0.1	0.1	0.1	0.3	0.2	0.2	0.2	0.2
Apatite	0.1	0.2	0.2	0.2	....	0.1	tr.	0.2	0.3	0.1	0.1	0.1
Magnetite	0.2	0.3	0.4	0.4	0.8	0.2	....	0.1	0.2	0.2	tr.	0.3
Fluorite	tr.	....	....	0.1	tr.	....	....	tr.	tr.	0.3	0.1	0.1
Plagioclase	An_{41} An_{18}	An_{27}	An_{30}	An_{29}	An_{33} An_{25}	An_{35} An_{24}	An_{35} An_{26}	An_{30} An_{22}	An_{36} An_{27}	An_{28}	An_{36} An_{26}	An_{33} An_{13}
Johannsen symbol	126″P	126″P	226″P	226″P	126P	126″P	127″P	226″P	227″P	227″P	226P	226″P

	Outer zone			Chilled contact with wall-rock			Apophyses of the batholith in the metamorphic wall-rock					
	1	13	18	C_1	C_2	C_3	A_1	A_2	A_{2a}	A_{2b}	A_{2c}	$A_{2avg.}$
Quartz	37.4	24.7	29.3	33.5	42.3	25.5	27.7	33.8	43.6	35.7	41.9	40.4
Microcline	34.9	43.1	40.0	34.4	32.5	43.3	38.1	33.9	47.2	53.4	39.7	46.9
Andesine and/or oligoclase	18.4	21.1	21.2	26.6	14.7	22.6	19.8	24.2	5.2	7.5	13.8	8.8
Albite	4.6	5.0	4.6	1.3	4.0	3.3	1.6	2.1	2.0	2.0	3.0	2.3
Biotite	3.3	5.6	3.7	2.6	6.2	5.2	7.3	4.0	1.1	0.9	0.7	0.9
Hornblende	0.7	....	0.3	....	....	....	2.8	....	....	....	....	....
Sphene	0.2	0.1	0.6	0.6	tr.	....	0.8	....	....	....	....	....
Zircon	0.2	0.1	tr.	tr.	tr.	0.1	0.2	0.1	0.2	....	0.1	0.1
Apatite	0.1	0.1	0.1	0.2	0.1	tr.	0.3	0.1	tr.	0.1	tr.	tr.
Magnetite	0.2	0.1	0.2	0.8	0.2	....	1.4	1.8	0.6	0.4	0.7	0.6
Fluorite	tr.	0.1	....	....	....	....	....	....	....	....	....	....
Plagioclase	An_{38} An_{27}	An_{36} An_{12}	An_{26}	An_{32}	An_{25}	An_{35}	An_{36}	An_{26}	An_{20}	An_{30}	An_{25}	An_{28}
Johannsen symbol	126″P	226P	126″P	126″P	226″P	126″P	226P	226″P	126P	126P	126P	126P

types. Principal magma types are shown by separate symbols on Figure 10. From the convergence of composition—*i.e.*, where positions of the granite porphyry (llanite) plots approach those of Town Mountain granite plots of similar SiO_2 range—the granite porphyry is considered the closest to being representative of the composition of the magma from which

the Town Mountain granites in this SiO_2 range were crystallized. Aphanitic equivalents of lower SiO_2 range are not present to give better control in construction of the smooth curves in this range.

accompanied by a drop in the percentage of hornblende and biotite. With the decrease in mafites there is a corresponding increase in potash feldspar although the percentage of microcline is remarkably constant. Thus nor-

TABLE 3.—NORMS*

	Core	Intermediate central zone			Intermediate zone	Outer zone	
Sample No.	6	5	5a	3	2	1	1a
Quartz	32.28	24.54	23.46	25.02	34.50	29.64	33.12
Orthoclase	27.80	27.80	27.80	26.68	27.80	35.58	33.92
Albite	27.24	28.82	31.44	29.34	28.30	27.24	24.63
Anorthite	6.67	10.84	9.45	10.00	5.00	4.44	3.34
Corundum	0.61	.....	.....	0.31	0.41	0.20	0.92
Hypersthene	3.24	5.10	4.67	5.3	2.08	1.32	2.68
Magnetite	0.70	1.16	1.39	1.16	0.70	0.93	0.70
Ilmenite	0.46	0.76	0.91	0.91	0.30	0.30	0.46
Apatite	.....	.....	0.35	.....	.....	.....	0.09
Calcite	.....	.....	0.02	.....	.....	.....	0.14
Fluorite	.....	.....	0.47	.....	.....	.....	0.16
Pyrite	.....	.....	0.08	.....	.....	.....	0.06
Normative plagioclase	An_{20}	An_{27}	An_{23}	An_{25}	An_{14}	An_{14}	An_{12}

* 1a, 5a calculations by V. E. Barnes (1947, p. 69, 79); 1, 2, 3, 5, 6 calculations by R. M. Hutchinson.

The variation curves in a solid black line are the nearest approach to being representative of the liquid lines of descent for the igneous rocks of central Texas. The area encircled about the two granite porphyry samples probably approaches closest to composition of magmas of the Town Mountain type granite in this area. The dashed line was obtained for only Town Mountain granites and differs considerably. The Sixmile granites are clustered somewhat and do not seem to fit the curves.

Chemical changes for the rocks of Enchanted Rock batholith show that with increasing silica the variation curves for magnesia, lime, iron oxides, alumina, and accessories (titania and phosphorous pentoxide) decline. In the silica range from 69.5 to 75.0 per cent the K_2O curve rises slightly while the Na_2O shows a slight decline. Beyond 75.0 per cent the curves for K_2O and Na_2O converge. Modal composition of these same samples is given in Table 2. In terms of minerals, the shape of the potash curve is determined by the relative abundance of biotite and microcline. The decline in iron and magnesia with increasing silica content is

mative orthoclase in the outer zone is highest with a value of 35.6 per cent, but hypersthene drops from 5.3 to 1.3 per cent (Table 3). The biotite content of samples 1, 2, and 6 is almost the same.

X-ray Analysis of Feldspars

Phenocrysts of microcline were collected from representative samples of each rock zone, a chill border sample, and an apophysis in the schist wall rock. X-ray diffraction pattern tracings and powder photographs were obtained using CuKα radiation with a North American Phillips x-ray spectrometer and a powder camera, diameter = 143.2 mm, respectively. A tracing for plagioclase was also obtained and showed purity and phases present as well as being a standard of comparison for aid in distinguishing microcline from plagioclase.

The potash feldspar is in all cases, insofar as can be determined from optical and x-ray studies, a microcline perthite. Albite is present as a separate phase in the microcline both as poikilitic inclusions and as film or string micro-

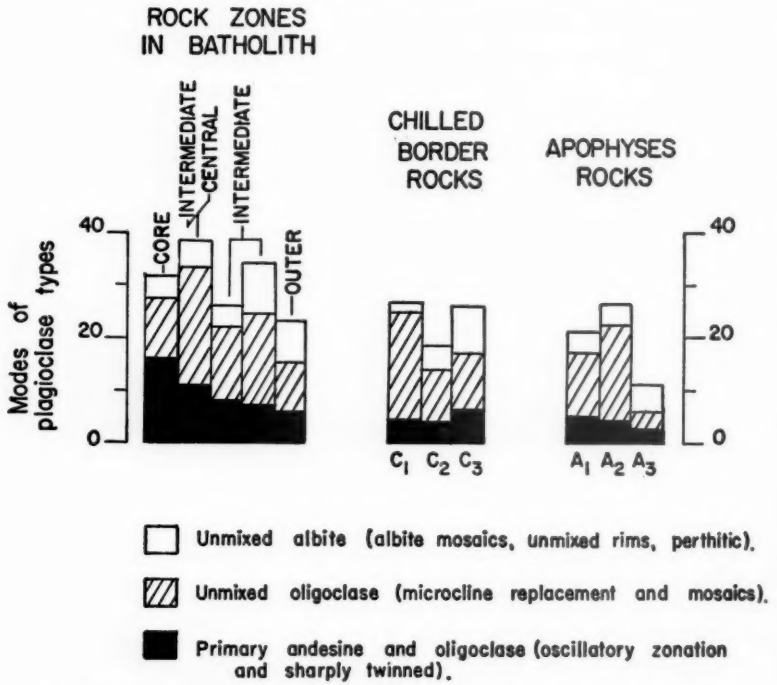

FIGURE 11.—MODAL COMPOSITION OF PLAGIOCLASE IN ROCKS OF THE BATHOLITH

perthite. "From powder and single-crystal x-ray-diffraction studies it was found that the microcline phenocrysts both from the core and the chilled border specimens had variable lattice parameters. Single-crystal x-ray-oscillation photographs of cleavage fragments from the microcline perthite phenocrysts in specimens T_9S_{32} of the core and C_3 of the chilled border zone showed that the exsolved sodium feldspar phase was comparable with low-temperature albite in lattice angles" (Wm. Scott MacKenzie, personal communication).

Plagioclase-Microcline Relationships

In the hand specimen microcline phenocrysts dominate the texture and stand out either because of their abundance or, where few in number as in the core, are in contrast to the groundmass (Pl. 6). Microscopically the most striking textural features are those of the plagioclase in both single grains and in grain-to-grain relationships with microcline. Sodic andesine, calcic to sodic oligoclase, and albite occur and have characteristic textural modes. These are as follows:

(1) Textures with albite
   1. Borders of clear albite on plagioclase at plagioclase-microcline contacts. Some of these rims contain radial and myrmekitic quartz channels.
   2. "Albite mosaics" of clear microcrystals interstitial granular between large microcline and plagioclase grains
   3. Film, string, and patchy bands of microcline perthite commonly arranged parallel to (010), (110), and (210). Automorphic to hypautomorphic microcrystals are also poikilitic in microcline commonly arranged parallel to (010), (110), and (210).

(2) Textures with oligoclase
   1. Partial reconstitution or replacement of microcline with development of rapakivilike texture (not true rapakivi where ovoidal structure is characteristic).

TABLE 4.—RELATION BETWEEN ALBITE RIMS ON PLAGIOCLASE AND MICROCLINE-PLAGIOCLASE BOUNDARY IN ROCK ZONES OF THE BATHOLITH

Location	No. of contacts	Mi-Pl	Mi-Mi	Mi-Q	Pl-Pl	Pl-Q	Q-Q	Total
Core	Total	49	16	56	14	34	34	200
	With 2ndary ab	45	0	0	2	3	0	
Intermediate central zone	Total	55	3	33	31	50	29	200
	With 2ndary ab	52	0	0	6	7	0	
Intermediate zone	Total	58	9	30	26	45	32	200
	With 2ndary ab	52	0	0	3	3	0	
Outer zone	Total	41	12	44	18	39	46	200
	With 2ndary ab	39	0	0	6	8	0	
Chilled border no. 1	Total	23	5	44	19	52	57	200
	With 2ndary ab	23	0	0	2	3	0	
Chilled border no. 2	Total	34	8	68	9	41	40	200
	With 2ndary ab	33	0	0	3	6	0	
Chilled border no. 3	Total	36	16	58	2	35	45	200
	With 2ndary ab	31	0	0	0	7	1	
Apophysis no. 1	Total	16	34	88	3	15	44	200
	With 2ndary ab	14	0	0	0	0	0	
Apophysis no. 2	Total	39	22	51	8	32	48	200
	With 2ndary ab	37	0	0	0	2	0	
Apophysis no. 3a	Total	18	62	72	0	4	43	200
	With 2ndary ab	18	0	0	0	1	0	
Apophysis no. 3b	Total	29	49	87	1	6	28	200
	With 2ndary ab	29	0	0	0	0	0	
Apophysis no. 3c	Total	35	47	78	1	5	34	200
	With 2ndary ab	35	0	0	0	0	0	

Have unreplaced microcline cores with mantles of oligoclase.

2. Almost complete replacement of microcline crystals with microscopic-sized strongly embayed remnants of microcline core (extreme rapakivi)
3. "Oligoclase mosaics", patchy with heavy sericite which has replaced small to large portions of microcline crystals

(3) Textures with oligoclase and sodic andesine

1. Zoned plagioclase, automorphic to hypautomorphic, with multiple narrow sericite zones. In places microscopic-sized microcline is poikilitically enclosed and is automorphic.

Andesine with some oligoclase is adjudged primary. In almost all places oligoclase, calcic to sodic, is attributed to unmixing. As the sodic feldspar unmixed it occupied some of the volume previously occupied by alkali feldspar, and unmixing and replacement operated at different places and at different times. Oligoclase in most crystals has replaced microcline but before doing so appears to have migrated from its initial site of unmixing. Albite in all places is regarded as secondary. In an effort to determine the variation in amount of these types, modal percentages of only these plagioclase types have also been run on the representative suites of thin sections from each rock zone and are shown in Figure 11.

Plagioclase (andesine and oligoclase), zoned and carrying multiple sericite zones (Fig. 17; Pl. 9, figs. 1, 3, 5; Pl. 10, fig. 1), suggests former oscillatory zoning and is adjudged to be primary.

Oligoclase with mottled mosaic structure containing sericite distributed at random with faintly visible albite twinning and Carlsbad twinning commonly has replaced parts of microcline (Pl. 8, fig. 1). In many places a few unreplaced heavily embayed microcline remnants remain (Pl. 8, figs. 2, 6). Plagioclase with multiple sericitic zoning surrounds some cores containing strongly embayed microcline remnants. Distribution of sericite within the interior is irregular and random (Pl. 8, fig. 2).

Calcic to sodic oligoclase mantles on micro-

cline cores (Fig. 18; Pl. 10, figs. 2, 3, 4) have embayments convex toward the microcline commonly with apophyses of oligoclase extending into the unreplaced core (Pl. 8, figs. 3, 4). Figures 3, 4, and 5 of Plate 8 are enlarged views of the oligoclase mantle-microcline core contact of the large rapakivi in Figures 3 and 4 of Plate 10. Microcline crystals in various stages of replacement are shown in Figures 3–6 of Plate 8. Xenomorphic fluorite commonly occurs in the oligoclase mantle, especially where there has been heavy sericitization (Pl. 8, figs. 3, 4). Sericite in some places is distributed evenly in one set of albite lamellae (Pl. 8, fig. 4) and in others is distributed uniformly throughout regardless of zoning (Pl. 8, figs. 3, 5, 6).

Fine aggregates of limpid grains—*i.e.*, "albite mosaics", (Pl. 7, fig. 6)—fill angular openings between large microcline and plagioclase grains. Narrow stringers and veinlets of perthitic albite commonly parallel (100), (110), and (210) crystallographic planes (Pl. 7, figs, 2, 4, 5, 6).

The type of boundary and the presence of secondary albite were recorded for 200 grain contacts in representative thin sections from all rock zones, chilled border zone, and apophyses in the schist wall rocks (Table 4). Table 4 indicates that nearly all the secondary exsolved rim albite external to microcline crystals lies at the microcline-plagioclase boundaries. The amount of secondary albite occurring as exsolution patches in microcline crystals and as rims on plagioclase at microcline-plagioclase boundaries shows a marked decrease in rocks of the chilled border zone and apophyses. Rims are narrowest in apophyses, thicker in chilled border rocks and the core, and thickest in intermediate central, intermediate, and outer zones. (*Compare* Figures 1, 2, 3, 4 of Plate 7.)

Twins and Zones in Plagioclase

Abundance of feldspar zoning and polysynthetic twinning in plagioclase seems to be related to location or particular rock zone in

---

PLATE 7.—PLAGIOCLASE-MICROCLINE RELATIONSHIPS

FIGURE 1.—Albite rim on plagioclase at plagioclase-microcline boundary. Rim is absent at quartz contact (white), and there is also absence of microperthite (Leucogranite from core, ×38, T_3S_{22}).

FIGURE 2.—String microperthite and albite rim on plagioclase at plagioclase-microcline boundary (Leucogranite from outer zone, ×13, T_2S_5).

FIGURE 3.—Albite rim on sodic oligoclase crystal bordered by quartz and microcline (intermediate central zone, ×13).

FIGURE 4.—Narrow albite rim on plagioclase at plagioclase-microcline boundary. Rim is absent at quartz contact (gray, white), and string microperthite is present (Apophysis, A_2, ×13).

FIGURE 5.—Veinlets of exsolved albite that have filled fractures in microcline phenocryst in porphyritic medium granite (outer zone, ×13, T_2S_5).

FIGURE 6.—"Albite mosaics", *i.e.*, aggregates of small unmixed albite grains recrystallized between large crystals of microcline (outer zone, ×13).

PLATE 8.—PLAGIOCLASE-MICROCLINE RELATIONSHIPS

FIGURE 1.—Oligoclase with mosaic structure of several crystals and randomly distributed sericite. Oligoclase has recrystallized between microcline crystals and partly replaced these (outer zone, ×13, T_2S_5).

FIGURE 2.—Plagioclase with multiple sericitic zoning surrounds microcline core almost completely replaced by oligoclase. Sericite irregularly distributed in replaced portion of the microcline core (intermediate central zone, ×13, T_3S_{22}).

FIGURES 3, 4.—Enlarged views of oligoclase mantle-microcline core contact of large rapakivi (Pl. 10, fig. 4, X and Y). Anhedral black grains are fluorite. Sericite occurs varyingly (outer zone, Fig. 3, ×13, Fig. 4, ×38, T_2S_5).

FIGURE 5.—Enlarged view of oligoclase mantle-microcline core contact of large rapakivi (Pl. 10, fig. 3, X). Remnants of microcline strongly embayed. Sericitization both irregularly and selectively distributed. Faint albite lamellae inherited from replaced microcline (intermediate central zone, ×38, T_3S_{22}).

FIGURE 6.—Splotchy sericite and faint narrow albite lamellae inherited from microcline replaced by oligoclase (outer zone, ×13, T_2S_5).

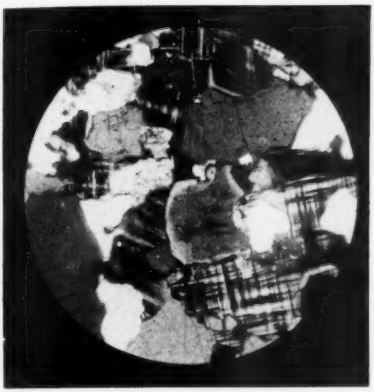

FIGURE 1

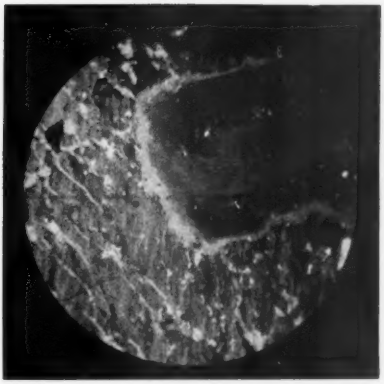

FIGURE 2

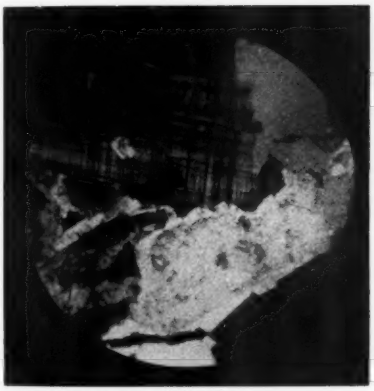

FIGURE 3

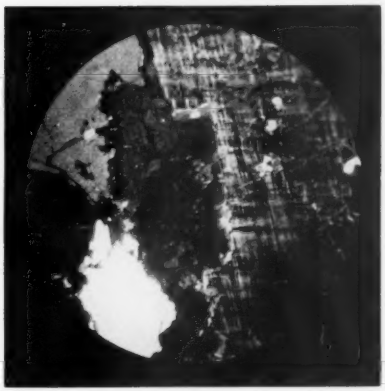

FIGURE 4

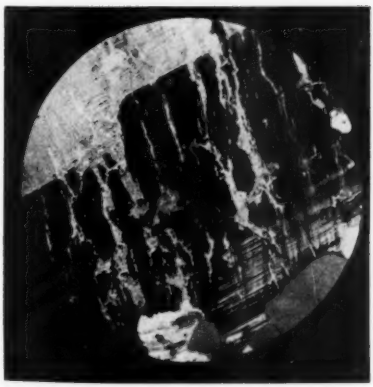

FIGURE 5

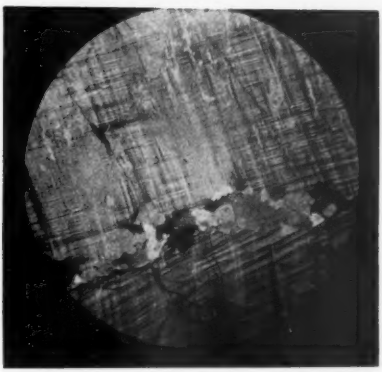

FIGURE 6

PLAGIOCLASE-MICROCLINE RELATIONSHIPS

FIGURE 1

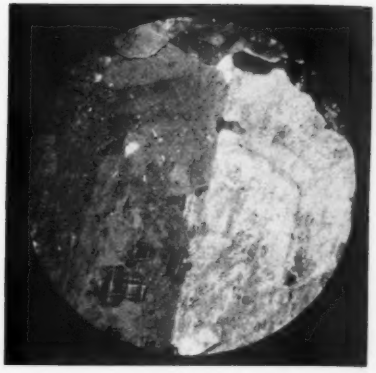

FIGURE 2

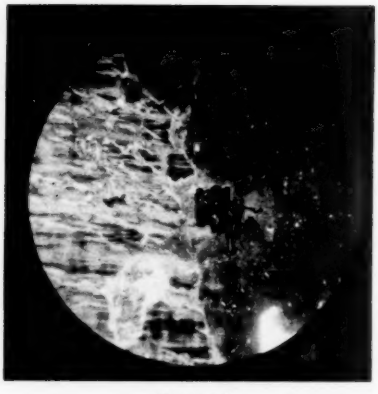

FIGURE 3

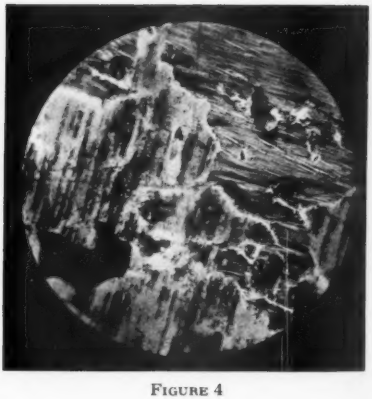

FIGURE 4

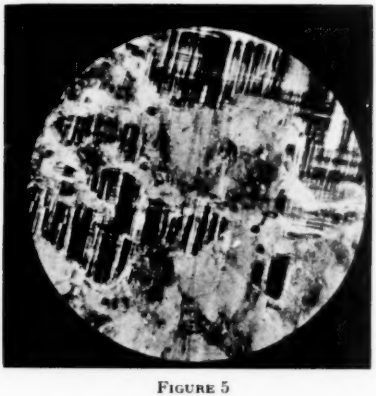

FIGURE 5

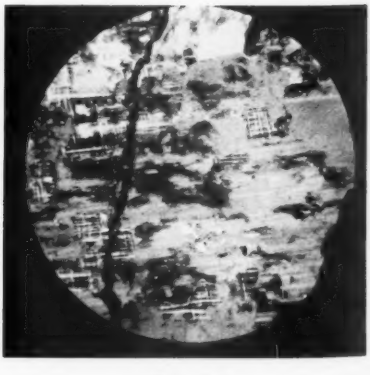

FIGURE 6

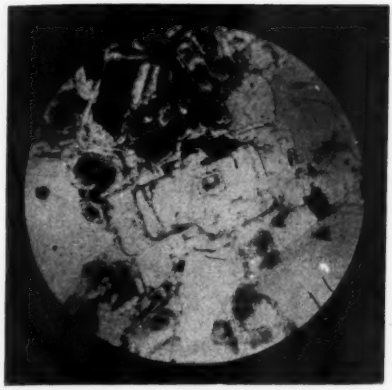

FIGURE 1

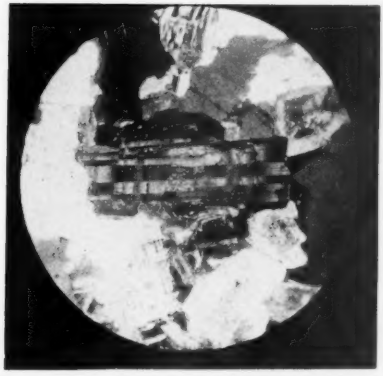

FIGURE 2

FIGURE 3

FIGURE 4

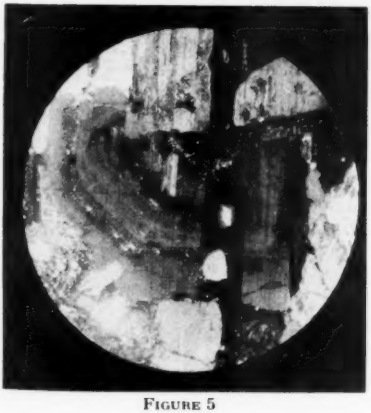

FIGURE 5

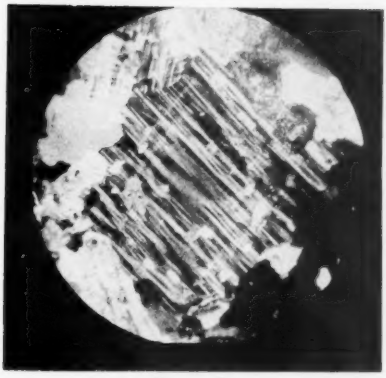

FIGURE 6

PLAGIOCLASE-MICROCLINE RELATIONSHIPS

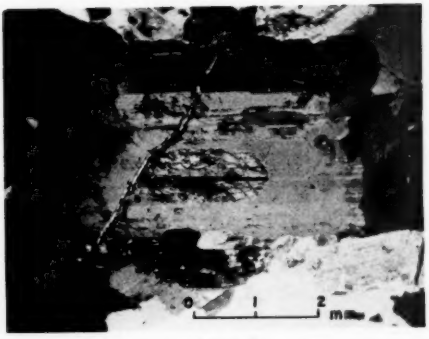

FIGURE 1

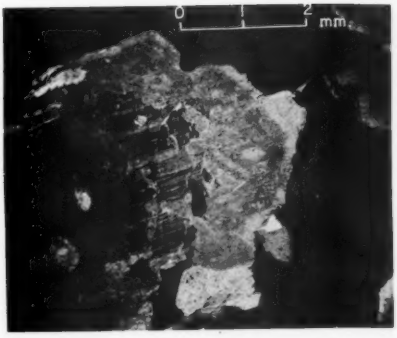

FIGURE 2

FIGURE 3

FIGURE 4

RAPAKIVI AND ZONED PLAGIOCLASE

the batholith. Plagioclase, zoned and carrying multiple sericite zones suggestive of former oscillatory zoning, occurs throughout all rock zones but shows marked increase in abundance throughout the rock zone transitional to the core and especially in the core. Polysynthetic twinning of the albite type in oscillatorily zoned plagioclase has involved only parts of crystals located in the core and the zone transitional to the core (Pl. 9, figs. 2, 3, 4).

Development of polysynthetic twinning across zoned crystals appears to eliminate the zone lines but fails to disturb the narrow bands of sericite (Pl. 9, figs. 1, 2, 3, 4, 5). Many zoned plagioclase crystals of the core are without polysynthetic twinning. In contrast, oscillatorily zoned crystals in the other rock zones where seen have always been polysynthetically twinned completely throughout. Microcline of the core rock commonly exhibits faint zonal growth bands with microscopic automorphic to hypautomorphic plagioclase crystals oriented parallel to zone lines (Pl. 9, fig. 6).

"Chill" Border and Metasomatism of Wall Rocks

Exposures of the contact between granite of the outer zone and metamorphic wall rocks are not continuous along the 45-mile perimeter of the batholith. Most of them occur along the south, east, and north sides where erosion by Sandy, Silvermine, Bullhead, and Bear Springs Branch creeks has exposed the contact. Along northeast, east, and southeast edges metasomatism seldom extends more than 5–10 feet into the wall rock. Contacts are either sharp with little or no replacement visible (Pl. 5, fig. 2), or microcline porphyroblasts extend into wall rocks with decreasing abundance for a distance of up to 10 feet (Pl. 5, fig. 1).

Porphyritic, fine to medium leuco-quartz monzonite occurs along the northeast, east, and southeast perimeter. The rock here has noticeably finer groundmass texture, smaller phenocrysts, and is interpreted as being a chilled texture. What is adjudged a "chill" zone of 10–20 feet in width consisting of leuco-quartz monzonite extends 11 miles, from H. Keese's ranch house to J. G. Moss's ranch house on the east side of Enchanted Rock. Contacts of this "chill" facies with gneissose and schistose wall rocks are either sharp with very little replacement evident (Pl. 5, fig. 2), or replacement of schist or gneiss extends up to 5 feet into the wall rocks (Pl. 5, fig. 1). Throughout

---

PLATE 9.—PLAGIOCLASE-MICROCLINE RELATIONSHIPS

FIGURE 1.—Plagioclase crystal carrying multiple sericite zones suggestive of former oscillatory zoning (core, ×13, plane light, T_3S_{41}).

FIGURE 2.—Same as Figure 1 except nicols are crossed which brings out zones and apparent partial elimination of zones by development of polysynthetic twinning (core, ×13, T_3S_{41}).

FIGURE 3.—Oscillatorily zoned plagioclase with narrow zones partially eliminated by polysynthetic twinning (core, ×13, T_3S_{39}).

FIGURE 4.—Enlarged view of Figure 3 showing straight-line edges of the zones, rectangularlike poikilitically enclosed microcline, and partial elimination of zones by polysynthetic twinning (core, ×38, Fig. 3, X).

FIGURE 5.—Completely polysynthetically twinned oscillatorily zoned plagioclase crystal (transition to core, ×13).

FIGURE 6.—Faint zonal growth in microcline with poikilitically enclosed albite grains. Microperthite is absent (core, ×13, T_3S_{32}).

PLATE 10.—RAPAKIVI AND ZONED PLAGIOCLASE

FIGURE 1.—Zoned plagioclase in alkalic granodiorite of the intermediate central zone. Oscillatory zonation is rough and irregular. Veinlet is calcite. Diagrammatic sketch shown in Figure 17.

FIGURE 2.—Rapakivi from intermediate central zone. Replacement mantle of oligoclase, An_{26}, surrounds core of unreplaced microcline. Veinlike penetrations of oligoclase partly controlled by (110). Sericitization followed (110) and albite lamellae. Diagrammatic sketch shown in Figure 18.

FIGURE 3.—Large thin section of porphyritic alkalic granodiorite of intermediate central zone. Replacement mantle of oligoclase, An_{23}, surrounds core of unreplaced microcline. Growth of crystal resulted in steplike offsetting of Carlsbad twin plane. Enlarged view of X is given in Figure 5 of Plate 8.

FIGURE 4.—Large thin section of porphyritic leucogranite from outer zone. Replacement mantle of oligoclase, An_{27}, surrounds core of unreplaced microcline. Rim of oligoclase thicker on ends of crystal than on edges. Enlarged views of X and Y are shown in Figures 3 and 4 of Plate 8.

this distance xenoliths of metamorphic wall rocks are not abundant and are small, angular, or rounded.

occurred at each area, the general relations of wall rock to granite of the outer zone differ at each area.

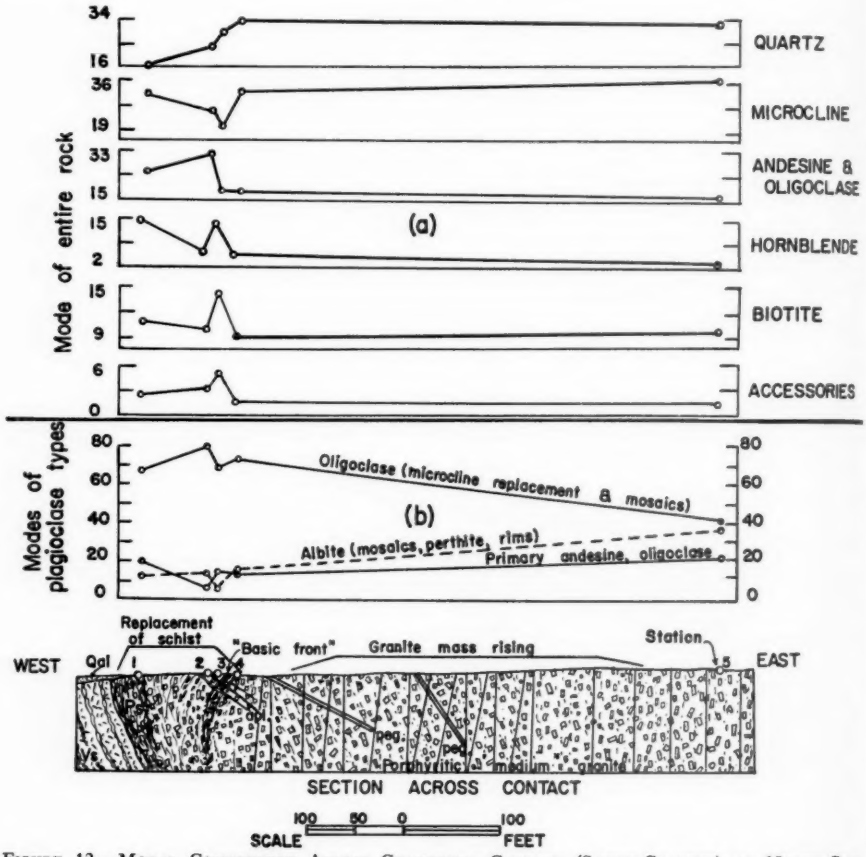

FIGURE 12.—MODAL COMPOSITION ACROSS GRANITIZED CONTACT (SCHIST-GRANITE) AT NORTH PART OF THE BATHOLITH

Very few are larger than those shown in Figures 4 and 5 of Plate 5. Most are smaller. "Chill" border features also occur on the southwest flank of the batholith where it crosses the Gillespie County line (Pl. 1).

Considerable replacement of schist wall rocks has occurred along two separated zones. One is south of the source of Sandy Creek at the extreme south tip of the batholith, and the other is at the north tip of the batholith, 500 feet north of where Bear Springs Branch Creek flows off granite of the outer zone onto Valley Spring gneiss. Although replacement has

At the south tip of the batholith, metasomatism has advanced as far as 1500 feet into blackish-gray schist. Light-gray microcline and quartz porphyroblasts have lightened color of the schist and partly eliminated its foliation. Several large elongate lenses of schist within the area of partial replacement are nonporphyroblastic and seem to have resisted replacement (Pl. 1). The zone of partial replacement is irregularly convex toward schist wall rock to the south and has altered the schist for about 2500 feet parallel to the granite-schist contact.

Throughout the length of this 2500 feet,

contact of granite with schist remains sharp and dips 80°–85° S. under the schist. The granite mass abuts and partly bypasses a narrow dike of aplite, 25–50 feet in width and about three-quarters of a mile in length. Some decrease in grain size occurs in the granite where it contacts schist. Granite of the outer zone of the intrusion north of this replacement area is singularly free of xenoliths and basic schlieren. Three-fourths of a mile north of the wall rock in the interior of the outer zone there are several 2- to 3-inch thick biotite schlieren 10–15 feet long.

Structural and mineralogic changes across the granite-schist wall-rock contact at the north tip of the batholith are shown in Figure 12. The modal changes shown represent a quantitative estimate of the changes that are thought to have occurred. Actual contact of unreplaced and partially replaced schist is covered by alluvium but is not more than 25 feet west of station 1 on Figure 12. Change from granite of the outer zone toward schistose wall rock is gradual and differs from that at the south tip by an accumulation of calco-ferromagnesian minerals in the form of a "basic front".

The zone of replacement and extreme porphyroblastesis is restricted to a 100-foot distance from stations 1 to 4. Microcline and quartz replace the schist throughout this zone. From wall rock outward the hornblende: biotite ratio is 14.7:11.1 at station 1 and 5.6:9.1 at station 4. Additional replacement of earlier-formed microcline by oligoclase also occurred (Fig. 12b).

At station 3 there is a sharp drop in modal microcline and plagioclase, coupled with an increase in hornblende, biotite, and accessories throughout a 5-foot rock zone. The entire 5-foot zone runs higher in the calco-ferromagnesian minerals throughout, approaches equigranular texture, and, what is most striking, has several ½–3 inch bands of dark minerals in higher concentration (Pl. 5, fig. 3).

Mineralogic changes throughout the 500 feet from station 4 to 5 appear to have become stabilized about the composition of granite. The basic minerals accumulated into a "basic front", averaging 5 feet in width, probably were expelled from the direction of the wall rock toward the outer zone. As shown by the mineral-variation diagrams it would seem the replacing materials sought to establish chemical and modal equilibrium about the composition of granite. Some ferrous iron, probably released as hornblende recrystallized to biotite, was oxidized and incorporated in newly formed microcline giving it a pinkish color. The microcline within the 100-foot replacement zone becomes less gray and increasingly pinkish to orangish red as the zone of stabilized granite is approached. Considerable hornblende is also lost.

It should be emphasized that this zone of replacement carries for a distance of only about 200 feet parallel to the wall rock in this area. Nowhere else along the border of the batholith has such a contact with the metamorphic wall rocks been seen as has been described here.

Metasomatism of Inclusions

About 600 xenoliths were mapped, and 95 per cent consisted of dark biotite-hornblende-quartz-feldspar schist. These disc-like xenoliths ranged from hand sized to as much as 10 by 40 feet. The most prevalent size averaged about 1 by 2 feet. Not all xenoliths in the batholith were mapped; an estimated 20–30 per cent of the possible total are shown on Plate 1. In total bulk and outcrop area less than 1 per cent and possibly not more than 0.5 per cent of the surface of the batholith consists of inclusions. (This figure includes inclusions not mapped.)

Some of the larger inclusions are much granitized, but probably not more than 15 per cent of those mapped have been so affected. Most are relatively little replaced and contain scattered microcline porphyroblasts. Rows and clusters of xenoliths have similar compositions, whereas those scattered as little as 100 feet apart may have a variety of schistose composition.

Three unusually large bands of igneous-appearing rock west of House Mountain near Hickory Creek may be severely granitized schist septa. Texture and composition of these is medium porphyritic granitic, but that of the enclosing rock is coarse porphyritic and is quartz monzonite. Textural change is sharp where they meet and contacts dip 36°–80° toward the core. Except for the uniformly

finer texture, the rocks do not run higher in biotite than surrounding granite. Several small dark schist inclusions within the igneous-appearing rock are oriented transverse to flow structures. Two miles north of House Mountain, a narrow band of quartzitic rock about 1200 feet long has been partially replaced by microcline porphyroblasts and some silica. These larger bands total about one-third of a square mile in area.

Petrology

Age Determinations

Two samples were collected for age determinations by the "Larsen Method" (Larsen *et al.*, 1952), one from the outer zone and the other from the intermediate central zone. Age of the outer-zone rocks is 795 million years (average) and the intermediate central zone is 835 million years (Table 5). Inasmuch as Larsen's Method is believed accurate to within ±10 per cent, rocks of the two zones cannot be shown to be of different ages. An overall average for both rock zones is 815 million years and may be taken as the age of Enchanted Rock batholith.

Alteration of the zircon to the metamict condition produced platy structure in the zircon with radiogenic lead concentrated more highly in some plates than others. Separate age determinations were made on the high-lead and low-lead portions of the platy metamict zircon and served as a check. These are shown in Table 5 and are labeled TM-1A and TM-1B.

Development of Rock Zones

A critical control in the development of the rock zones of the batholith was the time relation between intrusion and final crystallization. Continued upward bulge of the core of the batholith forced the granite against the wall rocks and produced tensional deformational effects which finally fractured the rigid exterior zones. Of great importance during the rise of the granite was the minor deformational effect of compressional squeezing which forced crystals together and filter-pressed off the yet-liquid fraction. For the level in the earth's crust at which the batholith was emplaced and now stands the liquid fraction was probably of minor quantity. During this time the potash feldspars were unmixing, and some of the unmixed material probably was carried and filter-pressed toward the core by a front of sodic-rich hydrothermal solutions moving inward ahead of an advancing front of crystalline immobility.

Unmixing of potash feldspars took place beyond the perthitic stage to give nearly potash-free plagioclase and soda-free microcline. The unmixed plagioclase fraction is believed to have consisted principally of oligoclase and albite, possibly with some sodic andesine. Tuttle (1952, p. 115) reported that the plagioclase component of perthite is commonly oligoclase and in some cases may be as calcic as andesine. Such a process of unmixing and recrystallization played a vital role in developing the mineralogical and textural relationships of the batholith.

Figure 11, showing the overall variation of plagioclase content in the rock zones of the batholith, illustrates two important changes: (1) the progressive increase in primary plagioclase from the outer zone to the core, and (2) the systematic variation in amount of unmixed oligoclase. The importance of the role of liquid in the formation of primary plagioclase (sodic andesine to calcic oligoclase) increased toward the core. Two principal concentration maxima of secondary unmixed oligoclase occur, one in the intermediate and the other in the intermediate central zone. The latter is flanked on either side by two oligoclase minima, one in the core and the other on the inner edge of the intermediate zone next to the intermediate central zone.

Field occurrence of these zones (Pl. 1) finds expression as arcuate ribs of rock, their contacts gradational and subparallel to the outline of the batholith. Boundaries between the zones of maximum and minimum oligoclase cut across flow structures of the rocks where these bands pinch out. The independent relationship as well as the gradational character of the contacts suggests both contemporaneity of development and emplacement of the mass of granite as a single unit.

Concentrations of oligoclase maxima to form quartz monzonite zones probably developed as the inward-moving front of crystalline immobility moved faster than did the front of

TABLE 5.—AGE DETERMINATIONS OF ZIRCONS FROM ENCHANTED ROCK BATHOLITH*

Source and number of sample	alpha/ mg./hr.	Lead (ppm)	Age (M.Y.)	
Outer rock zone TM-1A	340	116	771	795 (avg.)
Outer rock zone TM-1B	494	180	820	815 (avg.)
Intermediate central zone TM-2	404	150	835	

*All age determinations corrected for parent decay of the zircon. Analyses by David Gottfried and H. W. Jaffe.

TABLE 6.—CHEMICAL ANALYSES OF VALLEY SPRING GNEISS AND PACKSADDLE SCHIST

	11	12	13	14	15	16	17
SiO_2	72.62	74.11	76.47	71.10	74.91	70.92	63.21
Al_2O_3	12.93	13.58	11.64	12.16	11.78	15.72	16.81
Fe_2O_3	1.49	1.14	0.50	2.02	2.08	0.63	2.30
FeO	1.54	0.77	1.26	1.59	0.54	0.79	3.70
MgO	0.36	0.12	0.38	0.94	0.06	0.48	2.03
CaO	1.15	0.99	0.10	1.08	0.03	0.95	4.08
Na_2O	3.77	3.40	1.41	1.00	0.36	5.55	4.02
K_2O	4.71	5.13	7.79	8.75	10.06	4.31	1.92
H_2O+	0.28	0.05	0.18	0.13	0.00	0.11	0.55
H_2O-	0.05	0.03	0.02	0.08	0.02	0.04	0.04
CO_2	0.44	n.d.	0.02	0.41	0.01	0.03	0.05
TiO_2	0.21	0.24	0.11	0.33	0.14	0.33	0.57
P_2O_5	n.d.	n.d	0.02	n.d.	0.02	0.07	0.31
MnO	n.d.	n.d.	0.02	n.d.	0.01	0.01	0.16
F	n.d.	n.d.	n.d.	n.d.	n.d.	0.13	n.d.
BaO	.....	.....	.....	.....	.....	.....	0.12
	99.55	99.56	99.92	99.59	100.02	100.07	99.87

Analyses 11–16 by Barnes *et al.* (1947) analysis 17 by R. M. Hutchinson (PhD. thesis, Univ. Texas, May 1953).

11. Valley Spring gneiss, Llano Co.; 6 feet below top of west wall of Premier gray-granite quarry 2.7 miles south of Sixmile; sampled from light-colored portion of steeply dipping gneiss-schist series, collected by V. E. Barnes and G. A. Parkinson; R. W. Perlich, analyst

12. Valley Spring gneiss, Gillespie Co.; east side of highway cut north of Bell Mountain, 2 miles by road southwest of Legion Creek bridge, and about 500 feet south of a concrete culvert; collected by V. E. Barnes and G. A. Parkinson; R. W. Perlich, analyst

13. Valley Spring gneiss, Llano Co.; east side of highway cut near Baby Head and near llanite dike; collected by H. B. Stenzel; R. B. Ellestad, analyst

14. Valley Spring gneiss, Burnet Co.; 5 feet beneath surface in cut north side of Llano-Burnet highway, 7.2 miles west of highway intersection in Burnet; collected by V. E. Barnes and G. A. Parkinson; R. W. Perlich, analyst

15. Valley Spring gneiss, Llano Co.; 1.8 miles east of road intersection at Baby Head, on creek parallel to Wilberns Glen road, from a ledge which forms a water fall; collected by H. B. Stenzel; R. B. Ellestad, analyst

16. Valley Spring gneiss, Burnet Co.; from north ditch of old Llano-Burnet road, on east slope of a small hill, 1.56 miles west from point where this road forks from new Llano-Burnet highway; collected by H. B. Stenzel; R. B. Ellestad, analyst

17. Packsaddle schist, Llano Co.; 1 mile north-east of Enchanted Rock dome on east side of Sandy Creek, 1000 feet due east of granite-schist contact of Enchanted Rock batholith; collected by R. M. Hutchinson; J. A. Maxwell, analyst

the filter-pressed material thereby effectively fixing its position permanently. The position of the plagioclase-rich intermediate central zone next to the core probably resulted from behavior of the core during the last stages of cooling. Distinctly less seriate porphyritic texture and hiatal porphyritic texture begin with rocks of the intermediate central zone and increase toward the core where hiatal porphyritic texture prevails.

A last upward surge of the yet partially mobile core could have been initiated through partial failure of the roof and ensuing partial escape of volatiles. Such an escape of volatiles would affect all parts yet mobile and result in a "sweeping-out" action of interstitial liquid. The filter-pressing action was intensified during this time, as all materials free to move or capable of transport in solution sought positions of maximum equilibrium along the energy gradient. Contact between the inner edge of the intermediate zone and the outer edge of the intermediate central zone is less gradational than that between the core and the intermediate central zone. This probably developed after all available or movable oligoclase on the coreward side of the intermediate zone had been moved into the intermediate central zone. Depletion of the magma reservoir probably resulted in cessation of intrusion. This combined with failure of the roof rocks and partial loss of volatiles produced an increased rate of cooling and crystal growth throughout the core. Movement of sodic-rich hydrothermal solutions and unmixed sodic plagioclase was checked as the core stiffened and both were "dammed" in the present intermediate central zone.

Significance of Plagioclase-Microcline Relationships

The microscopic study of the twin-zone relationships of many hundreds of plagioclase crystals collected along traverses rim-core-rim across the batholith has shown that oscillatorily zoned plagioclases of the core and transition zone to the core may lack albite twinning or, as in most crystals, are only partially twinned as shown in Plate 9. This is in marked contrast to crystals in all other zones where they are strongly and completely twinned. Evidence is conflicting concerning the relative importance of the strain effect in the development of albite twinning in primary crystals. Emmons (1953) established the time of polysynthetic twinning as very late in the period of growth of the crystal and emphasized that polysynthetic twinning is, in feldpars as in metals, a strain effect, a mechanical feature which depends in part on environmental factors. MacKenzie (1955, personal communication) and Emmons (1953, p. 54) stated that when either albite or anorthite crystals are grown in the laboratory they are invariably multiply twinned. These crystals are sometimes quite outside the glass and have been free to develop crystal faces yet they are multiply twinned. It would appear that such crystals have not been twinned by any strain effect. Polysynthetic twinning can probably be produced by strain, but it need not be due to this alone.

The environmental factors described in the development of the rock zones would explain the partial twinning of oscillatorily zoned crystals in the transition zone and core. During the stages of inward crystallization the entire intrusion was bulging upward and outward. This motion produced deformational effects, tensional in character, which finally fractured the sufficiently rigid exterior zones. Of great importance during this stage was the minor deformational effect of compression which squeezed the crystals together and strained them. Interstitial quartz shows erratic, generally weak, undulatory extinction from zone to zone. Plagioclase crystals in each succeeding rock zone from the outer zone inward could have developed polysynthetic twinning as they were strained by the continued force of intrusion of the yet-mobile core. Partial and complete lack of polysynthetic twinning of the oscillatorily zoned plagioclases in the core indicates that crystallization probably took place in an environment of decreasing strain. The upward bulge of the core gradually ceased and the remaining plagioclase liquid probably formed as oscillatorily zoned untwinned crystals. The partly twinned crystals could have been formed in the waning stage of intrusion when tensional stresses and compressional squeezing were very weak to nonexistent.

The concept of a waning force of intrusion with an accompanying "strain effect" producing albite twinning in primary plagioclase of the batholith could be valid. Despite the fact that the structural and intrusive history of the batholith suggests such an influence, it is not definite that the twin-zone relationships are due to this, either in whole or in part, although it does seem probable that strain is partly responsible for polysynthetic twinning.

Examination of oscillatory zoning in detail shows regular inner boundaries between extremely thin zones (Pl. 9, figs. 3, 4, 5). Bowen's explanation that this type of zoning may arise from "the forcing of a hotter liquid magma through a crystal mesh" (1928, p. 275) satisfies the environmental conditions indicated by other lines of evidence and predicates the same conditions during intrusion as are indicated by the structural evidence. The progressive increase in number of oscillatorily zoned crystals from the outer zone inward to the core indicates liquid played an increasingly important role in formation of the granite toward the core.

Rapakivi are very abundant in the plagioclase-rich intermediate central zone. They have not been observed in the core and are rare in all other rock zones. One slab of rock from the intermediate central zone, 25 by 100 cm on a side, which is typical, contained four rapakivi and three completely replaced microcline crystals surrounded by oligoclase. Crystals of oligoclase-replaced microcline commonly range on cross section from 5 by 12 mm to 13 by 54 mm. Many are smaller.

The oligoclase mantle surrounding each microcline core invariably contains tiny disseminated hypautomorphic flakes of biotite. Microcline crystals completely replaced by oligoclase have biotite flakes ranging from .05 by .1 mm to .1 by .5 mm disseminated throughout. Part of the potassium displaced from the microcline probably contributed to formation of the secondary biotite. The biotite flakes in the oligoclase mantle are noticeably smaller than those elsewhere throughout the rock.

The almost complete limitation of the abundant rapakivi to the intermediate central zone developed after unmixed sodic plagioclase had migrated most probably from the intermediate zone into the intermediate central zone. The petrographic and structural evidence suggests that unmixed sodic plagioclase had a mobility allowing it to behave similar to the rest magma in a crystallizing magma. Gates (*in* Emmons, 1953, p. 58, 61) has proposed a similar approach in another area. Sodic-rich hydrothermal solutions derived from the cooling Enchanted Rock batholith probably aided in transporting the unmixed sodic plagioclase. Dr. O. F. Tuttle (Personal communication) has called attention to the fact that (1) his laboratory experiments have shown unmixing of sodic plagioclase from potash feldspar will go on in a few hours if water vapor is present to flux the reaction, and (2) potash feldspar of granite can carry 40–60 per cent plagioclase in solid solution. On this basis he suggests the oligoclase mantles around microcline cores in the intermediate central zone could be derived by unmixing from the very same crystal each mantle surrounds. A relationship such as this would mean that the chief role of the hot vapor phase in the intermediate central zone was to flux the unmixing reaction. This would require that considerably less unmixed sodic need be derived from the adjacent intermediate zone. Perhaps none (?). The hot-vapor phase, it is believed, moved from the intermediate into the intermediate-central zone, pushed toward the core by a filter-pressing action, and it carried some unmixed sodic plagioclase with it. The principal direction of compressional squeezing was maintained at right angles to the outline shape of the chamber. This is indicated by subparallelism of rock-zone boundaries to contact with the wall rocks.

Under the influence of a structural control imposed by the shape of the chamber, the inward movement of an "interface of immobility" (Compton, 1955, p. 28) began at the outer zone. Unmixed sodic plagioclase probably squeezed inward until, as it reached its present position in the batholith, relatively sudden dilatant effects above the roof of the intrusion caused chilling of the core. The way was then effectively blocked for further extensive migration of the plagioclase, and it was effectively dammed in the intermediate central zone. The outer zone and parts of the inter-

mediate zone were impoverished in plagioclase, and the area of concentration, the intermediate central zone, was enriched in sodic plagioclase with the characteristic textural relationships. The rapakivi are adjudged to be of replacement origin, developed during the autometamorphic stage of the batholith. As a consequence of the concentration of the sodic-rich plagioclase, textures characteristic of replacement and recrystallization are most abundant in the intermediate central zone rocks.

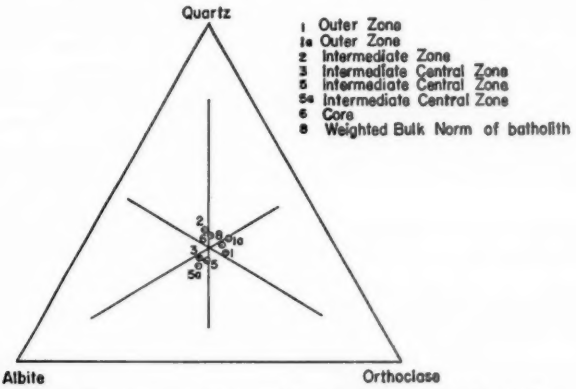

FIGURE 13.—NORMATIVE COMPOSITION (ALBITE+ORTHOCLASE+QUARTZ) OF ROCKS OF ENCHANTED ROCK BATHOLITH CONTAINING 80 PER CENT OR MORE OF THESE NORMATIVE CONSTITUENTS

Interpretation of Compositional Variation

For each rock type of the batholith the proportions of the normative constituents, albite + orthoclase + quartz, total more than 80 per cent, and these components have been plotted in Figure 13. The points for the granite are strikingly grouped about the composition having a 1:1:1 ratio of albite:orthoclase:quartz. The grouping of the Enchanted Rock granites illustrates the unusual extent to which the granite formation must have been dominated by factors tending to give the rocks a nearly constant composition.

The weighted bulk normative composition for the entire batholith has been plotted in Figure 13 and lies within the compositional range for rocks of the batholith. The bulk normative composition represents the approximate average composition throughout the batholith prior to its emplacement, and the scattering of points in Figure 13 probably developed during the structural and intrusive history of the batholith.

Although the granites of the batholith consist chemically (or normatively) of approximately equal amounts of albite + orthoclase + quartz, mineralogically there are considerable variations from equal ratios (Fig. 14). In the outer zone there are approximately equal ratios of microcline:quartz with subordinate plagioclase, and in the intermediate central zone there are approximately equal ratios of plagioclase:microcline with subordinate quartz. Rocks of the core come closest to having equal ratios of quartz:microcline:plagioclase. Chilled border rocks average higher in plagioclase than apophyses rocks, yet both are dominantly microcline. It is interesting to note that the weighted bulk mode for the batholith is closely similar to the average composition of the chilled border rocks. Rocks of the core also have the same microcline content but are higher in plagioclase.

The significance of the distribution of the points in Figure 14 can best be understood by referring to Figure 11 as well, for this shows both types and amounts of modal plagioclase in each of the rock zones of the batholith. Since only the average modal composition of the apophyses is plotted in Figure 14, the critical significance of the mode of apophysis A_3 must be shown in Figure 11. Apophysis A_3 is 1500 feet from the edge of the batholith, com-

pletely isolated from it in plan but most probably connected to it at depth. All three principal types of plagioclase in A_3 total less than 11 per cent of the rock (the lowest value obtained), and the texture is strongly hiatal porphyritic with fine groundmass. The texture particularly A_3, cooled rapidly enough to allow unmixing of only minor amounts of sodic plagioclase. The tendency of the apophyses rocks is toward the granite and leucogranite range of composition, whereas chilled border rocks are quartz monzonite to leuco-

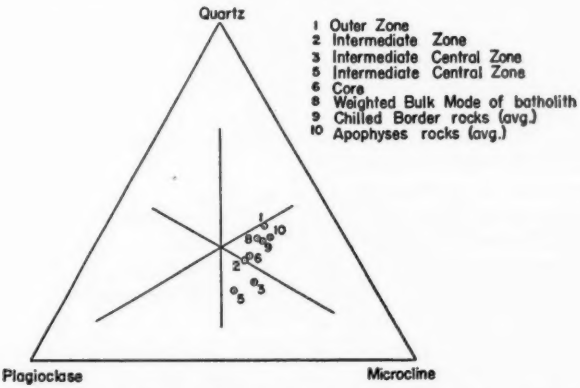

FIGURE 14.—MODAL COMPOSITION OF ROCKS OF ENCHANTED ROCK BATHOLITH
Albite included in microcline

is believed to be a "chill" texture, and the composition the earliest "chill" facies of all the batholith rocks. Microcline phenocrysts average 7 by 13 mm and are set in a fine-grained hypautomorphic groundmass with long dimension subparallel to the walls of the fissure.

The similarity in amount of primary plagioclase (4–6 per cent) for A_1, A_2, C_1, C_2, C_3, and the outer zone rocks is probably significant. The variation of secondary or unmixed oligoclase in A_1, A_2, C_1, C_2, and C_3 (in most crystals it seems to have replaced microcline) is probably due to the varying amounts of replacement of schist wall rock by microcline from the granite intruding it.

The closeness of the plots for average modal composition of apophyses rocks, chilled border rocks, and weighted bulk mode of the batholith indicates that (1) apophyses rocks mineralogically probably are most similar to the original modal composition of the batholith prior to the effects of autometamorphism; (2) there was a minimum of overall total contamination of chilled border rocks by wall-rock replacement, and (3) apophyses rocks, quartz monzonite. As stated, the generally lower total plagioclase content of apophyses rocks resulted from cooling rapidly enough to allow unmixing of only minor amounts of sodic plagioclase. Chilled border rocks, cooled not so fast, had time to partly unmix sodic plagioclase. Much less modal plagioclase is present in the outer zone than in the intermediate central zone in spite of the fact the normative plagioclase in the intermediate central zone is noticeably higher than the core. This suggests that the outer zone cooled in such a way that the plagioclase in solid solution in the potash feldspar unmixed to a lesser degree and that the potash feldspar of the outer zone must carry considerably more plagioclase in solid solution (or as submicroscopic perthite) than the potash feldspar of the intermediate central zone. The outer part of the core is a leucoquartz monzonite which grades imperceptibly into leucogranite in the center of the core.

Chilled border rock makes up about 0.5 to 1 per cent of the batholith. For rocks of the core a higher content of primary plagioclase moved the plot toward plagioclase (Fig. 14). The scattering of plots for rocks of the inter-

mediate and intermediate central zones is due mainly to increased sodic plagioclase (unmixed oligoclase). Primary plagioclase is less than in the core.

Migration inward of portions of the unmixed sodic plagioclase with consequent impoverishment of some rock zones and enrichment of others produced generally small differences in relative proportions of plagioclase and hence in rock types as well. Relative proportions of rock types in the batholith average 65 per cent granite to leucogranite, 30 per cent quartz monzonite to leuco-quartz monzonite, and 5 per cent alkalic granodiorite.

The presence of sericite commonly accompanied by anhedrons of fluorite and occasional veinlets of calcite in microcline crystals which have been partly or completely replaced by oligoclase indicates hydrothermal solutions played an important role during the period of unmixing, migration, and replacement by the sodic plagioclase. A front of sodic-rich hydrothermal solutions derived from the cooling batholith probably moved upward and inward ahead of the advancing front of crystalline immobility and aided in transporting the unmixed sodic plagioclase.

Additional evidence for a filter-pressing action that affected the rock zones is found in superposing the oxide analyses plots for Enchanted Rock batholith on the Harker variation diagram for igneous rocks of the surrounding central Texas region (Fig. 10). Distribution of the oxides K_2O and CaO with respect to the smooth curves drawn through the points obtained indicates the outer zone rocks depart from the curves in high K_2O content and the somewhat low CaO content. With crystallization of microcline as a first stable crystalline phase in response to supersaturation of the magma in this constituent, the outer zone rocks underwent partial loss of primary plagioclase liquid by filter-pressing action inward toward the intermediate and intermediate central zones. Peripheral crowding of magma first against the wall rocks of the chamber and then against the advancing front of crystalline immobility caused this.

If increasing silica content reflects decreasing age, the sequence of intrusion oldest to youngest would be intermediate central zone, core, outer zone, and finally the intermediate zone. Such is not thought to be the sequence because: (1) internal structures of the batholith, particularly the marginal fissures, indicate the outer zone cooled first; (2) development and distribution of textural relations between microcline and plagioclase as well as progressive variation of ratios of microcline:plagioclase fit in with the genetic sequence of intrusion and cooling outlined; and (3) the isolated position of an arcuate rib of leucogranite in the intermediate central zone a mile northeast of House Mountain is probably best explained as a band of original granite that was not penetrated by the unmixed sodic plagioclase and sodic-rich solutions at the time these were migrating toward the core.

The time-honored axiom that increasing silica content goes along with increasing age will not apply to the rock zones of the batholith, then, if their oxide contents are taken at face value. Once the physico-chemical effects produced by the tectonic setting of the batholith during the time of intrusion are understood, and the filter-pressed fractions are restored to their original positions, decreasing age of intrusion might be expressed by decreasing silica content. However, any differences in rock types would be so slight as to prevent any degree of certainty in applying this axiom to the rocks of the batholith. Probably the batholith was intruded as a unit, mostly crystals with some liquid, to complete the final phases of its cooling history as it moved into the structural position it now occupies.

Tuttle and Bowen (Adams, 1952, p. 39) have established the existence of a lowest-crystallizing composition for the system albite + orthoclase + quartz at approximately equal proportions of the three components. They have further shown that there is a moderate change in the position of the minimum-crystallizing composition depending on the amount of water (pressure of water) and that the proportions of the three components are more nearly equally balanced at the lower pressures (low water content). Their plot of the rock-forming oxides that constitute 80 per cent or more of the rock for the compositions of 571 analyzed granites and syenites shows a

concentration of the points that corresponds closely with their previously experimentally determined minimum. Such clustering of composition of granites is cited by Tuttle and Bowen (Adams, 1952, p. 39) as strong evidence of origin by crystallization of the liquid which is a residuum of fractional crystallization. One other hypothesis is the selective fusion (melting) of random rock material producing the same minimum crystallizing liquid. In such a process of selective fusion this would be the first liquid formed.

Similar normative and modal compositions of the rocks of Enchanted Rock batholith to that determined experimentally and also plotted by Bowen and Tuttle (Adams, 1952) would seem to require that the rocks be formed from a granitic liquid. This liquid would have as its origin one of the two, or maybe both of the processes of magma generation quoted: (1) crystallization of a liquid which is a residuum of fractional crystallization, or (2) selective fusion (melting) of random rock material producing the same minimum crystallizing liquid.

Source of the Granite

Generation of granitic magma was a product of the tectonic history that affected the rocks of this region during early middle Precambrian time. Restriction of the north end of the batholith to a syncline and enlargement of the granite mass to the south indicate that the syncline exerted partial structural control during emplacement. The generation of magma may have depended partly upon downfolding, as the Castell syncline has been depressed at least 3–4 miles, possibly as much as 6 miles. A less probable interpretation would allow for downbuckling resulting from and occurring above sites of previous magma generation. It is not known if the granite was derived from (1) a residuum of fractional crystallization or (2) selective fusion of either the sial or metamorphic rocks. In the first case, moderate-sized, rudely cylindrical, pluglike masses of granite probably detached themselves from the sial and rose into the framework of metamorphic rocks. Their emplacement was structurally controlled and guided by the major synclines. In the second case, because of the deeper position of the major synclinal troughs, temperature and pressure (of water) conditions could have been best for selective fusion (melting) of random rock material and production of granite liquid. The granite mass would then be in position to move up along the trough of the syncline immediately above.

A plot of the normative compositions of all known chemical analyses of Valley Spring gneiss from widely scattered localities of the surrounding region shows a fairly wide range in composition (Fig. 15). Two samples have compositions closely similar to rocks of the batholith; three are predominantly orthoclase and quartz; and one is high in plagioclase with subordinate quartz and orthoclase. Packsaddle schist collected 1000 feet east of the granite-schist contact a mile northeast of Enchanted Rock is mainly plagioclase and quartz with subordinate orthoclase.

Analysis 11 is from the 6000 feet or more of gneiss forming the northeast limb of the large syncline underlying the north part of the batholith. Close similarity of the normative and mineral compositions of this gneiss to the bulk normative and bulk modal compositions of the batholith indicate a maximum amount of granitic liquid could be obtained by selective fusion of the gneiss under the proper conditions of temperature and pressure (water pressure), of course, provided the gneiss maintains the composition of analysis 11 to the postulated locus of magma generation.

The structural and thermal conditions needed for the formation of granite by selective fusion (melting) of random rock material are most favorable during the later stages in the deformation of geosynclines. Tuttle and Bowen (Adams, 1952, p. 38) demonstrated it is improbable that many granites have crystallized at depths greater than 9 miles. Considering that a thickness of at least 6000 feet of Valley Spring gneiss and 5000 feet of Packsaddle schist is exposed; that the base of the gneiss is unknown; that many thousands of feet of rocks were deposited above the Packsaddle schist of which there is now no record and that the depth of folding in the metamorphic rocks approximates 3–4 miles, possibly as much as 6 miles, it is not unreasonable to assume a mini-

mum thickness of 15,000–20,000 feet of metamorphic rocks existed. Depth of folding may have lowered the rocks sufficiently to cause selective fusion (melting).

Geophysical data on the shape of the intrusion at depth is lacking for all except a 3-mile zone along the southwest flank of the batholith in Gillespie County. A magnetometer survey across the southwest flank of Enchanted Rock batholith (Barnes *et al.*, 1954) indicated the granite mass in this area extends to depth and widens with a near-vertical edge dipping steeply southwest. The granite mass is separated from another granite mass to the southwest, the Hilltop mass, by a thin septum of schist. Structural evidence seems good that the northern third of the Enchanted Rock batholith is phacolithic, but as shown in Figure 1 the southern two-thirds probably is cylindrical at depth.

An indirect method of predicting the dip of the outer edge of the batholith at depth is a correlation with abundance of pegmatites and aplites in the metamorphic rocks of the wall rock. Within a 500-foot zone next to the granite-schist contact, the pegmatites and aplites box the compass about the batholith. Considerable numbers of these are present in this zone extending from the east down to the south and up to the west side of the batholith suggesting that the flanks of the batholith dip steeply outward under the schist as shown in Figure 1. Where the dip of this contact is inward toward the batholith, as in the northern third of the intrusion, there are none or considerably fewer and smaller aplites and pegmatites in the wall-rock zone.

The locus of refusion lay at depth below the present level of the batholith. Location of the granite in the syncline is significant for this would seem to indicate that (1) temperature-pressure conditions for formation of granite by selective fusion obtained first in the locus of or beneath the lowermost level of the trough of the syncline, and (2) tensional stresses upward along the axis of the fold favored elongation and movement of the magma in this direction. The granite seems to have tried to move upward, wedging into and along the plane of contact between the Valley Spring gneiss and Packsaddle schist.

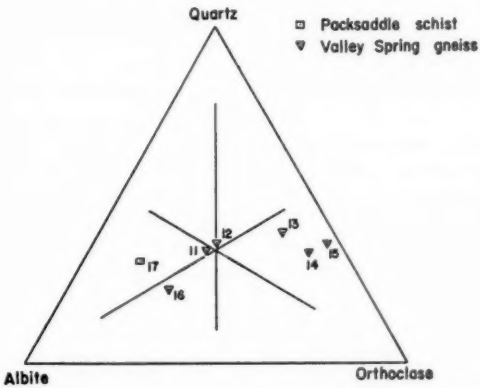

FIGURE 15.—NORMATIVE COMPOSITION (ALBITE+ORTHOCLASE+QUARTZ) OF VALLEY SPRING GNEISS AND PACKSADDLE SCHIST, PRECAMBRIAN OF CENTRAL TEXAS

The schist became the roof rock as the intrusion progressed. Of the 600 xenoliths mapped, about 95 per cent consisted mainly of Packsaddle schist and occurred in all parts of the batholith. Only one xenolith, of course, was found in the core. Tensional stress upward along the axis of the fold in combination with the incompetence of the schist supplied the granite mass with the impetus it needed to crowd against the schist wall rock which gave gradually under the combined forces of intrusion and lengthening upward. This tendency of the schist to give with both the force of intrusion and the tensile stress accompanying folding resulted in the schistosity boxing the compass

about the batholith. The walls were not rigid and completely immovable but gave slightly as the quantity of granite increased and attempted to extend its bulge upward. The internal flow structures of the batholith thus reflected the shape of the chamber they occupied and which they helped partly to form.

The pear-shaped outline of the batholith would be the one most likely to form if emplacement of the magma were structurally controlled as it followed up along the fold axis in the direction of greatest lengthening. Intrusion occurred during the later most severe stage of regional folding.

The most probable history then is one of the Packsaddle schist crowding into the trough of a syncline and exerting downward pressure, which forced up a roughly circular pluglike column of granite above the zone of refusion. The downward pressure of the more solid rocks above was maintained steadily upon the locus of magma generation crowding unmelted rocks into the site of selective fusion (melting) and squeezing together the newly formed granite liquid. It is not improbable that the locus of refusion could slowly mount as a result of continued deformational squeezing of the geosynclinal tract. Such selective melting and softening of the metamorphic frame would prepare the way for emplacement of the newly formed granite mass when the appropriate forces prevailed. One might compare the rise of the batholith to that of the "core of a large carbuncle" as downward pressure is applied

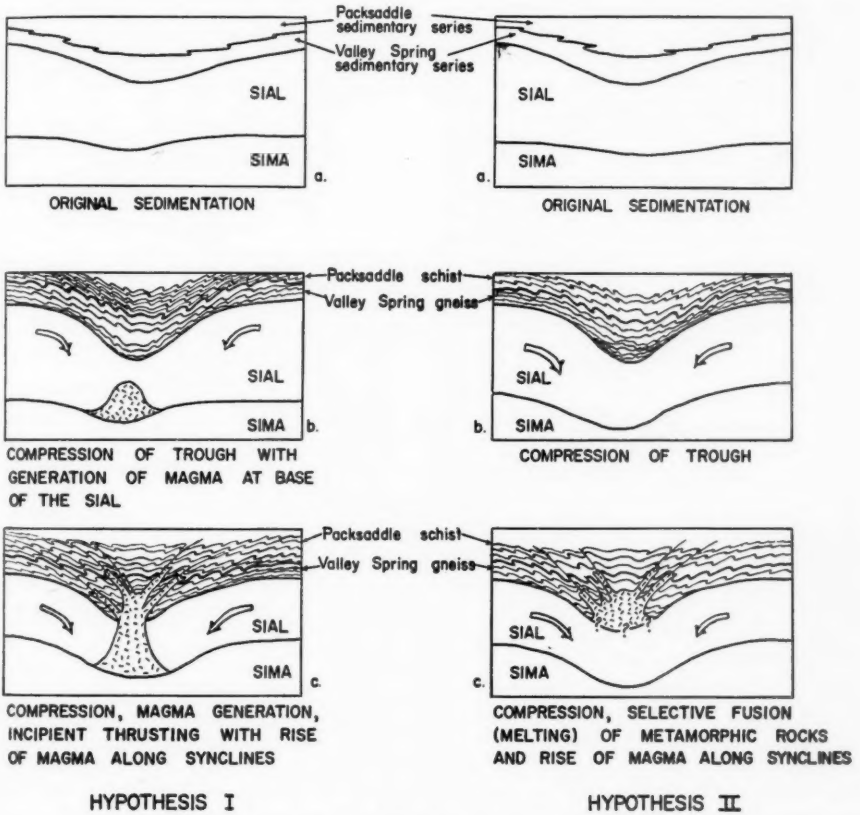

FIGURE 16.—HYPOTHESES FOR OCCUPANCY OF SYNCLINES BY RISING MAGMA

uniformly from all sides forcing it up from its site of development. The downward pressure of the upper-level rocks was initially greater and of more continued importance, for this placed the magma column under great hydrostatic pressure which was transmitted uniformly to all parts of the intrusion. With regional tectonism increasingly active, the harder the rocks pushed down, the stronger was the force of intrusion of the enlarging mass of granite. Pressure of the batholith upward was sufficient to hold back the schist and prevent it from crowding into the bottom of the syncline (Fig. 16).

Problem of the Schlieren

Depending upon which hypothesis is favored in formation of granitic liquid for the batholith, one might interpret biotite-rich schlieren as resulting from either (1) segregation of basic material during crystallization-differentiation of primary granitic magma, (2) remnants of undissolved schist wall rocks, (3) remnants of unreplaced schist wall rocks, or (4) rock material unfused at the locus of magma generation but which was carried up to its present position by the main body of rising granite.

The first possibility is ruled as improbable in view of the tectonic history of these rocks in early middle Precambrian time and the petrogenetic significance of the structural location of the batholith. In the case of (2) the solution of large quantities of material that would be needed does not appear to have been within the powers of the granitic magma when it reached the level in the crust it now occupies. From the overall continuity and circular pattern of the flow structures in the batholith it would appear that the granite consisted of crystals and some liquid when it was emplaced at this level.

There is a minimum of evidence to use in estimating the quantity of liquid present when the granite rose to its present position. Modal analyses of representative suites of thin sections from each rock zone have shown a general predominance of a microcline and quartz mixture over plagioclase. Porphyritic texture in chilled border and apophyses rocks as well as interior zones of the batholith indicates crystallization of potash feldspar before all other major components. Increase in oscillatorily zoned plagioclase from the outer zone

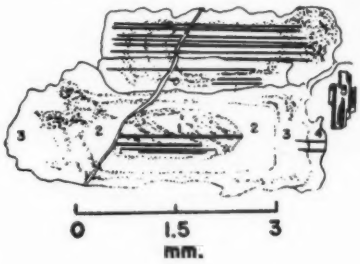

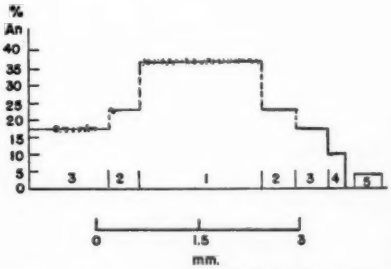

FIGURE 17.—ZONATION AND ANORTHITE CONTENT OF THE CONSECUTIVE ZONES

Ordinate = anorthite content. Abscissa = width of the zones. Specimen from the intermediate central zone (Pl. 10, fig. 1).

inward to the core does not necessarily afford a measure of the relative quantity of liquid present at the time of intrusion. On the contrary, considerable oscillatorily zoned plagioclase in the outer and intermediate zones may have had all such zonation eliminated by the mechanical strain induced during intrusion and peripheral stretching of the batholith. Such evidence indicates the presence of a minimum amount of liquid as the batholith intruded to its present level.

The magma should have had only the power to transform or replace to a limited extent but not to dissolve such material, as indicated by the small amount of metasomatism of wall rocks. Several sizable downward extensions of schist roof rocks were probably replaced and granitized into "igneous-looking" rock in the

vicinity of House Mountain. These, however, total about 0.3 square mile. Including the wall-rock replacement visible along the border rocks and granitized xenoliths, probably not more than 5 per cent of the granite of the batholith at this level of exposure is of replacement origin.

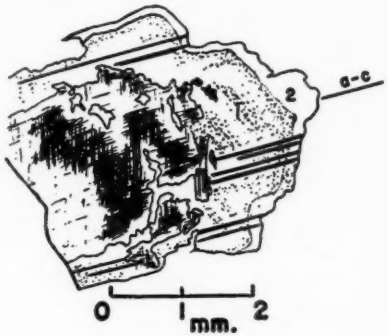

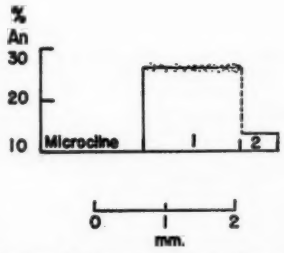

FIGURE 18. RAPAKIVI FROM INTERMEDIATE CENTRAL ZONE

Curves represent anorthite content of consecutive zones. Ordinate = anorthite content. Abscissa = width of zones (Pl. 10, fig. 2).

Hypothesis (4) is accepted as most probable in explaining the origin and structural position of the biotite-rich schlieren. At the site of partial refusion of granite or selective fusion of metamorphic rocks, we might, as stated by Bowen (1947, p. 276), expect a tendency to produce a mass with a granitic liquid at the top, unfused lighter crystalline material of general granitic character immediately below, and the more mafic crystalline material still lower. This is the ideally developed condition and would not prevent nonhomogenous distribution of some mafic layers in the lower levels at the site of liquid generation. With downward buckling and severe folding of such a locus of magma generation, the lower-level mafic crystalline material, if some of it were carried upward by the rising granite, would find its position adjacent to the wall rocks. Its position in the field suggests that the biotite-rich schlieren were possibly derived from adjacent wall rocks. The structural and intrusive evidence, again, would seem to invalidate such an interpretation.

Within the batholith biotite-rich schlieren of the type shown on Figure 5 of Plate 3 occur sparingly along the series of exfoliation domes on the southeast side in the vicinity of Enchanted Rock. North of House Mountain 1–2 miles, along Hickory Creek, narrow mafic schlieren also occur. The circular swirl-like pattern of large biotite-rich schlieren in the north tip of the batholith (Pl. 1) suggests that the granite had a spiral-like motion as it rose up the keel of the Castell syncline.

Microcline-rich schlieren occur mostly in the intermediate zone and are small-scale structures (Pl. 3). These might be interpreted as either (1) schist with development of microcline from the replacing granite, or, more probably, (2) local concentrations of microcline due to compositional inhomogeneities of the crystallizing liquid initially formed at the site of selective fusion. One is impressed with the strikingly constant uniformity, mile after mile, of the textural and mineralogical composition of the granites. If replacement were the mechanism of granite formation for these rocks, there would have to be a widespread downward migration of mafic material accompanying a replacement so complete that no biotite-rich schlieren would be left over these distances. Such complete replacement does not seem to have been possible considering the minor replacement visible in the metamorphic wall rocks at the present level of exposure.

Arcuate biotite-rich schlieren are very small, and all but 4 of the 15 mapped occur in the outer zone. The mafic material probably represents narrow layers of unfused mafic material. Frictional retardation of solid wall rock and interlamellar movement of magma sheets during intrusion produced swirl-like

movements. This would be most commonly effected in the locale of selective fusion as granite liquid concentrated and initially began to rise.

Significance of Color

The pinkish to reddish colors of the granites of the batholith are attributable to ferric iron in the feldspars. Outer and intermediate zone rocks are moderate reddish orange (10R 6/6). Intermediate central zone rocks are grayish orange pink (5YR 7/2), and core rocks are moderate reddish brown (10R 4/6). Grains of iron oxide in the core rocks are coarser than in other zones and much more apparent in thin section. Minute hematite scales are banked up around feldspars forming heavy reddish rims. Many feldspar grains have heavy disseminations of hematite grains uniformly throughout.

Niggli (1954, p. 86) states the reddish color shown by some alkali feldspars is due to inclusions of minute hematite scales which are usually formed by exsolution which results from the replacement of some Al by Fe. This does not locate the source of the Fe. Whether the hematite be derived by Niggli's process or by oxidation of ferrous iron, the bulk of the iron oxide probably was derived at the site of magma generation. Indirectly, this possibly favors selective fusion of Valley Spring gneiss at depth, for present exposures of the gneiss forming the floor of the Castell syncline have a color very similar to the rocks of the batholith.

The contention that there will be absolute enrichment in iron oxides in final residual liquids is not supported by experimental results (Bowen, 1954), although Bowen states that probably in early stages of fractional crystallization the relative concentration in the liquid of FeO with respect to MgO will give a transient absolute enrichment of the liquid in FeO. Should the rocks of the batholith be the product of fractional crystallization (which they probably are not), surface oxygen would probably be needed to supply oxygen on the scale needed to convert ferrous to ferric iron throughout the batholith.

That some surface oxygen played a part in the increase of grain size and in amount of iron oxide for core rocks seems most probable. Structural and petrogenic evolution of rock zones has shown probable failure of the roof rocks in the last stages of intrusion. Faulting combined with incipient thrust movements in wall rocks of the west flank of the batholith might have allowed surface oxygen to enter.

In thin sections, hornblende is partly altered to biotite, and considerable iron oxide has been released which diffused partly into surrounding material. If the biotite of the rocks were derived from the recrystallization of initial hornblende and the released iron oxide were incorporated in the potash feldspars, this would require all conversion of hornblende to biotite before potash feldspar began to crystallize. This is improbable since the radioactive salts used in age determination are concentrated in zircons which are mostly enclosed in biotite.

Probably at least some of the granite of the batholith crystallized with such direct access to the surface that the environment of crystallization had surface aspects. This appears the most probable explanation of the increase in iron oxide of the core rocks. The pressure differentials necessary for the partial escape of volatiles and accelerated rate of cooling experienced by the core rocks would seem to require near-surface conditions.

References Cited

Adams, L. H., 1952, Annual report of the director of the geophysical laboratory, 1951–52: Carneigie Inst. Wash. Year Book 51, p. 35–63.

Barnes, V. E., 1952, Crabapple creek quadrangle, Gillespie and Llano Counties, Texas: Univ. Texas (Bur. Econ. Geology) Geol. quad. maps.

Barnes, V. E., Dawson, R. F., and Parkinson, G. A., 1947, Building stones of central Texas: Univ. Texas Bull. 4246, 198 p.

Barnes, V. E., Romberg, F., Anderson, W. A., 1954, Correlation of gravity and magnetic observations with the geology of Blanco and Gillespie Counties, Texas: Rept. 19th Internat. Geol. Congres, Algiers, Section IX, Contributions de la Géophysique á la Géologie, p. 151–162.

Bowen, N. L., 1928, Evolution of the igneous rocks: Princeton Univ. Press, 334 p.

——, 1947, Magmas: Geol. Soc. America Bull., v. 58, p. 263–280.

——, 1954, Experiment as an aid to the understanding of the natural world: Acad. Nat. Sci. Phila. Proc., v. CVI, p. 1–12.

Compton, R. R., 1955, Trondhjemite batholith near Bidwell Bar., California: Geol. Soc. America Bull., v. 66, p. 9–44.

Emmons, R. C. (editor), 1953, Selected petrogenic relationships of plagioclase: Geol. Soc. America Mem. 52, 142 p.

Fairbairn, H. W., 1949, Structural petrology of deformed rocks: Cambridge, Mass., Addison Wesley Press, Inc., 344 p.

Goldich, S. S., 1941, Evolution of central Texas granites: Jour. Geology, v. 49, p. 697–720.

Hutchinson, R. M., 1952, Statistical study of texture of Enchanted Rock pluton, southwestern Llano County, Texas (Abstract): Geol. Soc. America Bull., v. 63, p. 1266.

——, 1953, Petrology of Enchanted Rock pluton, Llano and Gillespie Counties, Texas (Abstract): Geol. Soc. America Bull., v. 64, 1438.

Hutchinson, R. M., Jaffe, H. W., and Gottfried, David, 1954, Magmatic trends and absolute age determinations of Precambrian intrusives of central Texas (Abstract): Geol. Soc. America Bull., v. 65, p. 1266.

Johannsen, A., 1931, A descriptive petrography of the igneous rocks: Univ. of Chicago Press., v. 1.

Keppel, David, 1940, Concentric patterns in the granites of the Llano-Burnet region, Texas: Geol. Soc. America Bull., v. 51, p. 971–1000.

Larsen, E. S., Jr., Keevil, N. B., and Harrison, H. C., 1952, Method for determining the age of igneous rocks using the accessory minerals: Geol. Soc. America Bull., v. 63, p. 1045–1052.

Niggli, P., 1954, Rocks and mineral deposits: San Francisco, W. H. Freeman and Co.

Paige, S., 1911, Mineral resources of the Llano-Burnet region, Texas, with an account of the pre-Cambrian geology: U. S. Geol. Survey Bull. 450, 103 p.

Paige, S., Spencer, A. C., Kay, F. H., 1909, Geologic map of the Llano-Burnet region, Texas: U.S. Geol. Survey Atlas, Llano-Burnet folio (no. 183).

——, 1912, Llano-Burnet folio: U. S. Geol. Survey Geol. Atlas No. 183.

Sander, B., 1926, Zur. petrographisch-tektonischen analyse III: Jahrbuch d.B. A. 76, p. 323–406.

——, 1930, Gefugekunde der gesteine: Wien, Julius Springer, 352 p.

Stenzel, H. B., 1934–1935, Pre-Cambrian structural conditions in the Llano region, *in* The Geology of Texas, Vol. II, Structural and economic geology: Univ. Texas Bull. 3401, p. 74–79.

——, 1936, Structural study of a phacolith: 16th Internat. Geol. Cong. Rept., Wash., 1933, p. 361–367.

Tuttle, O. F., 1952, Origin of the contrasting mineralogy of extrusive and plutonic salic rocks: Jour. Geology, v. 60, p. 106–124.

Department of Geology, Kansas State College, Manhattan, Kansas.

Manuscript Received by the Secretary of the Society, June 8, 1954.

Project Grant 601–52

Short Notes

BULLETIN OF THE GEOLOGICAL SOCIETY OF AMERICA
VOL. 67, PP. 807-810, 2 PLS. JUNE 1956

UNUSUAL PATTERNED GROUND IN GREENLAND

BY A. L. WASHBURN

Field Observations

At "Thule Take-Off" ("Tuto") about 16 km southeast of Thule, northwest Greenland, small well-developed sorted nets[1] occur on an ice-cored moraine of the Greenland Icecap. Where studied the nets were developed in material 5–7.5 cm thick, resting directly on clear glacier ice (Pl. 1). This material formed the western toe of a shear moraine (Thule Ramp moraine) located along the marginal zone of the Icecap about 1 km east (iceward) of the ice edge at "Lake Tuto".

These sorted nets were on a slope of about 5°, and the irregular meshes were commonly elongate downslope. Diameters of central areas of the meshes ranged from about 15 by 25 cm to 50 by 75 cm. Stone borders were 15–30 cm across. The central areas consisted mainly of sand, granules, and pebbles,[2] and the borders, of pebbles and cobbles. In the centers in general the cobbles were smaller than those in the borders. Tabular stones in the borders tended to be flat lying at the surface and on edge beneath it. In places the borders were one stone thick in that a single cobble extended from the surface to the ice. Sand and granules lay at the base of some borders, and both in central areas and borders the material tended to be finer-grained at the base than at the top.

Where best developed the borders lay in furrowlike depressions in the ice (Pl. 1, fig. 2), regardless of the orientation of the border with respect to slope. These depressions were up to about 1.5 cm deep, and in general the material of the borders was about 1.5 cm thicker than that of the centers. Upon excavation of border areas, muddy water trickled along the depressions but cleared within an hour or so, although a few sand grains continued to roll along the depressions. Large cobbles directly on the ice, or separated from it by a thin layer of sandy material, commonly rested in individual pockets up to 1.5 cm deep that conformed to their shapes. Except for being in clear ice, the furrows beneath the borders were similar to the border gutters observed by various authors (Högbom, 1914, p. 312; Huxley and Odell, 1924, p. 211–212; Elton, 1927, p. 180–181, 186–187).

In a few places the rather even surface of the sorted nets was interrupted by a pronounced knob of ice-cored sandy material, and other similar knobs occurred immediately upslope on gradients as steep as 10°–15° (Pl. 2, fig. 1). Except for their shape, the knobs were like sorted circles in composition of central areas and borders, the stones of the borders being concentrated around the base of a knob. In Figure 1 of Plate 2 the central area was about 3 cm thick over clear glacier ice, and the knob shape reflected the ice core. The knobs were somewhat similar to, but much smaller than, certain forms of ablation moraine described by Ward (1952, p. 13–22) as strikingly like patterned ground. Marked cases of differential thawing occurred in the same general area as the knobs in places where distribution of material over the ice was very spotty and gave rise to dirt cones (*cf.* Swithinbank, 1950) surrounded by stones at their bases (Pl. 2, fig. 2).

[1] A sorted net is patterned ground whose mesh is intermediate between that of a circle and a polygon and has a sorted appearance due to a border of stones surrounding finer material (Washburn, 1956).

[2] Grain-size analysis of a typical central area showed the following percentages by weight: >4 mm, 17.5%; 4–2 mm, 8.3%; 2–1/16 mm, 67.2%; 1/16–1/256 mm, 6.1%; <1/256 mm, 0.8%. Analysis made by R. W. Dixon.

Interpretation

It seems certain that the furrowlike depressions beneath the stones of the sorted nets owe their origin in considerable part to differential thawing and that the sandy covering material of the near-by ice-cored knobs protected the ice beneath from melting. The trickling of water beneath the stone borders of the nets and the observed movement of sand grains indicate eluviation of fines from the morainal material. These points suggest that these sorted nets may owe their origin to differential thawing and eluviation.

According to this idea, an accumulation of fines is a better insulator than a stone if other conditions including thickness and color are equal. The better insulating quality of the fines is attributable to their lower diffusivity, as expressed by the following equation (*cf.* Terzaghi, 1952, p. 7–12):

$$a = \frac{k_h}{c_h \times w_t}$$

where a denotes heat diffusivity, k_h thermal conductivity, c_h heat capacity, and w_t unit weight (solid and water combined). The following diffusivities are taken from Terzaghi (1952, p. 11):

Quartzite	45	$\times 10^{-3}$ cm^2 sec^{-1}
Granite	15	$\times 10^{-3}$ cm^2 sec^{-1}
Ice	11.2	$\times 10^{-3}$ cm^2 sec^{-1}
Dense saturated sand	8±	$\times 10^{-3}$ cm^2 sec^{-1}
Soft saturated clay	4±	$\times 10^{-3}$ cm^2 sec^{-1}
Dry soil	2.5±	$\times 10^{-3}$ cm^2 sec^{-1}
Water	1.9±	$\times 10^{-3}$ cm^2 sec^{-1}

The superior insulating qualities of fine, as compared with coarse material in patterned ground was discussed by Schenk (1955, p. 51–52) and, on a glacier, by Sharp (1949, p. 298–299). Sharp (1942, p. 288–290) also analyzed some of the complex variations and even reversals that may occur in insulation with changes in moisture in patterned ground.

Differences in diffusivity in a mixture of fines and stones at the surface of the ground cause thawing next to stones sooner than at comparable levels in the finer material, and the stones come to lie in thaw depressions. (*Cf.* Meinardus, 1912, p. 21–22; Huxley and Odell, 1924, p. 220; Schmid, 1955, p. 16, 87, 90.) As thawing progresses downward and laterally from the stones, the thaw depressions become interconnected and act as meltwater channels around irregular islands of frozen material.

With continued thawing and adequate drainage, fines are gradually eluviated and leave stony channels. The possible importance of eluviation in the origin of sorted patterns has been suggested from various points of view (De Geer, 1904, p. 465; Huxley and Odell, 1924, p. 220–223; Ahlmann, 1930). The irregular islands of dominantly finer material between the stony channels thaw most rapidly at corners where there is maximum surface exposure, and in equal periods of time more material is released from a frozen condition at corners than between them. Thus, the islands become rounded by differential eluviation of fines from the corners.

If the surfaces of the islands lie appreciably above the adjacent coarser material by virtue of the insulating effect of the dominantly finer material as illustrated by the knobs and dirt cones, stones and other particles on the surfaces will creep and slide radially toward the margins of the islands, with the stones accumulating there and the fines washing away. Continued decrease in thickness of finer material and increase in marginal accumulation of coarser might reverse the insulating effect and lead to the border areas rising slightly above the centers.

On gentle slopes differential thawing and eluviation gradually form sorted nets with almost equidimensional meshes. On steeper slopes, corners of islands become eroded, and

PLATE 1.—SORTED NETS ON GLACIER ICE

FIGURE 1.—Sorted net on glacier ice, western toe of Thule Ramp moraine at "Thule Take-Off", Thule, Greenland. Ruler is 15 cm (6 inches) long. "X" marks identical stone in Figures 1 and 2.

FIGURE 2.—Excavation across sorted net on glacier ice. "X" marks identical stone in Figures 1 and 2. View looking up about 5-degree slope. Ice axe (80 cm long) rests on ice with head next to downslope-oriented furrow in the ice. Material above ice is 5–7.5 cm thick.

FIGURE 1

FIGURE 2

SORTED NETS ON GLACIER ICE

FIGURE 1

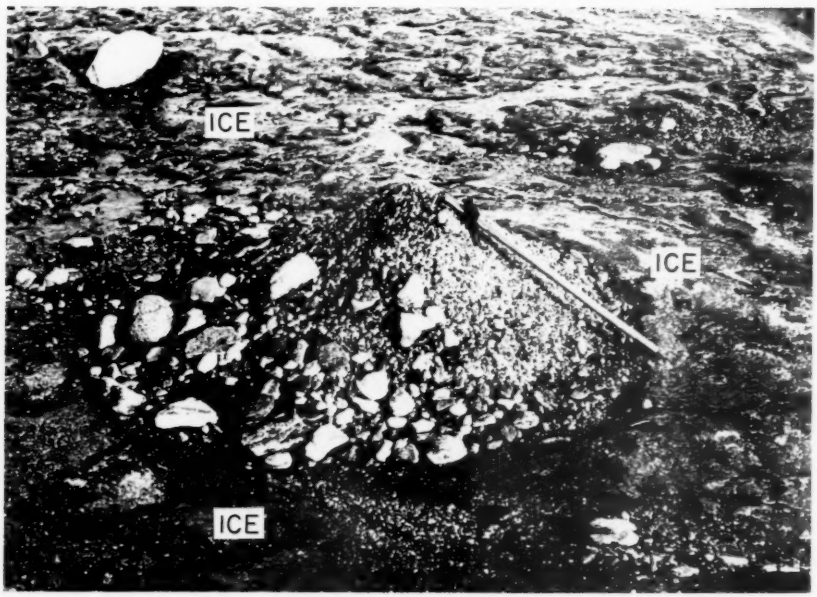

FIGURE 2

KNOB AND DIRT CONE ON GLACIER ICE

stones accumulate at the borders in a similar manner, but because the gradient exerts a stronger control on eluviation the islands of dominantly finer material develop a marked downslope orientation. Freeze-thaw cycles cause differential thawing and eluviation to rework the same area repeatedly and strengthen the patterns.

Upfreezing of stones to the surfaces of the islands and gravity movements of stones to the borders might produce a high degree of sorting between central areas and borders. Recent experiments by A. E. Corte and A. Higashi (Personal communication), at the U. S. Army Corps of Engineers, Snow, Ice and Permafrost Research Establishment, show that repeated freezing and thawing can move ceramic spheres upward through sand having excess water. Local differential heaving (Taber, 1943, p. 1458–1459) of moisture-retaining fine material would increase relief of the vegetation-free central areas during freezing and thereby promote gravity movements during thawing.

The hypothesis of differential thawing and eluviation, combined with upfreezing of stones and local differential heaving, as an explanation of the Thule-Ramp-moraine sorted patterns is speculative, but other combination hypotheses of patterned-ground origin (Washburn, In press) seem even less applicable. Qualitatively, the key processes might operate in any ground having a high ice content subject to annual thawing;[3] however, this does not imply that this grouping of processes explains sorted patterns in general.

Objections

Objections to the hypothesis as applied to the Thule-Ramp-moraine sorted nets include: (1) Channel-like depressions beneath borders may be a strictly secondary effect without significant influence on pattern evolution (Högbom, 1914, p. 312–313; Sharp, 1942, p. 290). (2) The development of a netlike drainage system is inconsistent with running water, which would eventually develop some routes at the expense of others and wipe out the net pattern (Högbom, 1914, p. 313). However, drainage might be too weak to accomplish much integration. (3) Border drainage is too weak to cause significant eluviation (Beskow, 1930). Some eluviation, however, was noted in the Thule-Ramp-moraine sorted patterns, and rapid border drainage elsewhere has been reported (Sapper, 1912, p. 267–268).

Objections to the hypothesis as applied more generally to sorted patterns in ground having a high ice content include the following: (1) Thawing sometimes extends to greater depth below central areas than below stony borders. This relationship was observed in sorted stripes by Sharp (1942, p. 280–281), and in sorted polygons near Thule late in the thaw season by J. Arthur and R. H. Espach Jr. (Personal communication) of the U. S. Army Corps of Engineers, Snow, Ice and Permafrost Research Establishment. Conceivably, the relationship could reflect reduced drainage along borders and accompanying increase in total volume of insulating air spaces between stones. (*Cf.* Sharp, 1942, p. 288–290.) (2) Although reasonable, it is not demonstrated that upfreezing of stones and radial gravity movements can explain absence of stones such as that occurring in the central areas of some sorted patterns. (3) The hypothesis does not apply to highly regular polygonal patterns.

Quantitative data are essential before these objections can be properly evaluated.

Conclusions

Differential thawing and eluviation are operative in the Thule-Ramp-moraine sorted nets, and perhaps these processes, combined with upfreezing of stones and local differential

[3] The report of Huxley and Odell (1924, p. 209) that sorted polygons occur ". . . apparently rarely (at least when well developed) on perfectly level ground" may be significant in this connection. However, the statistical validity of the reported distribution requires confirmation.

PLATE 2.—KNOBS AND DIRT CONES ON GLACIER ICE

FIGURE 1.—Knob on glacier ice, western toe of Thule Ramp moraine at "Thule Take-Off", Thule, Greenland. Ruler is 15 cm (6 inches) long. Material beneath ruler is about 3 cm thick over clear glacier ice.

FIGURE 2.—Dirt cone below Thule Ramp moraine at "Thule Take-Off", Thule, Greenland. Ice axe is 80 cm long. Note distribution of stones around base of cone.

heaving originated the nets. Wider application of this explanation to other sorted patterns is not excluded but is even more speculative. The occurrence of sorted nets in material only 5 cm thick overlying clear glacier ice, posing the unusual limiting conditions it does, warrants further and more detailed study in view of the information it may provide on processes of patterned-ground origin.

Acknowledgment

The writer is grateful to the U. S. Army Corps of Engineers for permission to cite these observations, which he made in 1954 while on a project for the Office of Chief of Engineers.

References Cited

Ahlmann, Hans W:son, 1930 [Discussion] Geol. Fören. Stockholm, Förh., band 52, p. 768.

Beskow, Gunnar, 1930 [Discussion] Geol. Fören. Stockholm, Förh., band 52, p. 770.

De Geer, [G.], 1904 [Discussion] Geol. Fören. Stockholm, Förh., band 26, p. 465–466.

Elton, C. E., 1927, The nature and origin of soil-polygons in Spitsbergen: Geol. Soc. London Quart. Jour., v. 83, p. 163–194.

Högbom, Bertil, 1914, Über die geologische Bedeutung des Frostes: Upsala Univ., Geol. Inst. Bull., v. 12 (1913–1914), p. 257–389.

Huxley, J. S., and Odell, N. E., 1924, Notes on surface markings in Spitsbergen: Geog. Jour., v. 63, p. 207–229.

Meinardus, Wilh., 1912, Über einige charakteristische Bodenformen auf Spitzbergen: Naturh. Ver. Preuss. Rheinlande u. Westfalens, Medizinisch-naturwiss. Gesell. Münster Sitzungsber., Sitzung 26, p. 1–42.

Sapper, K., 1912, Über Fliesserde und Strukturboden auf Spitzbergen: Gesell. Erdkunde Berlin Zeitschr., 1912, p. 259–270.

Schenk, Erwin, 1955, Die Mechanik der periglazialen Strukturböden: Hessischen Landesamtes für Bodenforschung Abh., Heft 13, 92 p.

Schmid, Josef, 1955, Der Bodenfrost als morphologischer Faktor: Heidelberg, Dr. Alfred Hüthig Verlag, 144 p.

Sharp, R. P., 1942, Soil structures in the St. Elias Range, Yukon Territory: Jour. Geomorphology, v. 5, p. 274–301.

—— 1949, Studies of superglacial debris on valley glaciers: Am. Jour. Sci., v. 247, p. 289–315.

Swithinbank, Charles, 1950, The origin of dirt cones on ice: Jour. Glaciology, v. 1 (1947–1951), no. 8, p. 461–465.

Taber, Stephen, 1943, Perennially frozen ground in Alaska: its origin and history: Geol. Soc. America Bull., v. 54, p. 1433–1548.

Terzaghi, Karl, 1952, Permafrost: Boston Soc. Civil Eng. Jour., v. 39, Jan. 1952, p. 1–50.

Ward, W. H., 1952, The physics of deglaciation in central Baffin Island [The glaciological studies of the Baffin Island Expedition, 1950, Part II]: Jour. Glaciology, v. 2, no. 11, p. 9–22.

Washburn, A. L., In press, Classification of patterned ground and review of suggested origins: Geol. Soc. America Bull.

Dept. of Geology, Dartmouth College, Hanover, N. H.

Manuscript Received by the Secretary of the Society, February 2, 1956

COMPOSITION OF WESTERLY GRANITE G-1 AND CENTERVILLE DIABASE W-1

By Samuel S. Goldich and Eileen H. Oslund

Introduction

Since the publication of U. S. Geological Survey Bulletin 980, *A cooperative investigation of precision and accuracy in chemical, spectrochemical and modal analysis of silicate rocks* (Fairbairn *et al.*, 1951), a number of papers have appeared discussing one or more aspects of the problems of accuracy of silicate analyses (Fairbairn and Schairer, 1952; Schlecht, 1951; 1953; Fairbairn, 1953). The samples of granite (G-1) from Westerly, Rhode Island, and of diabase (W-1) from Centerville, Virginia, are exceedingly useful to the analyst who is interested in comparing his methods and skill with the results of many other laboratories. These samples also are valuable to the spectroscopist (Ahrens, 1955).

In January 1955 the writers made routine analyses of G-1 and W-1 (Table 1, Nos. 1, 2). The results of replicate determinations for some constituents are given in Table 2. These values have been used to arrive at the averages in Table 1.

Methods

Fairbairn's (1953) statistical approach to the so-called "silica-alumina discrepancy" led him to make arbitrary corrections to the values of SiO_2 and Al_2O_3; 0.5 per cent is added to SiO_2 for G-1, and 0.35 per cent to W-1. These amounts are subtracted from the respective average values for Al_2O_3 (Table 4). We have attempted to recover the silica entrapped with the alumina and iron by evaporating the solution of the pyrosulfate fusion to fumes of sulfuric acid. The additional silica recovered in this way was 0.15 per cent for G-1 and 0.29 per cent for W-1 following two evaporations and filtrations (EHO). With three evaporations and filtrations the silica recovered from the ammonia group was 0.06 per cent for G-1 and 0.11 per cent for W-1 (SSG). Our experience is that following two evaporations with an intervening filtration rarely will more than 0.15 per cent of silica be recovered from the ammonia precipitate of a rock containing more than 70 per cent of SiO_2, if double precipitations of the ammonia group are made. Likewise, 0.30 per cent of SiO_2 is about the most ever recovered from the ammonia group of a rock containing 45–55 per cent of SiO_2. Larger amounts of silica are not retained but pass through the ammonium hydroxide precipitations. This silica may contaminate the lime or magnesia, but, if double precipitations are made of the alkaline earths, the silica more than likely will pass completely through the analysis and be lost. The summation then will be low, unless there are positive compensating errors.

Although the "silica-alumina discrepancy" may be due in part to the silica not recovered from the ammonia-group precipitate, other sources of error not readily apparent must be considered. Failure to wash out alkali salts from the bulky silica precipitate or an incomplete decomposition of the sample in the sodium carbonate fusion may lead to serious negative errors in silica and positive errors in alumina. Because these errors tend to compensate each other, they commonly are unsuspected and overlooked. These problems and others relating to the determination of silica have been discussed by Hillebrand (1902; Hillebrand *et al.*, 1953, p. 681–683).

In the determinations of the alkalies, the samples were decomposed by the J. Lawrence Smith method, and generally the chloroplatinate technique was used to separate potassium and sodium. Rubidium accompanies potassium and was determined by flame spectrophotometry after reduction of the potassium and rubidium chloroplatinates and conversion to sulfates. In the determination by Goldich and Horstman (Table 2) chloroplatinic acid was not used, and the alkalies, after extraction as chlorides by the J. Lawrence Smith method, were converted to sulfates and flamed directly. R. A. Burwash made four determinations of alkalies for G-1, and his average values are

included in Table 2. His chloroplatinate separations were reduced, converted to sulfates, and tested for completeness of separation by E. L. total iron on G-1 by the same method and also colorimetrically with *o*-phenanthroline (Table 2).

TABLE 1.—CHEMICAL ANALYSES OF G-1 AND W-1

1. Eileen H. Oslund; 2. S. S. Goldich; average (Table 2)

	Granite G-1			Diabase W-1		
	1	2	Av.	1	2	Av.
SiO_2	72.50	72.45	72.48 (4)	52.59	52.51	52.55 (2)
Al_2O_3	14.22	14.18	14.20 (2)	14.99	14.97	14.98 (2)
Fe_2O_3	.83	.75	.78 (5)	1.44	1.41	1.41 (5)
FeO	.95	.98	.97 (5)	8.69	8.70	8.71 (5)
MnO	.02	.02	.025 (3)	.16	.16	.161 (3)
MgO	.38	.35	.37 (2)	6.58	6.59	6.59 (2)
SrO	.02	.02	.02 (2)	n.d.	.01	.01 (1)
CaO	1.34	1.36	1.35 (2)	10.97	10.98	10.98 (2)
BaO	.10	.10	.10 (2)	n.d.	n.d.	
Rb_2O	.02	.02	.022	.00	.00	.00
K_2O	5.49	5.54	5.52 (5)	.61	63	.62 (2)
Na_2O	3.35	3.28	3.29 (5)	2.15	2.12	2.14 (2)
H_2O^+	.24	.26	.25 (2)	.43	.46	.45 (2)
H_2O^-	.04	.03	.04 (2)	.16	.13	.14 (2)
CO_2	.08	.08	.08 (3)	.07	.06	.07 (3)
TiO_2	.26	.26	.26 (2)	1.07	1.10	1.08 (2)
P_2O_5	.08	.09	.08 (4)	.14	.13	.12 (4)
F	.07	n.d.	.07 (3)	.02	n.d.	.02 (2)
S	n.d.	.01	.01 (1)	n.d.	.02	.02 (1)
	99.99	99.78	99.92	100.07	99.98	100.05
Less O ≡ F and S.....	.03		.03	.01	.01	.02
	99.96		99.89	100.06	99.97	100.03
Total Fe as Fe_2O_3.....	1.89	1.85	1.86	11.10	11.08	11.09
R_2O_3.....	16.45	16.38	16.40	27.30	27.28	27.27
$R_2O_3 + SiO_2$.....	88.95	88.83	88.88	78.89	79.79	79.82

Horstman using the flame spectrophotometer. A similar procedure was used by Oslund and Baadsgaard, except that double fusions and extractions were made.

Greenewalt, Herzog, and Pinson (1955, p. 45) found 0.62 per cent of K_2O in W-1, using the mass spectrometer and an isotopic dilution method. This value falls between our determinations of 0.61 per cent K_2O (EHO) and 0.63 per cent (SSG).

Ferrous iron was determined with potassium permanganate, and total iron, potentiometrically, with potassium dichromate and stannous chloride. R. B. Ellestad determined

Total water was determined with PbO as a flux using a modification of the Penfield tube method to take into account the CO_2 present in both G-1 and W-1. Geologists should realize that H_2O+ and H_2O- are a convention. H_2O- is commonly considered the moisture in the sample that can be driven off by heating for an hour or two in an oven at a temperature near 110° C. Finely ground silicates may adsorb water which is held very tightly and may not be driven off by heating at 110° C.

Phosphorus was weighed as ammonium phosphomolybdate (EHO, SSG, DT, Table 2).

H. Baadsgaard determined P_2O_5 by the molybdovanadophosphoric acid method (Baadsgaard and Sandell, 1954). The results for P_2O_5 are

A single determination of Co by R. A. Burwash gave 30 ppm for W-1. This is less than the recommended value of 36 ppm (Ahrens, 1955)

TABLE 2.—REPLICATE DETERMINATIONS OF CONSTITUENTS OF G-1 AND W-1

	Granite G-1	Diabase W-1		Granite G-1	Diabase W-1
SiO_2	72.50 (EHO) 72.45 (SSG) 72.51 (EHO) 72.46 (EHO) 72.48 Av.		Na_2O	3.35 (EHO) 3.28 (SSG) 3.25 (SSG & ELH) 3.27 (RAB-4) 3.32 (EHO & HB) 3.29 Av.	
Total Fe as Fe_2O_3	1.89 (EHO) 1.85 (SSG) 1.84 (SSG) 1.85 (SSG) 1.86 (SSG) 1.85 (RBE) 1.85 (RBE) 1.86 Av.	11.10 (EHO) 11.08 (SSG) 11.07 (SSG) 11.09 (SSG) 11.10 (SSG) 11.09 Av.	K_2O	5.49 (EHO) 5.54 (SSG) 5.52 (SSG & ELH) 5.54 (RAB-4) 5.52 (EHO & HB) 5.52 Av.	
FeO	0.95 (EHO) .98 (SSG) .98 (SSG) .98 (EHO) .97 (COI) .97 Av.	8.69 (EHO) 8.70 (SSG) 8.72 (SSG) 8.75 (SSG) 8.70 (COI) 8.71 Av.	CO_2	0.08 (EHO) .08 (SSG) .09 (DT) .08 Av.	0.07 (EHO) .06 (SSG) .07 (DT) .07 Av.
Fe_2O_3	0.78 Av.	1.41 Av.	F	0.067 (EHO) .07 (EHO) .068 (EHO) .07 Av.	0.02 (EHO) .02 (EHO) .02 Av.
MnO	0.024 (EHO) .025 (SSG) .026 (DT) .025 Av.	0.156 (EHO) .163 (SSG) .164 (DT) .161 Av.	P_2O_5	0.08 (EHO) .09 (SSG) .07 (DT) .08 (HB) .08 Av.	0.14 (EHO) .13 (SSG) .11 (DT) .11 (HB) .12 Av.

not in good agreement, and further work is indicated.

Minor Constituents

Ahrens (1955) has summarized much of the available data for the minor constituents of G-1 and W-1. A few determinations have been made in the Rock Analysis Laboratory. Ahrens' recommended value of 22 ppm of Li for G-1 agrees closely with 22.5 ppm found by Ellestad and Horstman (1955); however, his figure of 9 ppm for W-1 is much less than the 14 ppm of Li reported by Ellestad and Horstman.

and considerably less than the average of 49 ppm for six determinations by neutron activation reported by Smales (1955). Two determinations of Ni by Burwash gave 72 and 74 ppm of Ni for W-1. Six determinations reported by Smales (1955) range from 63 to 78 ppm of Ni and average 73 ppm. The 90 ppm of Ni recommended for W-1 by Ahrens (1955) appears to be too high.

Although a high precision in the determination of Rb with the optical spectrograph is obviously possible (Ahrens, 1955), results obtained in the Rock Analysis Laboratory by flame photometry are much lower than those

TABLE 3.—COMPARISON OF AVERAGES FOR 12 MAJOR CONSTITUENTS RECALCULATED TO 100 PER CENT

	Granite G-1			Diabase W-1		
	1	2	3	1	2	3
SiO_2	72.22	72.64	72.79	52.25	52.66	52.66
Al_2O_3	14.44	14.13	14.26	15.23	14.87	15.01
Fe_2O_3	.94	.86	.78	1.85	1.41	1.41
FeO	1.00	1.06	.97	8.51	8.91	8.73
MnO	.03	.03	.03	.19	.17	.16
MgO	.39	.44	.37	6.52	6.51	6.60
CaO	1.42	1.34	1.36	10.95	10.95	11.00
K_2O	5.51	5.43	5.54	.71	.68	.62
Na_2O	3.26	3.43	3.30	2.05	2.20	2.14
H_2O^+	.37	.31	.25	.62	.45	.45
TiO_2	.26	.25	.26	1.09	1.03	1.08
P_2O_5	.10	.10	.08	.13	.15	.12
	99.94	100.02	99.99	100.10	99.99	99.98
Total Fe as Fe_2O_3*	2.05	2.04	1.86	11.31	11.31	11.11
R_2O_3†	16.85	16.52	16.46	27.76	27.36	27.32
$R_2O_3 + SiO_2$	89.07	89.16	89.25	80.01	80.02	79.98

*$\Sigma\ Fe_2O_3 + 1.1114 \times FeO$.

†$\Sigma\ Fe_2O_3 + (1.1114 \times FeO) + TiO_2 + P_2O_5 + Al_2O_3$.

1. Average for 24 laboratories. (Fairbairn *et al.*, 1951, Table 14, p. 37.)

2. U. S. Geological Survey; average for 7 analysts for G-1, 6 analysts for W-1 (Fairbairn *et al.*, 1951, Table 17, p. 38).

3. Rock Analysis Laboratory.

TABLE 4.—COMPARISON OF AVERAGE COMPOSITIONS FOR G-1 AND W-1

	Granite G-1		Diabase W-1	
	1	2	1	2
SiO_2	72.36 → 72.86*	72.48	52.34 → 52.69*	52.55
Al_2O_3	14.44 → 13.94†	14.20	15.07 → 14.72†	14.98
Fe_2O_3	.93	.78	1.50	1.41
FeO	.99	.97	8.71	8.71
MnO	.027	.025	.165	.16
MgO	.39	.37	6.63	6.59
CaO	1.41	1.35	10.96	10.98
K_2O	5.42	5.52	.63	.62
Na_2O	3.25	3.29	2.00	2.14
H_2O	.365	.25	.56	.45
TiO_2	.25	.26	1.10	1.08
P_2O_5	.09	.08	.126	.12
	99.92	99.57	99.79	99.79
Fe as Fe_2O_3	2.03	1.86	11.18	11.09
R_2O_3	16.81 → 16.31	16.40	27.48 → 27.13	27.27
$R_2O_3 + SiO_2$	89.17	88.88	79.82	79.82

1. "Revised statistical data" (Fairbairn, 1953, Table 1, p. 146)

2. Averages, Rock Analysis Laboratory from Table 1

* Fairbairn's preferred estimate 0.5% higher for G-1; 0.35% higher for W-1

† Fairbairn's preferred estimate 0.5% lower for G-1; 0.35% lower for W-1

recommended by Ahrens. The average of a number of determinations by E. L. Horstman is 205 ppm of Rb for G-1 and 22 ppm for W-1. Two determinations by H. Baadsgaard gave 210 and 213 ppm of Rb for G-1. Ahrens (1955) recommends 570 and 64 ppm of Rb for G-1 and W-1. Herzog and Pinson (1955) report 218 and 215 ppm of Rb for G-1 and 27.9 and 29.1 ppm for W-1 by a stable isotope dilution technique. Results reported by Smales (1955) by neutron activation are 221, 254, and 243 ppm of Rb for G-1 and 27, 29, and 26 ppm for W-1.

Acknowledgments

This investigation was made possible by a grant from The Geological Society of America to the Rock Analysis Laboratory staff in support of research in methods of silicate analysis. We are indebted to R. B. Ellestad and E. B. Sandell for reading the manuscript and discussing various problems with us. We are pleased to acknowledge the assistance of past and present coworkers in the Rock Analysis Laboratory who contributed many of the determinations listed in the tables where they are identified by initials as follow: (HB) Halfdan Baadsgaard, (RAB) Ronald A. Burwash, (RBE) R. B. Ellestad, (COI) C. Oliver Ingamells, (ELH) Elwood Horstman, and (DT) Doris Thaemlitz.

References Cited

Ahrens, L. H., 1955, Quantitative spectrochemical analysis of silicates: London, Pergamon Press, p. 122

Baadsgaard, H., and Sandell, E. B., 1954, Photometric determination of phosphorus in silicate rocks: Anal. Chim. Acta, v. 11, p. 183

Ellestad, R. B., and Horstman, E. L., 1955, Flame photometric determination of lithium in silicate rocks: Anal. Chemistry, v. 27, p. 1229

Fairbairn, H. W., 1953, Precision and accuracy of chemical analysis of silicate rocks: Geochim. et Cosmochim. Acta, v. 4, p. 143

Fairbairn, H. W., and Schairer, J. F., 1952, A test of the accuracy of chemical analysis of silicate rocks: Am. Mineralogist, v. 37, p. 744

Fairbairn, H. W., Schlecht, W. G., Stevens, R. E., Dennen, W. H., Ahrens, L. H., and Chayes, F., 1951, A cooperative investigation of precision and accuracy in chemical, spectrochemical and modal analysis of silicate rocks: U. S. Geol. Survey Bull. 980, p. 71

Greenewalt, D., Herzog, L. F., and Pinson, W. H., Jr., 1955, Isotopic dilution analyses for potassium in W-1, and the Homestead and Forest City meteorites: Annual Progress Report 1954–5, Nuclear Geophysics Section, Dept. Geology and Geophysics, Mass. Inst. Technology, Cambridge, Mass., NYO 3935-II, p. 45

Herzog, L. F., and Pinson, W. H., Jr., 1955, The Sr and Rb contents of the granite G-1 and the diabase W-1: Geochim. et Cosmochim. Acta, v. 8, p. 296

Hillebrand, W. F., 1902, Common errors in the determination of silica: Am. Chem. Soc. Jour., v. 24, p. 362

Hillebrand, W. F., Lundell, G. E. F., Bright, H. A., and Hoffman, J. I., 1953, Applied inorganic analysis: New York, John Wiley and Sons, Inc.

Schlecht, W. G., 1951, Cooperative investigation of precision and accuracy: Anal. Chemistry, v. 23, p. 1568

—— 1953, The probable error of a chemical analysis: U. S. Geol. Survey Bull. 992, p. 57

Smales, A. A., 1955, Some trace-element determinations in G1 and W1 by neutron activation: Geochim. et Cosmochim. Acta, v. 8, p. 300

Rock Analysis Laboratory, Department of Geology and Mineralogy, University of Minnesota, Minneapolis, Minn.

Project Grant 397-41-S53

Manuscript Received by the Secretary of the Society, February 29, 1956

INDEX TO VOLUME 67 (JANUARY–JUNE)*

Age determination, Uranium-lead method of. By W. R. Eckelmann and J. L. Kulp 35
Albemarle, Geology of Galápagos. By A. F. Banfield *et al.* ... 215
Aleutian Ridge, Interpretation of configuration of. By Olcott Gates and William Gibson 127
American Falls, Idaho, Stratigraphic sequence in Eagle Rock volcanic area near. By H. T. Stearns and Andrei Isotoff 19
Analyses
  Chemical
    Rocks of Isabela Island, Archipielago de Colón (Galápagos). By A. F. Banfield *et al.* 215
    Rocks of the Sittampundi complex, Salem district, India. By A. P. Subramaniam 317
  Modal
    Gneisses, Franklin, New Jersey. By J. M. Hague *et al.* 435
  Statistical
    Chuska sandstone, Arizona-New Mexico. By H. E. Wright, Jr. 413
    Drainage systems in badlands at Perth Amboy, New Jersey. By S. A. Schumm 597
    Quantitative slope analysis. By A. N. Strahler .. 571
    Radioactivity of Pennsylvanian black fissile shale in Illinois. By W. C. Krumbein and H. A. Slack 739
Anorthosites, Sittampundi complex, India. By A. P. Subramaniam 317
Appalachian Valley, Middle Ordovician coarse conglomerates. By J. M. Kellberg and L. F. Grant 697
Archipielago de Colón (Galápagos), Geology of Isabela Island. By A. F. Banfield *et al.* 215
Areal geology
  Geology of the Blue Ridge near Harpers Ferry, West Virginia. By R. P. Nickelsen 239
Arizona, Origin of the Chuska sandstone. By H. E. Wright, Jr. 413
Arizona, Paleomagnetic survey in. By S. K. Runcorn 301
Atlantic Coastal Plain, Geophysical investigations in emerged and submerged. Part X. By C. R. Bentley and J. L. Worzel 1
Atlantic Ocean basin, west of Bermuda, Seismic refraction measurement in. By Samuel Katz and Maurice Ewing 475
†Ault, W. U. (With J. L. Kulp *et al.*): Lead and sulfur isotopic abundances in Mississippi Valley galenas 123
Austinville, Virginia, Three-dimensional applied potential studies. By H. V. McMurry and A. D. Hoagland 683

Badlands, Perth Amboy, New Jersey, Evolution of drainage systems and slopes. By S. A. Schumm 597
Baffin Island, Geomorphology and glacial history. By J. H. Mercer 553
Banfield, A. F., Behre, C. H., Jr., and St. Clair, David: Geology of Isabela (Albemarle) Island, Archipielago de Colón (Galápagos) 215
†Bate, G. L. (With J. L. Kulp *et al.*): Lead and sulfur isotopic abundances in Mississippi Valley galenas 123
Batholith (Enchanted Rock, Llano and Gillespie counties, Texas), Structure and petrology of. By R. M. Hutchinson 763
Baum, J. L. (With J. M. Hague *et al.*): Geology and structure of the Franklin-Sterling Area, New Jersey 435
Behre, C. H., Jr. (With A. F. Banfield and David St. Clair): Geology of Isabela (Albemarle) Island, Archipielago de Colón (Galápagos) 215
Bentley, C. R., and Worzel, J. L.: Geophysical investigations in the emerged and submerged Atlantic Coastal Plain. Part X: Continental Slope and Continental Rise south of the Grand Banks 1
Bermuda, Seismic refraction measurements west of. By Samuel Katz and Maurice Ewing 475
Bihar, India, Porphyritic granite and associated metamorphic rocks of East Manbhum. By S. Sen 647
Blue Ridge near Harpers Ferry, West Virginia, Geology of. By R. P. Nickelsen 239
†Bokman, John: Terminology for stratification in sedimentary rocks 125
Boulder County, Colorado, Petrology and weathering of the Iron Dike. By E. E. Wahlstrom 147
†Bradley, W. C.: Carbon-14 date for a marine terrace at Santa Cruz, California 675
British Columbia, Limnology and sedimentation, Lake Garibaldi. By W. H. Mathews 537

†Cambro-Ordovician age of the "Inwood" limestone and "Manhattan" schist near Peekskill, New York. By Sidney Paige 391
Canis condoni n. sp. By J. A. Shotwell 717
†Carbon-14 date for a marine terrace at Santa Cruz, California. By W. C. Bradley 675
Chemical analyses
  Rocks of Isabela Island, Archipielago de Colón (Galápagos). By A. F. Banfield *et al.* 215
Chronology of the Lake Michigan basin correlated with pollen studies, Late Wisconsin. By J. H. Zumberge and J. E. Potzger 271
Citellus (*Citellus*) *mckayensis* n. sp. By J. A. Shotwell 717
Citellus (*Otospermophilus*) *wilsoni* n.sp. by J. A. Shotwell .. 717
Coarse conglomerates of the Middle Ordovician in the southern Appalachian Valley. By L. F. Grant and J. M. Kellberg 697
Colorado, Petrology and weathering of the Iron Dike, Boulder and Larimer counties. By E. E. Wahlstrom .. 147
Colorado, Post-Laramie stratigraphic correlations in Denver Basin. By S. O. Reichert 107
†Composition of Westerly granite G-1 and Centerville diabase W-1. By S. S. Goldich and E. H. Oslund 811
Continental Rise, Geophysical investigations in. By C. R. Bentley and J. L. Worzel 1
Continental Slope, Geophysical investigations in. By C. R. Bentley and J. L. Worzel 1
Croixan stratigraphy, Mississippi Valley, Upper. By C. A. Nelson 165
Cross-bedding, Chuska sandstone, Arizona-New Mexico. By H. E. Wright, Jr. 413

Dating by uranium-lead method. By W. R. Eckelmann and J. L. Kulp 135
Denver Basin, Colorado, Post-Laramie stratigraphic correlations in. By S. O. Reichert 107
Deuteric alteration
  Iron Dike, Boulder and Larimer counties, Colorado. By E. E. Wahlstrom 147
Direct radiometric measurement by gamma-ray scintillation spectrometer, Part I: Uranium and thorium series in equilibrium. By P. M. Hurley .. 395

* Full titles of papers are in boldface type
† Indicates Short Note

Direct radiometric measurement by gamma-ray scintillation spectrometer, Part II: Uranium, thorium and potassium in common rocks. By P. M. Hurley 405
Drainage systems in badlands at Perth Amboy, New Jersey, Evolution of. By S. A. Schumm 597
†Drakensberg scarp of South Africa: a clarification. By L. C. King 121

Eagle Rock volcanic area, Idaho, Stratigraphic sequence in. By H. T. Stearns and Andrei Isotoff 19
ECKELMANN, W. R., and KULP, J. L.: Uranium-lead method of age determination. Part I: Lake Athabasca problem 35
Economic geology
Three-dimensional applied potential studies at Austinville, Virginia. By H. V. McMurry and A. D. Hoagland 683
Enchanted Rock batholith, Texas, Structure and petrology of. By R. M. Hutchinson 763
Eolian sediment
Origin of the Chuska sandstone, Arizona-New Mexico. By H. E. Wright, Jr. 413
Erosion
Evolution of drainage systems and slopes in badlands at Perth Amboy, New Jersey. By S. A. Schumm. 597
Evolution of drainage systems and slopes in badlands at Perth Amboy, New Jersey. By S. A. Schumm 597
EWING, MAURICE (With SAMUEL KATZ): Seismic refraction measurements in the Atlantic Ocean. Part VII: Atlantic Ocean basin west of Bermuda 475
EWING, MAURICE (With G. L. SHURBET): Gravity reconnaissance survey of Puerto Rico 511

Faulting, Aleutian Ridge. By Olcott Gates and William Gibson 127
†FEELY, H. W. (With J. L. KULP *et al.*): Lead and sulfur isotopic abundances in Mississippi Valley galenas 123
Felis longignathus n. sp. By J. A. Shotwell 717
Formation C (new name) (Pliocene?), Idaho, By H. T. Stearns and Andrei Istotoff 19
Formation E (new name) (Pliocene?), Idaho. By H. T. Stearns and Andrei Isotoff 19
Franklin-Sterling area, New Jersey, Geology and structure of. By J. M. Hague *et al.* 435

Galápagos, Geology of Isabela Island. By A. F. Banfield *et al.* 215
Garibaldi Lake, British Columbia, Limnology and sedimentation in. By W. H. Mathews 537
GATES, OLCOTT, and GIBSON, WILLIAM: Interpretation of the configuration of the Aleutian Ridge 127
Geochemistry
Uranium-lead method of age determination. By W. R. Eckelmann and J. L. Kulp 35
Geology and structure of the Franklin-Sterling area, New Jersey. By J. M. Hague, J. L. Baum, L. A. Hermann, and R. J. Pickering 435
Geology of Isabela (Albemarle) Island, Archipielago de Colón (Galápagos). By A. F. Banfield, C. H. Behre, Jr., and David St. Clair 215
Geology of the Blue Ridge near Harpers Ferry, West Viginia. By R. P. Nickelsen 239
Geomorphology
Baffin Island. By J. H. Mercer 553
Evolution of drainage systems and slopes in badlands at Perth Amboy, New Jersey. By S. A. Schumm .. 597
Origin of the Chuska sandstone, Arizona-New Mexico. By H. E. Wright, Jr. 413
Geomorphology and glacial history of southernmost Baffin Island. By J. H. Mercer 553
Geophysics
Geophysical investigations in emerged and submerged Atlantic Coastal Plain. Part X: Continental Slope and Continental Rise south of Grand Banks. By C. R. Bentley and J. L. Worzel 1
Seismic refraction measurements in Atlantic Ocean basin west of Bermuda. By Samuel Katz and Maurice Ewing 475
Three-dimensional applied potential studies at Austinville, Virginia. By H. V. McMurry and A. D. Hoagland 683
Geophysical investigations in the emerged and submerged Atlantic Coastal Plain. Part X: Continental Slope and Continental Rise south of the Grand Banks. By C. R. Bentley and J. L. Worzel 1
Georgia, Coarse conglomerates of the Middle Ordovician. By J. M. Kellberg and L. F. Grant 697
GIBSON, WILLIAM (With OLCOTT GATES): Interpretation of the configuration of the Aleutian Ridge 127
Glacial lake, Limnology and sedimentation, Lake Garibaldi, British Columbia. By W. H. Mathews 537
Glaciation
Baffin Island. By J. H. Mercer 553
Limnology and sedimentation, Garibaldi Lake, British Columbia. By W. H. Mathews 537
Gneisses. Franklin, New Jersey. By J. M. Hague *et al.* 435
†GOLDICH, S. S., and OSLUND, E. H.: Composition of Westerly granite G-1 and Centerville diabase W-1 811
Grand Banks, Geophysical investigations on Continental Slope and Continental Rise south of. By C. R. Bentley and J. L. Worzel 1
Granite of East Manbhum, Bihar, India, Structures of porphyritic. By S. Sen 647
GRANT, L. F. (With J. M. KELLBERG): Coarse conglomerates of the Middle Ordovician in the southern Appalachian Valley 697
Gravity anomalies
Reconnaissance survey of Puerto Rico. By G. L. Shurbet and Maurice Ewing 511
Gravity reconnaissance survey of Puerto Rico. By G. L. Shurbet and Maurice Ewing 511
Grenland, Pegmatites in west. By Hans Ramberg 185
†GUSSOW, W. C.: Late Keweenawan or early Cambrian glaciation in Upper Michigan? 235

HAGUE, J. M., BAUM, J. L., HERRMANN, L. A., and PICKERING, R. J.: Geology and Structure of the Franklin-Sterling area, New Jersey 435
Hemphillian mammalian assemblage from northeastern Oregon. By J. A. Shotwell 717
HERRMANN, L. A. (With J. M. HAGUE *et al.*): Geology and structure of the Franklin-Sterling area, New Jersey .. 435
†HIGGINS, C. G.: Unusual "pothole" 671
HOAGLAND, A. D. (With H. V. MCMURRY): Three-dimensional applied potential studies at Austinville, Virginia 683
HURLEY, P. M.: Direct radiometric measurement by gamma-ray scintillation spectrometer Part I: Uranium and thorium in equilibrium 395
—: Direct radiometric measurement by gamma-ray scintillation spectrometer, Part II: Uranium, thorium, and potassium in common rocks 405
HUTCHINSON, R. M.: Structure and petrology of Enchanted Rock batholith, Llano and Gillespie counties, Texas .. 763
Hydrology
Evolution of drainage systems and slopes in badlands at Perth Amboy, New Jersey. By S. A. Schumm. 597
Hydroscapheus americanus n. gen. n. sp. By J. A. Shotwell .. 717
Hypolagus oregonensis n. sp. By J. A. Shotwell 717

Idaho, Stratigraphic sequence in Eagle Rock volcanic area. By H. T. Stearns and Andrei Isotoff 19
Igneous rocks
Enchanted Rock batholith, Llano and Gillespie counties, Texas. By R. M. Hutchinson 763
Petrology and weathering of the Iron Dike, Boulder and Larimer counties, Colorado. By E. E. Wahlstrom 147
Sittampundi complex, Salem district, India. By A. P. Subramaniam 317
Structure of lopoliths. By H. D. B. Wilson 289
Illinois, Statistical analysis of low-level radioactivity of Pennsylvanian black fissile shale in. By W. C. Krumbein and H. A. Slack 739
India
Mineralogy and petrology of the Sittampundi complex, Salem district, Madras State. By A. P. Subramaniam 317
Structures of porphyritic granite and associated metamorphic rocks of East Manbhum, Bihar. By S. Sen. 647
Interpretation of the configuration of the Aleutian Ridge. By Olcott Gates and William Gibson 127
Iron Dike, Boulder and Larimer counties, Colorado, Petrology and weathering of. By E. E. Wahlstrom .. 147
Isabela Island, Galápagos, Geology of. By A. F. Banfield *et al.* 215
ISOTOFF, ANDREI (With H. T. STEARNS): Stratigraphic sequence in Eagle Rock volcanic area near American Falls, Idaho 19

KATZ, SAMUEL, and EWING, MAURICE: Seismic refraction measurements in the Atlantic Ocean. Part VII: Atlantic Ocean basin west of Bermuda 475
KAY, MARSHALL: Ordovician limestones in Western Anticlines of the Appalachians in West Virginia and Virginia northeast of the New River 55
KELLBERG, J. M., and GRANT, L. F.: Coarse conglomerates of the Middle Ordovician in the southern Appalachian Valley 697
†KERR, P. F.: United Nations Conference on the Peaceful Uses of Atomic Energy: Geological aspects 113
†KING, L. C.: Drakensberg scarp of South Africa: a clarification 121
KRUMBEIN, W. C., and SLACK, H. A.: Statistical analysis of low-level radioactivity of Pennsylvanian black fissile shale in Illinois 739
†KULP, J. L., *et al.*: Lead and sulfur isotopic abundances in Mississippi Valley galenas 123
KULP, J. L. (With W. R. ECKELMANN): Uranium-lead method of age determination: Part I: Lake Athabasca problem 35

Lake Athabasca uranium province, Age determinations of. By W. R. Eckelmann and J. L. Kulp 35
Lake Michigan basin, Late Wisconsin chronology of. By J. H. Zumberge and J. E. Potzger 271
Larimer County, Colorado, Petrology and weathering of the Iron Dike. By E. E. Wahlstrom 147
†Late Keweenawan or early Cambrian glaciation in Upper Michigan? By W. C. Gussow 235
†Late Keweenawan or early Cambrian ice shove in Upper Michigan—a reply. By R. C. Murray 237
Late Wisconsin chronology of the Lake Michigan basin correlated with pollen studies. By J. H. Zumberge and J. E. Potzger 271
†Lead and sulfur isotopic abundances in Mississippi Valley galenas. By J. L. Kulp, G. L. Bate, W. U. Ault, and H. W. Feely 123
Lead used in age determination. By W. R. Eckelmann and J. L. Kulp 35
Leptodontomys oregonensis n. gen. n. sp. By J. A. Shotwell .. 717
Limestones in Western Anticlines, West Virginia and Virginia. By Marshall Kay 55
Limnology
Lake Garibaldi, British Columbia. By W. H. Mathews 537
Limnology of a glacial lake. By W. H. Mathews 537
Lineation
Enchanted Rock batholith, Llano and Gillespie counties, Texas. By R. M. Hutchinson 763
Structures of the porphyritic granite and associated metamorphic rocks of East Manbhum, Bihar, India. By S. Sen 647
Lopoliths, Structure of. By H. D. B. Wilson 289
Low-water stages of Lake Michigan, Correlation of. By J. H. Zumberge and J. E. Potzger 271
Lurich formation (new name) (Ordovician), Virginia and West Virginia. By Marshall Kay 55

Madras State, India, Mineralogy and petrology of Sittampundi complex. By A. P. Subramaniam 317
Magnetization of sediments. By S. K. Runcorn 301
Manghum, Bihar, India, Porphyritic granite and associated metamorphic rocks of East. By S. Sen 647
Marble at Franklin, New Jersey. By J. M. Hague *et al.* .. 435
MATHEWS, W. H.: Physical limnology and sedimentation in a glacial lake 537
McGlone limestone (new name) (Ordovician), Virginia and West Virginia. By Marshall Kay 55
McGraw limestone (new name) (Ordovician), Virginia and West Virginia. By Marshall Kay 55
MCMURRY, H. V., and HOAGLAND, A. D.: Three-dimensional applied potential studies at Austinville, Virginia 683
MERCER, J. H.: Geomorphology and glacial history of southernmost Baffin Island 553
Metamorphic rocks of East Manbhum, Bihar, India, Structures of. By S. Sen 647
Metamorphism
Pegmatites in west Greenland. By Hans Ramberg .. 185
Metasomatism
Pegmatites in west Greenland. By Hans Ramberg ... 185
Mineralogy
Pegmatites in west Greenland. By Hans Ramberg 185
Sittampundi complex, Salem district, Madras State, India. By A. P. Subramaniam 317
Mineralogy and petrology of the Sittampundi complex, Salem district, Madras State, India. By A. P. Subramaniam 317
Minnesota, Upper Croixan stratigraphy of. By C. A. Nelson 165
Mississippi Valley, Upper Croixan stratigraphy of. By C. A. Nelson 165
†MURRAY, R. C.: Late Keweenawan or early Cambrian ice shove in Upper Michigan—a reply 237

Near Islands, Interpretation of topography of. By Olcott Gates and William Gibson 127
NELSON, C. A.: Upper Croixan stratigraphy, Upper Mississippi Valley 165
New Jersey
Drainage systems and slopes in Perth Amboy badlands. By S. A. Schumm 597
Geology and structure of the Franklin-Sterling area. By J. M. Hauge *et al.* 435
New Mexico, Origin of the Chuska sandstone. By H. E. Wright, Jr. 413
NICKELSEN, R. P.: Geology of the Blue Ridge near Harpers Ferry, West Virginia. By R. P. Nickelsen 239

Oceanography
Gravity reconnaissance survey of Puerto Rico. By G. L. Shurbet and Maurice Ewing ... 511
Ochotona spangelei n. sp. by J. A. Shotwell ... 717
Ordovician limestones in Western Anticlines of the Appalachians in West Virginia and Virginia northeast of the New River. By Marshall Kay ... 55
Oregon, Hemphillian mammalian assemblage. By J. A. Shotwell ... 717
Origin of the Chuska sandstone, Arizona-New Mexico—A structural and petrographic study of a Tertiary eolian sediment. By H. E. Wright, Jr. ... 413
†OSLUND, E. H. (With S. S. GOLDICH): Composition of Westerly granite G-1 and Centerville diabase W-1 ... 811

†PAIGE, SIDNEY: Cambro-Ordovician age of the "Inwood" limestone and "Manhattan" schist near Peekskill, New York ... 391
Paleoecology
Hemphillian mammalian assemblage from northeastern Oregon. By J. A. Shotwell ... 717
Paleomagnetic survey in Arizona and Utah: Preliminary results. By S. K. Runcorn ... 301
Paleontology
Hemphillian mammalian assemblage from northeastern Oregon. By J. A. Shotwell ... 717
Pegmatites in west Greenland. By Hans Ramberg ... 185
Perognathus sargenti n. sp. By J. A. Shotwell ... 717
Perth Amboy, New Jersey, Evolution of drainage systems and slopes in badlands. By S. A. Schumm ... 597
Petrography
Iron Dike, Boulder and Larimer counties, Colorado. By E. E. Wahlstrom ... 147
Origin of the Chuska sandstone, Arizona-New Mexico. By H. E. Wright, Jr. ... 413
Petrology
Enchanted Rock batholith, Llano and Gillespie counties, Texas. By R. M. Hutchinson ... 763
Iron Dike, Boulder and Larimer counties, Colorado. By E. E. Wahlstrom ... 147
Sittampundi complex, Salem district, India. By A. P. Subramaniam ... 317
Petrology and weathering of the Iron Dike, Boulder and Larimer counties, Colorado. By E. E. Wahlstrom ... 147
Physical limnology and sedimentation in a glacial lake. By W. H. Mathews ... 537
PICKERING, R. J. (With J. M. HAGUE *et al.*): Geology and structure of the Franklin-Sterling area, New Jersey ... 435
Pleistocene formations, Idaho. By H. T. Stearns and Andrei Isotoff ... 19
Pliocene
Hemphillian mammalian assemblange from northeastern Oregon. by J. A. Shotwell ... 717
Idaho. By H. T. Stearns and Andrei Isotoff ... 19
Polar wandering
Paleomagnetic survey in Arizona and Utah. By S. K. Runcorn ... 301
Pollen studies, Late Wisconsin chronology of the Lake Michigan basin correlated with. By J. H. Zumberge and J. E. Potzger ... 271
Post-Laramie stratigraphic correlations in the Denver Basin, Colorado. By S. O. Reichert ... 107
Potassium in common rocks, Direct radiometric measurement by gamma-ray scintillation spectrometer. By P. M. Hurley ... 405
POTZGER, J. E. (With J. H. ZUMBERGE): Late Wisconsin chronology of the Lake Michigan basin correlated with pollen studies ... 271
Prosomys mimmus n. gen. n. sp. By J. A. Shotwell ... 717
Prosthennops brachirostris n. sp. By J. A. Shotwell ... 717
Puerto Rico
Gravity reconnaissance survey. By G. L. Shurbet and Maurice Ewing ... 511

Quantitative slope analysis. By A. N. Strahler ... 571

Radioactivity
Measurement of uranium, thorium, and potassium by gamma-ray scintillation spectrometer. By P. M. Hurley ... 395, 405
Statistical analysis of low-level radioactivity of Pennsylvanian black fissile shale in Illinois. By W. C. Krumbein and H. A. Slack ... 739
Radiometric measurement of uranium, thorium, and potassium in common rocks by gamma-ray scintillation spectrometer. By P. M. Hurley ... 395, 405
RAMBERG, HANS: Pegmatites in west Greenland ... 185
REICHERT, S. O.: Post-Laramie stratigraphic correlations in the Denver Basin, Colorado ... 107
Replacement in metamorphosed regions
Pegmatites in west Greenland. By Hans Ramberg ... 185
RUNCORN, S. K.: Paleomagnetic survey in Arizona and Utah: Preliminary results ... 301

ST. CLAIR, DAVID (With A. F. BANFIELD and C. H. BEHRE, JR.): Geology of Isabela (Albemarle) Island, Archipielago de Colón (Galápagos) ... 215
Salem district, India, Mineralogy and petrology of Sittampundi complex. By A. P. Subramaniam ... 317
SCHUMM, S. A.: Evolution of drainage systems and slopes in badlands at Perth Amboy, New Jersey ... 597
Scintillation spectrometer in radiometric measurement of uranium, thorium, and potassium in common rocks, Use of By P. M. Hurley ... 395, 405
Sedimentation
Chuska sandstone, Arizona-New Mexico. By H. E. Wright, Jr. ... 413
Lake Garibaldi, British Columbia. By W. H. Mathews. ... 537
Post-Laramie stratigraphic correlations in Denver Basin, Colorado. By S. O. Reichert ... 107
Sedimentation in a glacial lake. By W. H. Mathews ... 537
Seismic refraction measurements in the Atlantic Ocean. Part VII: Atlantic Ocean Basin, west of Bermuda. By Samuel Katz and Maurice Ewing ... 475
Seismic-refraction profiles, Atlantic Coastal Plain south of Grand Banks. By C. R. Bentley and J. L. Worzel ... 1
SEN, S.: Structures of the porphyritic granite and associated metamorphic rocks of East Manbhum, Bihar, India ... 647
Shale, Radioactivity of black. By W. C. Krumbein and H. A. Slack ... 739
SHOTWELL, J. A.: Hemphillian mammalian assemblage from northeastern Oregon ... 717
SHURBET, G. L., and EWING, MAURICE: Gravity reconnaissance survey of Puerto Rico ... 511
Sittampundi complex (new name), Salem district, India, Mineralogy and petrology. By A. P. Subramaniam ... 317
†Size and roundness in sediments: A discussion. By W. F. Tanner ... 535
SLACK, H. A. (With W. C. KRUMBEIN): Statistical analysis of low-level radioactivity of Pennsylvanian black fissile shale in Illinois ... 739
Slope analysis, Quantitative. By A. N. Strahler ... 571
Space problem of batholithic emplacement, Enchanted Rock batholith. Llano and Gillespie counties, Texas. By R. M. Hutchinson ... 763
Statistical analyses
Chuska sandstone, Arizona-New Mexico. By H. E. Wright, Jr. ... 413
Drainage systems in badlands at Perth Amboy, New Jersey. By S. A. Schumm ... 597
Quantitative slope analysis. By A. N. Strahler ... 571

Statistical analysis of low-level radioactivity of Pennsylvanian black fissile shale in Illinois. By W. C. Krumbein and H. A. Slack ... 739
Statistical geology
Quantitative slope analysis. By A. N. Strahler ... 571
STEARNS, H. T., and ISOTOFF, ANDREI: Stratigraphic sequence in Eagle Rock volcanic area near American Falls, Idaho ... 19
Sterling Mine, New Jersey, Geology and structure of. By J. M. Hague *et al.* ... 435
†STOYANOW, ALEXANDER: Types of *Bathyuriscus howelli* var. *lodensis* Clark ... 679
STRAHLER, A. N.: Quantitative slope analysis ... 571
Stratigraphic sequence in Eagle Rock volcanic area near American Falls, Idaho. By H. T. Stearns and Andrei Isotoff ... 19
Stratigraphy
Correlations in Denver Basin, Colorado, Post-Laramie. By S. O. Reichert ... 107
Geology and structure of the Franklin-Sterling area, New Jersey. By J. M. Hague *et al.* ... 435
Geology of the Blue Ridge near Harpers Ferry, West Virginia. By R. P. Nickelsen ... 239
Ordovician limestones in Western Anticlines, West Virginia and Virginia. By Marshall Kay ... 55
Upper Croixan, Upper Mississippi Valley. By C. A. Nelson ... 165
Structure
Franklin-Sterling area, New Jersey. By J. M. Hague *et al.* ... 435
Geology of the Blue Ridge near Harpers Ferry, West Virginia. By R. P. Nickelsen ... 239
Gravity reconnaissance survey of Puerto Rico. By G. L. Shurbet and Maurice Ewing ... 511
Structure, Aleutian Ridge. By Olcott Gates and William Gibson ... 127
Structure and petrology of Enchanted Rock batholith, Llano and Gillespie counties, Texas. By R. M. Hutchinson ... 763
Structure of lopoliths. By H. D. B. Wilson ... 289
Structures of the porphyritic granite and associated metamorphic rocks of East Manbhum, Bihar, India. By S. Sen ... 647
Submarine topography, Aleutian Ridge. By Olcott Gates and William Gibson ... 127
SUBRAMANIAM, A. P.: Mineralogy and petrology of the Sittampundi complex, Salem district, Madras State, India ... 317

†TANNER, W. F.: Size and roundness in sediments: A discussion ... 535
Tectonics, Aleutian Ridge. By Olcott Gates and William Gibson ... 127
Tennessee, Coarse conglomerates of the Middle Ordovician. By J. M. Kellberg and L. F. Grant ... 697
†Terminology for stratification in sedimentary rocks. By John Bokman ... 125
Tertiary
Origin of the Chuska sandstone, Arizona-New Mexico. By H. E. Wright, Jr. ... 413
Texas, Structure and petrology of Enchanted Rock batholith, Llano and Gillespie counties. By R. M. Hutchinson ... 763
Thorium in common rocks, Direct radiometric measurement by gamma-ray scintillation spectrometer. By P. M. Hurley ... 395, 405
Three-dimensional applied potential studies at Austinville, Virginia. By H. V. McMurry and A. D. Hoagland ... 683
Topography, Aleutian Ridge. By Olcott Gates and William Gibson ... 127
Turbidity currents
Aleutian Ridge. By Olcott Gates and William Gibson. 127
Garibaldi Lake, British Columbia. By W. H. Mathews 537
†Types of *Bathyuriscus howelli* var. *lodensis* Clark. By Alexander Stoyanow ... 679

†United Nations Conference on the Peaceful Uses of Atomic Energy: Geological aspects. By P. F. Kerr ... 113
†Unusual patterned ground in Greenland. By A. L. Washburn ... 807
†Unusual "pothole". By C. G. Higgins ... 671
Upper Croixan stratigraphy, Upper Misaisippi Valley. By C. A. Nelson ... 165
Uranium in common rocks, Direct radiometric measurement of, by gamma-ray scintillation spectrometer. By P. M. Hurley ... 395, 405
Uranium-lead method of age determination. Part I: Lake Athabasca problem. By W. R. Eckelmann and J. L. Kulp ... 35
Utah, Paleomagnetic survey in. By S. K. Runcorn ... 301

Virginia
Coarse conglomerates of the Middle Ordovician. By J. M. Kellberg and L. F. Grant ... 697
Geology of the Blue Ridge near Harpers Ferry, West Virginia By R. P. Nickelsen ... 239
Ordovician limestones in Western Anticlines of. By Marshall Kay ... 55
Three-dimensional applied potential studies at Austinville. By H. V. McMurry and A. D. Hoagland ... 683
Volcanic rocks, Idaho. By H. T. Stearns and Andrei Isotoff 19
Volcanism
Geology of Isabela Island, Archipielago de Colón (Galápagos). By A. F. Banfield *et al.* ... 215

WAHLSTROM, E. E.: Petrology and weathering of the Iron Dike, Boulder and Larimer counties, Colorado ... 147
Walcott welded tuff (new name) (Pliocene?). Idaho. By H. T. Stearns and Andrei Isotoff ... 19
†WASHBURN, A. L.: Unusual patterned ground in Greenland ... 807
Weathering
Iron Dike, Boulder and Larimer counties, Colorado. By E. E. Wahlstrom ... 147
Welded tuff, Eagle Rock volcanic area, Idaho. By H. T. Stearns and Andrei Isotoff ... 19
West Virginia
Geology of the Blue Ridge near Harpers Ferry. By R. P. Nickelsen ... 239
Ordovician limestones in Western Anticlines of. By Marshall Kay ... 55
WILSON, H. D. B.: Structure of lopoliths ... 289
Wisconsin Upper Croixan stratigraphy of. By C. A. Nelson ... 165
WORZEL, J. L. (With C. R. BENTLEY): Geophysical investigations in the emerged and submerged Atlantic Coastal Plain. Part X: Continental Slope and Continental Rise south of the Grand Banks ... 1
WRIGHT, H. E., JR.: Origin of the Chuska sandstone, Arizona-New Mexico—A structural and petrographic study of a Tertiary eolian sediment ... 413

ZUMBERGE, J. H., and POTZGER, J. E.: Late Wisconsin chronology of the Lake Michigan basin correlated with pollen studies ... 271

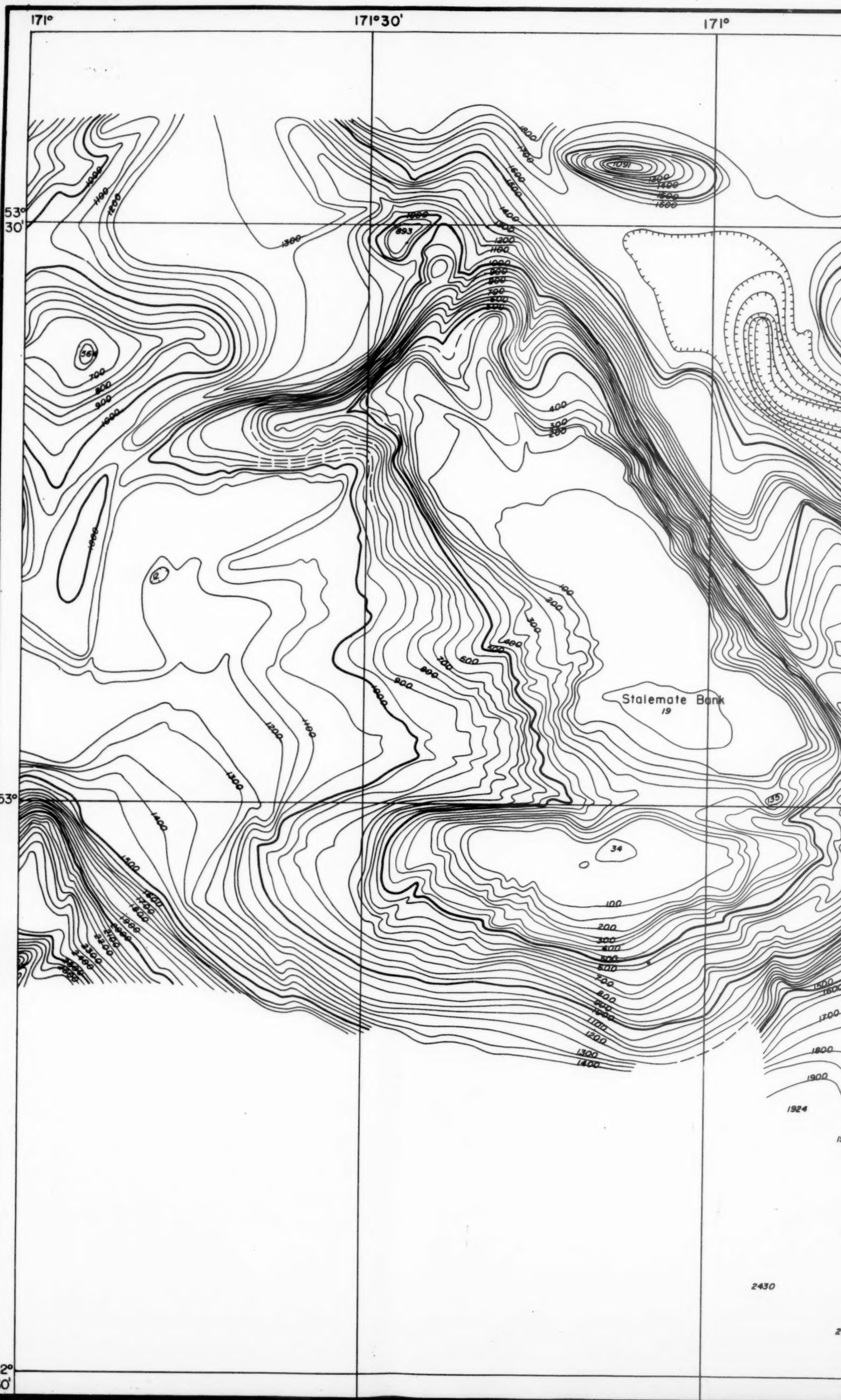
171°
171°30'
171°
53°
30'
53°
52°
30'
Stalemate Bank
19
34
1924
2430

171° 30

172°

172° 3

2142 2142 2142 2142 2142

2142

185

222

302

262

1630

81

172

795

1955

1900

176

2350

2162

2214

2006

2631

2812

Stalemate Sea Valley

Etienne Sea Valley

Abraham Sea Valley

172°

172°30'

2142 2142 2142 2142 2142 2142

2142 2147 2142

185 185

2100 2000 1900 1800 1700 1600 1500 1400 1300

31

2142 2142

827 804

1200 1100 1000 900 800 700 600 500 400 300 200

81 172 197

30 40 50 60 70 80 90 100 200 300 400 500

Etienne Bay

Abraham Bay

Etienne Sea Valley

Abraham Sea Valley

1840 2812 2528

177 200 300 400 500 600 700 800 900 1000

173°

173° 30'

BERING SEA

2152 2142

2142

2137 2137 2137

2137

2137 2127

2142

2137

2137 2132

2132

2122

2126

2137 2137

2132

2132

2132

2080

2100

2122

1900

Stellar Cove

Holtz Bay

ATTU IS.

Sarana Bay

Massacre Bay

Temnaia Bay

ALEUTIAN

Near Islands Platform

73° 30'

174°

RING SEA

2132

2137 2137 2137 2137 2130

2127 2137 2100

2100

2137

2132

2132 2100 2100

2137 2137

2132 2132

2132 2100

2080 2100

2150

2122 2097

2060 2090

2085

2090 2128

NORTH INSULAR

Sarana Bay

Massacre Bay

2095

SEMICHI IS.

ALEUTIAN

CREST

Near Islands Platform

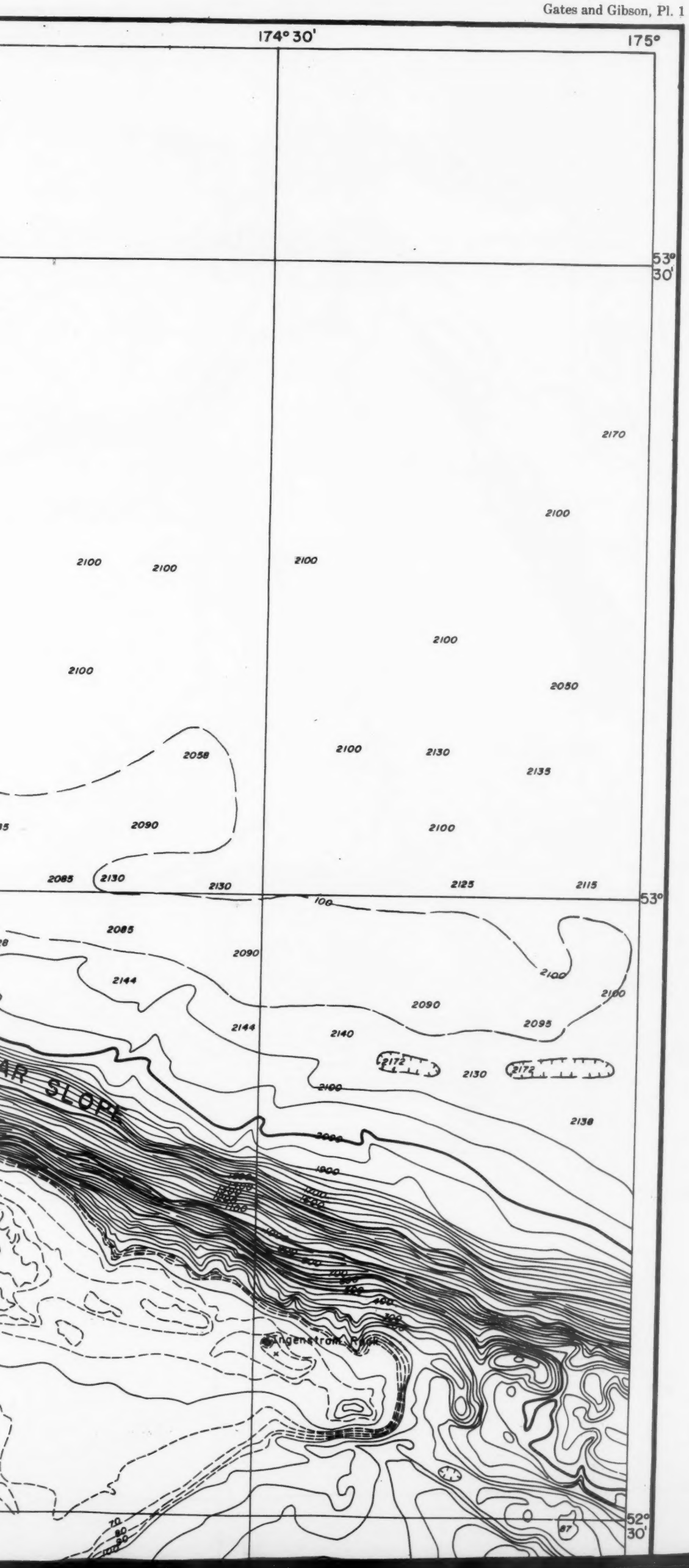
174° 30'
175°
53° 30'
53°
52° 30'
2170
2100
2100
2100
2100
2100
2100
2050
2058
2090
2085
2130
2130
2100
2130
2135
2100
2125
2115
2085
2090
2144
2144
2140
2090
2095
2100
2100
2172
2172
2130
2138
AR SLOPE
Ingenstrom Rock
70
80
90
100
87

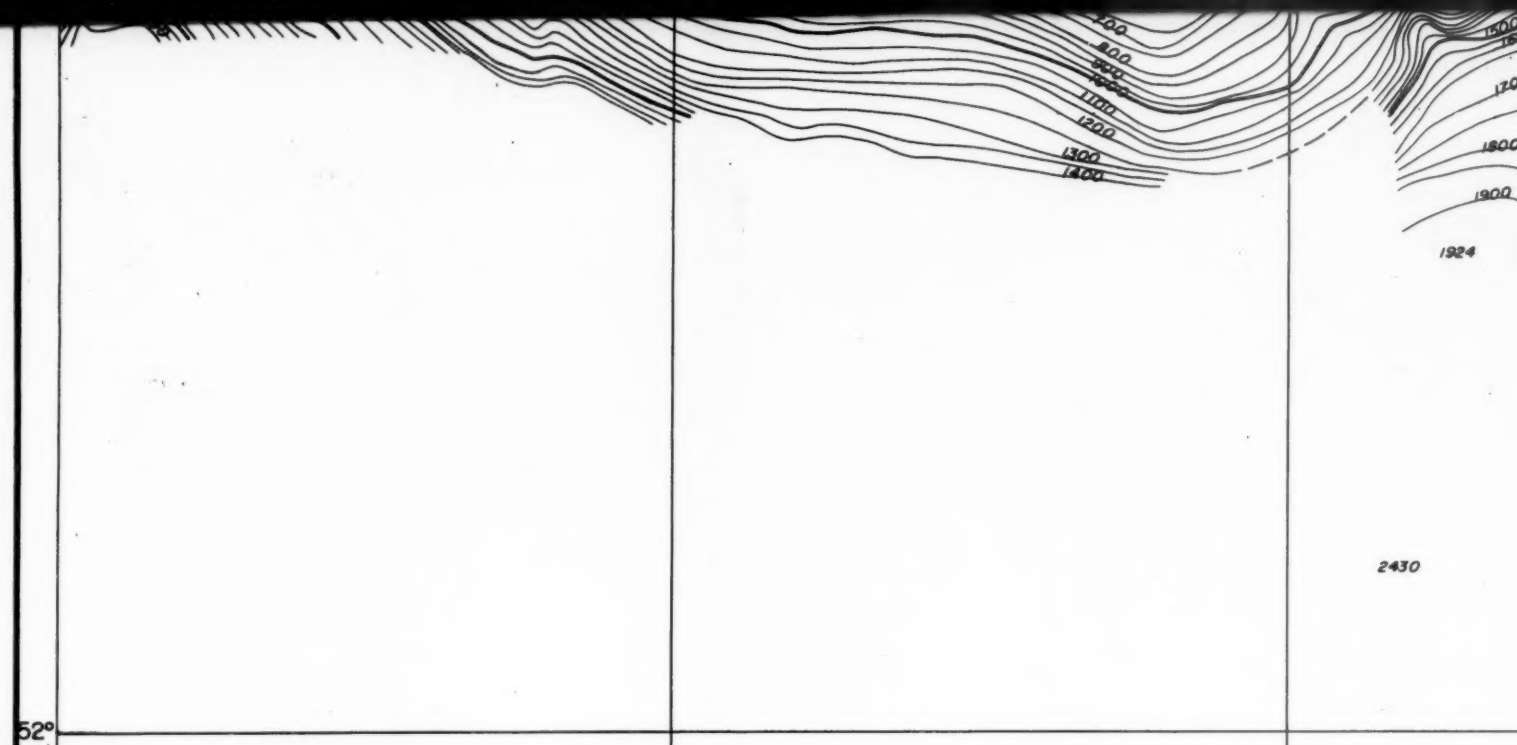

52° 30'

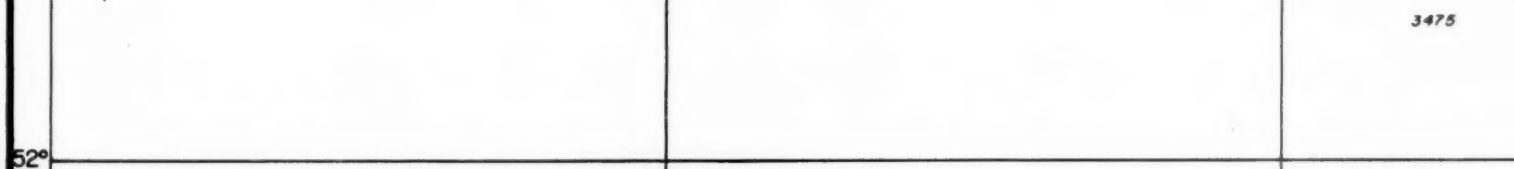

52°

UNITED STATES
ALEUTIAN ISLAND–ALASKA
CONFIGURATION OF THE ALEUTIAN RIDGE
NO. 2—NEAR ISLANDS GROUP

Contours by W.M. Gibson and Olcott Gates

Marine contour interval, 50 fathoms (300 ft.)
Land contour interval, 500 feet

Soundings from hydrographic surveys by U.S. Coast and Geodetic Survey 1934–1952 and Chart 8865

Shoreline and elevation contours adopted from U.S. Geologic Survey topographic quadrangle map–Attu, Alaska. Mercator Projection

10 5 0 10 20

Nautical miles

51° 30'

170° 170°30' 171°

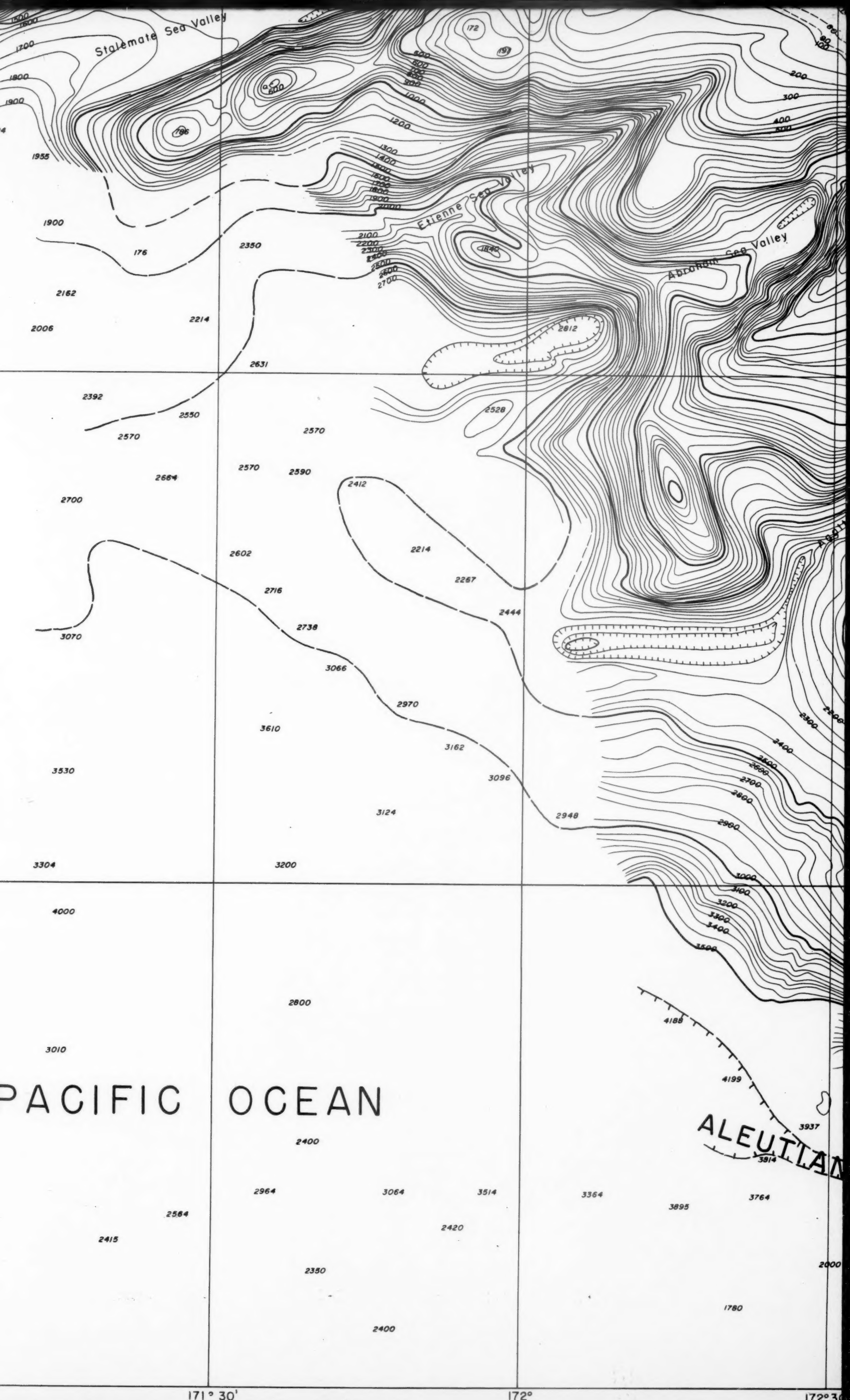

CONFIGURATION OF ALEUTIAN R

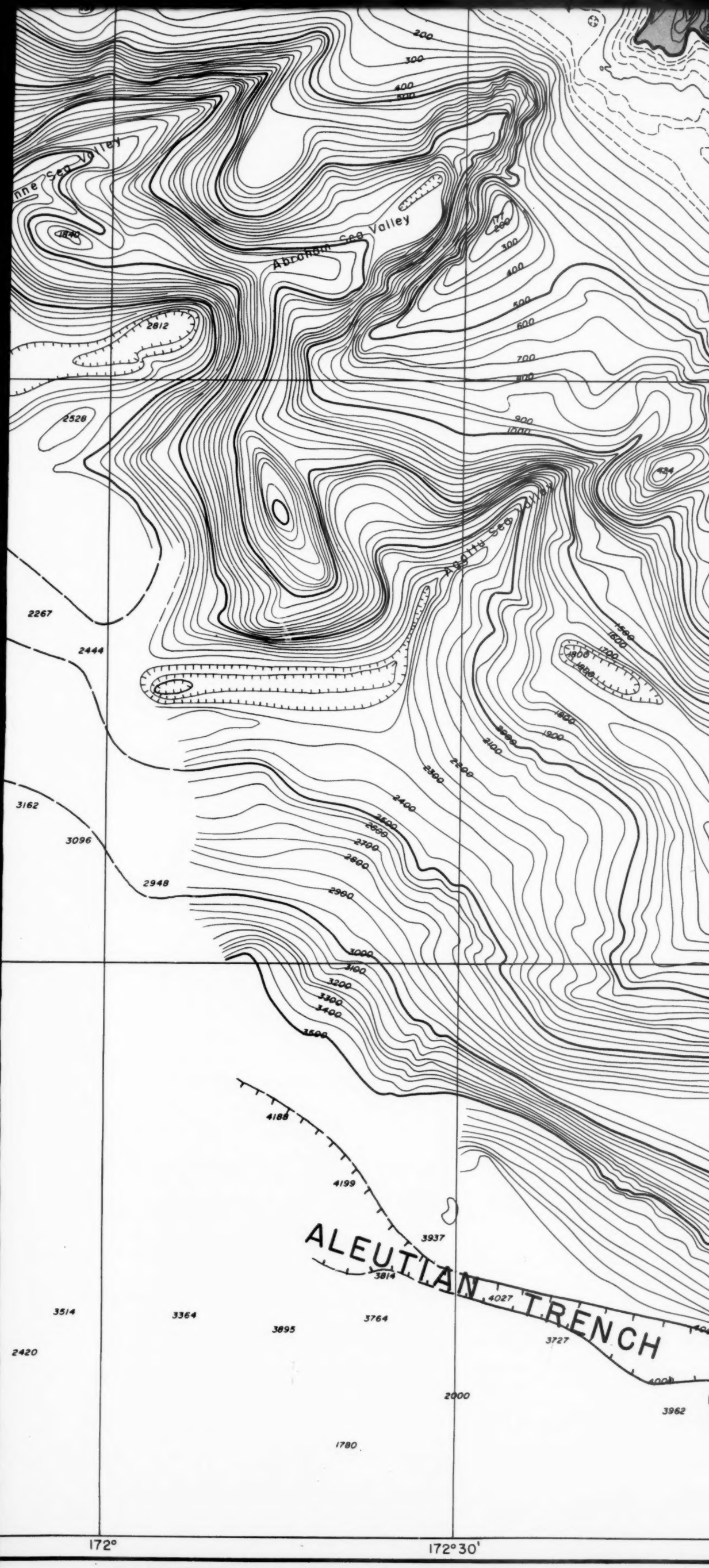

CONFIGURATION OF ALEUTIAN RIDGE, NEAR ISLANDS

Temnaia Bay

ALEUTIAN

Near Islands Platform

AGATTU IS.

SOUTH INSULAR SLOPE

173°

173° 30'

DS GROUP

SEMICHI IS.

ALEUTIAN CREST

Near Islands Platform

AGATTU IS.

SOUTH INSULAR SLOPE

ALEUTIAN B

173° 30'

174°

Ingenstrom Rock

Heck Sea Valley

BENCH

52°
30'

52°

51°
30'

174°30'

175°

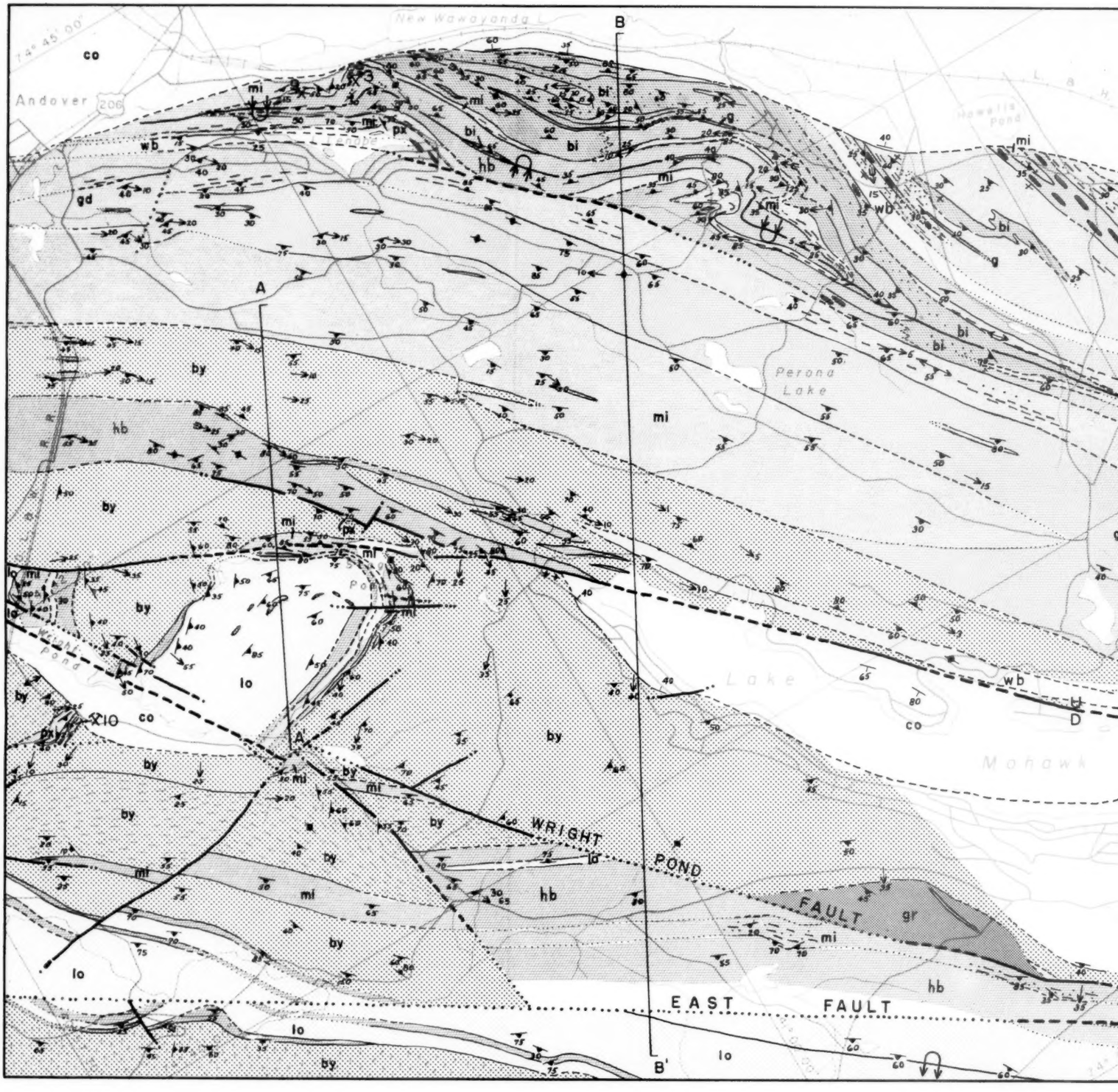
B
A
A'
B'
WRIGHT POND FAULT
EAST FAULT
Perona Lake
Andover
co
mi
by
hb
lo
bi
wb
gd
gr
px
D

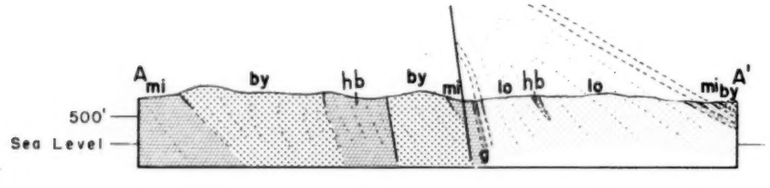
A
A'
500'
Sea Level
mi
by
hb
lo
g

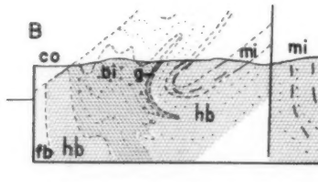
B
co
bi
g
mi
hb
fb

GEOLOGY AND STRU
AREA

Geology by J. M. Hague, J. L. Baum,
L. A. Herrmann, R. J. Pickering,
and others, 1946 - 1954

1 1/2

5,000

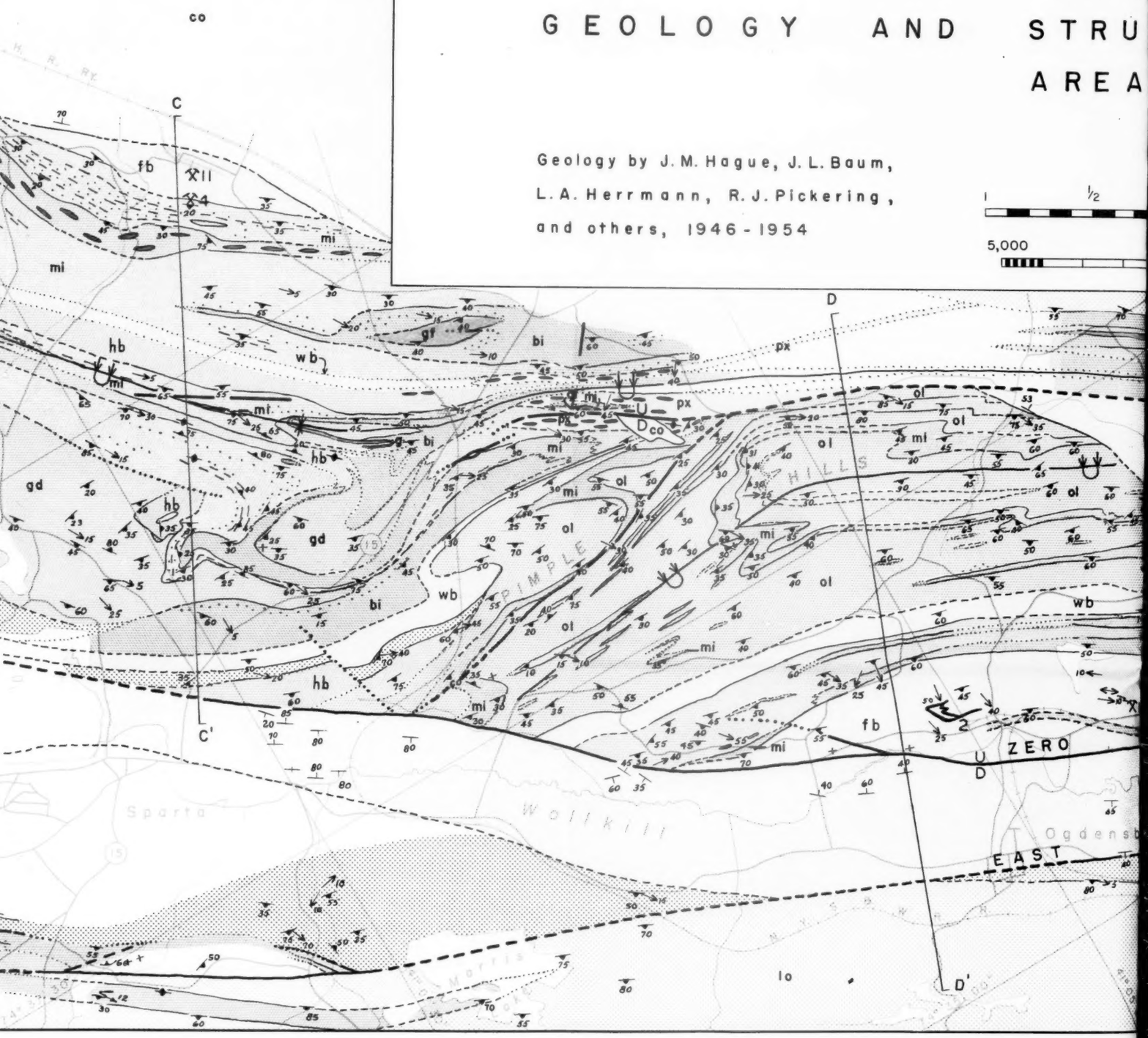

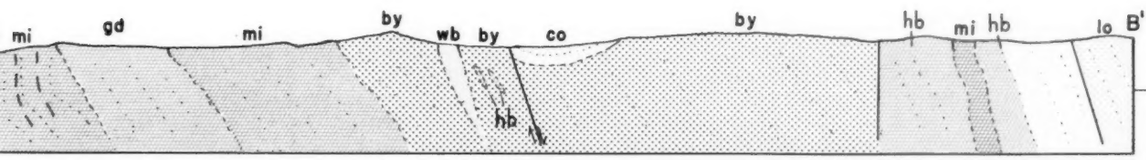

EOLOGY AND STRUCTURE OF THE FRA
AREA, NEW JERSEY

ogy by J. M. Hague, J. L. Baum,
Herrmann, R. J. Pickering,
others, 1946 - 1954

SCALE

1 ½ 0 1 2 MIL

5,000 0 5,000 10,000 FEE

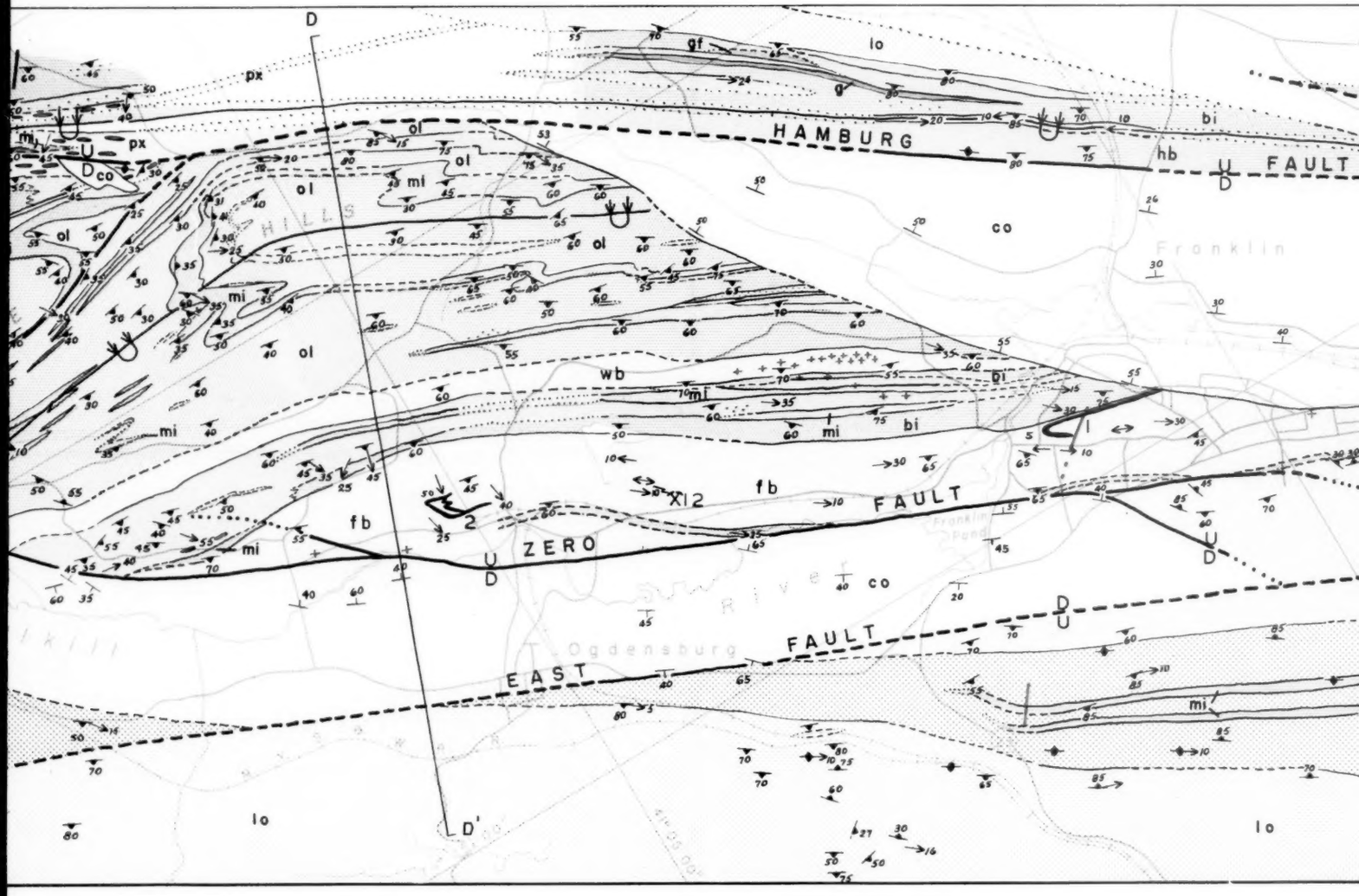

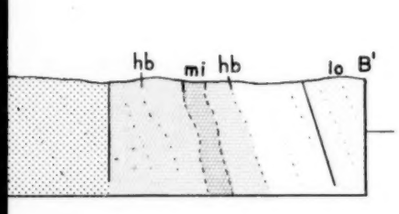

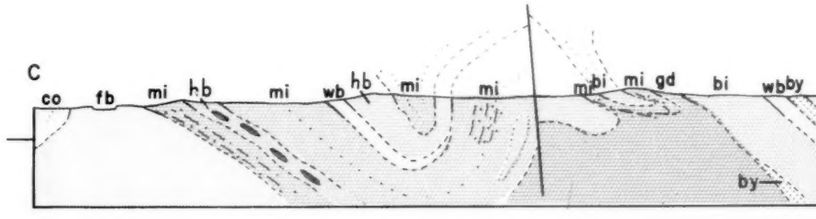

GEOL

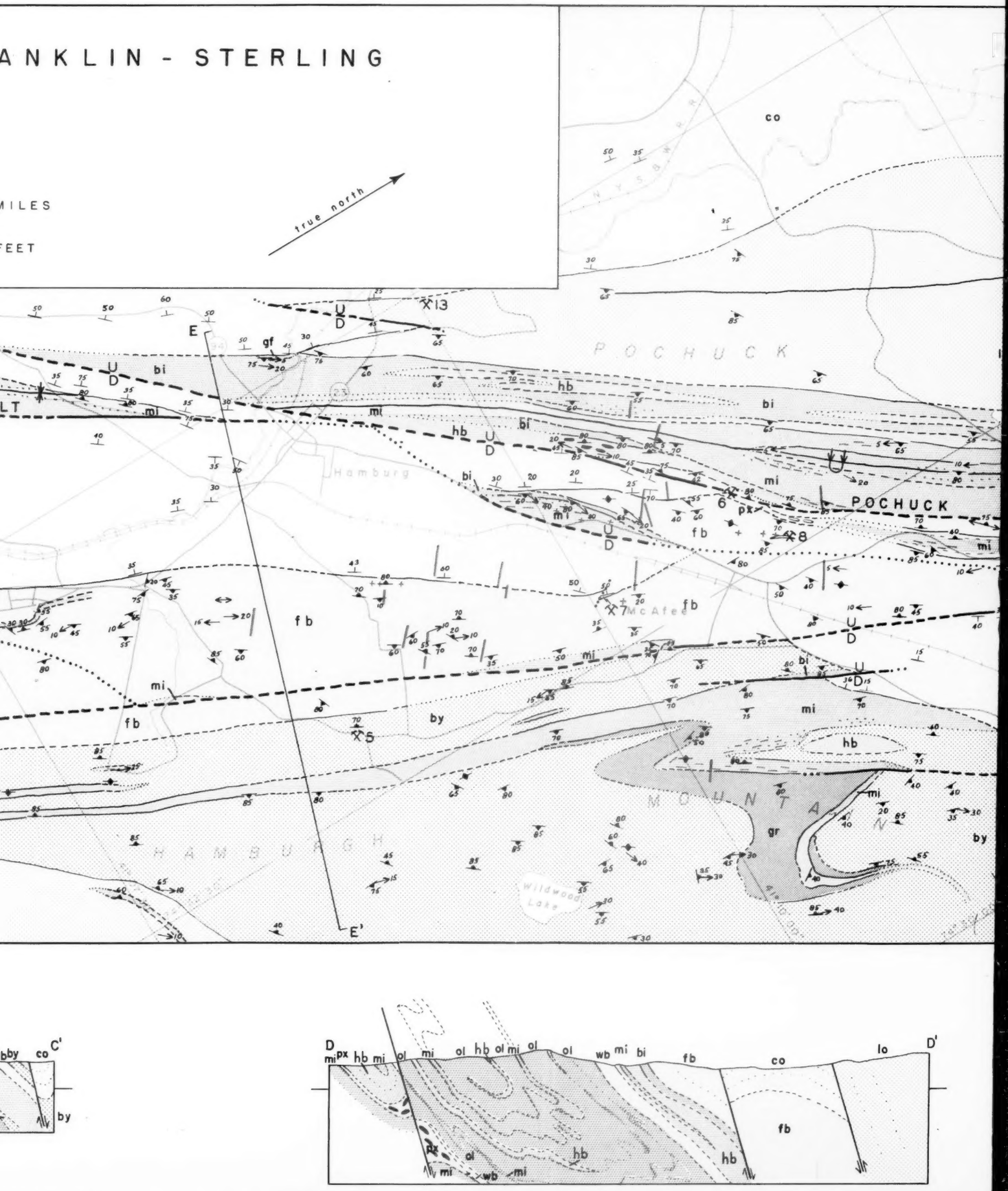

OLOGICAL AND STRUCTURAL MAP OF THE FRANKLIN-STERLING AREA, NEW

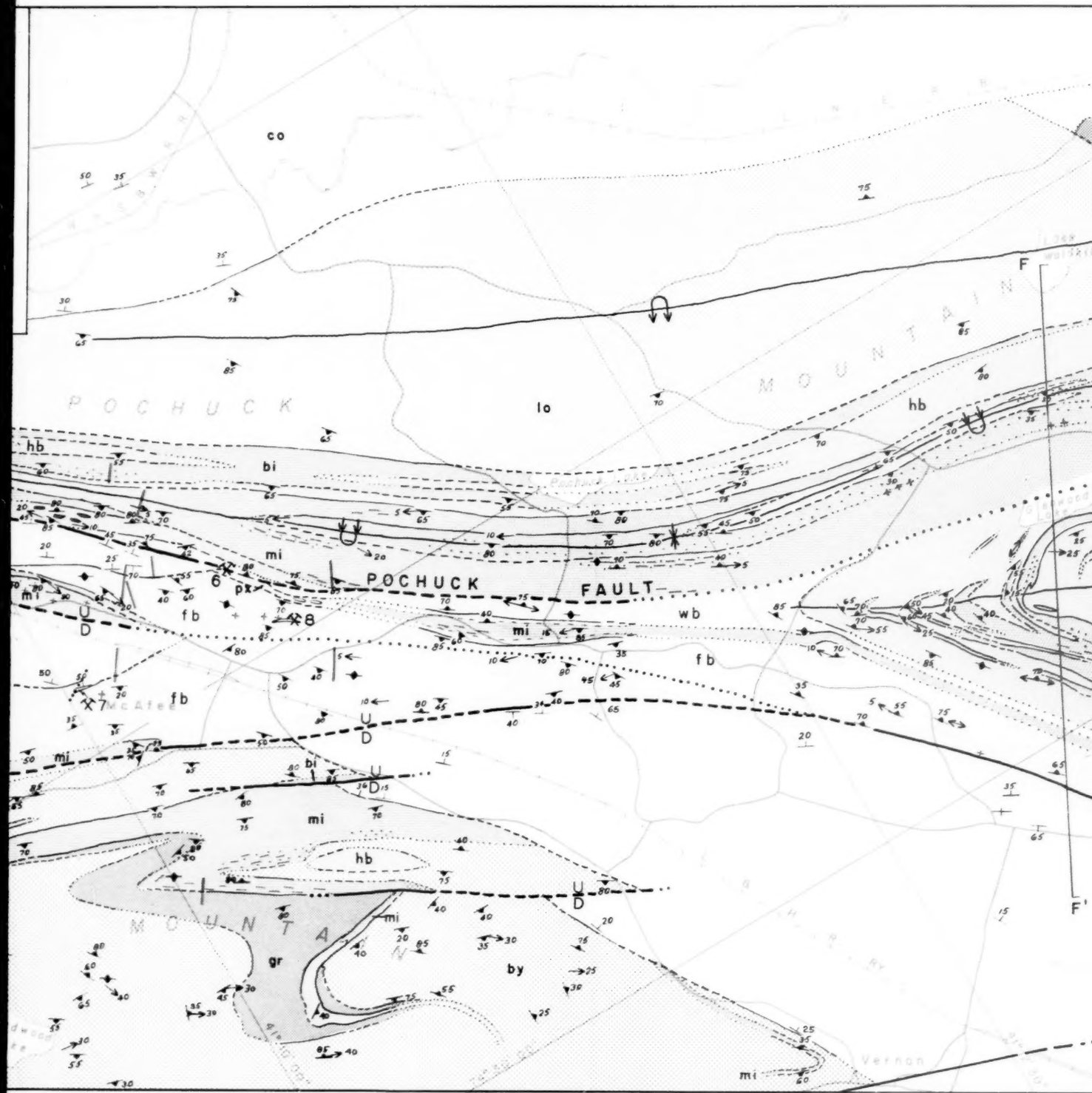

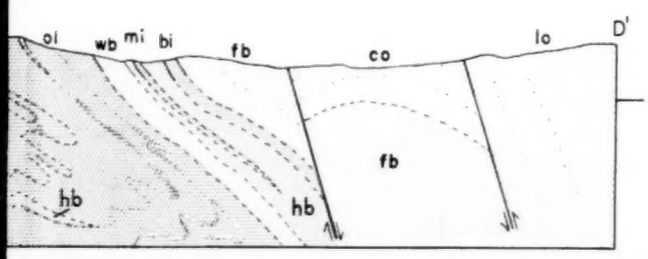

E

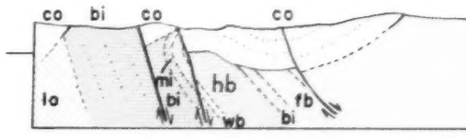

E FRANKLIN-STERLING AREA, NEW JERSEY

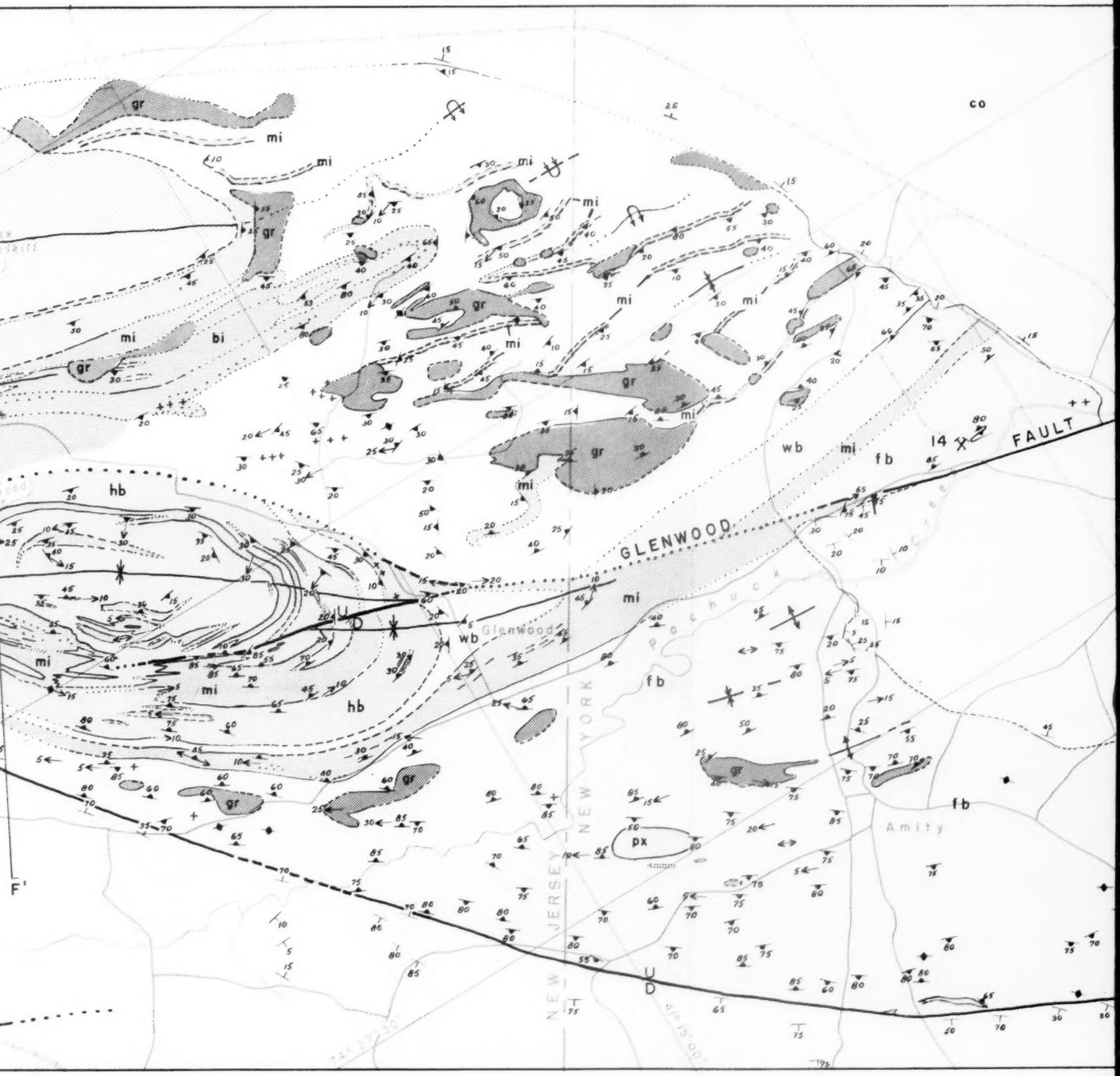
co
gr
mi
bi
hb
wb
fb
px
14
FAULT
GLENWOOD
Glenwood
NEW JERSEY
NEW YORK
Pochuck
Amity
F'
U
D

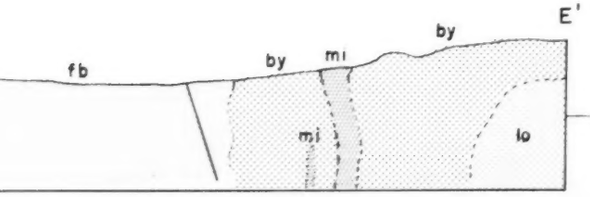
E'
fb
by
mi
lo

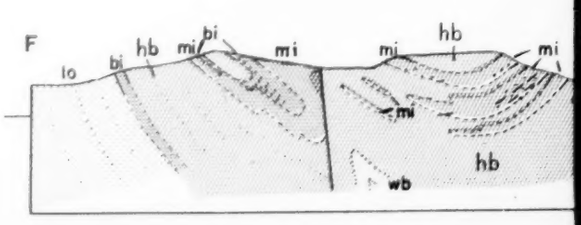
F
lo
bi
hb
mi
wb

CAMBRIAN AND
LATER ROCKS

Camptonite Dikes

co

Cambro-Ordovician
Sediments

PRECAMBRIA
IGNEOUS ROCK

+++

Pegmatites

A

gr

Granite
(A= granitic gneiss)

1 2 3

by

Byram Gneiss
types 1,2,3

GLENWOOD FAULT

Glenwood

Pochuck Creek

Amity

NEW JERSEY — NEW YORK

74° 27' 30"

41° 15' 00"

74° 25' 00"

E E'

F F'

Plate I

EXPLANATION

gd — Granodiorite Gneiss

ol — Oligoclase Gneiss

lo — Losee Gneiss

PRECAMBRIAN META-SEDIMENTARY AND METAVOLCANIC ROCKS

fb | wb — Marble
fb = Franklin Band
wb = Wildcat Band

mi — Microcline Gneiss

A: hb — Hornblende Gneiss
(A = calcareous facies)

bi — Biotite Gneiss

A: px — Pyroxene Gneiss and Related Rocks
(A = calcareous facies)

g — Garnet Gneiss

gf — Graphitic Gneiss

STRUCTURES

60 — Strike and Dip of Banding and Foliation

30 — Strike and Dip of Bedding

15 — Strike and Plunge of lineation

15 — Strike and Plunge of Small Folds

(1) (2) — Trace of Axial Plane of (1) Normal Syncline and (2) Overturned Syncline

Trace of Axial Plane of Overturned Anticline

FAULTS

solid line where observed, dashed line where approximate, dotted line where projected

CONTACTS

solid line where observed, dashed line where approximate, dotted line where projected

SPECIAL SYMBOLS

Sillimanite

Garnets

Zinc Ore Body

Mines and Quarries

1. Franklin	8. Cedar Hill
2. Sterling	9. Andover
3. Sulphur Hill	10 Roseville
4. Indian	11. Limecrest
5. Edsall	12. Farber
6. Pochuck	13. Sussex
7. Simpson	14. Pine Island

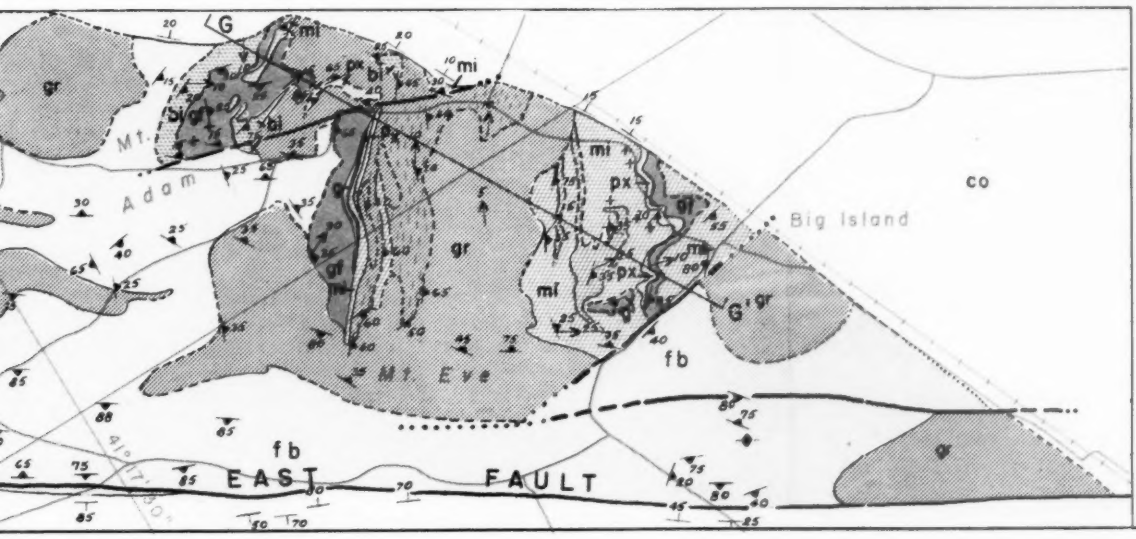

F'

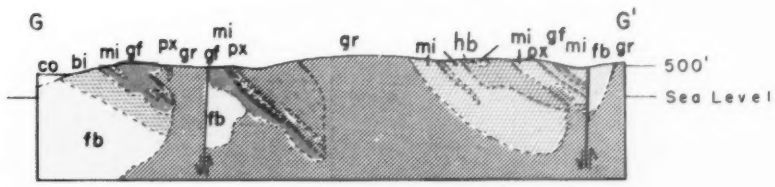

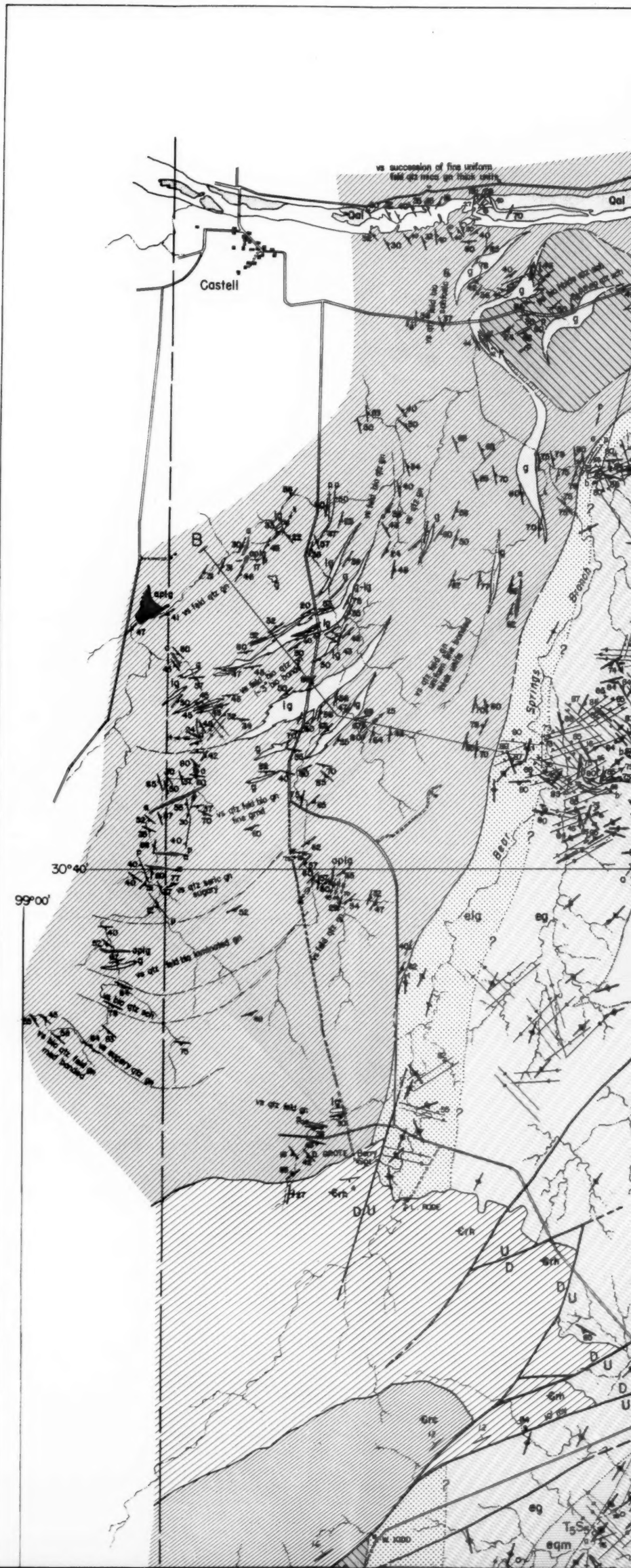
Castell
Qal
B
30°40'
99°00'
Bear Branch Springs
eg
eqm

LLANO RIVER
Qal
A
A'
B
B'
eg
eqm
elg
ig
apig-ig
Vaughn Creek
E. RHEINHARD
T. B. MOSELY
CREEK
Branch

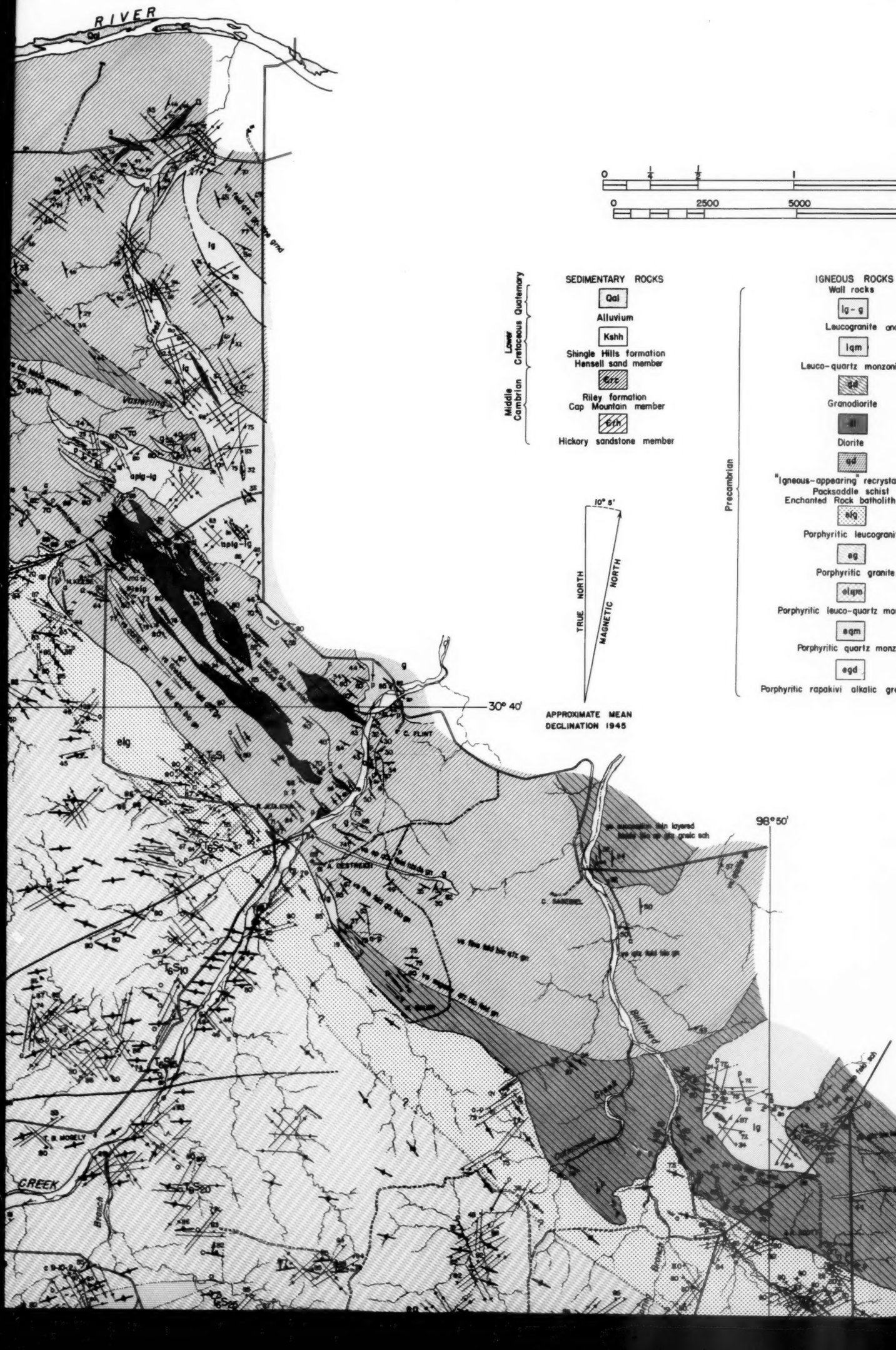
RIVER
0 1/4 1/2 1
0 2500 5000
SEDIMENTARY ROCKS
Qal
Alluvium
Kshh
Shingle Hills formation
Hensell sand member
Cch
Riley formation
Cap Mountain member
Cchh
Hickory sandstone member
Lower Cretaceous
Quaternary
Middle Cambrian
IGNEOUS ROCKS
Wall rocks
lg - g
Leucogranite
lqm
Leuco-quartz monzoni
gd
Granodiorite
di
Diorite
Packsaddle schist
Enchanted Rock batholith
elg
Porphyritic leucograni
eg
Porphyritic granite
elqm
Porphyritic leuco-quartz mo
eqm
Porphyritic quartz monz
egd
Porphyritic rapakivi alkalic gr
Precambrian
10° 5'
TRUE NORTH
MAGNETIC NORTH
APPROXIMATE MEAN
DECLINATION 1945
30° 40'
98° 50'
Vaxterling
C. FLINT
C. BARNEL
CREEK

SCALE

2 3 4 MILES

10000 15000 20000 FEET

FIELD WORK 1950-52

EXPLANATION

OCKS

e and granite

onzonite

e

crystallized
chist
holith

ogranite

granite

tz monzonite

monzonite

ic granodiorite

Precambrian

Dike or irregular lens of aplite

Dike or irregular lens of pegmatite

Irregular intrusion of aplogranite

Large pod or lens of quartz pegmatite

Narrow vein of quartz

Quartz-enriched zone

METAMORPHIC ROCKS

Packsaddle schist formation

Valley Spring gneiss formation

Strike and plunge of linear elements in metamorphics

Strike and dip of foliation, banding in metamorphics, normal and overturned

Strike and dip of vertical, inclined and horizontal joints

Strike and dip of joint and plunge of slickensides

FLOW STRUCTURES IN IGNEOUS ROCKS

Strike and plunge of lineation

Platy parallelism of feldspar crystals. Strike and dip of inclined and vertical flow structure

Strike and dip of flow layers (schlieren). b = biotite m = microcline

Strike and dip of xenoliths. Size has been exaggerated.

Strike and vertical dip of rows of xenoliths

Axis of anticline. Dashed where inferred

Axis of syncline. Dashed where inferred

Plunge of minor anticline

Plunge of minor syncline

Strike and dip of beds

Strike and dip of cross bedding (foreset beds)

Strike and dip of recently exposed Precambrian erosion surface

Fault zone with mylonite showing thickness in feet

Fault dashed where inferred, solid line where observed

Contact of lithologic units. Dashed where approximately located. Dotted where gradational.

o T_2S_{20}

Symbol for Traverse 2, Station 20

x c T_5S_{21}

Chemical analysis made for sample taken at this location.

x A_1

Apophysis in wall rock

x C_2

Chilled border rock

x T. M.$_1$

Sample for age determination

HICKORY
Marshall
J. KINSEY
eqm
eg
Qal
Ig to g
Ig sanukite
Igneous- appearing septum
Igneous- appearing septum
pa flaky musc qtz sch
pa fine-bio qtz sch
pa bio qtz fold sch becomes increasingly gneissic to N
pa qtzite gr
pa musc-bio qtz sch
pa qtz mono gr
pa musc-bio gneiss
pa musc-bio qtz sch
pa musc-bio qtz sch
pa musc-bio qtz sch

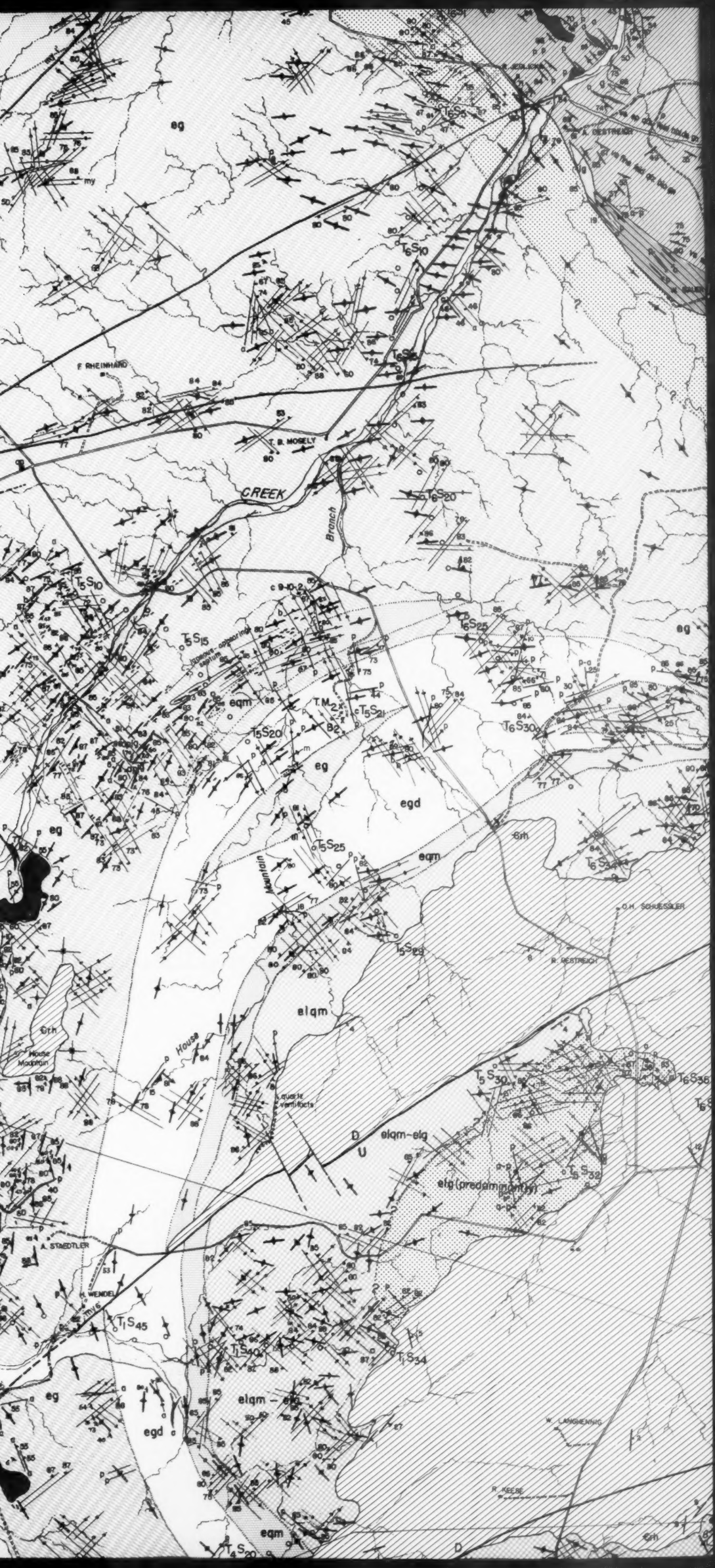
eg
F. RHEINHARD
T. B. MOSELY
CREEK
Branch
eqm
egd
elqm
elqm-elg
elg (predominantly)
D
U
Mountain
House
Mountain
R. BESTREICH
O.H. SCHUESSLER
A. STAEDTLER
R. WENDEL
W. LANGHENNIG
R. KEESE
T5S10
T5S15
T5S20
T5S25
T5S29
T5S30
T5S32
T6S10
T6S15
T6S20
T6S25
T6S30
T6S34
T6S36
T1S45
T1S40
T1S34
T4S20

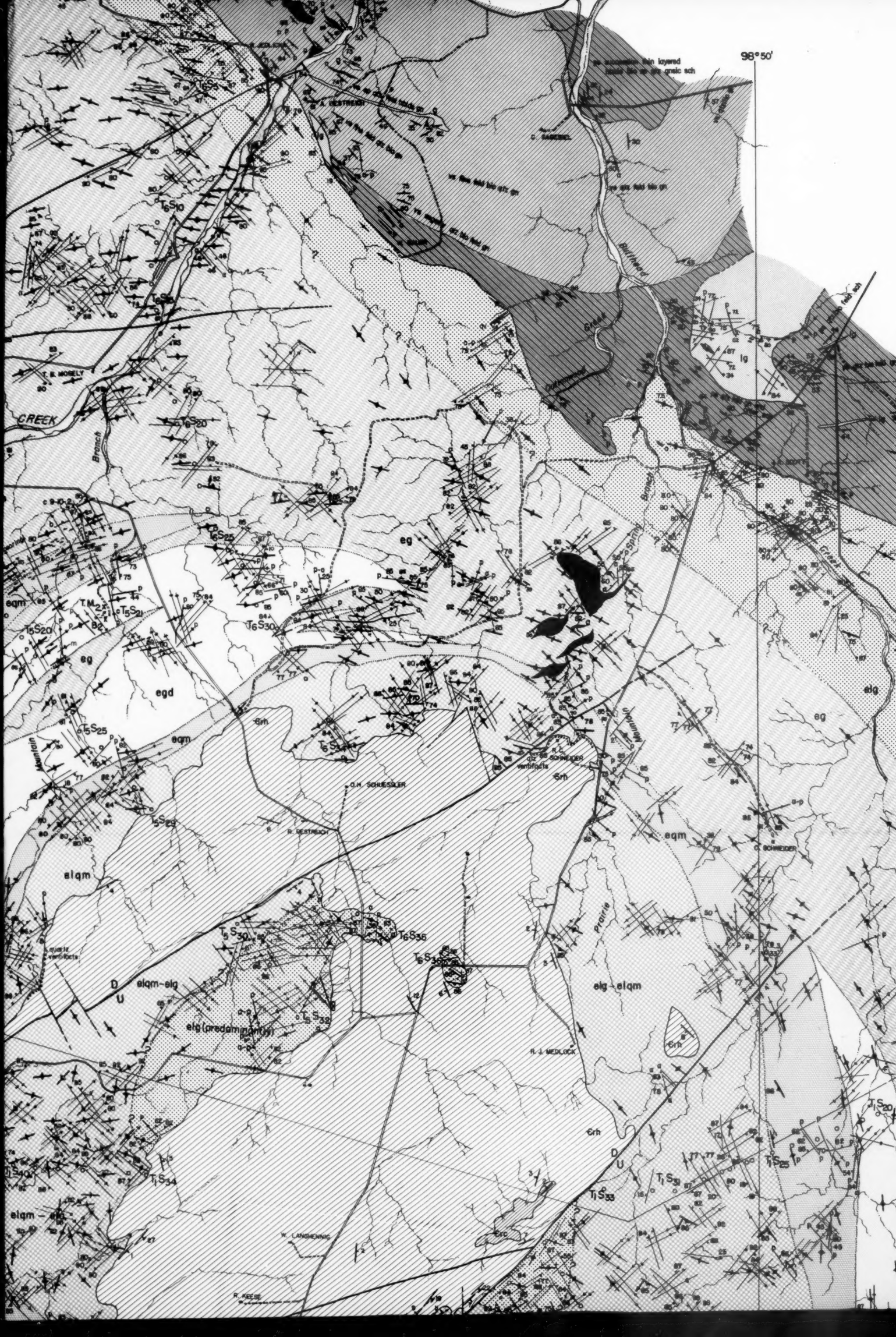
98°50'
CREEK
Branch
Mountain
Prairie
eg
egm
egd
elg
elqm
elqm-elg
elg-elqm
elg (predominantly)
Crh
lg
T. R. MOSELY
O. H. SCHNEIDER
R. BESTREICH
R. J. MEDLOCK
W. LANGHENNIG
R. KEESE
T5S10
T5S20
T5S25
T5S21
T6S30
T6S36
T1S34
T1S33
T1S31
T1S25
T1S20

Strike and dip of vertical, inclined and horizontal joints

Strike and dip of joint and plunge of slickensides

Strike and dip of cross bedding (foreset beds)

Strike and dip of recently exposed Precambrian erosion surface

Fault zone with mylonite showing thickness in feet

Fault dashed where inferred, solid line where observed

Contact of lithologic units. Dashed where approximately located. Dotted where gradational.

o T_2S_{20}

Symbol for Traverse 2, Station 20

x c T_5S_{21}

Chemical analysis made for sample taken at this location.

x A_1

Apophysis in wall rock

x C_2

Chilled border rock

x $T.M._1$

Sample for age determination

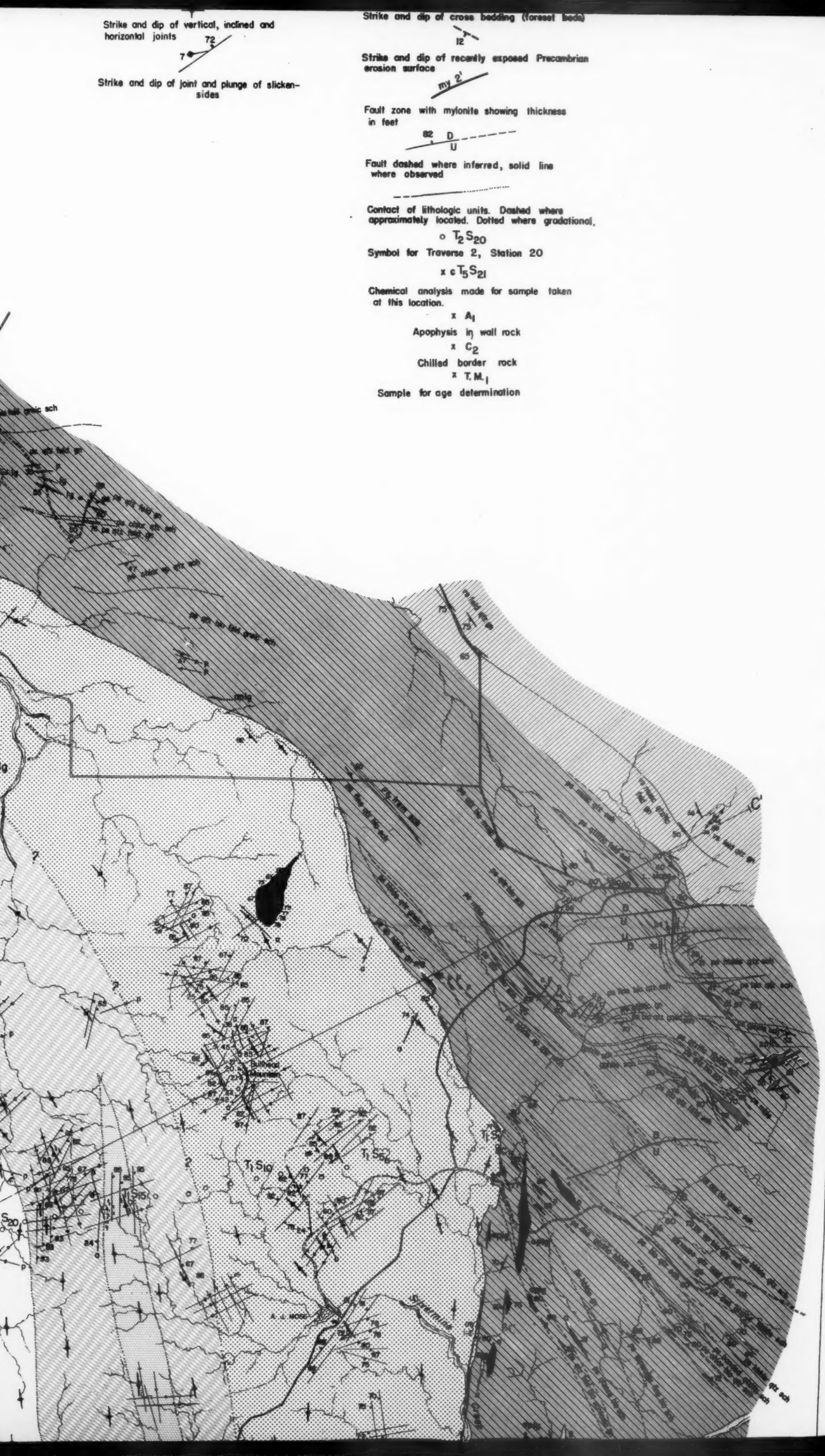

MASON COUNTY
LLANO COUNTY

99°00'

30°30'

LLANO CO
GILLESPIE

Index map of Texas showing location of area

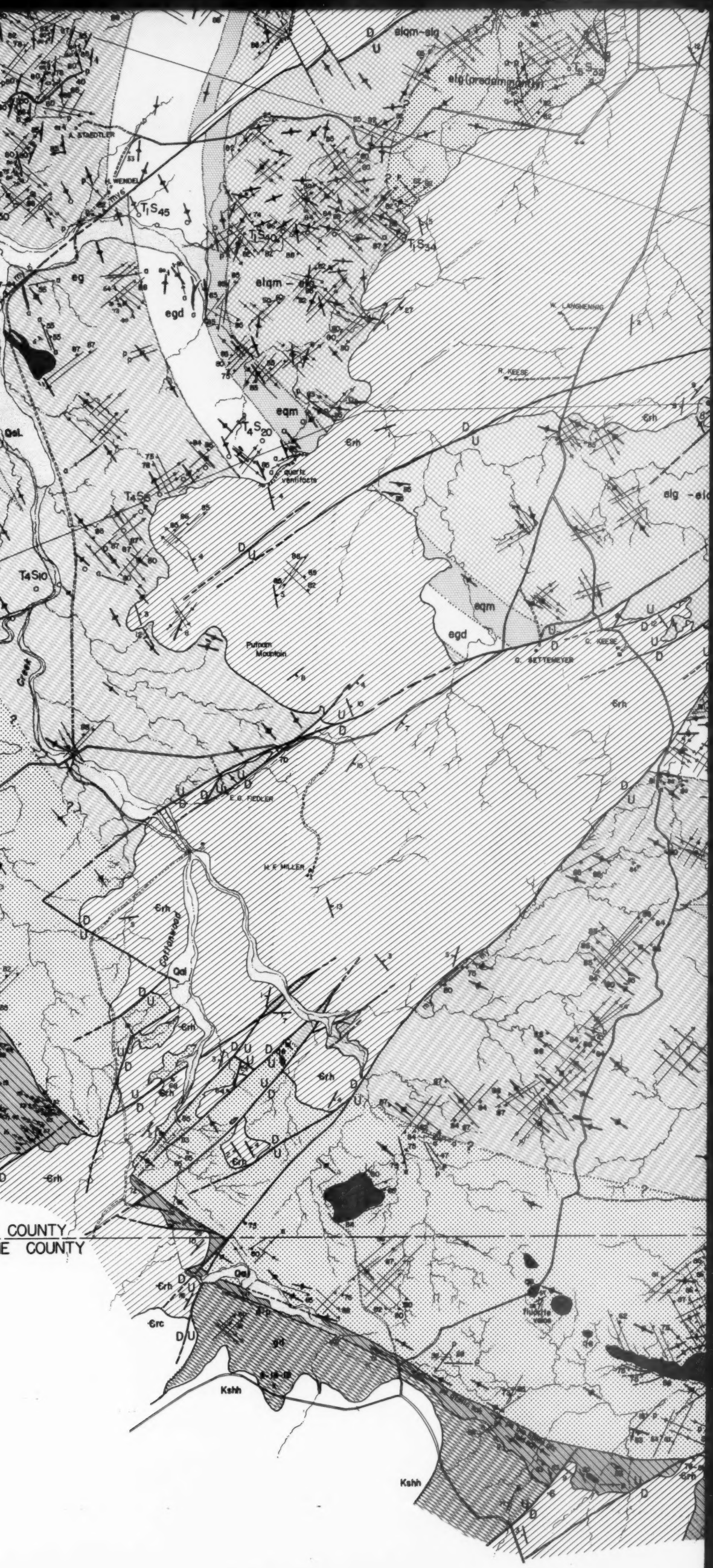

ENCHANTED ROCK BATHOLITH, LLA

ENCHANTED ROCK BATHOLITH, LLANO AND GILLESPIE COUNTIES, TEXAS

Bullhead Mountain

A. J. MOSS

Strathmore

Creek

Qal

Watch Hill

Creek

H. ETHRIDGE

Sandy

Qal

Duckenfield Park

Qal

ig intrusion strongly foliated along border

ig to igm

ig to qm

ig

egd

eg

eqm

eg

elg

elg

D

D'

E'

30°30'

T_1S_{20}

T_1S_{19}

T_1S_{16}

T_1S_{16}

T_2S_{18}

T_2S_{10}

T_2S_{10}

cT_2S_{10}

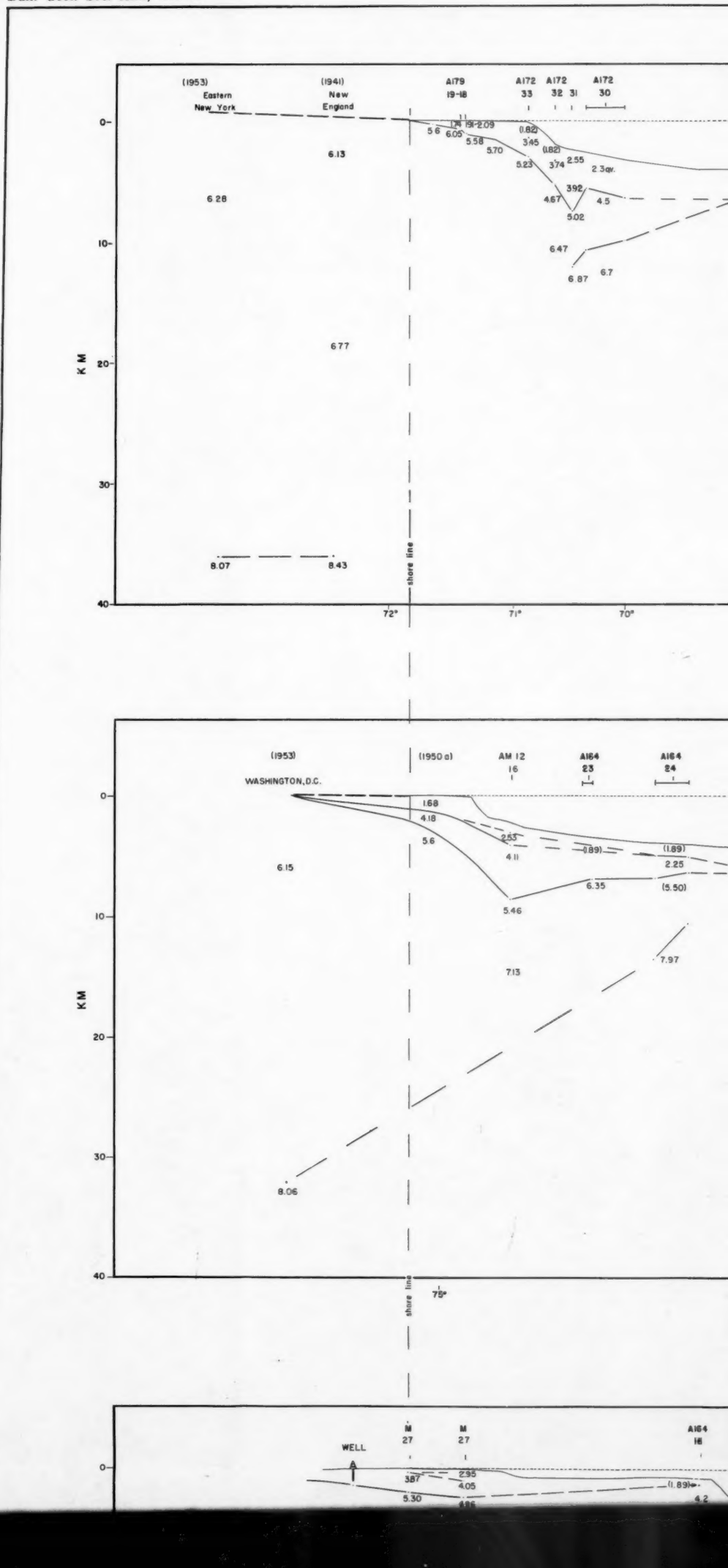
(1953)
Eastern
New York
(1941)
New
England
A179
19-18
A172
33
A172
32
31
A172
30
0
10
20
30
40
KM
6.13
6.28
6.77
8.07
8.43
shore line
72°
71°
70°
(1953)
WASHINGTON, D.C.
(1950 a)
AM 12
16
A164
23
A164
24
6.15
8.06
7.13
7.97
75°
WELL
M
27
M
27
A164
18

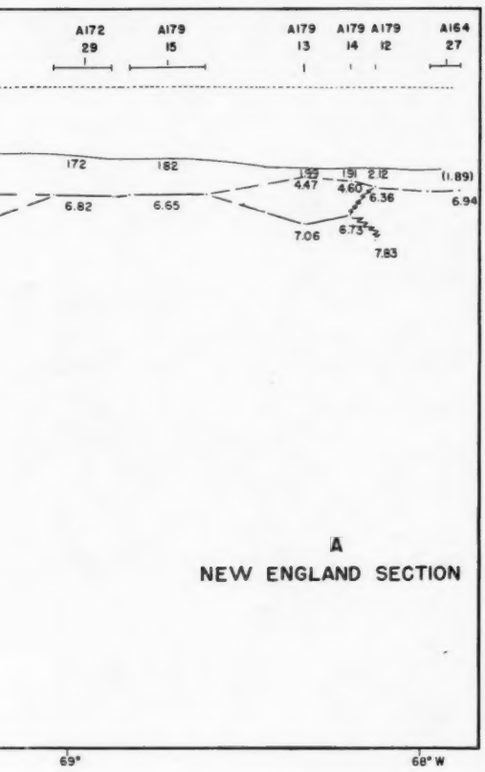

A
NEW ENGLAND SECTION

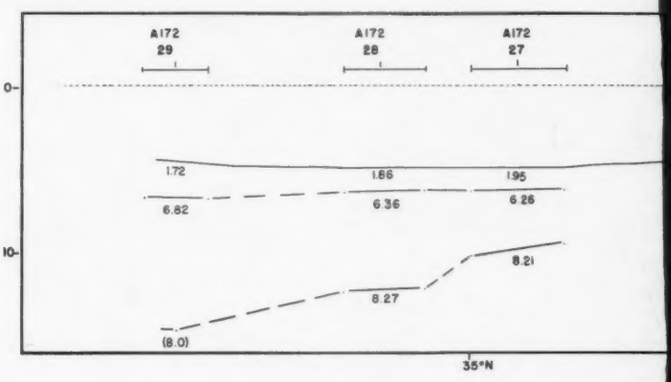

SCALES FOR SEISMIC SECTIONS

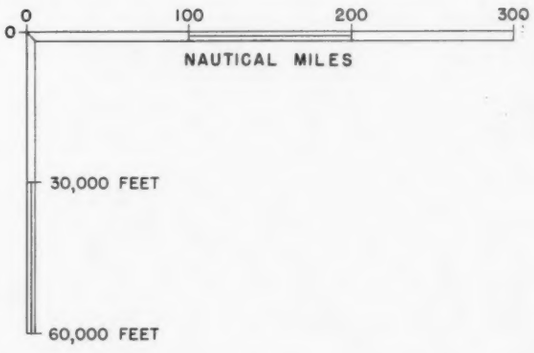

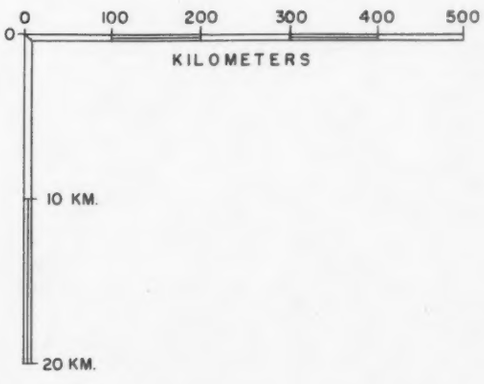

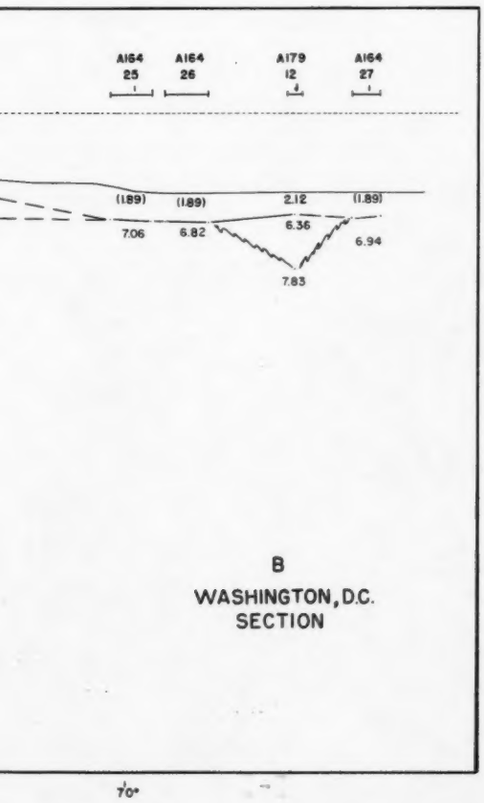

B
WASHINGTON, D.C.
SECTION

VERTICAL EXAGGERATION: 18.6 = 1

COMPRESSIONAL WAVE VELOCITIES IN
KILOMETERS/SECOND

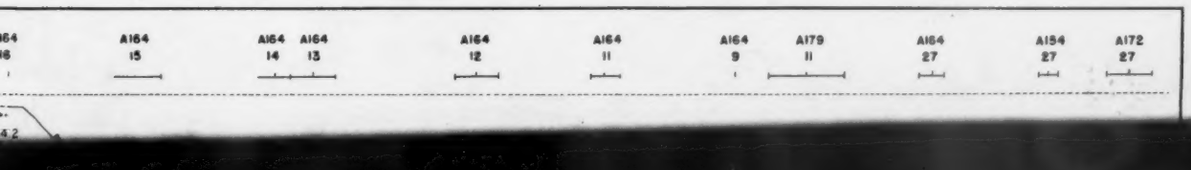

A
ENGLAND SECTION

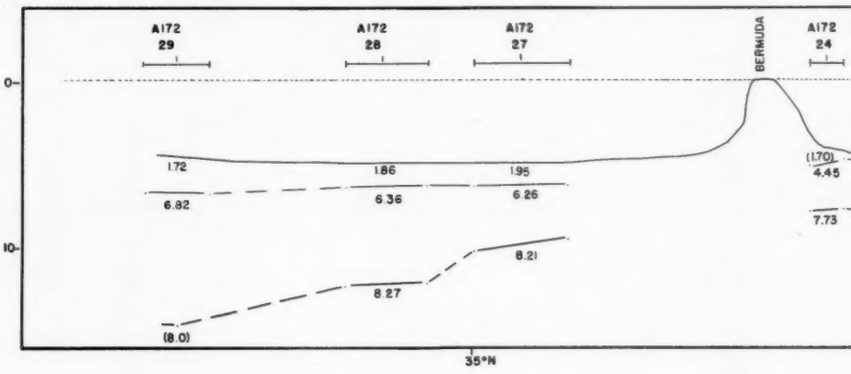

SCALES FOR SEISMIC SECTIONS

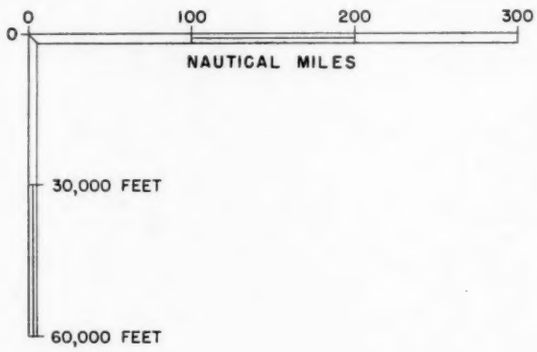

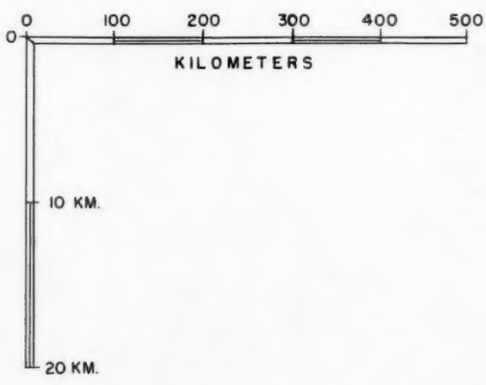

VERTICAL EXAGGERATION: 18.6=1

COMPRESSIONAL WAVE VELOCITIES IN
KILOMETERS/SECOND

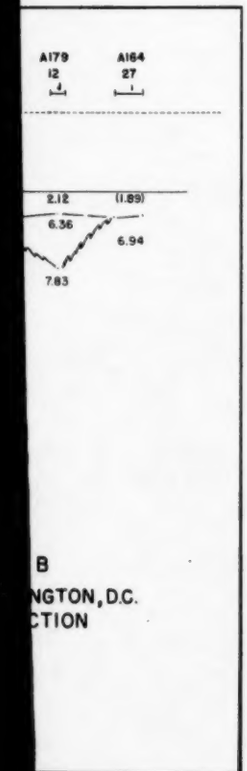

B
NGTON, D.C.
CTION

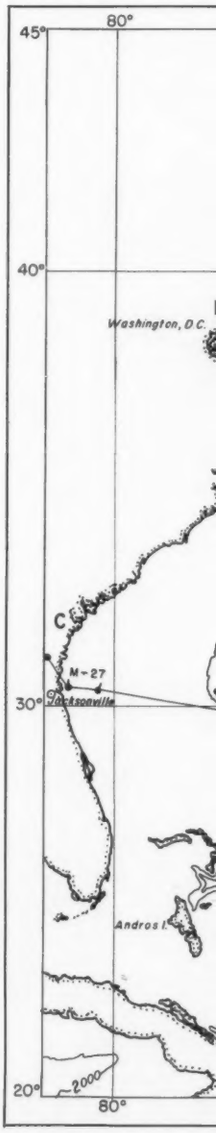

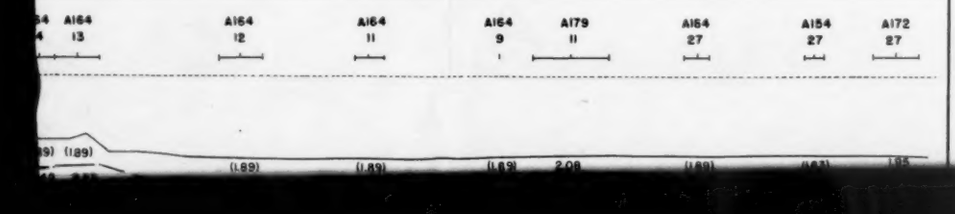

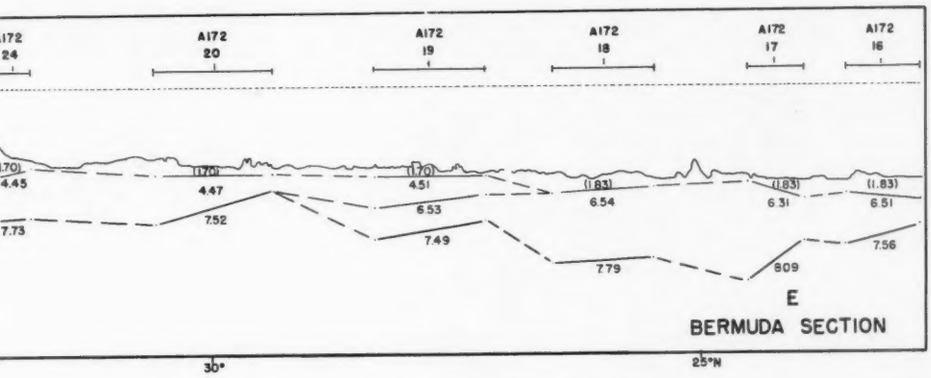

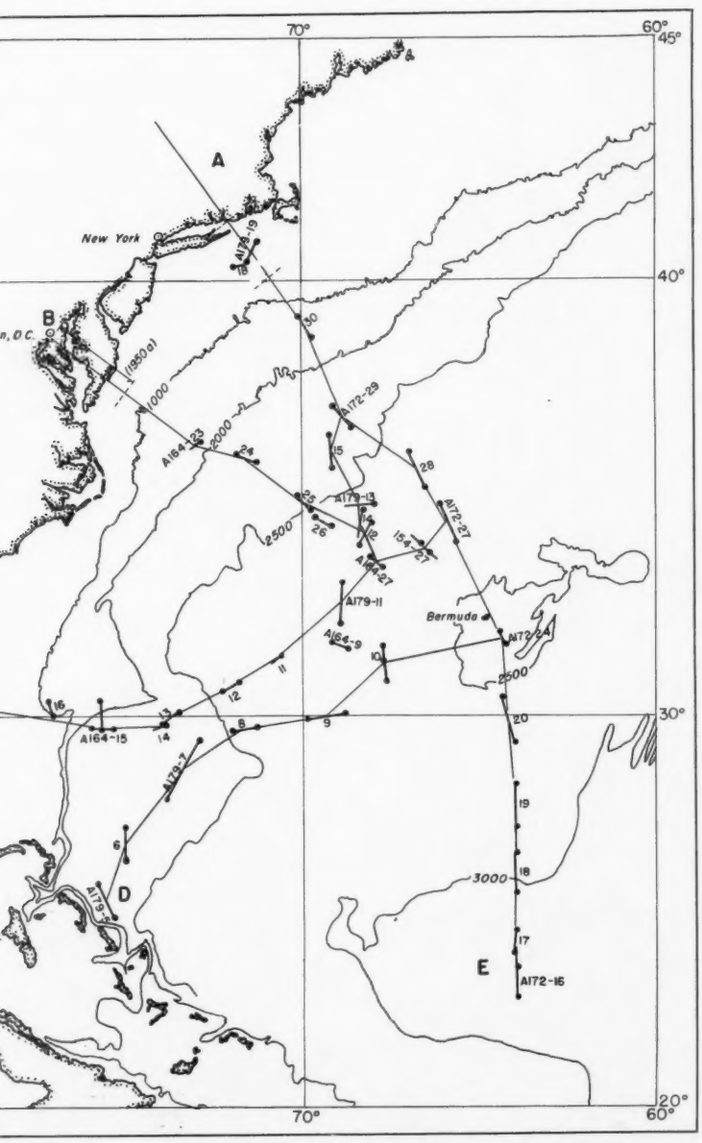

INDEX MAP FOR SEISMIC SECTIONS

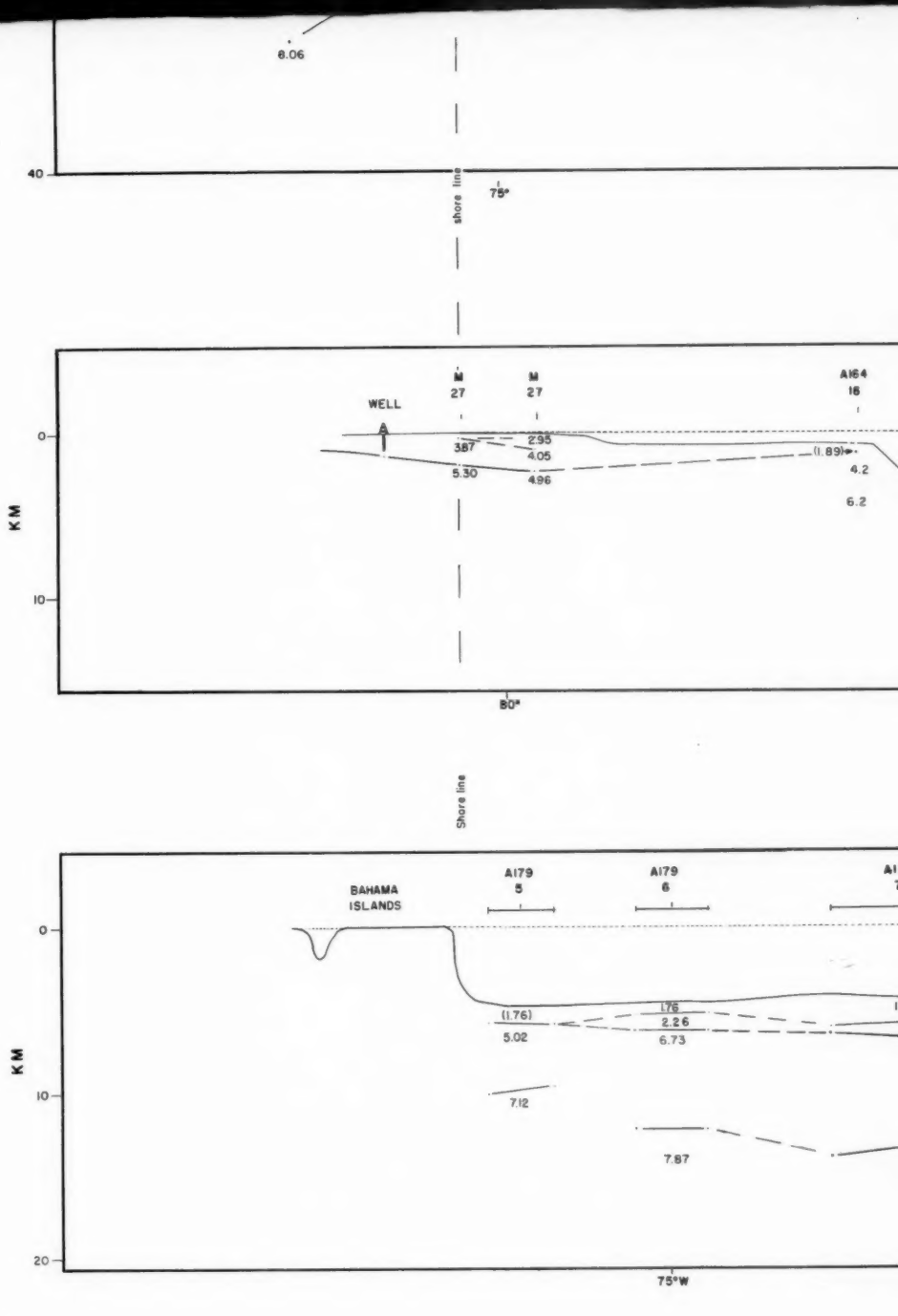
8.06
40
shore line
75°
M
27
M
27
A164
16
WELL
0
3.87
2.95
4.05
(1.89)
4.2
5.30
4.96
6.2
KM
10
80°
Shore line
BAHAMA
ISLANDS
A179
5
A179
6
0
(1.76)
1.76
2.26
5.02
6.73
7.12
7.87
KM
10
20
75°W

SECTION

VERTICAL EXAGGERATION: 18.6 = 1

COMPRESSIONAL WAVE VELOCITIES IN
KILOMETERS/SECOND

70°

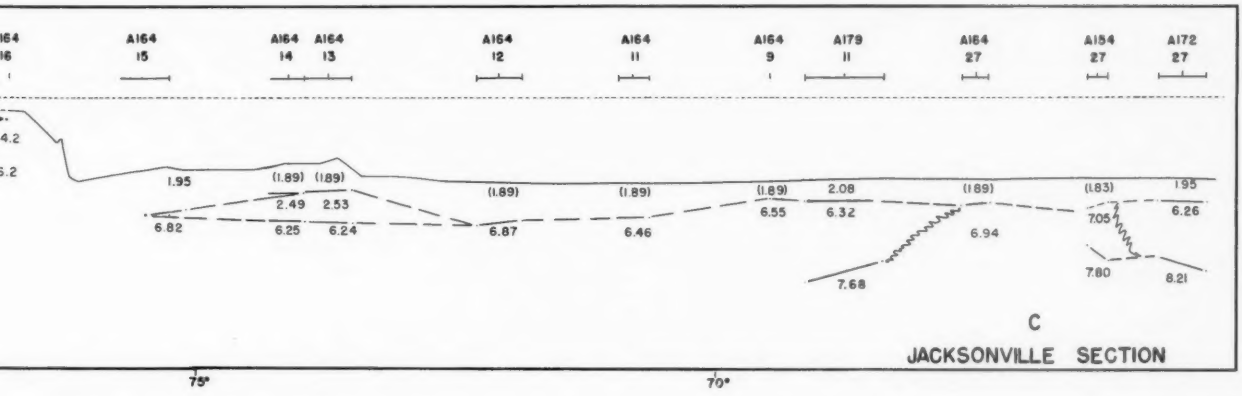

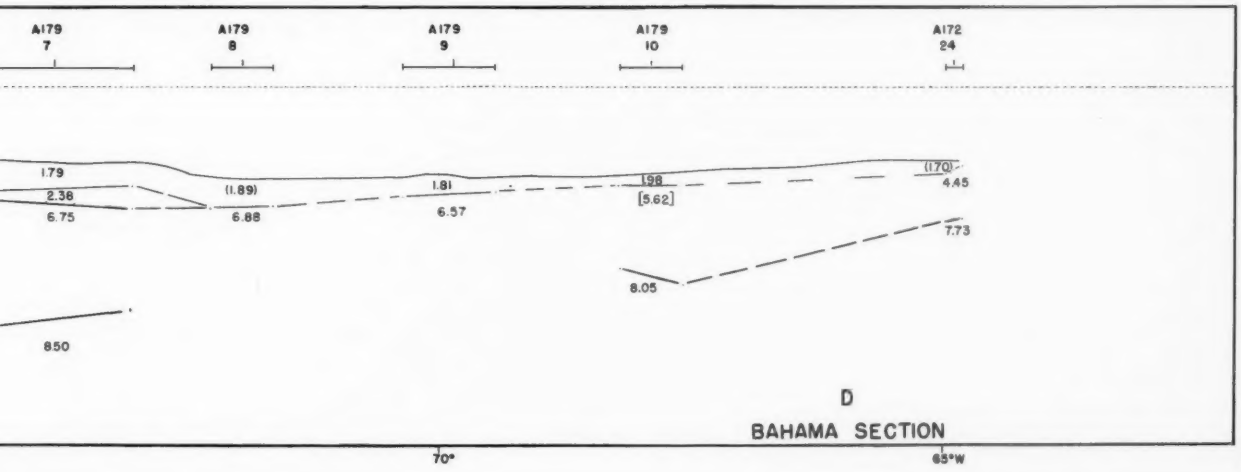

SEISMIC SECTIONS, WESTERN ATLANTIC OCEAN

SECTION

VERTICAL EXAGGERATION: 18.6 = 1

COMPRESSIONAL WAVE VELOCITIES IN
KILOMETERS/SECOND

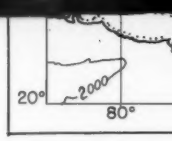

70°

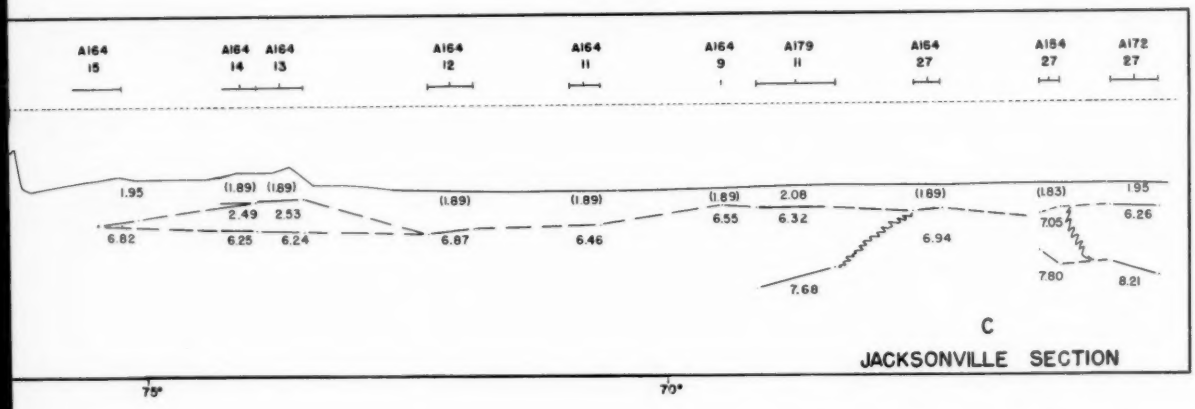

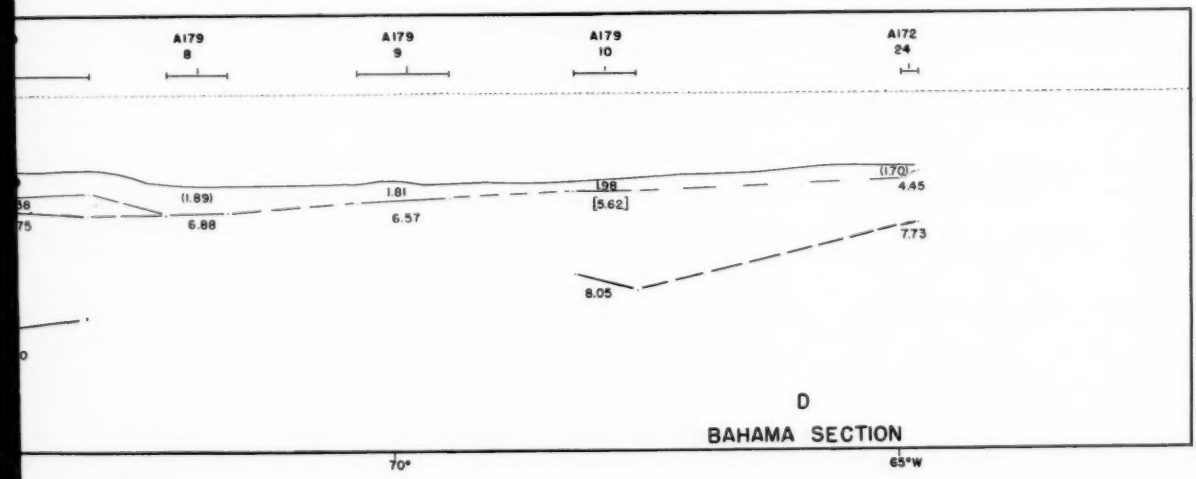

SEISMIC SECTIONS, WESTERN ATLANTIC OCEAN

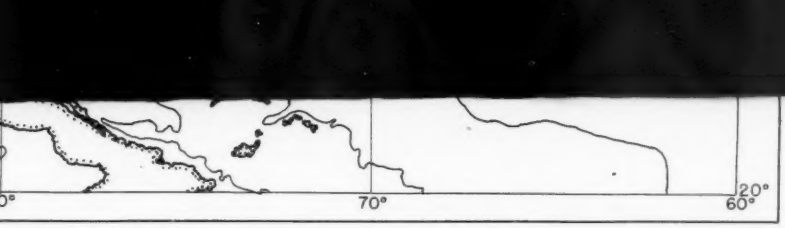

INDEX MAP FOR SEISMIC SECTIONS

LAMONT GEOLOGICAL OBSERVATORY
COLUMBIA UNIVERSITY

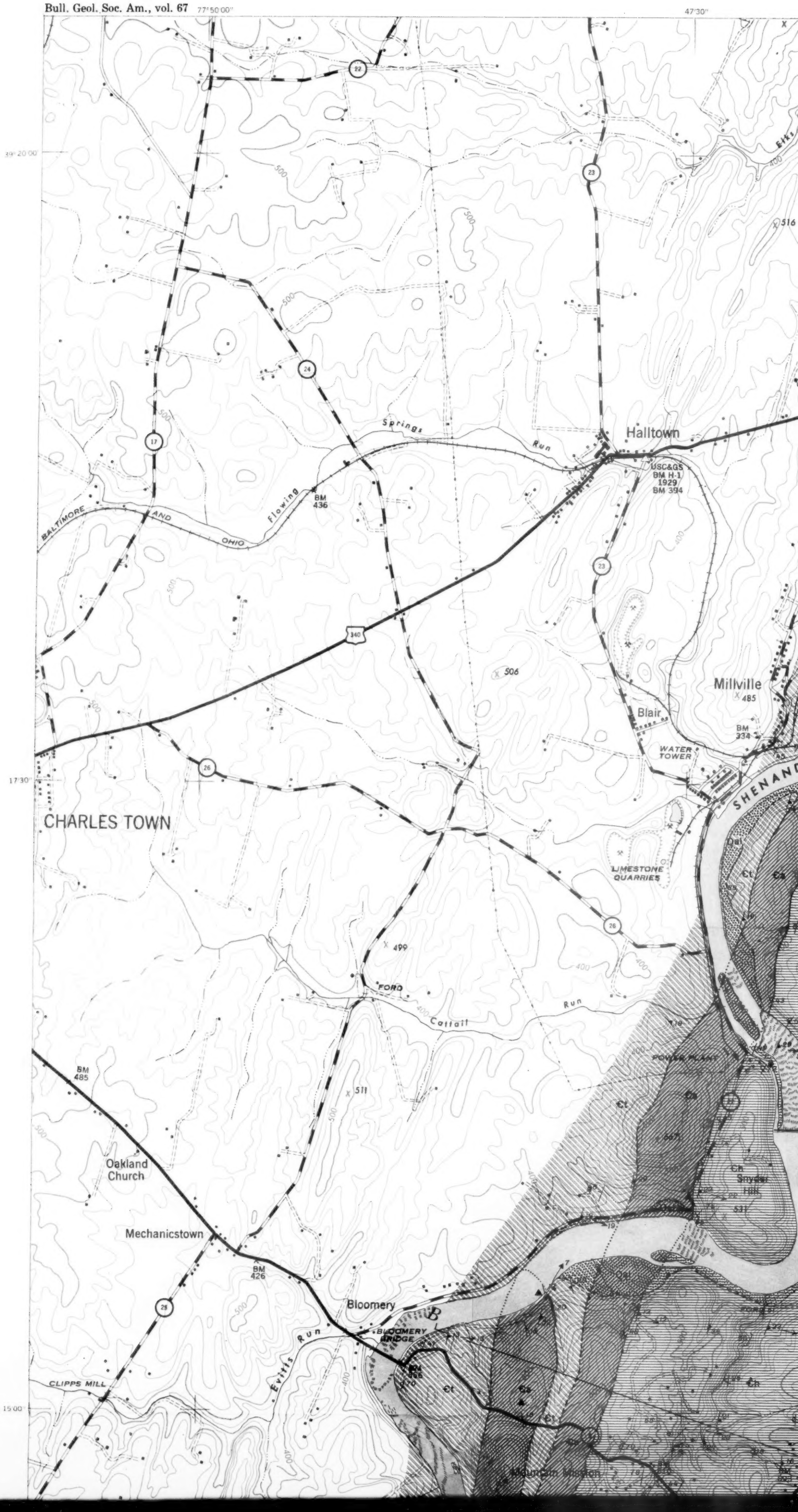
77°50'00"
47'30"
39°20'00"
17'30"
15'00"
22
23
24
17
26
28
340
500
400
Halltown
USC&GS
BM H-1
1929
BM 394
Springs
Run
Flowing
BM
436
BALTIMORE AND OHIO
Millville
485
Blair
BM
334
WATER
TOWER
SHENAND
516
506
CHARLES TOWN
LIMESTONE
QUARRIES
Qal
Ct
Cs
499
FORD
Cattail
Run
POWER PLANT
511
BM
485
Oakland
Church
Mechanicstown
BM
426
Bloomery
BLOOMERY
BRIDGE
Evitts Run
CLIPPS MILL
Snyder
Hill
667
531
Ch
Mountain Mission

45'00"

USC&GS MARYLAND HEIGHTS 1869

Pleasantville

C&O CANAL

WEST VIRGINIA

MARYLAND

BM 313

John Brown's Cave

Harpers Ferry

Bolivar

BM 285

BM 287

STORER COLLEGE

WATER TOWER

MARYLAND

VIRGINIA

SHENANDOAH RIVER

Loudoun Heights

BLUE RIDGE

JEFFERSON COUNTY

LOUDOUN COUNTY

LIMESTONE QUARRY

Silver Grove

Ebenezer Church

Church of the Nazarene

St Pauls Church

Neersville

Chestnut Hill Church

Keyes Gap

Purcell Knob

Run

Ch

CEM

Qal

Cwu

Cwm

Cwl

Cl

p€c

p€csrs

p€csrp

p€g

45'00"

42'30"

USC&GS
MARYLAND HEIGHTS
1869

Pleasantville

C & O CANAL

WEST VIRGINIA

MARYLAND

John Brown's Cave

WATER TOWER

Harpers Ferry

Bolivar

STORER COLLEGE

SHENANDOAH RIVER

Loudoun Heights

LIMESTONE QUARRY

Silver Grove

BALTIMORE

JEFFERSON COUNTY

Ebenezer Church

Church of the Nazarene

St Pauls Church

Neersville

Chestnut Hill Church

Keyes Gap

RIDGE

Run

Qal

Ch

CEM

Ot

Ca

Cwu

Cwl

Cwm

p€g

p€c

p€srs

p€srp

p€cs

77°40'00"

39°20'00"

17'30"

15'00"

WASHINGTON COUNTY
FREDERICK COUNTY
Weverton
USC&GS BM T 35 1938
OHIO CANAL (ABANDONED)
BALTIMORE AND OHIO CHESAPEAKE
Sandy Hook
Knoxville
B&O
POTOMAC RIVER
MARYLAND
VIRGINIA
BLUE RIDGE CLUB
Georges Mill
Mt Olivet Church
Britain
FORD
BM 335
BM 261
BM 471
p€srp
p€srs
p€g
p€cd
p€cc
p€cs
€wu
€wl
€l
Ch

Oakland Church
Mechanicstown
Bloomery
BLOOMERY BRIDGE
Evitts Run
CLIPPS MILL
Cattail Run
FORD
POWER PLANT
Snyder Hill
Mountain Mission
Blue Ridge School
SHENANDOAH RIVER
Bullskin Run
Fairmont Church
BLUE RIDGE
APPALACHIAN TRAIL
WEST VIRGINIA
VIRGINIA
Jefferson Lookout
BM 485
BM 426
BM 556
BM 665
BM 659
BM 582
BM 593
BM 610
Qal
Ct
Ca
Ch
Cwm
Cwu
Cwl
pCcm
pCca
A
B
C
D
15 00
12 30

Chestnut Hill Church
Keyes Gap
St Pauls Church
Neersville
Purcell Knob
Mannings
USC&GS BEACON 1942
USC&GS NEERSVILLE 1942
Salem Church
Mechanicsville
SAWMILL
Hillsboro
Arnold Grove Church
Asbury Church
CRGS TOWER
BM 636
BM 589
BM 596
BM 541
BM 523
BM 818
BM 883
BM 888
JEFFERSON COUNTY
LOUDOUN COUNTY
BLUE RIDGE
WEST VIRGINIA
FOUNTAIN
Cwu
Cwl
Cwm
Cl
Ch
p€srs
p€g
p€c
p€ccm
p€ccs
p€ccd
p€srp
U.D.

Chestnut Hill Church
Keyes Gap
Snyder Hill
St Pauls Church
Neersville
Mannings
Mechanicsville
Salem Church
Hillsboro
Arnold Grove Church
Asbury Church
SAWMILL
FOUNTAIN
JEFFERSON COUNTY
LOUDOUN COUNTY
USC&GS BEACON 1942
USC&GS NEERSVILLE 1942
BM 636
BM 580
BM 596
BM 618
CAGS TOWER
p€g
p€c
p€srs
p€srp
p€ccs
p€ccm
p€cd
€wu
€wl
€l
€h

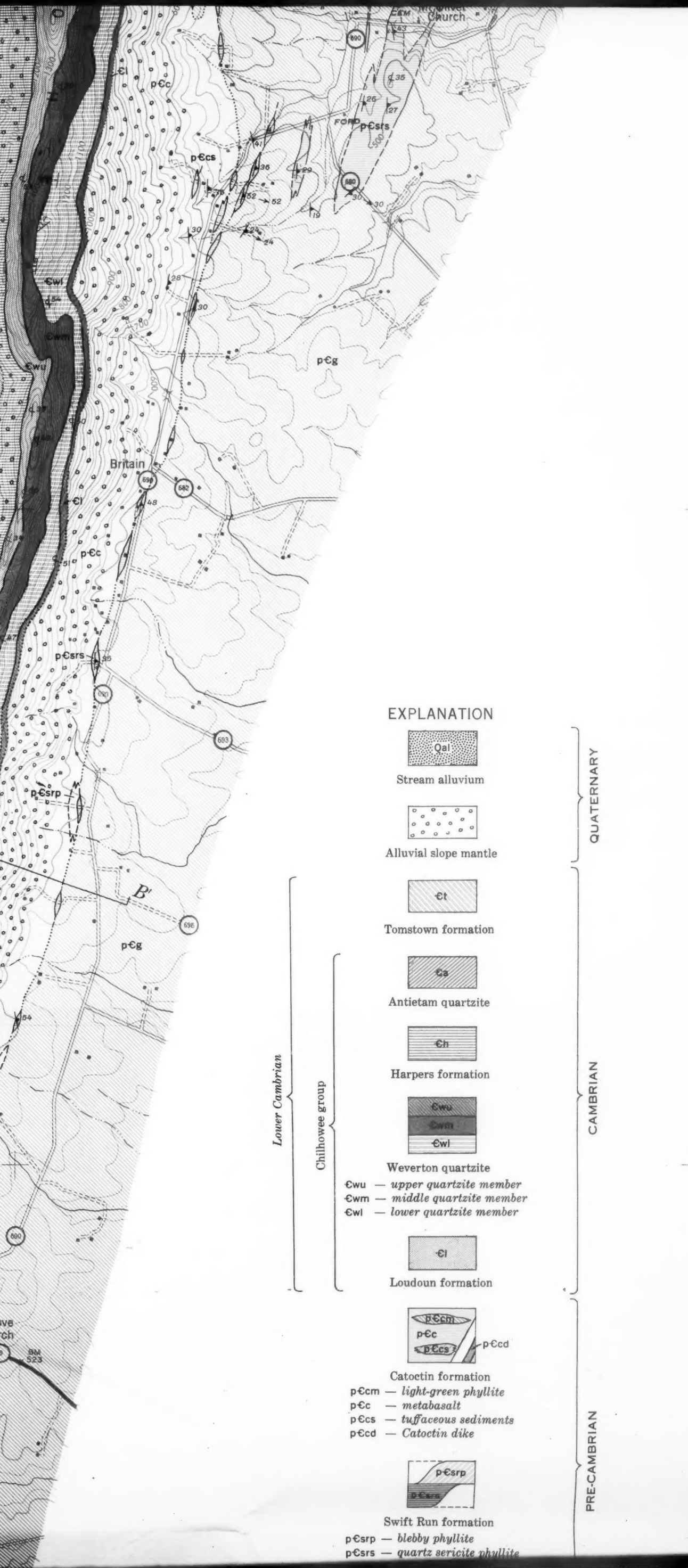

EXPLANATION

QUATERNARY

Qal — Stream alluvium

Alluvial slope mantle

CAMBRIAN

€t — Tomstown formation

Chilhowee group

€a — Antietam quartzite

€h — Harpers formation

€wu / €wm / €wl — Weverton quartzite

€wu — *upper quartzite member*
€wm — *middle quartzite member*
€wl — *lower quartzite member*

Lower Cambrian

€l — Loudoun formation

PRE-CAMBRIAN

p€cm / p€c / p€cs / p€cd — Catoctin formation

p€cm — *light-green phyllite*
p€c — *metabasalt*
p€cs — *tuffaceous sediments*
p€cd — *Catoctin dike*

p€srp / p€srs — Swift Run formation

p€srp — *blebby phyllite*
p€srs — *quartz sericite phyllite*

Chestnut Hill Church
Keyes Gap
St Pauls Church
Neersville
Mannings
Salem Church
Mechanicsville
SAWMILL
Hillsboro
Arnold Grove Church
Asbury Church
JEFFERSON COUNTY
LOUDOUN COUNTY
pCsrs
pCg
pCc
pCcm
pCcs
pCsrs
pCcd
pCsrp
Cwu
Cwl
Cl
Ch
Cwm
BM 636
BM 589
BM 596
BM 541
687
689
718
719
715
716
714
275
9

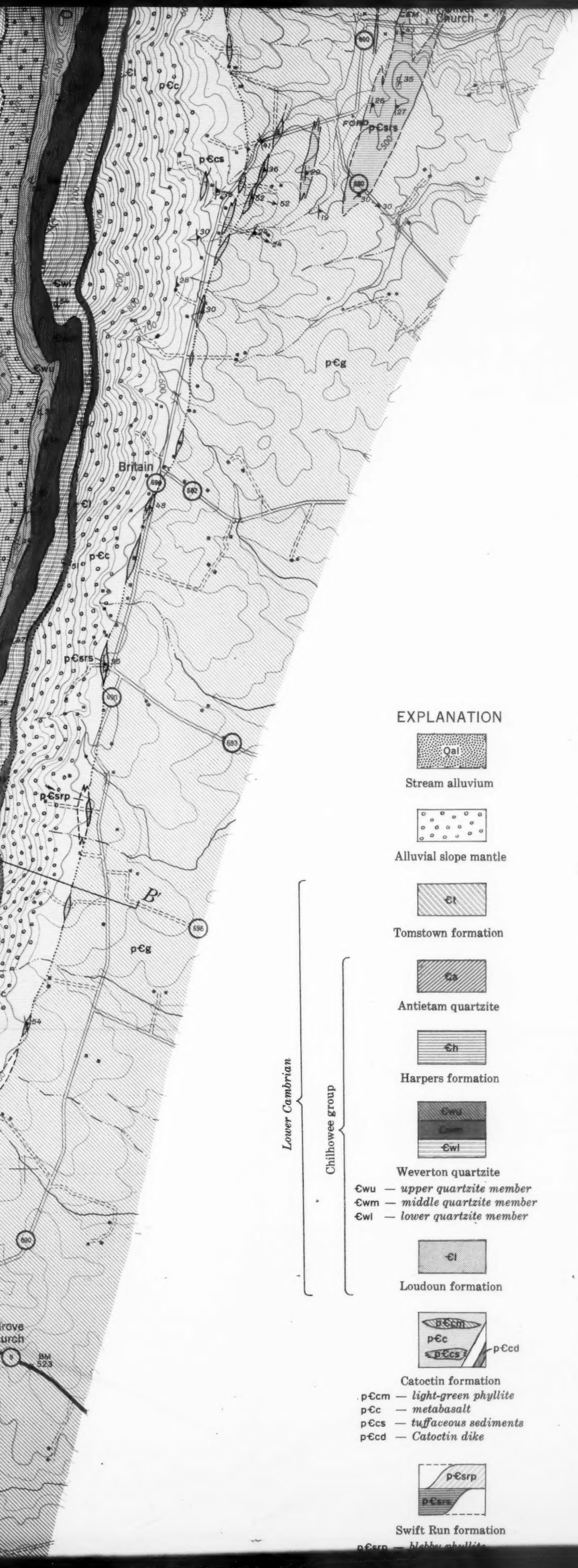

15'00"

12'30"

EXPLANATION

QUATERNARY

Qal — Stream alluvium

Alluvial slope mantle

CAMBRIAN

Lower Cambrian

€t — Tomstown formation

Chilhowee group

€a — Antietam quartzite

€h — Harpers formation

€wu / €wm / €wl — Weverton quartzite

€wu — *upper quartzite member*
€wm — *middle quartzite member*
€wl — *lower quartzite member*

€l — Loudoun formation

PRE-CAMBRIAN

p€cm / p€c / p€cs / p€cd — Catoctin formation

p€cm — *light-green phyllite*
p€c — *metabasalt*
p€cs — *tuffaceous sediments*
p€cd — *Catoctin dike*

p€srp / p€srs — Swift Run formation

p€srp — *blabby phyllite*

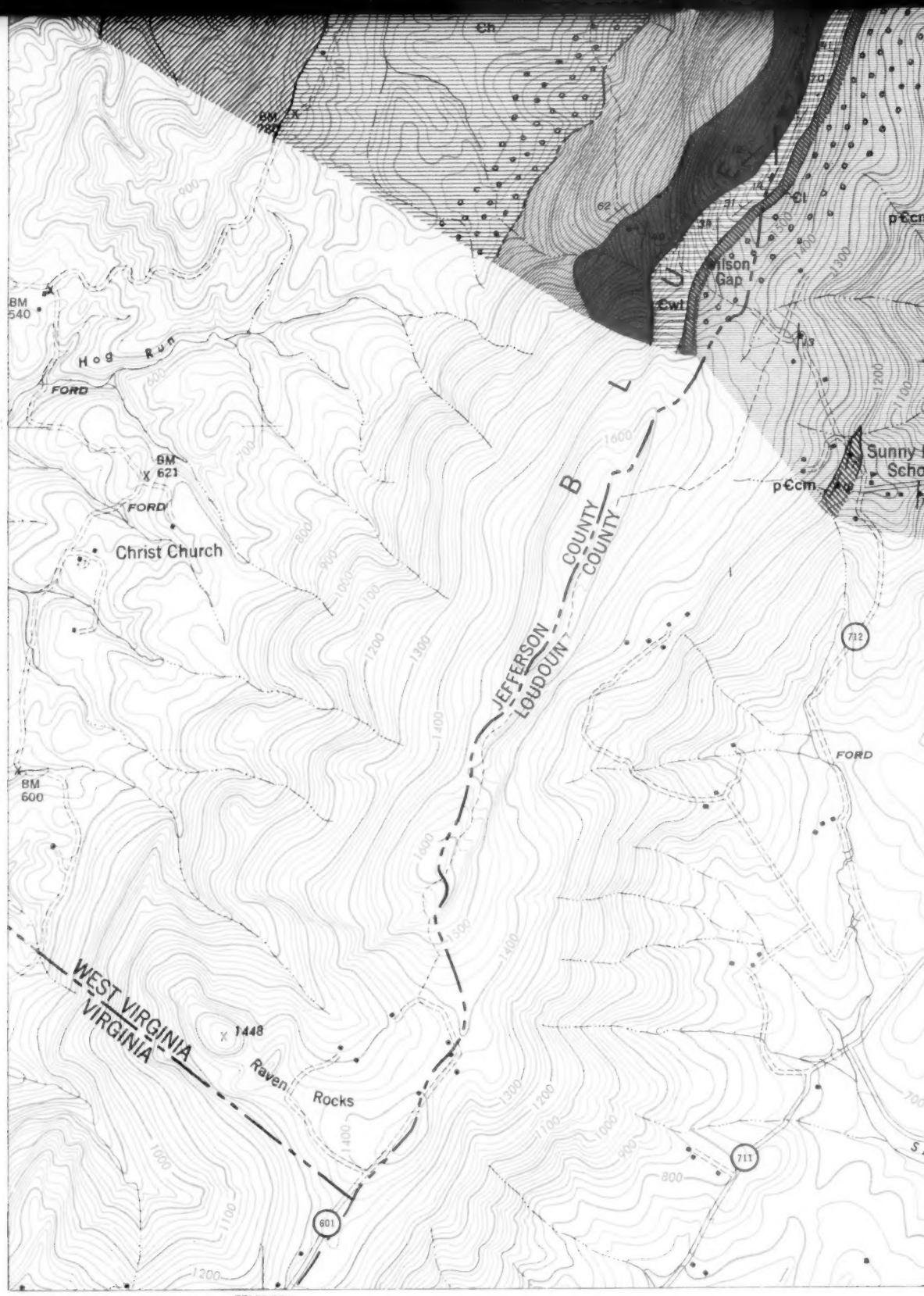

Base from U.S. Army Map Service; Charles Town, Harpers Ferry, Purcellville, and Round Hill 7½ minute quadrangles. 1946 Editions

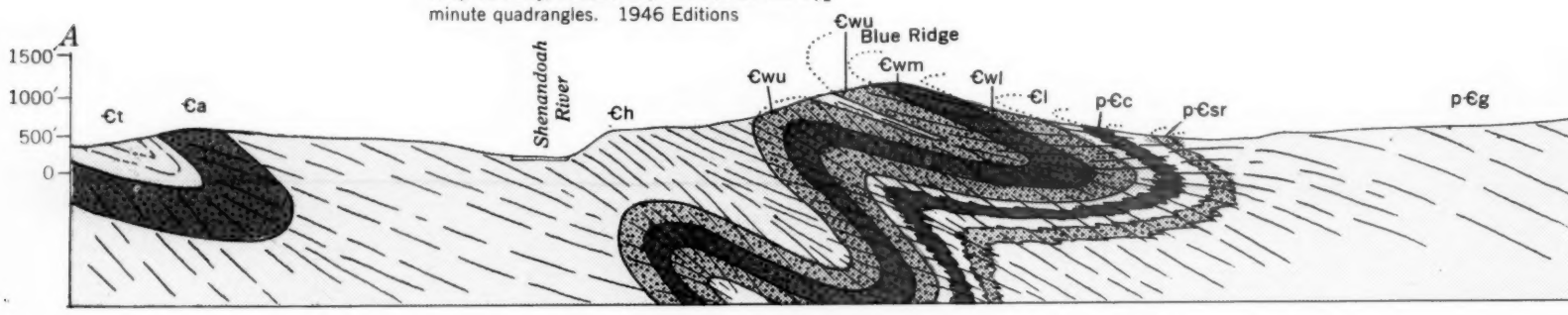

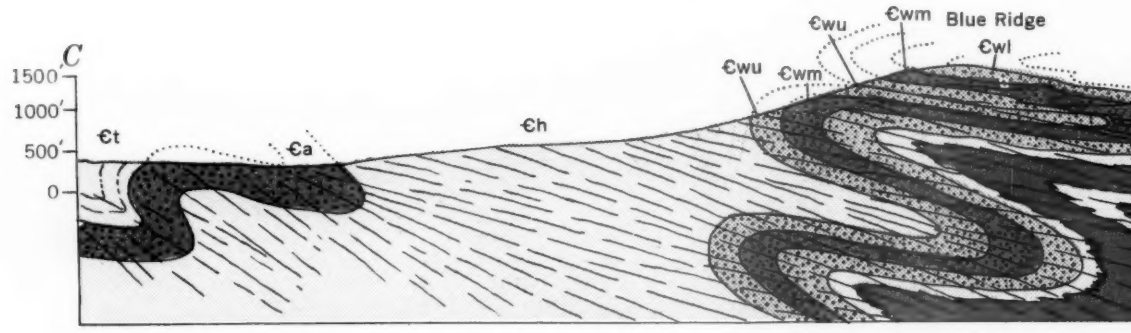

GEOLOGIC M

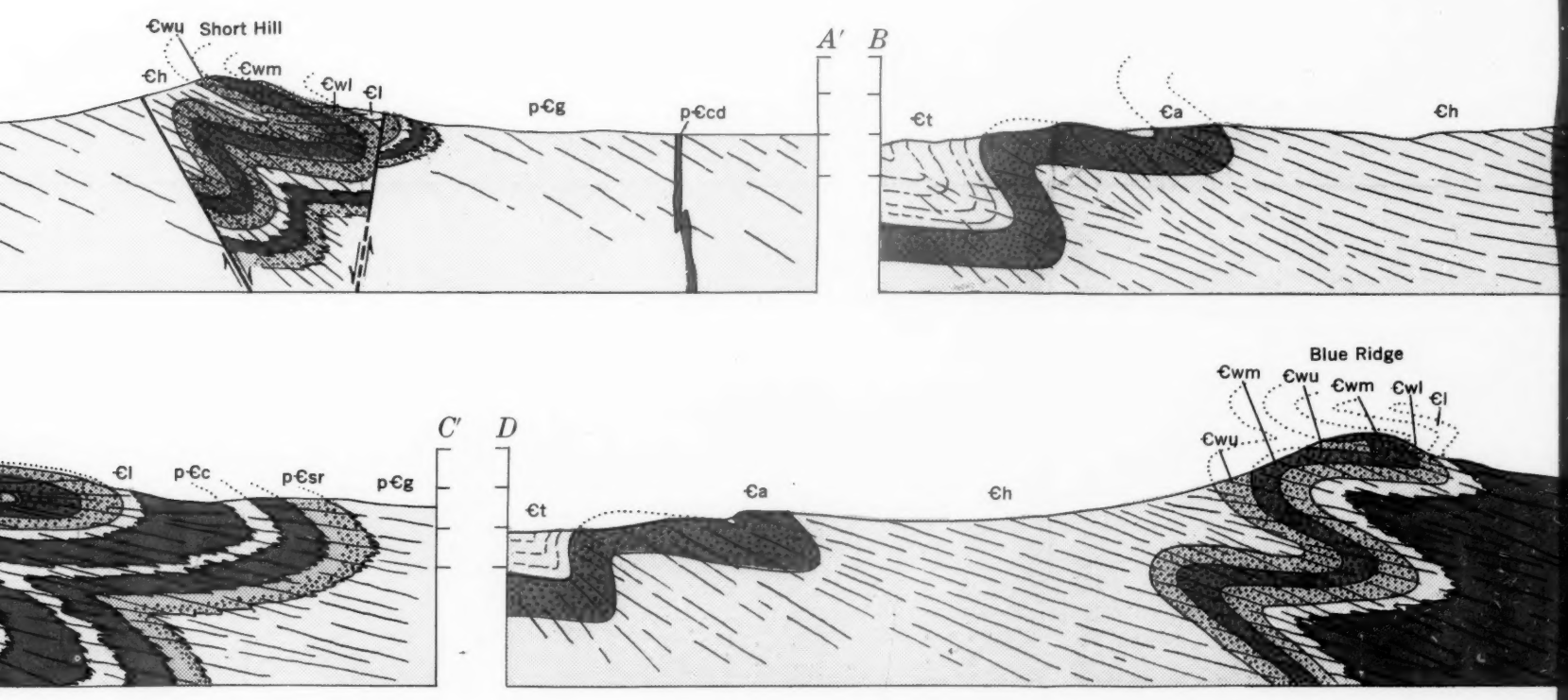

MAP AND SECTIONS OF NORTHWESTERN LOU

Scale 1:25,000

1 ½ 0 1 Mile

Contour interval 20 feet
Datum is mean sea level

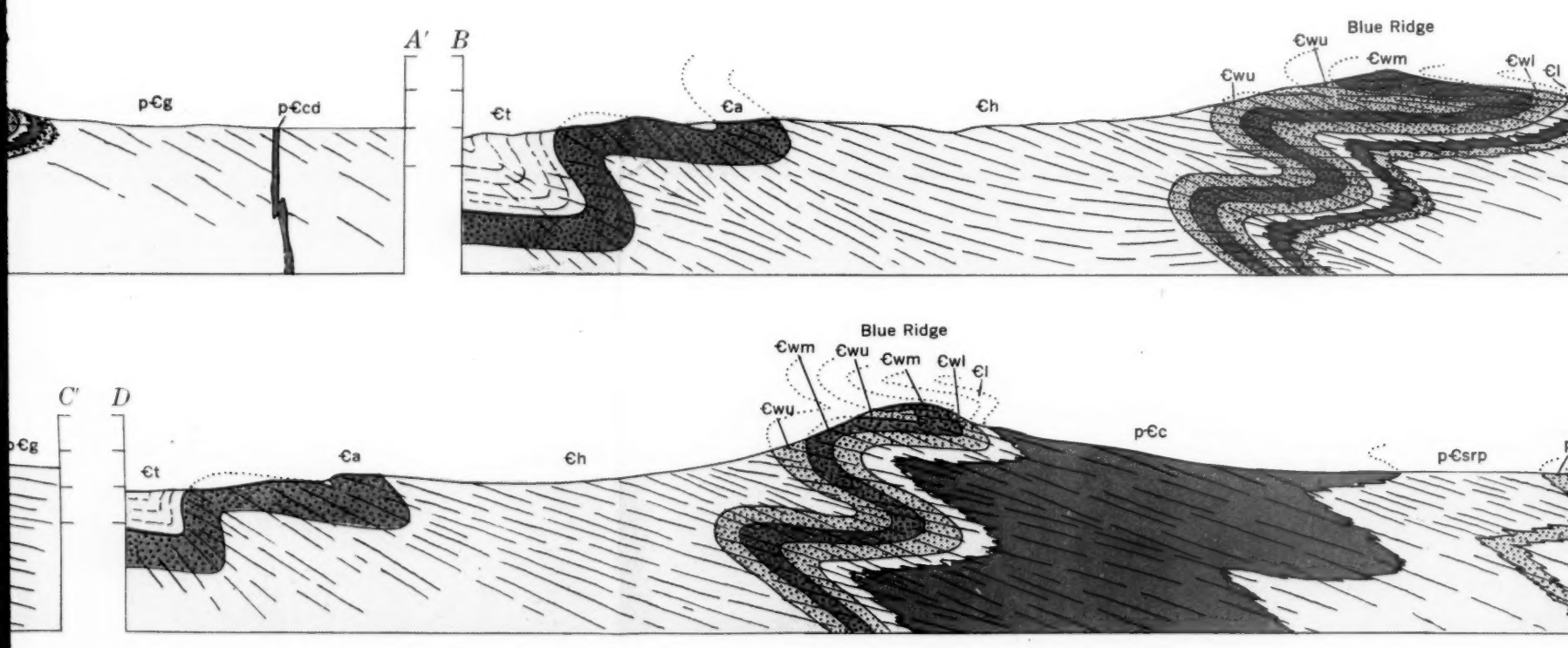

ECTIONS OF NORTHWESTERN LOUDOUN COUNTY,

Scale 1:25,000

1 ½ 0 1 Mile

Contour interval 20 feet
Datum is mean sea level

p€srp — *blebby phyllite*
p€srs — *quartz sericite phyllite*

p€g

Gneissic basement

Fossil locality

D
U
Normal fault, dashed where approximately located

D
U
Concealed normal fault

Contact, dashed where approximately located

Concealed contact

Strike and dip of bedding

Strike and dip of overturned bedding

Strike and dip of bedding overturned more than 180 degrees

Strike of vertical bedding

Strike and dip of flow cleavage

Strike and dip of slip cleavage

Strike and dip of gneissic foliation

Horizontal projection and plunge of lineation

Horizontal projection and plunge of fold axis

39°10'00"

77°40'00"

Geology by R. P. Nickelsen, 1951-52

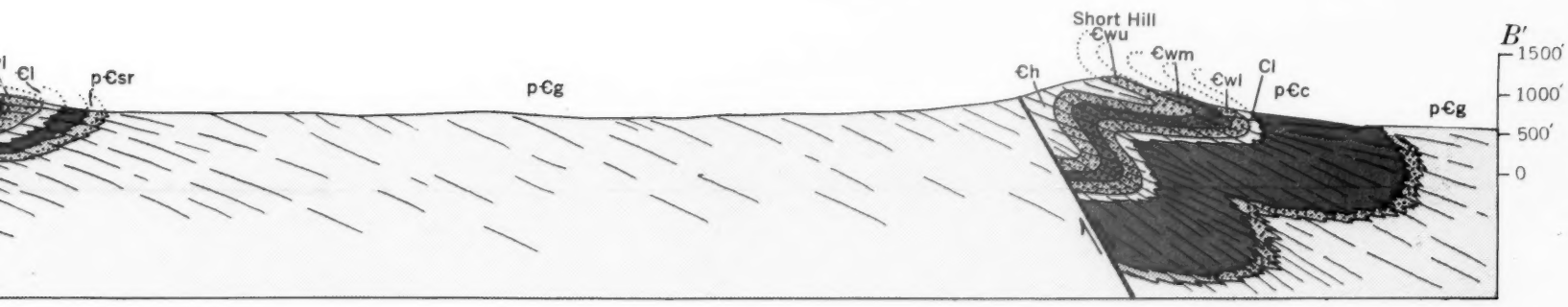

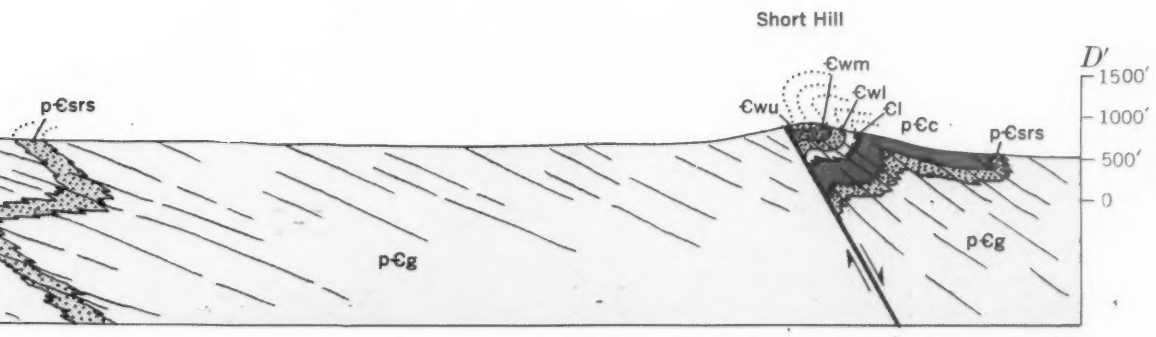

Note: See Figure 11 for Sections X-X′ and Y-Y′.

Y, VIRGINIA

TRUE NORTH

MATE MEAN
ATION 1946

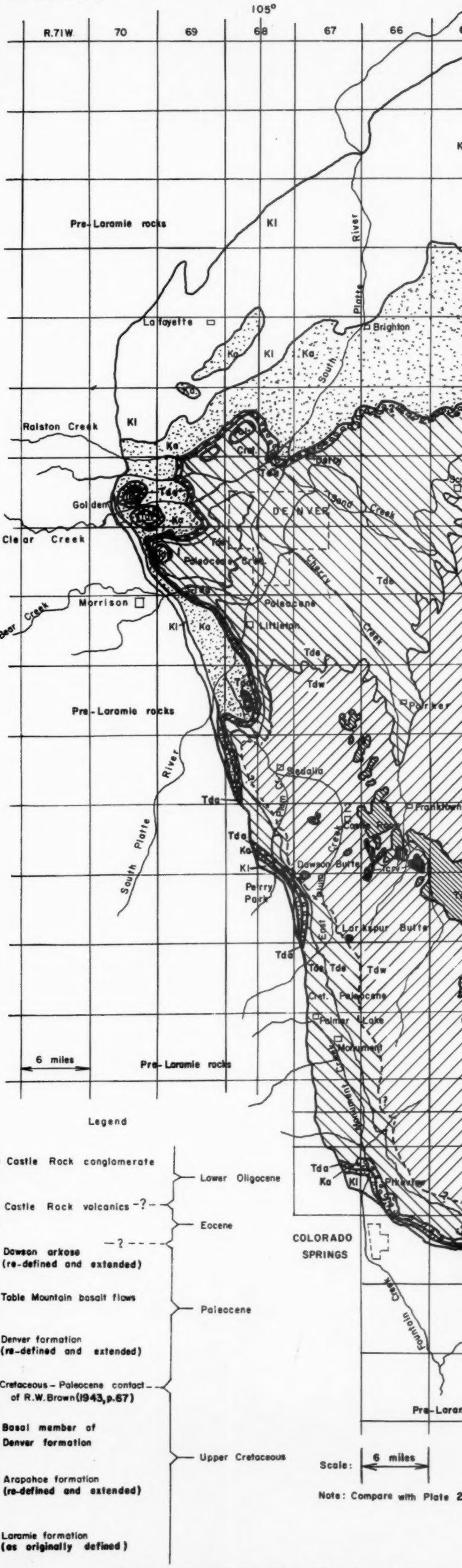

POST-LARAMIE CORRELATION MAP

PET-PUB-LIB

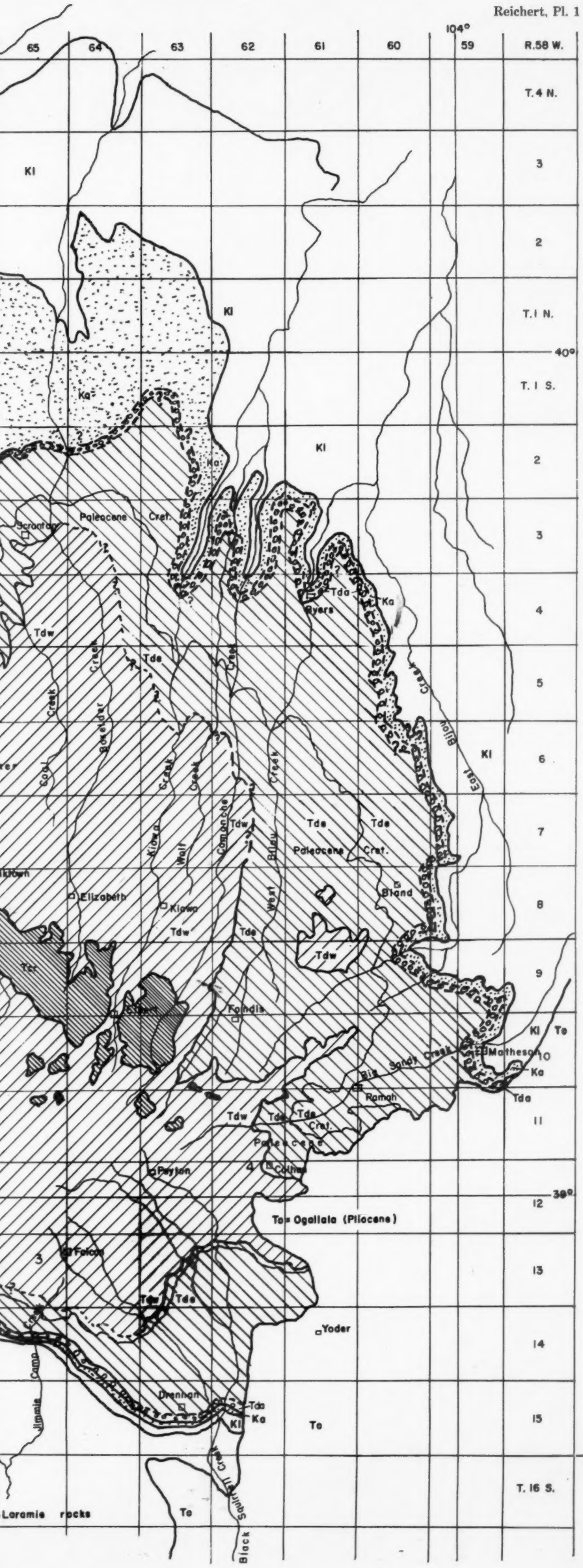
104°
65
64
63
62
61
60
59
R.58 W.
T. 4 N.
3
2
T. 1 N.
40°
T. 1 S.
2
3
4
5
6
7
8
9
10
11
12
39°
13
14
15
T. 16 S.
Kl
Ka
Tda
Tde
Tdw
Tcr
Cret.
Paleocene
Scranton
Elizabeth
Kiowa
Elbert
Falcon
Peyton
Calhan
Yoder
Bennett
Bijou
Bennett
Bijou
Byers
Strasburg
Deer Trail
Agate
Bijou
Comanche
Kiowa
Wolf
Box Elder
Coal
Jimmie
Camp
Bijou
Creek
Sand
Creek
Bijou
Creek
Bijou
Creek
Bijou

EXPLANATION

PRE CAMBRIAN

- Peninsular gneiss and younger granite — GNEISSIC COMPLEX
- Pyroxenite (Websterite)
- ECLOGITE GABBRO SERIES — Pyroxene garnet rock, Garnet-hornblende plagioclase rock, etc.
- ANORTHOSITE SERIES — Perknite and Chromitite bands, Anorthite edenite gneiss, Anorthite clinozoisite corundum rock, Bytownite clinozoisite gneiss, Cordierite corundum anthophyllite rock, etc. Chromitite bands shown by heavy lines. — SITTAMPUNDI COMPLEX
- Peridotite
- Amphibolite
- Magnetite quartzite
- Calciphyre & crystalline limestone — DHARWAR

Contact, dashed where approximately located

Strike of vertical foliation

Strike and dip of foliation with inclined lineation

Horizontal lineation

Railway line

Country road

District highway

Height above mean sea level 702

N

SCALE OF MILES

0 ¼ ½ 1 2

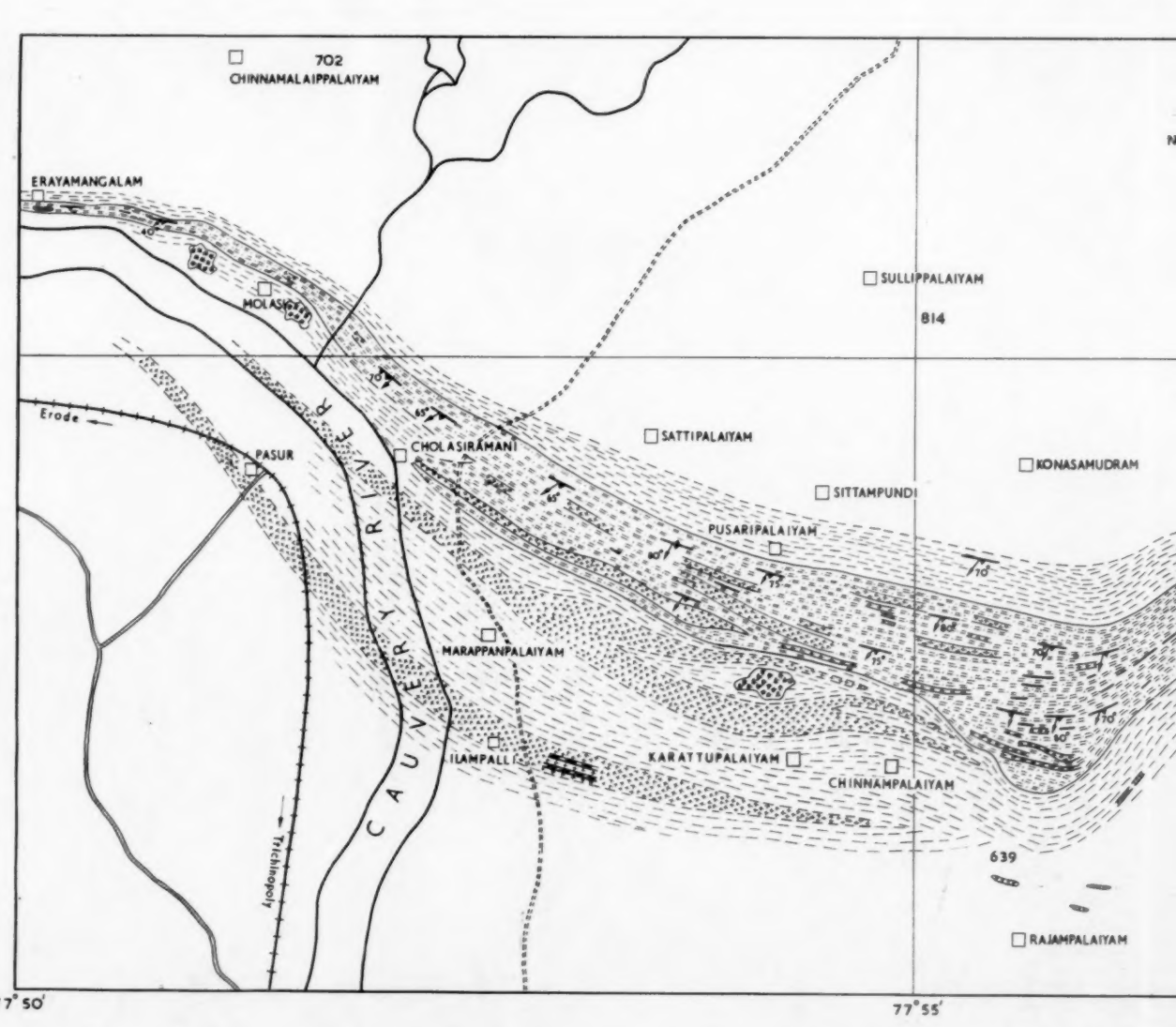

PETROLOGICAL MAP OF THE SITTAMPUNDI ANORTHOS

DET-PUB-LIB

HOSITE-GABBRO COMPLEX, SALEM DISTRICT, MADRAS, INDIA